

THE ROLE OF CHAPERONES AND BAMA IN THE OUTER MEMBRANE PROTEIN
BIOGENESIS PATHWAY OF ESCHERICHIA COLI

by
Ashlee Marie Plummer

A dissertation submitted to Johns Hopkins University in conformity with the requirements for
the degree of Doctor of Philosophy

Baltimore, Maryland

June 2017

© 2017 Ashlee Plummer

All Rights Reserved

Abstract

Outer membrane protein (OMP) biogenesis in Gram-negative bacteria is a multi-step, complex process that spans several cellular compartments. OMPs are post-translationally secreted across the bacterial inner membrane and subsequently encounter the aqueous periplasm. In this milieu, nascent OMPs interact with chaperone proteins that prevent the formation of off-folding-pathway species and deleterious aggregates. Here we investigate how two *Escherichia coli* periplasmic chaperones, FkpA and SurA, bind to unfolded OMP clients to facilitate trafficking. We find that FkpA populates both monomeric and dimeric species and these oligomers have differential affinities for unfolded OMP clients. We present the first structural model for a SurA-OMP complex, in which the unfolded OMP is expanded and makes delocalized contacts with the SurA chaperone. Upon reaching the outer membrane, OMPs are assembled via interactions with the *E. coli* β -Barrel Assembly Machinery (BAM) multi-protein complex. We consider the functional mechanism for the OMP component of the BAM complex, BamA, and determine that this enzyme works via a catalytic cycle to facilitate the folding of OMPs with an activity similar to the entire BAM complex. Lastly, we interrogate this pathway in a holistic manner by constructing a computational model to simulate OMP flux through this pathway. Our modeling suggests that together the concentrations of periplasmic chaperones and the kinetic and thermodynamic parameters for chaperone-OMP binding are poised for this system to act as a reservoir for OMP flux towards the OM. Our studies highlight the importance of both chaperone-OMP and BAM-OMP interactions in the accurate and efficient process of OMP biogenesis.

Thesis advisor: Dr. Karen Fleming

Second reader: Dr. Doug Barrick

Thesis committee: Dr. Bertrand Garcia-Moreno, Dr. Jungsan Sohn, & Dr. Vince Hilser

Acknowledgements

First and foremost, I would like to thank my family and friends for their continued encouragement throughout my time at Johns Hopkins University. I am incredibly fortunate to have fantastic parents, Donald and Rosemary, and two amazing sisters, Melissa and Rachel. I also have the best friends, both inside and outside of the Jenkins Biophysics Department, who have always been there for me. I am forever grateful to these folks for their unconditional love and support.

Throughout my career in academic science, I have continually had excellent role models to admire and strive to emulate. From my high school Chemistry class to my lab bench at Hopkins, I have been fortunate to be surrounded by passionate mentors who have blazed the way for my success. I attribute the most profound developments in my career trajectory to Dr. Karen Fleming. Thank you Karen for constantly pushing me to develop the analytical and communication skills required for me to excel as a scientist. And also, thanks for giving me the independence to explore scientific questions in a supportive, creative environment. We make a great, productive team, and I look forward to keeping up with the lab's continual growth and new discoveries. Additionally, I would like to acknowledge the members of my thesis committee at Johns Hopkins University for their assistance and constructive feedback: Dr. Barrick, Dr. Garcia-Moreno, Dr. Sohn, Dr. Hilser, and Dr. Lau. I would particularly like to thank Doug for letting me hang around his lab space, in hopes of securing that ever-elusive rotation spot. Finally, I would like to thank Fleming lab collaborators, Dr. Susan Kreuger and Dr. Harris Bernstein for their continued encouragement and guidance throughout several years of collaborations.

Five years in any laboratory would be daunting without the everyday support of lab mates. I would like to thank past members of the Fleming lab for welcoming me with open arms. I especially would like to recognize the current Fleming lab members – Henry Lessen and

Dagan Marx for working with me to create a fun lab environment over countless hours in lab and many bar tabs. Henry, thanks for laughing at my very best jokes and acknowledging all the others. Dagan, thanks for being a great running buddy and good listener. I am excited to see how your thesis work and subsequent careers turn out – I know you will achieve great things. Thanks to Dr. Patrick Fleming for guidance in all computational aspects of the work presented here and for also keeping me up-to-date on the happenings of Florida. Also, I would like to acknowledge the two “wonder-grads” with whom I worked during my time at Hopkins: Quenton Bubb and Shawn Costello. These two taught me how to be a patient mentor, and I would like to point out their invaluable contributions to Chapters 2 and 5, respectively.

According to an old proverb, “it takes a village to raise a child.” I believe this also applies to adults – particularly those writing dissertations. My Baltimore and Hopkins village have helped me at every step along the way towards finishing the work presented here. And for that, I express my deepest gratitude.

List of Abbreviations

Acr: *Escherichia coli* Acridine resistance multi-protein complex

AUC: Analytical ultracentrifugation

BAM: β -barrel assembly machinery complex

BamABCDE: BAM proteins A, B, C, D, E respectively

CD: Circular Dichroism

CN: Copy number

COM: Center of mass

DegP: *Escherichia coli* periplasmic endoprotease protein

DiC₁₀: didecanoyl-*sn*-glycero lipids

FkpA: *Escherichia coli* FkpB binding protein A

fOMP: Folded outer membrane protein

GF: Gel-filtration

HSP: Heat shock protein

IM: Inner membrane

LUV: Large unilamellar vesicle

MD: Molecular dynamics

MP: Membrane protein

NMR: Nuclear magnetic resonance

OM: Outer membrane

OMP: Outer membrane protein

OmpBioM: Outer membrane protein biogenesis model

PC: Phosphatidyl choline lipid head group

PE: Phosphatidyl ethanolamine lipid head group

PG: Phosphatidyl glycerol lipid head group

POTRA: Polypeptide-transport associated motif

PPIase: Peptidyl-prolyl isomerase

RMSD: Root-mean squared distance

R_G: Radius of Gyration

SANS: Small-angle neutron scattering

SASA: Solvent accessible surface area

SE: Sedimentation equilibrium

σ^E : Sigma-E stress response

SecYEG: *Escherichia coli* Sec-translocase proteins Y, E, and G

Skp: *Escherichia coli* Seventeen kilodalton protein

SurA: *Escherichia coli* survival factor protein A

SV: Sedimentation velocity

TAMD: Torsion angle molecular dynamics

TM: Transmembrane

uOMP: Unfolded outer membrane protein

WT: Wild type

Table of Contents

| | |
|---|-------------|
| List of Tables | xii |
| List of Figures | xiii |
| Chapter 1 – Introduction to the Biogenesis Pathway of Outer Membrane Proteins in <i>Escherichia coli</i> | 1 |
| 1.1 Overview of the membrane system of Gram-negative bacteria..... | 2 |
| <i>Gram-negative bacteria are surrounded by a double membrane system.</i> | 2 |
| <i>OMP's have similar topologies yet distinct functions.</i> | 3 |
| 1.2. The role of chaperones in outer membrane protein biogenesis..... | 5 |
| <i>Chaperones are critical to the maintenance of the membrane proteome.</i> | 5 |
| <i>Redundancy in the chaperone network provides built-in stress response mechanism.</i> | 6 |
| <i>Periplasmic chaperones bind to unfolded OMP ensembles.</i> | 7 |
| <i>Skp and DegP form cavities to accommodate and safeguard uOMP's.</i> | 8 |
| <i>It is currently unknown how SurA and FkpA interact with uOMP's.</i> | 9 |
| <i>SurA, FkpA, and DegP are bifunctional enzymes.</i> | 10 |
| <i>The relevant oligomerization states of the periplasmic chaperones are unknown.</i> | 11 |
| <i>Chaperones bind uOMP's with different rates and affinities.</i> | 12 |
| <i>Many unanswered questions remain about the roles of periplasmic chaperones.</i> | 13 |
| 1.3. The role of the BAM complex in OMP biogenesis | 15 |
| <i>The OM-localized BAM complex facilitates uOMP assembly into the OM.</i> | 15 |
| <i>Recently published structures of the BAM complex highlight novel features of BamA.</i> | 16 |
| <i>The BamA POTRA domain mediates BamA contacts with BAM lipoproteins.</i> | 17 |
| <i>How do the BamA POTRA motifs interact with uOMP's?</i> | 18 |
| <i>OMP's spontaneously insert into bilayers in vitro.</i> | 19 |
| <i>BamA accelerates OMP folding in vitro.</i> | 20 |
| <i>Unanswered questions abound on BAM complex function.</i> | 21 |

| | |
|---|-----------|
| 1.4. A holistic understanding of OMP partitioning through the biogenesis pathway is lacking. | 22 |
| | 22 |
| <i>Thermodynamic partitioning may drive OMPs towards their folded state.</i> | 22 |
| <i>The E. coli OMP biogenesis system is an ideal network for computational modeling.</i> | 22 |
| <i>Outstanding questions on the OMP biogenesis pathway.</i> | 23 |
| 1.5. Outline of the data presented here. | 25 |
| Chapter 2 – Chaperone FkpA Populates Oligomers that Exhibit Distinct Functions | 32 |
| 2.1. Introduction..... | 33 |
| <i>Periplasmic chaperone network assists OMP trafficking in Gram-negative bacteria.</i> | 33 |
| <i>FkpA functions as a chaperone, prolyl-isomerase, and is a heat-shock protein.</i> | 34 |
| 2.2. Methods | 37 |
| 2.3. Results | 41 |
| <i>FkpA populates both monomeric and dimeric states at physiological concentrations.</i> | 41 |
| <i>Monomeric FkpA binds uOMP with an affinity 1000 fold weaker than dimeric FkpA.</i> | 42 |
| 2.4. Discussion..... | 45 |
| <i>SE findings highlight the importance of the FkpA dimerization equilibrium.</i> | 45 |
| <i>FkpA monomer and dimer species exhibit distinct functions.</i> | 46 |
| <i>Moving forward: HSP upregulation as a control mechanism for distinct oligomer functions.</i> | 47 |
| 2.5. Figures | 48 |
| 2.6. Tables..... | 57 |
| Chapter 3 – Novel Binding Mechanism for the Chaperone SurA and unfolded OMPs .. | 60 |
| 3.1. Introduction..... | 61 |
| <i>Biochemical characterization of SurA suggests this chaperone is specific for uOMPs.</i> | 62 |
| <i>Crystallographic studies of SurA hint at mechanisms for uOMP chaperone function.</i> | 62 |
| 3.2. Methods | 64 |

| | |
|--|-----|
| <i>Determination of proline content and cis/ trans isomer classification.</i> | 64 |
| <i>SurA protein was expressed and purified for analysis.</i> | 64 |
| <i>SE analysis was utilized to investigate SurA oligomerization.</i> | 65 |
| <i>SANS analysis provides global structural information of macromolecules in solution.</i> | 66 |
| <i>Biochemical crosslinking was used to map the interaction interface between SurA and OMP clients.</i> | 69 |
| <i>SANS was used to interrogate a SurA-uOMP complex.</i> | 71 |
| <i>Experimental R_G values were integrated into a SurA-OMP complex model.</i> | 72 |
| <i>SurA-OMP binding was quantitated by sedimentation velocity experiments.</i> | 73 |
| 3.3. Results | 76 |
| <i>SurA is monomeric at physiological concentrations.</i> | 76 |
| <i>SurA monomer has solution properties similar to crystallized conformation.</i> | 77 |
| <i>SurA interacts with uOMP clients with a delocalized interface.</i> | 77 |
| <i>uOMP exists in an expanded conformation when in complex with SurA.</i> | 78 |
| <i>Constrained MD simulations yield SurA-uOMP complex structures consistent with experimental results.</i> | 80 |
| <i>SurA binds to uOMP client with a K_D in the micromolar range.</i> | 81 |
| 3.4. Discussion | 83 |
| <i>SurA is a dedicated chaperone for uOMP biogenesis.</i> | 83 |
| <i>SurA exhibits unique oligomerization properties and uOMP binding mechanism.</i> | 84 |
| <i>Structural model of SurA-uOMP complex suggests how SurA may facilitate uOMP folding in coordination with the BAM complex.</i> | 85 |
| <i>Moving Forward: Expanding our understanding of how SurA accommodates uOMPs.</i> | 86 |
| 3.5. Figures | 87 |
| 3.6. Tables | 103 |
| Chapter 4 – BamA Alone Accelerates OMP Folding <i>in vitro</i> through a Catalytic Mechanism | 110 |
| 4.1. Introduction | 111 |

| | |
|--|------------|
| <i>Recently solved crystal structures reveal that the BamA β-barrel has a unique seam.</i> | 111 |
| <i>How do the soluble POTRA motifs contribute to BamA function?</i> | 113 |
| <i>In vitro folding studies complement structural investigations of BamA function.</i> | 114 |
| 4.2. Methods | 115 |
| 4.3. Results | 118 |
| <i>BamA acts as an enzyme to accelerate uOMP folding in vitro.</i> | 118 |
| <i>BamA accelerates uOMP folding through a catalytic mechanism.</i> | 119 |
| 4.4. Discussion | 122 |
| <i>BamA function involves two substrates: uOMPs and lipids.</i> | 122 |
| <i>In vitro studies offer insight into function of BAM lipoproteins.</i> | 123 |
| <i>Moving Forward: Mechanistic insight into BamA-catalyzed OMP folding.</i> | 124 |
| 4.5. Figures | 125 |
| 4.6. Tables | 137 |
| Chapter 5 – Dynamic Periplasmic Chaperone Reservoir Facilitates Biogenesis of Outer Membrane Proteins | 138 |
| 5.2. Methods | 142 |
| <i>OMPBioM Treatment: uOMP Synthesis.</i> | 142 |
| <i>OMPBioM Treatment: Chaperone Synthesis and Oligomerization.</i> | 143 |
| <i>OMPBioM Treatment: Chaperone Binding of uOMP.</i> | 144 |
| <i>OMPBioM Treatment: OMP Folding.</i> | 144 |
| <i>OMPBioM Treatment: uOMP Aggregation, Degradation and Dilution.</i> | 146 |
| <i>Kinetic Simulations.</i> | 146 |
| <i>Calculation of uOMP Periplasmic Lifetimes.</i> | 148 |
| <i>Model Assumptions.</i> | 149 |
| 5.3. Results | 150 |
| <i>OmpBioM reproduces experimentally observed folded OMP levels and lifetimes.</i> | 150 |

| | |
|---|-----|
| <i>Single chaperone null mutant phenotypes reveal the importance of SurA activity and σ^E response.</i> | 150 |
| <i>Simulations of double null chaperone strains suggest distinct roles for Skp and DegP.</i> | 152 |
| <i>DegP functions primarily as a protease and is under kinetic control.</i> | 154 |
| <i>Skp-uOMP complexes are highly populated and display dynamic behavior.</i> | 155 |
| <i>The folding rate enhancement provided by SurA is necessary but modest.</i> | 155 |
| <i>The estimated effective rate of uOMP folding by BAM is faster than in vitro observations.</i> | 156 |
| 5.4. Discussion | 159 |
| <i>Chaperones are dynamic uOMP periplasmic reservoirs.</i> | 159 |
| <i>A strictly ordered set of reactions is not required to accurately represent OMP biogenesis.</i> | 160 |
| <i>Skp and DegP may not form a productive parallel folding pathway.</i> | 161 |
| <i>Kinetic partitioning prevents uOMP aggregation and degradation under WT conditions.</i> | 162 |
| <i>Periplasmic conditions provide simple solutions to challenges faced by OMP biogenesis.</i> | 163 |
| 5.5. Figures | 165 |
| 5.6. Tables | 180 |
| Concluding Remarks | 202 |
| <i>FkpA populates monomeric and dimeric species, which exhibit distinct functions.</i> | 204 |
| <i>Proposed model of SurA-uOMP complex raises exciting prospects.</i> | 205 |
| <i>In vitro analysis of BamA function complement structural studies.</i> | 207 |
| <i>OMPBioM is the first computational model of OMP biogenesis.</i> | 208 |
| References | 211 |
| Curriculum Vitae | 235 |

List of Tables

| | |
|--|------------|
| Chapter 2 – Chaperone FkpA Populates Oligomers that Exhibit Distinct Functions | 32 |
| Table 2.1. Summary of fitting for SE data on FkpA dimerization (20 mM Tris). | 57 |
| Table 2.2. Summary of fitting for SE data on FkpA dimerization (20 mM Tris, 1 M urea). | 58 |
| Table 2.3. Primers for FkpA-G28K cloning. | 59 |
| Chapter 3 – Novel Binding Mechanism for the Chaperone SurA and unfolded OMPs .. | 60 |
| Table 3.1. Summary of number of prolines in abundant OMPs and periplasmic proteins. | 103 |
| Table 3.2. Percentage of proline content in abundant OMPs and periplasmic proteins. | 104 |
| Table 3.3. Scattering lengths of common atoms. | 105 |
| Table 3.4. Summary of SANS experiments and Guinier fitting parameters. | 106 |
| Table 3.5. Primers used for cloning SurA- Δ AF variants. | 107 |
| Table 3.6. Primers used for cloning SurA ^{-4W} | 109 |
| Chapter 4 – BamA Alone Accelerates OMP Folding <i>in vitro</i> through a Catalytic Mechanism | 110 |
| Table 4.1. Summary of BamA-catalyzed folded OmpA concentrations | 137 |
| Chapter 5 – Dynamic Periplasmic Chaperone Reservoir Facilitates Biogenesis of Outer Membrane Proteins | 138 |
| Table 5.1. Summary of reactions and WT rate constants within the model. | 180 |
| Table 5.2. Ordinary Differential Equations for each species within the model. | 192 |
| Table 5.3. Chaperone concentrations determined by proteomics studies. | 195 |
| Table 5.4. Rate constant values implemented in the σ^E response. | 196 |
| Table 5.5. Enumeration of binding events and lifetimes from stochastic simulations. | 199 |
| Table 5.6. Tabular form of Figure 5.3. | 201 |

List of Figures

| | |
|---|-----------|
| Chapter 1 – Introduction to the Biogenesis Pathway of Outer Membrane Proteins in <i>Escherichia coli</i> | 1 |
| Figure 1.1. The <i>E. coli</i> Outer Membrane Protein Trafficking Network. | 28 |
| Figure 1.2. Structures and biological activities of representative β -barrel OMPs. | 29 |
| Figure 1.3. Structural model showing uOMP encapsulated by Skp. | 30 |
| Figure 1.4. BamBCDE lipoproteins contact BamA periplasmic POTRA motifs. | 31 |
| Chapter 2 – Chaperone FkpA Populates Oligomers that Exhibit Distinct Functions | 32 |
| Figure 2.1. Crystal structure of FkpA. | 48 |
| Figure 2.2. Representative fits for FkpA sedimentation equilibrium data. | 49 |
| Figure 2.3. Species plot and van't Hoff analysis of FkpA dimerization reaction. | 50 |
| Figure 2.4. Characterization of FkpA-G28K variant. | 51 |
| Figure 2.5. Sedimentation velocity data suggests FkpA dimer binds to uOMPs 1000-fold stronger than FkpA monomer. | 52 |
| Figure 2.6. Simulations suggest FkpA dimer and monomer bind to uOMP with μM and mM K_D values, respectively. | 54 |
| Figure 2.7. Thermodynamic cycle to summarize the new model for FkpA dimerization and uOMP binding reactions. | 55 |
| Chapter 3 – Novel Binding Mechanism for the Chaperone SurA and unfolded OMPs .. | 60 |
| Figure 3.1. Analysis of Proline content for abundant periplasmic proteins and OMPs. | 87 |
| Figure 3.2. SE analysis of SurA at varying concentrations. | 88 |
| Figure 3.3. SANS data and structural model for apo-SurA. | 90 |
| Figure 3.4. Summary of the SurA sequence and sites of all mutations. | 91 |
| Figure 3.5. <i>pAF</i> structure and representative SDS-PAGE gel of crosslinking reaction. | 92 |

| | |
|--|------------|
| Figure 3.6. Summary of crosslinking efficiencies for SurA- <i>p</i> AF variants and uOMPs..... | 93 |
| Figure 3.7. Map of SurA _{<i>p</i>AF} -uOmpA ₁₇₁ crosslinking results. | 94 |
| Figure 3.8. Scatter length density and contribution to total scattering calculations for protonated SurA and deuterated uOmpA ₁₇₁ | 95 |
| Figure 3.9. Summary of SANS datasets and fitting for SurA-uOmpA ₁₇₁ complex. | 97 |
| Figure 3.10. MD analysis and SANS calculations for SurA-uOmpA ₁₇₁ complex model. | 98 |
| Figure 3.11. SV data for SurA ^{-4W} and uOmpA ₁₇₁ mixtures and controls..... | 99 |
| Figure 3.12. Simulation of SV data for SurA ^{-4W} and uOmpA ₁₇₁ as a function of K_D | 100 |
| Figure 3.13. Summary of structures of chaperone bound uOMP complexes..... | 101 |
| Figure 3.14. Mechanistic insight into SurA-uOMP interactions with the BAM complex..... | 102 |
| Chapter 4 – BamA Alone Accelerates OMP Folding <i>in vitro</i> through a Catalytic Mechanism | 110 |
| Figure 4.1. Crystallographic studies suggest BamA β -barrel contains two domains and has unique seam. | 125 |
| Figure 4.2. Established protocols for intrinsic and BamA-mediated OMP folding <i>in vitro</i> | 127 |
| Figure 4.3. Unfolded and folded OMP species are distinguished by their distinct migration via SDS-PAGE..... | 129 |
| Figure 4.4. BamA functions as an enzyme to accelerate OMP folding into LUVs..... | 131 |
| Figure 4.5. Under modified setup, OmpA folds in the presence of prefolded BamA than OmpX..... | 132 |
| Figure 4.6. Kinetic trace of OmpA folding in the presence of BamA and OmpX..... | 133 |
| Figure 4.7. Concentration of OmpA folded by BamA exceeds the concentration of folded BamA. | 134 |
| Figure 4.8. Linear range for concentration determination of OmpA by SDS-PAGE..... | 135 |

| | |
|--|------------|
| Figure 4.9. The BamA β -barrel may create defects in neighboring bilayer..... | 136 |
| Chapter 5 – Dynamic Periplasmic Chaperone Reservoir Facilitates Biogenesis of Outer Membrane Proteins | 138 |
| Figure 5.1. Diagram of mechanistic treatment used in OMPBioM. | 165 |
| Figure 5.2. Phenotype construction in OMPBioM..... | 166 |
| Figure 5.3. Simulated phenotypes in OMPBioM. | 168 |
| Figure 5.4. Summary of simulations to investigate folding rate enhancement provided by SurA..... | 169 |
| Figure 5.5. Representative steady state simulation..... | 170 |
| Figure 5.6. Lifetime measurements by stochastic and deterministic modeling methods..... | 171 |
| Figure 5.7. OMP populations for simulations with varying σ^E treatments..... | 172 |
| Figure 5.8. Change in [uOMP] + [Agg] for various phenotypes treatments. | 173 |
| Figure 5.9. Fraction of degraded OMP for phenotype simulations. | 174 |
| Figure 5.10. Concentrations of free and bound chaperone species in WT simulations. | 175 |
| Figure 5.11. Summary of simulations to determine SurA rate-enhancement for OMP folding. | 176 |
| Figure 5.12. Assessment of <i>in vivo</i> BAM folding rates..... | 177 |
| Figure 5.13. Summary of stochastic simulations of uOMP flux..... | 178 |
| Figure 5.14. Summary of phenotypes with hypothetical folding mechanism..... | 179 |

Chapter 1 – Introduction to the Biogenesis Pathway of Outer Membrane

Proteins in *Escherichia coli*

Excerpts published as: Plummer, A. M., Fleming, K.G., (2016) Trends in Biochemical Sciences,

41(10): 872-882.

1.1 Overview of the membrane system of Gram-negative bacteria

Annually 2 million people acquire antibiotic resistant infections in the United States. Of those infected 23,000 die each year. The most severe threats identified by the U.S. Center for Disease Control include antibiotic resistant forms of *Escherichia coli* and *Neisseria gonorrhoeae* (CDC 2013). For both of these Gram-negative bacteria, it has been particularly challenging to deduce how antibiotic molecules permeate the barrier presented by the bacterial membrane system (Brown and Wright 2016). Understanding the mechanisms by which antibiotics enter Gram-negative bacteria and how these cells subsequently acquire resistance are therefore pressing biomedical issues. Studies to elucidate these pathways are prerequisite to efficiently targeting these bacteria by therapeutic treatments.

Gram-negative bacteria are surrounded by a double membrane system.

Two membranes surround the bacterium cells of *E. coli* and *N. gonorrhoeae*, and drugs must traverse both to enter the cytoplasm (Figure 1.1). The innermost membrane is termed the inner membrane (IM), while the outermost one is termed the outer membrane (OM). Both membranes are lipid bilayer structures with a hydrophobic interior containing lipid acyl chains and more hydrated interfacial regions composed of lipid head groups. With regard to lipid composition, the inner membrane is composed of a symmetric phospholipid bilayer. The outer membrane is asymmetric in that the inner leaflet is made of phospholipids and the outer leaflet contains lipopolysaccharide.

In addition to lipids, both the bacterial IM and OM contain membrane proteins (MPs). These two membranes contain distinct classes of MPs. The IM and OM primarily contain α -helical and β -barrel MPs, respectively. Because these two classes of MPs reside in separate cellular membranes, they proceed through different biogenesis pathways. Briefly, α -helical IM

proteins are co-translationally inserted into the IM by the SecYEG translocase (Dalbey, Wang, and Kuhn 2011). However, β -barrel OM Proteins (OMPs) must bypass the IM in order to reach the OM, therefore they utilize a more complex assembly pathway. OMPs are translated with an N-terminal export sequence that signals for their export from the bacterial cytoplasm; therefore OMPs are post-translationally secreted across the IM through the SecYEG translocase (Ruiz, Kahne, and Silhavy 2006). As shown in Figure 1.1, an aqueous compartment termed the periplasm separates the bacterial IM and OM. This space contains soluble periplasmic proteins and peptidoglycan, which is a polymer of sugars and amino acids that forms a mesh in the periplasm and provides mechanical strength to the cell (Vollmer and Bertsche 2008). Little work on the interactions of peptidoglycan with periplasmic proteins has been published; therefore it is excluded from Figure 1.1 and further discussions. OMPs must traverse the bacterial IM and the periplasm to arrive at their native location – the OM. The accurate biogenesis and trafficking of both MP classes is a prerequisite to the formation of a functional membrane system and subsequent healthy bacterium.

OMPs have similar topologies yet distinct functions.

OMPs typically exhibit a β -barrel topology composed of a closed cylinder of antiparallel β -strands. The β -strands of OMPs contain an alternating pattern of hydrophobic and hydrophilic residues; because of this geometry, the inside and outside of these β -barrel proteins possess hydrophilic and hydrophobic character, respectively (Fairman, Noinaj, and Buchanan 2011). This yields a tertiary structure in which the interior of an OMP β -barrel is water-accessible, while the exterior is lipid-exposed. Adjacent β -strands interact through hydrogen bonding and are covalently connected by short periplasmic turns and longer extracellular loops.

Although OMPs have canonical secondary and tertiary structures, various OMPs exhibit a breadth of biologically relevant functions. Figure 1.2 illustrates this point by showing several *E. coli* OMPs with similar topologies yet unique functions. Three 8 stranded β -barrel OMPs are shown with their associated functions: PagP exhibits palmitoyltransferase activity (Bishop 2005); OmpX has been implicated in bacterial virulence (Vogt and Schulz 1999); OmpA plays a role in cell-cell adhesion (Ortiz-Suarez et al. 2016). Each of these OMPs is composed of a transmembrane (TM) β -barrel domain, yet OmpA additionally contains a soluble, periplasmic domain that is required for *in vivo* function. OMPs also exhibit different numbers of β -strands and can range in size from 8 β -strands to 26 β -strands. Figure 1.2 includes several larger OMPs, such as OmpT (protease with 10 β -strands), OmpLA (phospholipase with 12 β -strands), and BamA (OMP-folding enzyme with 16 β -strands). Each of these OMPs contains a β -barrel domain, yet exhibits distinctive functional properties.

1.2. The role of chaperones in outer membrane protein biogenesis

Chaperones are critical to the maintenance of the membrane proteome.

Each unique OMP shown in Figure 1.2 utilizes the same OMP trafficking pathway in *E. coli* to traverse the periplasm. Biogenesis of OMPs is known to involve several periplasmic chaperone proteins that associate with OMPs en route to the OM. Through genetic experiments each of these chaperones has been implicated in functioning in this trafficking. These experiments suggest that when these chaperones are removed from the bacterial genome individually or in pairs, the integrity of the OM is compromised to varying extents (Arié, Sassoon, and Betton 2001; Sklar, Wu, Kahne, et al. 2007). Chaperones identified through these types of experiments are: Seventeen Kilodalton protein (Skp) (Schäfer, Beck, and Müller 1999), Survival protein A (SurA) (Tormo, Almirón, and Kolter 1990), FkpB binding protein A (FkpA) (Ge, Lyu, et al. 2014), and the protease DegP (Ge, Wang, et al. 2014a; Lipinska, Zylicz, and Georgopoulos 1990). SurA was identified as a particularly important chaperone through experiments of this nature, as removing SurA from the *E. coli* genome (i.e., Δ_{surA}) results in cells with compromised membrane systems as evidenced by sensitivity to detergents and antibiotics (Lazar et al. 1998; Lazar and Kolter 1996). Single deletions of Skp (Δ_{skp}), DegP (Δ_{degP}), or FkpA (Δ_{fkpA}) have little effect on the integrity of the OM (Justice et al. 2005; Sklar, Wu, Kahne, et al. 2007).

One may ask, why have *E. coli* evolved four seemingly redundant chaperones to manage the OMP biogenesis pathway? To address this question, Rizzitello *et al.* systematically depleted Skp, SurA, and DegP from the *E. coli* genome and assessed the phenotypes associated with these genotypes (Rizzitello, Harper, and Silhavy 2001). Here the authors constructed bacterial strains with depletions (δ) or deletions (Δ) of the chaperone genes of interest in pairs. The authors

present the first evidence that depletion/deletion combinations of either SurA and Skp (i.e., $\delta_{surA}\Delta_{skp}$) or SurA and DegP (i.e., $\delta_{surA}\Delta_{degP}$) are lethal. Interestingly, the strain with a $\delta_{degP}\Delta_{skp}$ genotype exhibits no observable growth defects. These results lead to the realization that each of these proteins is likely redundant in possessing chaperone function, yet two distinct pathways for OMP biogenesis may exist: one involving both DegP and Skp, and SurA is involved in a separate “parallel pathway.”

Redundancy in the chaperone network provides built-in stress response mechanism.

As mentioned above, Δ_{surA} bacterial cells have compromised membrane systems that leads to observable phenotypes (Lazar et al. 1998; Lazar and Kolter 1996). Under such conditions, *E. coli* are known to induce transcriptional stress responses, such as the sigma-E (σ^E) response (Danese and Silhavy 1997; De Las Peñas, Connolly, and Gross 1997; Onufryk et al. 2005). This response involves the modulation of transcription of many genes, including the upregulation of the periplasmic chaperones and down-regulation of OMPs themselves (Dartigalongue, Missiakas, and Raina 2001). The observation that the Δ_{surA} genotype induces the σ^E response begs the question – what is it about the loss of SurA that signals a stress response? It has been proposed that the accumulation of unfolded OMP species in the periplasm signal the induction of the σ^E response; the loss of SurA must allow the unfolded OMP population to surpass the threshold level for bacterial stress induction (Lazar and Kolter 1996; Sklar, Wu, Kahne, et al. 2007; Ureta et al. 2007).

OMP biogenesis has been suggested to proceed through varying routes that consist of distinct chaperones, termed “parallel pathways” (Ureta et al. 2007). This type of trafficking allows alternate avenues for OMPs to reach the OM under stress conditions, such as the genetic knockout of SurA and subsequent σ^E induction. Indeed, it was found that under these

conditions, OMPs are able to achieve their native conformations through interacting with Skp/DegP, albeit on a slower timescale than in the presence of SurA (Ureta et al. 2007). Furthermore, parallel pathways allows for differential flux through the various routes for OMP clients that preferentially interact with one chaperone over another (Chen and Henning 1996; Ureta et al. 2007; Vertommen et al. 2009).

Overall, genetics studies have identified which periplasmic proteins are involved in OMP assembly, along with the associated phenotypes for their removal from *E. coli*. However, interpreting results from experiments of this nature is complex – phenotypes may arise for many reasons. For instance, the interpretation of a lethal phenotype is impossible. For more detailed insight into the functions of the periplasmic proteins SurA, Skp, FkpA, and DegP, we turn to *in vitro* biochemical and structural studies.

Periplasmic chaperones bind to unfolded OMP ensembles.

To explain the changes in OM integrity upon the loss of SurA or pairs of other chaperones, it was suggested that each of these proteins works as a chaperone in the periplasm for the trafficking of unfolded OMPs to the OM (Lazar and Kolter 1996; Rizzitello, Harper, and Silhavy 2001; Schäfer, Beck, and Müller 1999). This implies that each periplasmic protein (i.e., SurA, Skp, FkpA, and DegP) interacts with OMPs in the periplasm – indeed, reported phenotypes include a decrease in the amount of certain OMPs in the OM in $\Delta surA$ (Sklar, Wu, Kahne, et al. 2007). Understanding this association between chaperones and OMPs involves identifying the conformation of each protein involved. This raises the question: what conformation of OMP is bound by these chaperones? In the periplasm, OMPs remain unfolded (i.e., uOMPs) until they reach the asymmetric outer membrane into which they fold (Figure 1.1). Because uOMPs require a lipid bilayer to fold into their native conformation, they must traverse the 165 Å aqueous periplasm in this unfolded, yet folding-competent state (Murakami et al.

2002). Herein lies a dilemma: uOMPs are prone to aggregate in aqueous environments (Danoff and Fleming 2015a; Ebie Tan et al. 2010). The thermodynamically favorable, yet kinetically slow process of uOMP aggregation directly competes with the productive folding pathway of uOMPs. This potential dead-end fate for an unfolded OMP is avoided *in vivo* by the association of uOMPs with periplasmic chaperones.

The mechanism of chaperone activity and subsequent prevention of uOMP aggregation in the periplasm is complicated by the fact that the periplasm lacks ATP (Wülfing and Plückthun 1994). Therefore, periplasmic chaperones must prevent uOMP aggregation and its associated cell stress (i.e., σ^E) in the absence of an external energy source. To accomplish this important cellular feat, the thermodynamics and kinetics of chaperone-uOMP interactions must be fine-tuned to maintain uOMP proteostasis in the absence of ATP (Fleming 2015; Ge, Lyu, et al. 2014; Moon et al. 2013; Wu et al. 2011).

Skp and DegP form cavities to accommodate and safeguard uOMPs.

The periplasmic chaperones mentioned above have been expressed and purified for *in vitro* investigation by several research groups. Crystallographic structures of each chaperone have been solved and are presented in Figure 1.1 (Bitto and McKay 2002; Krojer, Sawa, et al. 2008; Saul et al. 2004; Walton and Sousa 2004). Additionally, structural characterization and modeling of chaperone-uOMP complexes have revealed various mechanisms that chaperones utilize to protect uOMPs from aggregation: one such mechanism periplasmic chaperones employ to prevent subsequent aggregation is to protect uOMPs by sequestering them within a defined internal uOMP-cavity. Skp and DegP are both oligomeric chaperones with defined internal binding cavities that accommodate uOMPs (Figure 1.1) (Krojer, Sawa, et al. 2008; Strauch, Johnson, and Beckwith 1989; Walton and Sousa 2004). Most structural studies have focused on uOMP-Skp interactions (Moon et al. 2013; Wu et al. 2011). In the apo (i.e., uOMP free) state,

three α -helical Skp polypeptide chains associate to form a trimer with an internal cavity (Sandlin, Zaccai, and Fleming 2015; Walton et al. 2009). Nuclear Magnetic Resonance (NMR) analyses suggest that the uOMP inside of Skp is highly dynamic, makes many weak local interactions with the chaperone, and populates a “fluid globule” conformational ensemble (Burmam, Wang, and Hiller 2013).

Small-angle Neutron Scattering (SANS) experiments have subsequently demonstrated that the α -helical arms of Skp are flexible to accommodate the unstructured uOMP (Zaccai et al. 2015). Structural modeling of the uOMP bound to Skp revealed that the uOMP (i.e., OmpW) is not entirely encapsulated but protrudes from the Skp cavity (Figure 1.3). Also, modeling of Skp bound to OmpA, which contains a folded soluble domain (Figure 1.2), suggests this uOMP client binds to Skp as an ensemble with the soluble OMP domain in a variety of orientations outside of the Skp trimer. Overall, it seems that both the bound uOMP and Skp exist in multiple conformations in the complex, all of which shield the uOMP from the aqueous periplasm and prevent deleterious uOMP aggregation. This type of uOMP capturing mechanism has also been observed for the periplasmic chaperone/protease DegP, which binds uOMPs in an internal cavity as evidenced by cryo-electron microscopy (Krojer, Sawa, et al. 2008).

It is currently unknown how SurA and FkpA interact with uOMPs.

The second mechanism for safeguarding uOMPs from aggregation involves chaperones that are not known to form defined cages. The periplasmic proteins SurA and FkpA both lack internal cavities but are still known to bind uOMPs (Figure 1.1) (Arié, Sassoon, and Betton 2001; Bitto and McKay 2002; Rouviere and Gross 1996; Saul et al. 2004). It is unclear how these chaperones bind to uOMP clients to prevent their aggregation. Recent studies have suggested that both SurA and FkpA may exist in a variety of conformations that play a role in uOMP

binding. Crosslinking and genetic experiments suggest that SurA may explore several conformations and these structural changes mediate SurA activity by modulating populations of “open” and “closed” SurA states (Soltes et al. 2016). Flexibility in one of the N-terminal α -helices of FkpA may allow this chaperone to exist in many uOMP-binding conformations (Hu, Galius, and Pervushin 2006). Structural information on these complexes would prove immensely valuable in understanding how these chaperones safeguard uOMPs via a mechanism distinct from that of Skp/DegP.

SurA, FkpA, and DegP are bifunctional enzymes.

A complicating feature to the periplasmic trafficking of OMPs is that several chaperones involved in this pathway are multi-functional. It has been reported that all cellular compartments contain peptidyl-prolyl cis-trans isomerase enzymes (PPIases) and the periplasm is no exception. *Cis-trans* isomerization of the peptide backbone is required for folding of some proteins and is often the rate-limiting step for this process; PPIase enzymes catalyze the conversion between these two states to facilitate protein folding (for a review, see Gothel and Marahiel, 1999). The periplasm contains four proteins with PPIase activity: FkpA, PpiA, PpiD, and SurA (Justice et al. 2005). FkpA falls into the FKBP family of PPIases, while the other three periplasmic PPIases are classified as parvulin type PPIases. The PPIase activity of FkpA and SurA are additional factors for consideration of their activity in the periplasm.

DegP also possesses an enzymatic activity distinct from its role as a chaperone: it is a processive endoprotease of the HtrA family that degrades misfolded proteins (Krojer, Pangerl, et al. 2008; Lipinska, Zylicz, and Georgopoulos 1990). DegP forms higher order oligomers, including hexamers that assemble to catalytically active 12-mer and 24mer states; it has been suggested that the oligomerization state is modulated to accommodate substrates for degradation of varying sizes (Krojer, Sawa, et al. 2008). Although the protease activity of DegP is

biologically important, expression of a protease-deficient variant of DegP (i.e., catalytic Ser-210 mutated to Ala) rescues otherwise lethal phenotypes, highlighting the importance of the DegP chaperone activity (Castillo-Keller and Misra 2003; Misra, Castillo-Keller, and Deng 2000).

While it is established that SurA, FkpA, and DegP are bifunctional, it is currently unknown how these various functions relate to the chaperone activity of SurA, FkpA, and DegP. It could be that clientele pool for PPIase activity for SurA and FkpA overlaps with their preferred OMP binding client pool; the same may be true for DegP protease/chaperone activities. Studies to define the relevant clients of each activity of these chaperones are lacking in the literature. Additionally, it is unknown if these proteins are constitutively active as enzymes and chaperones or if different cellular conditions modulate their activities.

The relevant oligomerization states of the periplasmic chaperones are unknown.

Crystallographic evidence has traditionally been utilized to assign oligomerization states to proteins. As mentioned above, structures of DegP have been solved in a variety of oligomerization states, including hexamers, 12-mers, and 24-mers (Iwanczyk, Leong, and Ortega 2011; Kim, Grant, and Sauer 2011; Kim and Sauer 2012; Krojer, Sawa, et al. 2008; Sassoon, Arié, and Betton 1999; Thompson et al. 2014). Skp has also been reported to form trimers both in the apo- and OMP-bound states (Walton and Sousa 2004; Zaccai et al. 2015). FkpA and SurA were crystalized in dimeric and monomeric conformations, respectively (Bitto and McKay 2002; Saul et al. 2004). One shortcoming of determining oligomerization by structural studies is that the oligomer present in a highly concentrated crystal lattice is not necessarily the one present in more dilute solution conditions. This type of incongruity was recently observed for Skp, as it was observed that the Skp monomer is significantly populated at biologically relevant protein concentrations (Sandlin, Zaccai, and Fleming 2015). This type of rigorous solution investigation

of oligomerization has not been performed for DegP, FkpA, or SurA; therefore, it is not definitively known which oligomeric species are populated *in vivo* for these proteins.

Chaperones bind uOMPs with different rates and affinities.

Previous studies have additionally aimed to differentiate between the periplasmic chaperones based on the kinetics of their interactions with OMP clients. Stopped-flow fluorescence experiments have measured the extent of association of each chaperone with a client OMP by labeling each with a fluorescent dye and quantitating the FRET between the two fluorophores. The half-time for binding (i.e., $t_{1/2}$) for binding of OmpC to FkpA, SurA, Skp, and DegP (S210A) were reported as: 6.6 ± 0.4 ms; 58.5 ± 0.7 ms; 18.8 ± 0.3 ms; and 28.3 ± 0.1 s, respectively (Ge, Lyu, et al. 2014; Wu et al. 2011). Although these values are not rigorously determined rate constants for chaperone-uOMP binding, trends from these data are telling – DegP binds to OmpC three orders of magnitude slower than FkpA, SurA, or Skp under these experimental conditions. These data suggest that different kinetics of binding may allow OMPs to preferentially interact with SurA, Skp, or FkpA over DegP, creating a kinetic partitioning mechanism to sort OMPs away from DegP. However the experimental conditions presented in this study do not allow for the definitive exclusion of OMP aggregation in this set-up; additionally, the oligomeric state of chaperones in these studies cannot be determined from the published protocol.

Equilibrium dissociation constants (K_D) for the binding reactions of OmpC to FkpA, SurA, Skp, and DegP (S210A) have also been reported as follows: 23.2 ± 3.5 nM; 106 ± 84 nM; 15.9 ± 7.2 nM; and 8.6 ± 0.4 nM, respectively (Ge, Lyu, et al. 2014; Wu et al. 2011). These results suggest that SurA associates with this OMP client with the weakest K_D . As with the previously published kinetics experiments, the oligomeric states of chaperones and uOMP in this study cannot be determined from the published protocol. Additionally, control experiments to

ensure these reported measurements were made on a system at equilibrium were not published; these reported K_D values report on the apparent equilibrium constant for this system. Other studies have investigated the thermodynamics of uOMP-chaperone binding reactions as well. The K_D of Skp binding to OmpLA was reported to be 10.8 ± 0.2 nM (Moon et al. 2013) – this K_D is ten times tighter than the Skp-uOmpC affinity (Ge, Lyu, et al. 2014; Wu et al. 2011). SurA also binds weakly to peptides: the K_D of SurA association with aromatic-rich peptides was determined by phage-display assays to be in the μ M range (Bitto and McKay 2003, 2004; Xu et al. 2007). These experiments are non-equilibrium measurements and are therefore not thorough, quantitative descriptions of the SurA-OMP interaction energy. Overall, there are few reported measurements of the association energies for periplasmic chaperones and uOMPs, and certainly no rigorous comparisons between these energies under conditions in which the uOMP is monomeric and the chaperone oligomerization state is known.

Many unanswered questions remain about the roles of periplasmic chaperones.

The *E. coli* periplasmic chaperone network has been studied for decades, yet many questions remain about the specific roles of FkpA, SurA, DegP, and Skp. These chaperones seem redundant but may form parallel pathways for OMP flux to proceed through the periplasm. Preferential bindings of uOMPs to each chaperone will depend on the specific kinetic and thermodynamic parameters for each association. To understand how uOMPs associate with the various periplasmic chaperones, we must first answer several questions: which oligomeric states are functionally relevant for each chaperone? How do these functional states accommodate an unstructured OMP binding partner? How do SurA and FkpA bind to uOMPs without forming an internal cavity? After the formation of chaperone-uOMP complexes, do these chaperones limit the population of OMP misfolded conformations or do they actively

promote the formation of folded OMP? Do these chaperones work together to facilitate the assembly of OMPs or do they function independently?

Key questions regarding the catalytic and chaperone activities of the bifunctional periplasmic proteins also remain unanswered: how do the enzymatic activities of FkpA, SurA, and DegP relate to their chaperone activities? Are the PPIase activities of FkpA and SurA relevant for OMP assembly? That is, does the clientele pool for PPIase and chaperone activity overlap? How is a balance between the DegP protease and chaperone activity maintained to ensure the OMPs are not degraded en route to the OM? We currently do not understand how these bifunctional proteins work as both enzymes and chaperones.

1.3. The role of the BAM complex in OMP biogenesis

The OM-localized BAM complex facilitates uOMP assembly into the OM.

Once OMPs reach the OM, they are assembled in their TM topology with the assistance of the OM-localized β -Barrel Assembly Machinery (BAM) multi-protein complex (BamABCDE). BAM protein A is itself a β -barrel OMP that is evolutionarily conserved from bacteria to eukaryotes and is known to play an essential role in uOMP assembly (Voulhoux, Bos, Geurtsen, Mols and Tommassen 2003). In *E. coli*, four periplasmic lipoproteins associate with BamA, BamBCDE, to form the BAM complex (Malinverni et al. 2006; Onufryk et al. 2005; Sklar, Wu, Gronenberg, et al. 2007; Wu et al. 2005). Each BAM component has been implicated in maintaining OM integrity, but only BamA and BamD are required for cell viability (Malinverni et al. 2006; Werner and Misra 2005). The essentiality of the BAM complex stems from its role in assembling uOMPs into the bacterial OM.

The BAM complex facilitates OMP folding into the OM, which is an asymmetric bilayer composed of a phospholipid inner leaflet and outer leaflet made of lipopolysaccharide. The phospholipids in the inner leaflet have both phosphoethanolamine (PE) and phosphoglycerol (PG) head groups (Kamio and Nikaido 1976; Osborn, Gander, Parisi, Carson 1972). This is consequently similar to the head group composition of the bacterial IM lipids. It has been proposed that the presence of the BAM complex in the OM effectively targets OMPs for insertion into the OM – uOMP folding into the IM would certainly lead to dissipation of the proton gradient essential to sustain cell viability (Gessmann et al. 2014). Therefore OMP client recognition by the BAM complex and accurate assembly of OMPs into the OM is critical to both OM integrity and cell survival.

Recently published structures of the BAM complex highlight novel features of BamA.

In the past 4 years, several structures have been presented for the BAM complex and functional mechanisms have been proposed (Gu et al. 2016; Han et al. 2016; Iadanza et al. 2016; Noinaj et al. 2013). In 2013, the first crystallographic structure of a full-length bacterial BamA homologue was presented (Noinaj et al. 2013). This structural model indicated that BamA is composed of two domains: one TM 16-stranded β -barrel domain and a series of five soluble POlypeptide-TRansport-Associated (POTRA) motifs (Figures 1.1 and 1.4). Each of these structural subunits has unique features that may contribute to the catalytic ability of BamA to accelerate uOMP folding (See Chapter 4). The structure of the BamA β -barrel domain structure revealed a surprising feature: instead of exhibiting a geometry that maximizes the number of hydrogen bonds between the N- and C-terminal β -strands, the crystal structure of the *N. gonorrhoeae* BamA revealed that the N- and C-terminal β -strands of the β -barrel interact with only two hydrogen bonds to close the β -barrel. Also, the C-terminal β -strand is twisted and bends into the β -barrel. This “open” β -barrel conformation has since been observed in crystallographic studies of *E. coli* BamA (Gu et al. 2016). Molecular dynamics (MD) simulations and biochemical analyses have been utilized to suggest that lateral opening or dynamic motion of these BamA seam β -strands may play a pivotal role in the function of BamA (i.e., “lateral gating”) (Noinaj et al. 2014).

Because lipids in the OM surround OMPs, this lateral gating hypothesis for the functional mechanism of BamA seems contradictory to the basic principles of thermodynamics. The BamA β -barrel interior is large enough to accommodate hundreds of water molecules, which would be exposed to hydrophobic lipids as the BamA β -barrel laterally opens. This process should result in a large energetic penalty that must be overcome by another

compensating source of energy. Reconciling these thermodynamic considerations with the available structural information must be accomplished to elucidate the catalytic mechanism of BamA.

The BamA POTRA domain mediates BamA contacts with BAM lipoproteins.

Both *in vitro* and *in vivo* studies have indicated that the presence of the POTRA motifs are required for BamA acceleration of OMP folding and cell viability, respectively (Gessmann et al. 2014; Kim et al. 2007). These POTRA motifs of BamA interact with the BamBCDE lipoproteins, as shown in Figure 1.4. Prior to the solution of the most recent crystallographic structures of the BAM complex, crystal structures of individual POTRA motifs fused to BAM lipoproteins revealed that BamB and BamD interact with POTRA motifs 3 and 5, respectively (Bergal et al. 2015; Jansen, Baker, and Sousa 2015). The recently solved crystal structures of BamACDE and the entire BAM complex suggest that the most extensive contacts between BamA and the BAM lipoproteins occurs between BamA POTRA 5 and BamD (Bakelar, Buchanon, and Noinaj 2016; Gu et al. 2016; Han et al. 2016). This interaction between BamA and BamD may be functionally important, because outcompeting this interaction with a BamD-derived peptide inhibits BAM complex formation (Hagan, Wzorek, and Kahne 2015).

One possible conformation of the BamA POTRA domain was elucidated in recent crystallographic studies of BamACDE and the BAM complex where it was observed that the BamA POTRA motifs encircle the periplasmic face of the BamA β -barrel and were suggested to create a funnel to direct the uOMP client to the β -barrel of BamA (Figure 1.4) (Bakelar, Buchanon, and Noinaj 2016; Gu et al. 2016; Han et al. 2016). However, the observed conformation of POTRA 5 is inconsistent with this hypothesis. POTRA 5 occludes the β -barrel of BamA from the periplasm, and the ~ 15 Å opening at the periplasmic face of the BamA β -

barrel is too small to accommodate a uOMP client (Bakelar, Buchanon, and Noinaj 2016). Additionally, it is difficult to exclude the idea that the compactness of the POTRA domain in the crystal structure may result from crystal contacts between neighboring BAM proteins. Indeed, MD of BamABCDE suggests the BamA POTRA motifs sample a variety of less compact states (Gu et al. 2016). Although the reported conformation of the POTRA domain may have implications for the function of the BAM complex, structural studies that are non-crystallographic in nature will be required to further understand the role of the POTRA domain and BAM lipoproteins in modulating the conformational states of BamA.

How do the BamA POTRA motifs interact with uOMPs?

The POTRA motifs of BamA exhibit a conserved $\beta 1-\alpha 1-\alpha 2-\beta 2-\beta 3$ architecture and have been suggested to interact with client uOMPs through exposed β sheets (Knowles et al. 2008). NMR experiments have shown that the addition of peptide fragments from a representative OMP (i.e., PhoE) yield chemical shift perturbations in residues in the terminal β -sheets of the POTRA motifs. Although these experiments may suggest the nascent OMPs interact with the POTRA motifs through “ β -augmentation,” it is critical to point out that these NMR studies were completed on a soluble construct of the POTRA domain. Use of a soluble construct removes the POTRA domain from the biological context of full-length BamA; therefore it is unclear that the observed interactions would be recapitulated in an experimental setup that utilizes the full-length BamA protein.

Interestingly, it has been shown by several groups that SurA crosslinks to the BamA POTRA motif 5 (Bennion et al. 2010; Sklar, Wu, Kahne, et al. 2007). It is unknown if SurA mediates contacts between the BamA POTRA motifs and OMP clients through ternary complex

formation. It is an ongoing endeavor in the field to understand how the BamA POTRA domain contacts uOMP clients in both the presence and absence of the chaperone SurA.

OMPs spontaneously insert into bilayers *in vitro*.

Studies investigating the *in vitro* folding behavior of *E. coli* OMPs have been presented for over a decade (Bulieris et al. 2003; Burgess et al. 2008; Kleinschmidt 2015; Kleinschmidt and Tamm 2002). It has been established that OMPs will spontaneously insert into synthetic bilayers and folding is commonly assessed by the apparent electrophoretic mobility of OMPs. When not boiled, the folded and unfolded β -barrel species migrate differentially by SDS-PAGE, and this experimental tool has proven invaluable for monitoring the folding kinetics of various OMPs (Inouye and Yee 1973; Nakamura and Mizushima 1976). It was shown by Burgess *et al.* that OMPs fold with the fastest apparent kinetics into vesicles with shorter acyl chain lengths and phosphatidyl-choline (PC) head groups (Burgess et al. 2008). Importantly, because BamA is itself an OMP, it also exhibits this spontaneous insertion into synthetic bilayers *in vitro*.

Surprisingly, it was reported that incorporating lipids with PE head groups into vesicles used in folding assays significantly retards OMP folding (Burgess et al. 2008; Gessmann et al. 2014). In fact, no folding was observed into lipid extract from *E. coli*. It has been suggested that PE head groups present a kinetic barrier for OMP folding. This interpretation raises the question: if OMPs cannot insert into vesicles with PE head groups, how do they fold into the *E. coli* OM which contains lipids with 75% PE head groups (Lugtenberg and Peters 1976; White, Lennarz, and Schnaitman 1972)? The presence of BamA in the OM to target OMP folding to this membrane provides an elegant solution to this apparent paradox.

BamA accelerates OMP folding *in vitro*.

Because the biologically functional *E. coli* BAM complex contains five proteins, *in vitro* experiments have aimed to deconvolute the effects of these components by studying the individual BAM proteins in isolation. *In vitro* studies have established that prefolding BamA into vesicles prior to the introduction of a client OMP accelerates the folding of the client OMP; therefore it was shown that BamA alone can accelerate uOMP folding, albeit to a lesser extent than the entire BAM complex (Gessmann et al. 2014; Hagan, Kim, and Kahne 2010). Because uOMPs spontaneously insert into synthetic lipid bilayers *in vitro* and BamA accelerates this process, BamA exhibits properties of an enzyme in that it reduces the activation barrier to uOMP folding into biological membranes. The K_m for this catalytic process was determined to be high ($>20 \mu\text{M}$) suggesting the possibility that thermodynamically weak interactions occur between BamA and the uOMP client (Fleming 2015; Gessmann et al. 2014).

These results raise the question: how can BamA accelerate uOMP folding if it only weakly interacts with the uOMP? This conundrum can be addressed by realizing that these weak protein-protein interactions are only one facet of the role of BamA (Fleming 2015). BamA-accelerated uOMP folding is in fact a multi-order process, as BamA may interact with both the uOMP client and the surrounding lipid membrane. It is entirely plausible that BamA promotes the formation of a membrane defect. Because such structures are known to accelerate uOMP folding, this has been suggested as one possible catalytic mechanism for uOMP-BAM mediated folding (Danoff and Fleming 2015b). Such a membrane defect is poorly defined structurally but may be represented by a hydrophobic mismatch between the surrounding lipid bilayer and the BamA β -barrel (Fleming 2015; Noinaj et al. 2013). This membrane defect functional mechanism for BamA is currently speculative, as there has been no compelling evidence presented that BamA specifically interacts with lipids as a part of its catalytic mechanism.

Interestingly, it was shown previously that the entire BAM complex facilitates multiple rounds of catalysis. The “turnover number” or OMPs folded per BAM complex was reported as 1.5 OMPs/BAM. This finding led to the suggestion that the BamBCDE lipoproteins function to regenerate BamA upon client-OMP folding (Hagan and Kahne 2011). However, the turnover number of BamA alone has never previously been reported. This raises the question – can BamA itself catalyze the folding of more than one OMP client? By deconvoluting the roles of each BAM protein by modifying established biochemical assays, we can more precisely assign functions to each protein in this complex (Chapter 4). This allows for better understanding of the mechanism of BamA-mediated OMP folding *in vitro*, which likely parallels *in vivo* function.

Unanswered questions abound on BAM complex function.

Overall, crystal structures of the BAM complex and its individual components provide valuable snapshots of the catalytic cycle of BAM-mediated uOMP folding. The crystallographic conformations observed likely represent stable reaction intermediates; if so, these crystallographic data inherently only provide insight into local energetic minima along the functional pathway of BAM. Complementary *in vitro* studies of OMP folding kinetics in the presence of BamA have enabled the classification of this OMP as a MP-folding enzyme. But many questions remain about the functional mechanism of this enzyme: how are the “open” and “closed” crystallographic conformations of BamA related to the catalytic mechanism? How do the BamA β -barrel and POTRA domains work together to recognize OMP clients and subsequently facilitate their folding? What is the role of the BamBCDE lipoproteins in this process? Lastly, are BAM-chaperone-uOMP ternary complexes formed as intermediates in the biogenesis pathway?

1.4. A holistic understanding of OMP partitioning through the biogenesis pathway is lacking.

Thermodynamic partitioning may drive OMPs towards their folded state.

Figure 1.1 presents a series of possible reactions that a nascent uOMPs may make prior to reaching the OM for assembly by the BAM complex. It is currently unknown what is the biological driving force for productive OMP progression through this pathway. Consideration of the thermodynamics for all possible reactions has prompted a compelling suggestion – the thermodynamics of OMP folding may be the ultimate driving force towards to native state ensemble. Interestingly, the folding free energy for a representative OMP, OmpLA, was reported to be extremely favorable: $32.5 \text{ kcal mol}^{-1}$ (Moon et al. 2013). This immense stability of the folded OMP is proposed to serve as an energy sink for the sorting of OMPs through the periplasm. In addition to a thermodynamic-driven pathway, kinetic partitioning mechanisms have also been suggested for promoting OMP flux through certain chaperone pathways (Wu et al. 2011). It is likely that both thermodynamic and kinetic constraints affect the biogenesis pathway of OMPs; currently, the complex interplay between these features is not well understood.

The *E. coli* OMP biogenesis system is an ideal network for computational modeling.

One intrinsic limitation to *in vitro* studies is that they involve removing components of the OMP assembly system from their biological contexts to investigate their roles in isolation. These types of experiments are necessary for parsing out the details of the numerous protein-protein interactions that occur in this complex pathway. However, a holistic understanding of this trafficking system involves piecing information from all of these biochemical experiments back together to inspect the puzzle of OMP biogenesis in its entirety. Because this periplasmic

network has been studied for more than 20 years, a wealth of information has been published on both genetic and biochemical investigations of the individual system components. We posit that this system is ideal for analysis by a holistic modeling approach.

Network modeling has previously been utilized to investigate emergent properties of well-studied chaperone systems. The FoldEco model for protein folding in the *E. coli* cytoplasm was presented in 2012 (Powers, Powers, and Gierasch 2012). This model incorporates the known kinetic and thermodynamic parameters for reactions involving nascent protein interactions with the cytoplasmic quality control systems into a series of differential equations that quantitate the amount of nascent polypeptide that proceeds through different states, including: unfolded, native, misfolded, and aggregate protein ensembles. This type of modeling was pivotal in synthesizing decades of experimental work into a computational model to analyze the cytoplasmic chaperone network. This type of model has only been reported for the cytoplasmic proteostasis network, although we suggest that the amount of biochemical characterization presented in the literature on OMP biogenesis make this system a prime target for development of a model to describe *E. coli* membrane proteome maintenance.

Outstanding questions on the OMP biogenesis pathway.

Although several thermodynamic and kinetic studies are presented in the literature, no one has previously synthesized these decades of data to understand the OMP biogenesis pathway holistically. This approach raises several questions – will a computational model constructed using the published thermodynamic and kinetic constants recapitulate previously published results? Will this model be capable of simulating the well-established genetics experiments? What types of information will a model of this nature yield to us about the kinetics and thermodynamics of OMP assembly? Can we gain insight into the functions of the

periplasmic chaperones and BAM complex? These questions highlight the exciting possibilities that computational modeling holds with regard to the OMP assembly pathway.

1.5. Outline of the data presented here.

The OMP assembly pathway involves many protein-protein interactions that ensure the accurate assembly of these MPs. Understanding the intricacies of this process requires a detailed knowledge of both the kinetics and thermodynamics of the various interactions that occur prior to the folding of the bacterial OMPs. Here I have investigated the biogenesis pathway of OMPs from the Gram-negative bacteria *E. coli* in hopes to elucidate mechanistic details of this assembly process.

I studied the role of the two prolyl-isomerases shown in Figure 1.1 in the biogenesis pathway of OMPs, FkpA and SurA. In Chapter 2, I have determined the relevant oligomeric states of FkpA at biological concentrations and discovered that the previously unidentified monomeric species is significantly populated under these conditions. I further assessed the ability of both of the FkpA monomer and dimer to bind uOMP and determine that the dimeric species associates with uOMPs with an affinity that is 1000-fold greater than the monomer. I suggest that the monomer and dimer species exhibit the distinct functions of PPIase and uOMP-chaperone, respectively. The relative populations of these oligomers and subsequent functional states of this bifunctional protein are modulated by the σ^E stress response.

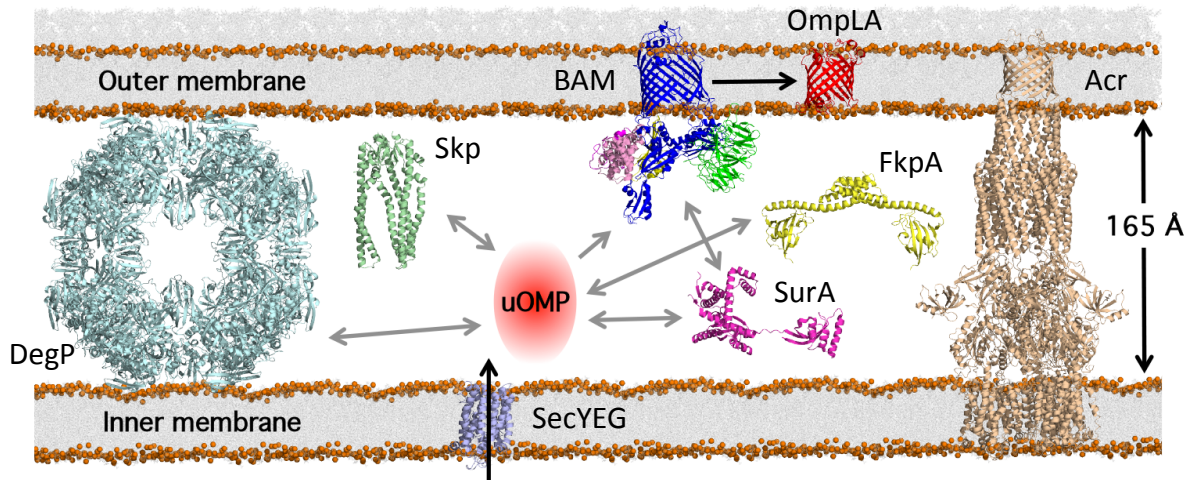
In Chapter 3, I determined that oligomerization is likely not important for the function of SurA, as SurA dimerizes with a K_D in the mM range. I have constructed a structural model for a complex between SurA and a representative uOMP client to explain how SurA accommodates these clients. SurA interacts with expanded uOMPs with a delocalized interface – this structural mechanism is quite distinct from the previously reported encapsulation motifs utilized by Skp and DegP. The discovery of this binding mechanism provides novel insight into the function of this chaperone and suggests how SurA may prime uOMP clients for interactions with the BAM complex.

I have also addressed the question – how does the catalytic activity of BamA compare to that of the whole BAM complex? To this end, I utilized *in vitro* folding assays to probe the mechanism of BamA-accelerated folding of OMPs to compare the activity of BamA to the previously determined BAM complex activity (Chapter 4) (Gessmann et al. 2014; Plummer and Fleming 2015; Plummer, Gessmann, and Fleming 2015). I found that BamA and the BAM complex have identical turnover numbers, suggesting that the BamBCDE lipoproteins are not required for regeneration of this OMP enzyme. These accessory proteins likely work to accelerate the intrinsic enzymatic function of BamA.

For a holistic understanding of how the individual components play a role in the entire process of OMP biogenesis in *E. coli*, we created a computational model to simulate the flux of uOMP through the trafficking system presented in Figure 1.1 (Chapter 5) (Costello et al. 2016). Our computational model incorporates previously reported kinetic and thermodynamic data into differential equations to simulate the flux of different OMP/chaperone species over time. This model recapitulates previously reported experimental results of both wild type and mutant strains of *E. coli*. Our model construction and details of our findings are presented in Chapter 5. Briefly, these simulations suggest that OMPs are highly dynamic in that they make hundreds of complexes with different chaperones prior to folding into the OM. These findings highlight the importance of the dynamic exchange of chaperone-uOMP complexes. These results are in contrast with previous biochemical studies that suggest that chaperones may form ternary complexes to facilitate OMP trafficking through the periplasm (Wu et al. 2011). Our data indicate ternary complex formation is likely not required for accurate trafficking of OMPs. Instead our data suggest a paradigm shift toward focusing on the dynamic OMP species moving non-directionally across the periplasm, towards the OM for folding (Chapter 5).

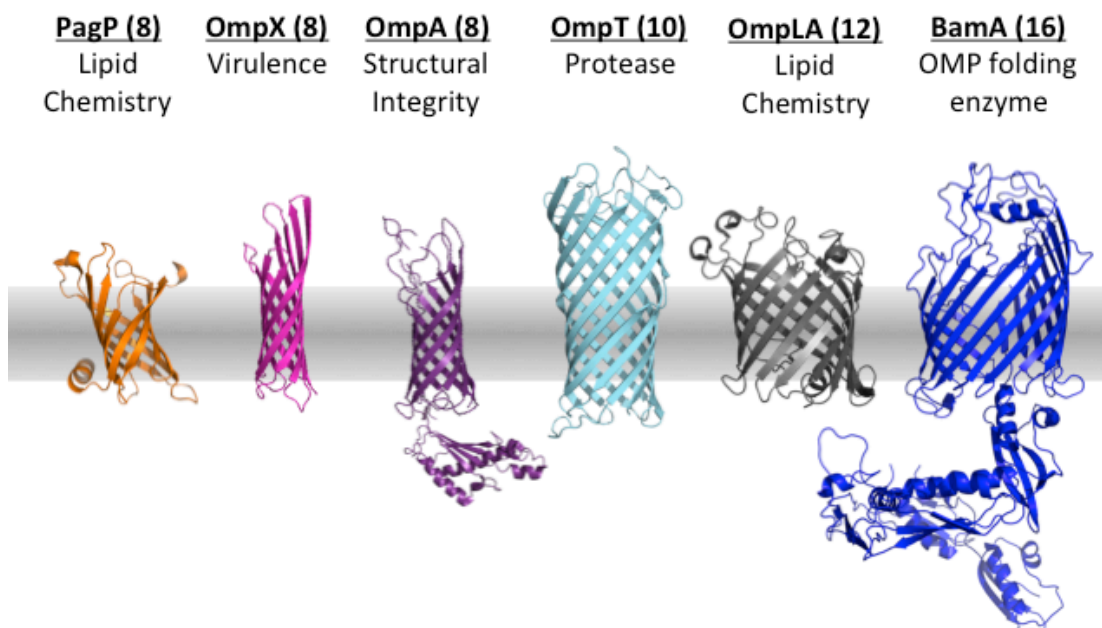
The novel insight provided through our investigations indicates several points along this pathway that are likely to be promising antibacterial drug targets, such as the chaperone-OMP or BAM-OMP interactions, as these binding events are required for the accurate assembly of OMPs into the OM and subsequent bacterial viability and virulence.

Figure 1.1. The *E. coli* Outer Membrane Protein Trafficking Network.



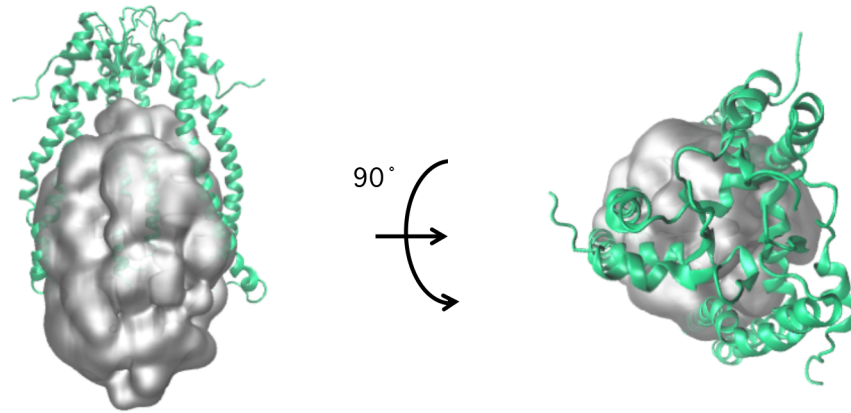
Depiction of Outer Membrane Protein biogenesis components in *E. coli* shown to scale. uOMPs enter the periplasm via the SecYEG translocase (light purple, PDB: 2CFQ), which is located in the bacterial inner membrane. Once in the periplasm, uOMPs interact with several chaperones, including: DegP (cyan, PDB: 3CSO), FkpA (yellow, PDB: 1Q6U), SurA (magenta, PDB: 1M5Y), and Skp (pale green, PDB: 1U2M). The outer-membrane localized BAM complex (BamABCDE shown in blue/green/magenta/pink/yellow respectively, PDB: 5D0O) facilitates uOMP folding into the OM (e.g., OmpLA; red, PDB: 1QD5). The multi-protein Acr complex (tan, PDBs: 1EK9, 2F1M, 2DHH) was used to position the inner and outer membranes. The structures of these membranes were derived from MD simulations of smaller patches that were concatenated to make this image (Wu et al. 2014); phosphate atoms of lipid head groups are shown in orange spheres. Arrows indicate known interactions, although the exact sequence and mechanisms of these interactions are unknown. Note the peptidoglycan is omitted from this figure. This figure is reproduced from (Plummer and Fleming 2016).

Figure 1.2. Structures and biological activities of representative β -barrel OMPs.



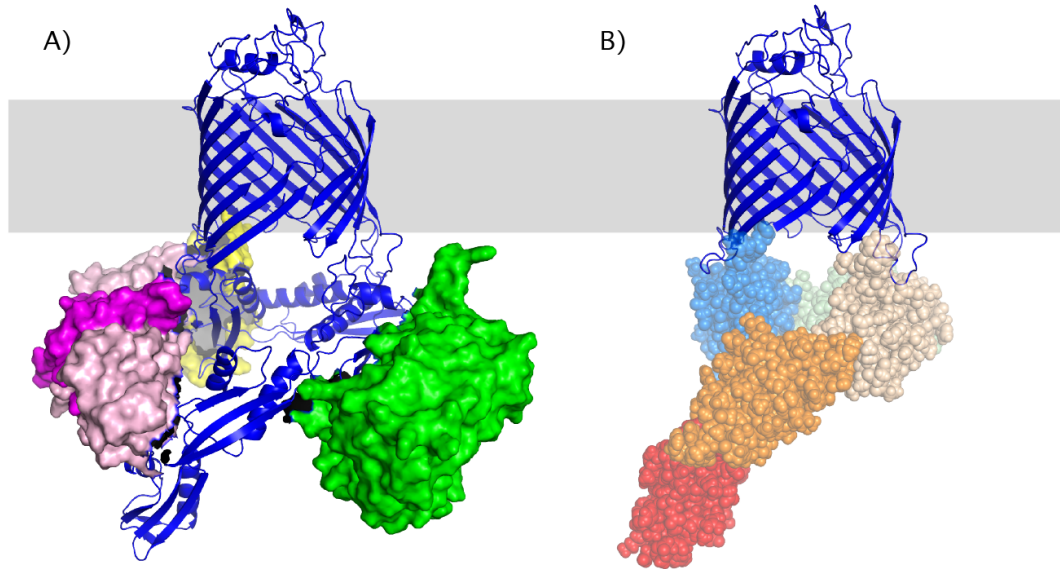
Six representative OMP structures are indicated: PagP (orange, PDB: 1THQ), OmpX (magenta, PDB: 1QJ8), OmpA (purple, PDBs: 2GE4 & 2MQE), OmpT (cyan, PDB: 1I78), OmpLA (grey, PDB: 1QD5), and BamA (blue, PDB: 5EKQ). The membrane in this figure is depicted as a gradient-shaded grey rectangle. The extracellular and periplasmic compartments are shown at the top and bottoms of the image, respectively. These OMPs range in size from 8 to 16 β -strands in the β -barrel TM domain and exhibit distinct functions; the number of β -strands and function of each OMP is listed above the respective PDB. Some OMPs, such as OmpA and BamA, contain soluble periplasmic domains. This figure is adapted from (Burgess et al. 2008).

Figure 1.3. Structural model showing uOMP encapsulated by Skp.



The uOMP protrudes from the internal binding cavity of Skp. This model was constructed from SANS experiments of Skp bound to unfolded OmpW (Zaccai et al. 2015). Skp is depicted as green cartoon, while uOMP is shown as grey surface. This figure is reproduced from (Plummer and Fleming 2016).

Figure 1.4. BamBCDE lipoproteins contact BamA periplasmic POTRA motifs.



(A) The crystallographic structure of the BAM complex (PDB: 5D0O) suggests how the BAM lipoproteins bind to the BamA POTRA motifs (Gu et al. 2016). BamD forms extensive contacts with BamA. BamABCDE are shown in blue, green, magenta, pink, and yellow respectively. (B) The BamA POTRA motifs encircle periplasmic face of β -barrel; the BAM lipoproteins are excluded from this view. POTRA motifs are colored red, orange, tan, green, and light blue (P1-5). This figure is reproduced from (Plummer and Fleming 2016).

Chapter 2 – Chaperone FkpA Populates Oligomers that Exhibit Distinct Functions

2.1. Introduction

Membranes play an essential role in cellular viability by separating intracellular molecules from extracellular ones and also mediating cellular responses to external stimuli. Intact membrane systems are composed of both lipid and membrane protein (MP) components. The accurate and efficient biogenesis of MPs is a prerequisite to the formation of the native, functionally active state of these MPs. MPs have a breadth of critical functions, including metabolite transport, various enzymatic activities, and stress sensing. Understanding how these MPs are trafficked is crucial to developing a holistic model of MP biogenesis and subsequent function.

Periplasmic chaperone network assists OMP trafficking in Gram-negative bacteria.

One MP biogenesis system that has received substantial attention is that of outer membrane proteins (OMPs) in Gram-negative bacteria. The OMP biogenesis and trafficking system has proven to be a promising target for antibacterial and virulence drug development (Hagan, Wzorek, and Kahne 2015). The biogenesis pathway of unfolded OMPs (uOMPs) is a multi-step and complex process that begins with uOMP secretion across the bacterial inner membrane. After translocation, uOMPs encounter the aqueous periplasm in an unfolded, yet folding-competent conformation. Binding of uOMPs to chaperones in the periplasm may prevent their misfolding prior to reaching the outer membrane for proper folding and assembly (Plummer and Fleming 2016). The periplasmic chaperone network is important for the efficient trafficking of uOMPs – it has been suggested that the thermodynamics of uOMP binding to chaperones and subsequent folding provides the biological driving force for uOMP partitioning through the periplasm, towards the bacterial outer membrane in the absence of an external chemical energy source (Moon et al. 2013). This seminal work was the first hint that nature likely

utilizes an intricate interplay between thermodynamics and biology to ensure accurate trafficking and assembly of MPs.

One complicating feature of the *E. coli* chaperone network is that several of the involved chaperones function as oligomers. Recent work has indicated that some chaperone proteins may populate lower order oligomeric species that were previously not implicated in uOMP trafficking (Sandlin, Zaccai, and Fleming 2015). This surprising finding raised several questions about the biologically relevant oligomers of those periplasmic chaperones involved in uOMP trafficking. One such chaperone is FkpA – this chaperone has been proposed to be a dimeric prolyl-isomerase with monomers composed of two domains (Horne and Young 1995; Missiakas, Betton, and Raina 1996). The structure of FkpA indicates that the N-terminal domain is predominantly α -helical and mediates dimerization (Figure 2.1). It has been suggested that the dimeric form of FkpA is the species involved as a chaperone for uOMPs (Ge, Lyu, et al. 2014; Saul et al. 2004).

FkpA functions as a chaperone, prolyl-isomerase, and is a heat-shock protein.

An additional facet of FkpA function is that the C-terminal domain is homologous to FK-506 binding proteins (FKBPs) and contains an active site for prolyl-isomerization (Saul et al. 2004). This domain contains high sequence and structural homology to the human protein FKBP-12, which has been implicated in critical signaling cascades (Van Duyne et al. 1993; Horne and Young 1995; Trandinh, Pao, and Saier 1992). FkpA accelerates the *cis/trans* isomerization of the proline backbone bond with a catalytic efficiency 100 fold greater than other periplasmic prolyl-isomerases (Behrens et al. 2001; Ramm and Plückthun 2000). Interestingly, all known FkpA clients for prolyl isomerization are soluble proteins (Bothmann and Pluckthun 2000; Braun et al. 2015; Hullmann et al. 2008). As FkpA has also been implicated in interacting with clients lacking *cis* prolines, it has been suggested that the prolyl-isomerase

activity of FkpA is not the sole factor for promoting folding of client proteins (Bothmann and Pluckthun 2000; Braun et al. 2015; Cumby et al. 2015; Dwyer et al. 2014; Gunnarsen et al. 2010, 2013; Hullmann et al. 2008; O'Reilly et al. 2014; Padiolleau-Lefèvre et al. 2006; Scholz et al. 2005; Veiga, De Lorenzo, and Fernández 2004). Therefore a prolyl-isomerase independent chaperone activity of FkpA has been proposed. FkpA assists the folding of soluble proteins, in addition to interacting with uOMPs (Ge, Lyu, et al. 2014; Schwalm et al. 2013). Interestingly, typical OMPs also lack *cis* prolines, further suggesting that FkpA has two distinct functions: uOMP chaperone and prolyl-isomerase for other client proteins.

Lastly, FkpA additionally plays a role in the stress response of *E. coli* (Arié, Sassoon, and Betton 2001). As with other bacterial heat shock proteins (HSPs), FkpA may function as a chaperone to prevent the misfolding and aggregation of its binding partners under non-native folding conditions. This role of HSPs in cellular proteostasis under temperature stress has been suggested to stem from an activation of HSPs under non-native temperatures, however changes in HSP expression sometimes complicate interpretations of HSP activation (Georgopoulos and Welch 1993; Haslbeck et al. 2005). As HSPs are upregulated in human cancers and neurodegenerative diseases, there are clear biomedical implications for understanding the mechanisms underlying HSP function under stress conditions (Cao and Konsolaki 2011; Jolly and Morimoto 2000).

Here we deconvolute the complex relationships between FkpA chaperone function and oligomerization. We investigate how various biologically relevant states of FkpA are populated and conclude that significant populations of both monomer and dimer are present at physiological protein concentrations. To investigate the functional importance of the FkpA monomer, we isolated a monomeric FkpA variant and determine that this variant may interact with uOMP clients, albeit with an affinity that is 1000 fold weaker than the FkpA dimer. We

suggest that the FkpA dimer functions as a chaperone by binding to uOMP's clients, while the FkpA monomer likely functions solely as a prolyl-isomerase. The transcriptional upregulation associated with the σ^E stress response likely modulates the relative populations of these oligomers and therefore relevant functional states of FkpA.

2.2. Methods

We introduced the gene of *E. coli* FkpA into the pET28b vector between the Nde I and Xho I restriction sites, following an N-terminal 6-Histidine tag and Tobacco Etch Virus (TEV) protease cleavage site. This construct lacks a signal sequence for export of protein to the periplasm. HMS *E. coli* cells from glycerol stocks containing this plasmid were used to inoculate 3 mL LB growths containing 50 µg/mL kanamycin. These cultures were grown for 8 to 10 hours at 37 °C. This growth was diluted 1:200 into a fresh 25 mL LB growth with antibiotics and grown overnight at 37 °C. This growth was diluted 1:40 into a fresh 500 mL of 2xYT with antibiotics in baffled flasks and grown at 37 °C to $A_{600} \sim 0.8$ prior to induction of FkpA overexpression by addition of IPTG (1 mM final concentration). After 6 additional hours of growth, cell pellets were collected by centrifugation at 5000 rpm (4410 x g) for 30 min in a Beckman J2-MI centrifuge in a JA-10 rotor. Cell pellets were frozen and stored at -20 °C.

Histidine-tagged TEV protease was prepared as previously described (Sandlin, Zaccai, and Fleming 2015). For FkpA purification, previously frozen cell pellets were thawed and solubilized in 25 mL of 20 mM NaPO₄, 500 mM NaCl, 20 mM imidazole buffer (Buffer A) with Pierce EDTA-free protease inhibitor tablets (Thermo Prod # 88266). Cells were subsequently lysed using an Avestin Emulsiflex homogenizer. The lysate was then centrifuged at 5000 rpm (4410 x g) for 30 min in a Beckman J2-MI centrifuge in a JA-10 rotor to pellet cell debris. The supernatant was filtered through a 0.45 mm Millex filter prior to being loaded onto a Ni Sepharose High Performance bench-top column (GE Prod # 17-5286-01) pre-equilibrated in Buffer A. The column was then washed with Buffer A. Protein was eluted with 20 mM NaPO₄, 500 mM NaCl, 300 mM imidazole buffer (Buffer B) and dialyzed with TEV-protease (1:25 molar ratio) into 2 L 20 mM Tris (pH = 8.0) utilizing 10 kDA MWCO Snakeskin dialysis tubing (Thermo Prod # 68100) overnight. The recovered dialysate was reapplied to a Ni Sepharose

High Performance bench-top column pre-equilibrated in Buffer A. The column was then washed with Buffer A and the FkpA was eluted in these wash fractions. TEV protease was eluted with the application of Buffer B to the column. Recovered FkpA was then dialyzed into 2 L 20 mM Tris (pH = 8.0) overnight with 10 kDa MWCO Snakeskin dialysis tubing. The recovered FkpA was then concentrated with an Amicon filter (Millipore) with a 10 kDa MWCO prior to use in experiments. Stock concentrations were determined with the theoretical extinction coefficient of $15930 \text{ M}^{-1} \text{ cm}^{-1}$ for the FkpA monomer (Gill and von Hippel 1989).

WT-FkpA was diluted into 20 mM Tris buffer (pH=8.0) and samples with $A_{280} = 0.90$, 0.60, and 0.30 at a path length of 1.2 cm (corresponding to concentrations of 56, 38, and 19 μM FkpA monomer units; $\epsilon_{280} = 15930 \text{ M}^{-1} \text{ cm}^{-1}$) were loaded into six-sector centerpieces and allowed to equilibrate at speeds of 20,000; 24,500; and 30,000 rpm in a Beckman Optima XL-A analytical ultracentrifuge with absorbance optics at each temperature. Data were collected at: 4, 26, 37, and 40 °C. Radial scans at 280 nm were acquired with 0.001 cm radial steps with 10 replicates. Equilibration was assessed with WinMatchv0.99 and data were subsequently trimmed to regions where Beer's law applies in WinReEdit v.0999.0028 (Johnson et al. 1981). Global fitting was completed in WinNonLin v.1.06 (Johnson et al. 1981). For data analysis, we calculated reduced molecular weight values, partial specific values and buffer densities using Sednterp (Laue et al. 1992). All data were fit with single-ideal species (i.e., obligate dimer) and dimerization models. Fitting output and parameters are indicated in Table 2.1 with representative data fits shown in Figure 2.2. These same experimental conditions were used for data collection of WT-FkpA in 20 mM Tris (pH=8.0) and 1 M urea for the thermodynamic value reported in Figure 2.7. A summary of fitting output and parameters for data collected in 20 mM Tris and 1 M urea are given in Table 2.2.

For analysis of a monomeric form of FkpA, site-directed mutagenesis was utilized to introduce the point mutation G28K into the WT-FkpA gene described above. Primers for cloning are given in Table 2.3. Protein expression and purification protocols for FkpA-G28K were identical to those used for WT-FkpA.

For apo-chaperone SV experiments, WT-FkpA and FkpA-G28K were diluted into 20 mM Tris buffer (pH=8.0) and 1 M urea to a final monomer protein concentration of 40 μ M and loaded into 1.2 cm double-sector SV centerpieces. For apo-uOMP SV experiments, unfolded OmpA₁₇₁ was diluted into 20 mM Tris buffer (pH=8.0) and 1 M urea to a final protein concentration of 5 μ M. For mixture SV experiments, either WT-FkpA or FkpA-G28K was diluted into 20 mM Tris buffer (pH=8.0) and 1 M urea to a final monomer protein concentration of 40 μ M in the presence of 5 μ M unfolded OmpA₁₇₁. Prior to starting each run, cells were thermally equilibrated in the centrifuge for 90 minutes prior to rotor acceleration. Experiments were performed in an An-Ti60 rotor at 50,000 rpm with radial scans at 280 nm were acquired with 0.003 cm radial steps in continuous mode with zero time interval between scans. SV experiments were conducted at 20 °C with a Beckman Optima XL-A analytical ultracentrifuge using absorbance optics. All data were analyzed in DCDT+ v.2.4.2 (Philo 2006). All simulations for Figure 2.6 were performed in SEDANAL v6.01.6926 (Stafford and Sherwood 2004).

For gel-filtration data presented in Figure 2.4B, 1 mL of WT-FkpA or FkpA-G28K with a protein concentration of 60 millimolar monomer units was injected onto a Superdex-200 10/300 GL (GE Healthcare Life Sciences) gel-filtration column in 20 mM Tris, 200 mM NaCl with a flow rate of 0.6 mL/min.

We estimated the sedimentation coefficient for the monomer-FkpA-uOmpA₁₇₁ and dimer-FkpA-uOmpA₁₇₁ by utilizing the previously published model of uOmpA₁₇₁ bound to

another chaperone, Skp (Zaccai et al. 2015). We combined the previously published structures of the FkpA monomer and dimeric species (PDB: 1Q6H) and uOmpA₁₇₁ with the uOMP placed in the proposed binding cavity of FkpA (Saul et al. 2004) (Figure 2.6 Panels A and D). The sedimentation coefficient of each complex was then calculated in HydroPro (García De La Torre, Huertas, and Carrasco 2000) for the buffer condition of 20 mM Tris, 1 M urea ($\rho = 1.01417 \text{ g mL}^{-1}$, $\eta = 0.01045 \text{ Poi}$) with appropriate molecular weights. Subsequent sedimentation velocity data was simulated in SEDANAL v6.01.6926 (Stafford and Sherwood 2004). Simulation input parameters are as follows: For monomeric FkpA, $\text{MW} = 26224 \text{ g mol}^{-1}$, $s = 1.70$ Svedbergs, ρ increment (defined as $1 - \nu\rho$) = 0.249, and $\epsilon_{\text{mass}} = 0.608 \text{ L cm}^{-1} \text{ g}^{-1}$. For uOmpA₁₇₁, $\text{MW} = 18875 \text{ g mol}^{-1}$, $s = 1.40$ Svedbergs, ρ increment = 0.266, and $\epsilon_{\text{mass}} = 2.483 \text{ L cm}^{-1} \text{ g}^{-1}$. For monomer-FkpA-uOmpA₁₇₁ complex, $\text{MW} = 45099 \text{ g mol}^{-1}$, $s = 2.70$ Svedbergs, ρ increment = 0.256, and $\epsilon_{\text{mass}} = 1.393 \text{ L cm}^{-1} \text{ g}^{-1}$. For dimeric FkpA, $\text{MW} = 52448 \text{ g mol}^{-1}$, $s = 2.86$ Svedbergs, ρ increment = 0.249, and $\epsilon_{\text{mass}} = 0.608 \text{ L cm}^{-1} \text{ g}^{-1}$. For dimer-FkpA-uOmpA₁₇₁ complex, $\text{MW} = 71323 \text{ g mol}^{-1}$, $s = 4.10$ Svedbergs, ρ increment = 0.256, and $\epsilon_{\text{mass}} = 1.104 \text{ L cm}^{-1} \text{ g}^{-1}$. Dimerization equilibrium association constants were varied from 1E+9 to 1E+1. Simulated data was then analyzed in DCDT+ v.2.4.2 (Philo 2006). Distributions of simulated sedimentation profiles for the monomer-FkpA-uOmpA₁₇₁ and dimer-FkpA-uOmpA₁₇₁ are shown in Figure 2.6 Panels B and E, respectively. Figure 2.6 Panels C and F indicate the weight average sedimentation coefficient of each complex as a function of simulated equilibrium dissociation constant.

2.3. Results

FkpA populates both monomeric and dimeric states at physiological concentrations.

In light of recent observations that previously unconsidered oligomeric states of periplasmic chaperones may be populated, we first investigate the dimerization equilibrium of FkpA. The crystallographic structure of FkpA was solved to be dimeric therefore it has been assumed that the solution state of FkpA is the dimeric form (Figure 2.1) (Saul et al. 2004). To probe the validity of that assumption, we utilized sedimentation equilibrium analytical centrifugation (SE) to determine the solution oligomerization state of FkpA. To our surprise, the SE data are not well described by a single ideal species fit, which would be expected if FkpA existed as an obligate dimer in solution (Figure 2.2). Rather, the SE data are best described by a monomer-dimer equilibrium model with an equilibrium dissociation constant (K_D) of 7.7 ± 2.8 μM at 37 °C ($\Delta G = 7.4$ kcal mol⁻¹). Interestingly, this equilibrium constant for FkpA dimer dissociation is on the same order of magnitude as the reported physiological concentration of FkpA in the *E. coli* periplasm (i.e., 10-20 μM , Figure 2.3A) (Arike et al. 2012; Masuda et al. 2009). These findings suggest that both the monomer and dimer species of FkpA are significantly populated at 37 °C.

In addition to discovering that the FkpA monomeric species is significantly populated at physiological concentrations and temperature, we utilized SE experiments to probe the thermodynamics of FkpA dimerization. For this analysis, we measured the equilibrium dissociation constant as a function of temperature (Figure 2.3B). This experimentally determined equilibrium constant increases slightly over the tested temperature range. To extract thermodynamic information from these data, we performed a Van't Hoff analysis, as shown in Figure 2.3C. This linear fit yields two thermodynamic parameters – the slope and intercept are

related to the enthalpy and entropy of FkpA dimerization, respectively. Fitted values of enthalpy and entropy of dimerization are $-4.57 \pm 1.06 \text{ kcal mol}^{-1}$ and $9.2\text{E-}3 \pm 3.6\text{E-}3 \text{ kcal mol}^{-1} \text{ K}^{-1}$. The individual contributions of each of these thermodynamic parameters to the free energy of dimerization can be calculated at any given temperature – for example, at 37 °C $T\Delta S$ is 2.9 kcal mol⁻¹ and ΔH is -4.6 kcal mol⁻¹. These values suggest that the FkpA dimerization equilibrium is driven by both the enthalpic and entropic components of the free energy. The enthalpic contribution may arise from favorable interactions at the FkpA dimer interface. Inspection of the crystal structure reveals that extensive surface area is buried on each FkpA monomer upon dimerization ($\sim 2200 \text{ \AA}^2$ per monomer) (Saul et al. 2004). This thermodynamic data complements the previous structural investigation of FkpA by providing quantitative insight into the dimerization equilibrium.

Monomeric FkpA binds uOMP with an affinity 1000 fold weaker than dimeric FkpA.

Our observation that the equilibrium constant for FkpA is similar to the expected physiological concentration raises an interesting question: what is the functional relevance of monomeric FkpA? To understand the importance of this species, we designed a point mutation to FkpA that mutates a glycine centrally located at the FkpA dimer interface to a lysine (i.e., FkpA-G28K). We reasoned that this mutation would disrupt the dimer interface and favor the monomeric conformation of FkpA. We assessed the oligomerization state of FkpA-G28K using several methods and determined this variant is indeed monomeric (Figure 2.4).

To investigate the functional relevance of the FkpA monomer, we developed a sedimentation velocity (SV) analytical ultracentrifugation assay to quantitate FkpA interactions with a uOMP client. This assay measures the sedimentation coefficient of both FkpA constructs in the presence and absence of a representative uOMP client to determine the extent of FkpA-

uOMP binding. Initial measurements of the sedimentation coefficients of both WT-FkpA and FkpA-G28K in the absence of uOMP client yielded values of 2.86 ± 0.08 Svedbergs and 1.70 ± 0.06 Svedbergs, respectively (Figure 2.4D). As expected, the sedimentation coefficient for FkpA-G28K is significantly smaller than WT-FkpA; this agrees with the observation that FkpA-G28K is monomeric while WT-FkpA is primarily dimeric under these conditions.

To quantify FkpA-uOMP interactions, we then measured the sedimentation coefficient of each FkpA construct in the presence of uOMP client. The client uOMP utilized for these studies is unfolded-OmpA₁₇₁ (uOmpA₁₇₁). Under our experimental conditions, uOmpA₁₇₁ is unfolded and monomeric (Danoff and Fleming 2011). This conformation of uOMP is likely the relevant one for binding to FkpA *in vivo*. The experimentally determined distributions of sedimentation coefficients for the WT-FkpA/uOmpA₁₇₁ and FkpA-G28K/uOmpA₁₇₁ mixtures are shown in Figure 2.5A (dark green) and Figure 2.5B (dark blue), respectively. Fitting these distributions yields average sedimentation coefficients for WT-FkpA/uOmpA₁₇₁ and FkpA-G28K/uOmpA₁₇₁ mixes of 3.18 ± 0.11 and 1.60 ± 0.10 Svedbergs, respectively. In addition to the experimental curves, we have indicated calculated curves (dashed lines) for hypothetical non-interacting mixtures of both FkpA proteins with uOmpA₁₇₁. These curves were calculated as a sum of the individual experimental sedimentation coefficient distributions for the appropriate FkpA construct and uOmpA₁₇₁. For WT-FkpA, calculated and experimental distributions for the mixture do not overlay, suggesting that WT-FkpA interacts with uOmpA₁₇₁ client. For FkpA-G28K, the calculated and experimental distributions overlay, suggesting that FkpA-G28K does not bind to the uOmpA₁₇₁ client. These results indicate that the dimeric form of FkpA binds to uOMP clients, while we are unable to detect an interaction between the monomeric construct and uOMP.

Although the above analysis provides us significant insight into the ability of each FkpA oligomer to interact with a uOMP client, it does not provide thermodynamic insight into this binding event. To determine interaction energies, we simulated SV data for association reactions of both monomeric and dimeric FkpA with uOmpA₁₇₁ with varying equilibrium dissociation constants (Figure 2.6). From these simulations, we determined a range of equilibrium constants that are consistent with our experimental observables. Despite the observation that there is no apparent shift in sedimentation coefficient upon mixing FkpA-G28K with uOmpA₁₇₁, we cannot definitively conclude that binding does not occur – it may be the case that the population of the bound complex is simply too low for detection. Our simulations suggest that K_D values in the millimolar range are consistent with our experimental findings for the FkpA-G28K/uOmpA₁₇₁ mixture. For WT-FkpA binding to uOmpA₁₇₁, we estimate a K_D in the micromolar range is consistent with our observed sedimentation coefficients. These observed and estimated interaction energies are incorporated into the thermodynamic cycle shown in Figure 2.7.

2.4. Discussion

SE findings highlight the importance of the FkpA dimerization equilibrium.

Although FkpA was initially identified as a component of the *E. coli* periplasmic chaperone network over 15 years ago (Arié, Sassoon, and Betton 2001), thermodynamic data on FkpA oligomerization and uOMP binding has been scarce. As shown in Figure 2.3, we determined that at physiological concentrations and temperature, FkpA likely exists as both monomeric and dimeric species. Interestingly, our experimentally determined micromolar K_D agrees well with previous estimations of the K_D for dimerization of the N-terminal domain of FkpA (Saul et al. 2004). In the context of these previous findings, our Van't Hoff analysis likely indicates that the N-terminal domain of FkpA is a contributor to the enthalpic component of the dimerization free energy. This suggests the N-terminal domain of FkpA mediates dimerization and the C-terminal domain likely makes a negligible contribution to the energy of dimerization.

One consequence of the equilibrium dimerization constant being similar to the physiological concentration of FkpA is that this chaperone is poised for participation in stress response. Upon exposure to stress, *E. coli* bacteria induce the σ^E stress response, which consists of complex transcriptional regulation. It has been previously reported that FkpA is among the periplasmic chaperones that are upregulated upon induction of the σ^E stress response (Dartigalongue, Missiakas, and Raina 2001). Even a slight increase in the expression of FkpA will subsequently shift the equilibrium of oligomerization to increase the population of FkpA dimers under stress conditions. This increase in FkpA dimer population may assist in coping with the accumulation of uOMP in the periplasm, as our data suggest the FkpA dimer is the oligomer responsible for the uOMP-client binding. These findings are in line with the recent realization

that the periplasmic chaperones effectively form a reservoir to capture free uOMPs (Costello et al. 2016). Also, our results agree with previous findings that overexpression of FkpA, and subsequent increase in dimeric population of FkpA, rescues lethal phenotypes at 37 °C (Ge, Lyu, et al. 2014).

FkpA monomer and dimer species exhibit distinct functions.

Emphasizing the thermodynamics of this system has allowed us to access information about the conformation states of FkpA that were previously undetected. We have summarized our observed and estimated free energies for the formation of various complexes in a thermodynamic cycle shown in Figure 2.7. We have measured the free energy of dimerization of FkpA to be $-7.6 \text{ kcal mol}^{-1}$ and estimated the binding free energies of monomeric and dimeric FkpA constructs to uOMP as -4 kcal mol^{-1} and -7 kcal mol^{-1} , respectively. Although we cannot experimentally access the free energy of monomer-FkpA/uOMP recruiting an additional FkpA monomer, the power of thermodynamics allows us to calculate this parameter as $\sim -11 \text{ kcal mol}^{-1}$. This suggests that a monomer-FkpA/uOMP complex would associate with another FkpA monomer with nanomolar affinity. It is worth noting that all free energies reported in Figure 2.7 were collected in experiments containing 1 M urea, which is required for measurements involving unfolded OMP clients. Therefore these values are likely upper bounds for energetic measurements made in the absence of denaturant.

The detection of FkpA monomer at concentration levels consistent with physiological expression suggests that both oligomers of FkpA are functionally important under wild type growth conditions. We propose that the dimer and monomer species of FkpA have distinct functions. Dimer FkpA likely participates in OMP biogenesis by binding to uOMPs. Monomer FkpA association with uOMP is weak – this suggests that the monomeric FkpA likely does not function as a chaperone for uOMPs. This type of oligomer-specific chaperone function has been

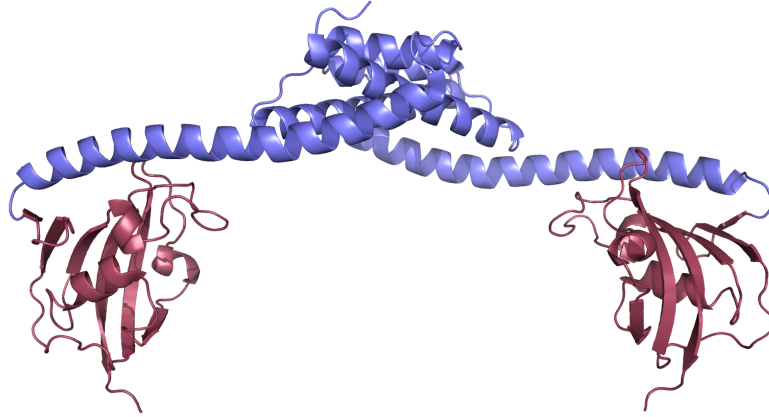
previously reported for other bacterial small HSPs (Giese and Vierling 2002). This discovery begs the question: why would the oligomerization equilibrium of FkpA be tuned in such a way to populate a chaperone-incompetent monomer under physiological conditions? Each FkpA monomer houses an inherent function – a C-terminal domain with peptidyl-prolyl isomerase activity. We propose that the monomeric form of FkpA may function as a prolyl-isomerase on non-OMP clients. This agrees with the finding that both domains of FkpA are required *in vivo* (Saul et al. 2004). The N-terminal domain is required to mediate dimerization and subsequent chaperone activity, while the C-terminal domain is necessary for monomer function as a PPIase.

Moving forward: HSP upregulation as a control mechanism for distinct oligomer functions.

There are immediate implications for our findings regarding the chaperone networks of both bacteria and eukaryotes. Modulation of the populations of FkpA monomer and dimer may promote different functions under different cellular conditions. It has been reported that HSPs are upregulated in human cancers and neurodegenerative disorders (Dattilo et al. 2015; Jagadish et al. 2016; Li et al. 2014; S. Wang et al. 2016). Future work will be required to understand the consequences of thermodynamics for the relative populations of various chaperone oligomers and chaperone-client complexes for this plethora of biologically important systems.

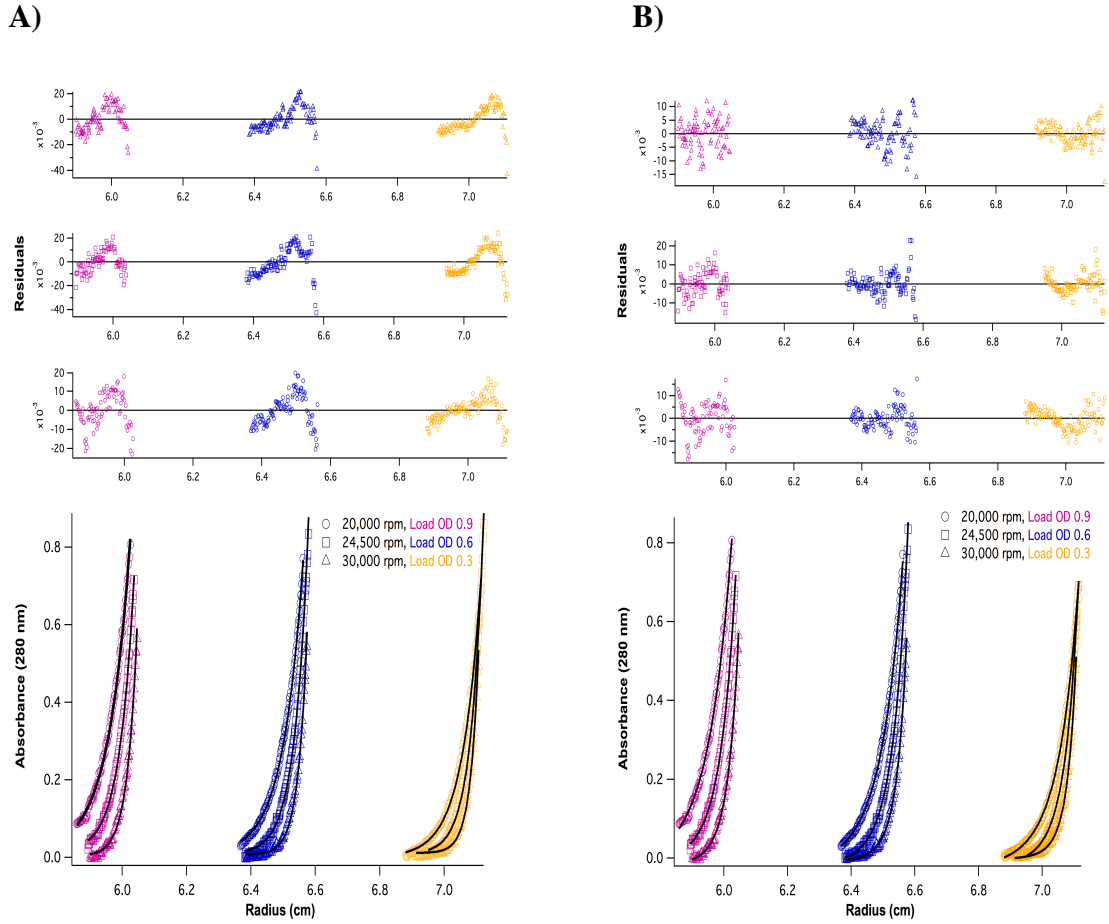
2.5. Figures

Figure 2.1. Crystal structure of FkpA.



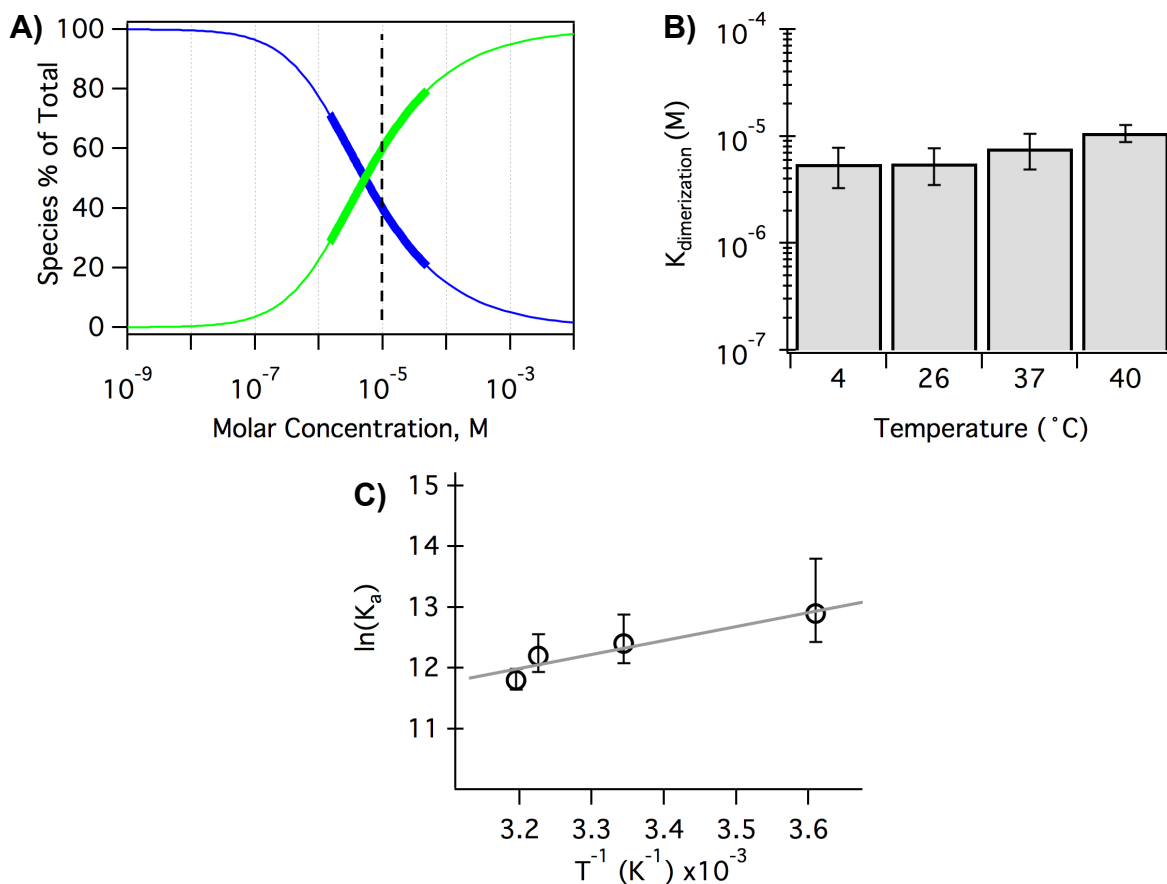
The FkpA α -helical N-terminal domain (blue) mediates dimerization, while the C-terminal domain (maroon) contains the catalytic site of prolyl-isomerization (Saul et al. 2004). PDB ID 1Q6U and Pymol were utilized to make this figure.

Figure 2.2. Representative fits for FkpA SE data.



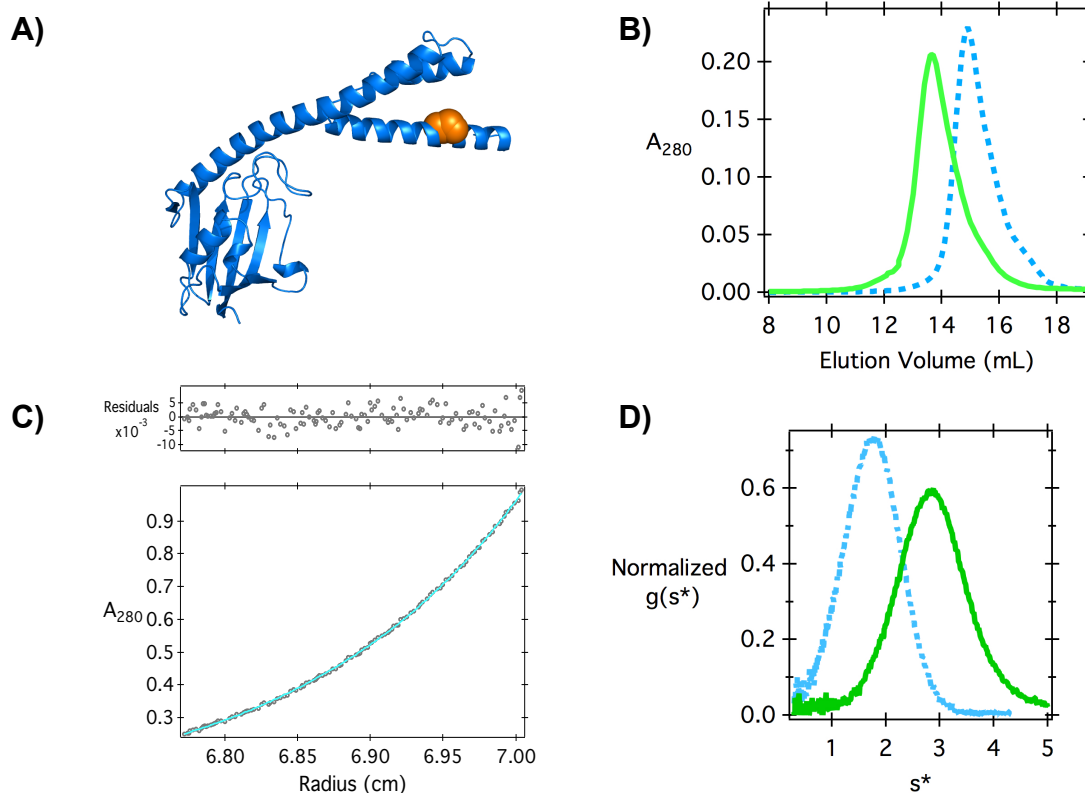
The sedimentation equilibrium data are not well described by single ideal species model (i.e., FkpA obligate dimer) as indicated by the non-random residuals shown in Panel A. A model accounting for monomer-dimer equilibrium better fit the data, as shown in Panel B. One representative dataset is shown with Channel A ($A_{280} = 0.9$), B ($A_{280} = 0.6$), and C ($A_{280} = 0.3$) shown in magenta, blue, and yellow respectively.

Figure 2.3. Species plot and Van't Hoff analysis of FkpA dimerization reaction.



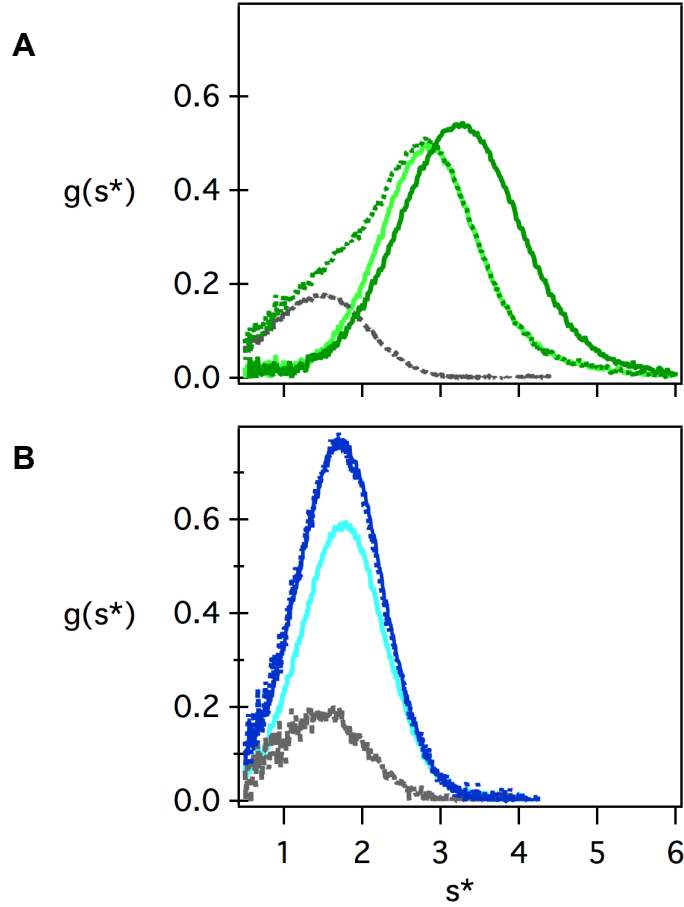
Species plot indicates appreciable population of both FkpA monomer (blue) and dimer (green) at physiological protein concentrations and 37 $^{\circ}\text{C}$, marked by vertical line (Panel A). Bolded regions indicate the concentration range accessed in the SE ultracentrifugation experiments. The equilibrium dissociation constant ($K_{\text{dimerization}}$) for FkpA dimerization changes slightly as a function of temperature (Panel B). A global analysis of these data with a linearized Van't Hoff equation reveals that this dimerization equilibrium is driven by both the enthalpic and entropic terms (Panel C). Note Panel C plots equilibrium association constants (K_a) on the y-axis. At 37 $^{\circ}\text{C}$, $T\Delta S$ is 2.9 ± 1.0 kcal mol $^{-1}$, ΔH is -4.6 ± 1.0 kcal mol $^{-1}$, and ΔG is -7.4 ± 0.2 kcal mol $^{-1}$.

Figure 2.4. Characterization of FkpA-G28K variant



(A) The position of G28 (orange sphere) on the FkpA monomer (PDB: 1Q6H). (B) Gel-filtration profiles of FkpA-G28K (blue dashed line) and WT-FkpA (green solid line) are distinct and suggest that FkpA-G28K has a lower apparent molecular weight than WT-FkpA. The measured molecular weight of FkpA-G28K by SE is 26.3 ± 0.3 kDa, consistent with the expected molecular weight of monomeric FkpA (i.e., 26.7 kDa). (C) Representative SE dataset fit with a single ideal species model. (D) The distribution of sedimentation coefficients for both WT-FkpA (green solid line) and FkpA-G28K (blue dashed line) – as expected, the weight average sedimentation coefficient of FkpA-G28K is smaller than that of WT-FkpA. These profiles are reproduced in Figure 2.5.

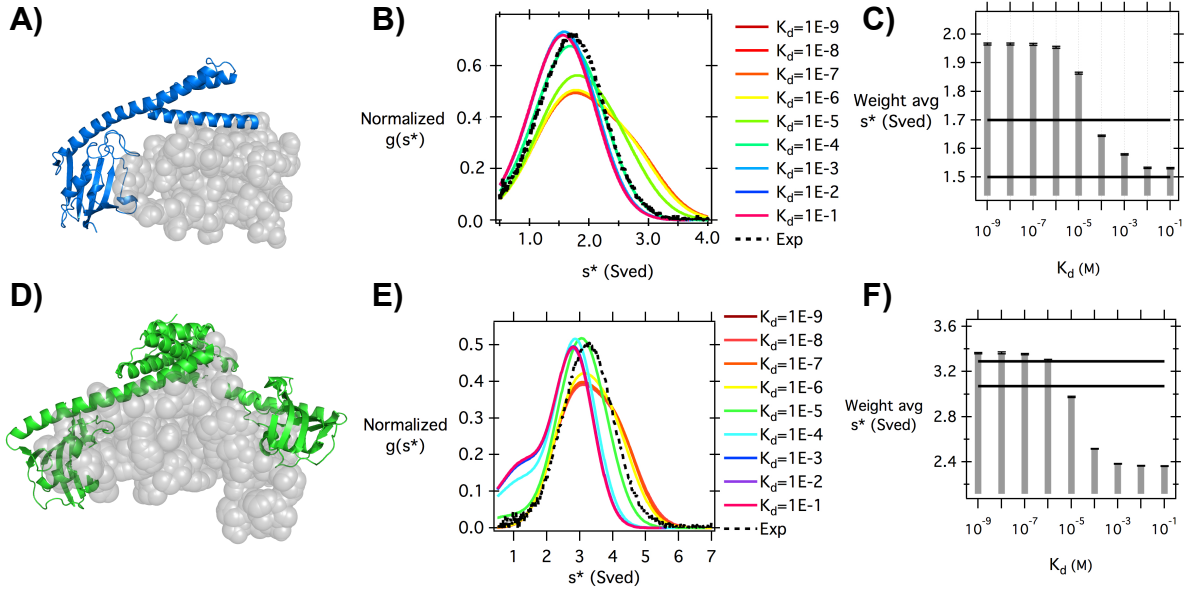
Figure 2.5. SV data suggests FkpA dimer binds to uOMPs 1000-fold stronger than FkpA monomer.



$g(s^*)$ distributions for 5 μ M uOmpA₁₇₁ (grey in Panel A and B) and 40 μ M WT-FkpA (light green, Panel A) and G28K-FkpA (light blue, Panel B). s^* values for WT-FkpA and G28K-FkpA are 2.86 ± 0.08 and 1.70 ± 0.06 Svedbergs, respectively. Calculated curves for FkpA-uOmpA₁₇₁ mixes are shown as dashed dark green (Panel A) and dark blue (Panel B) curves. Experimental curves for FkpA-uOmpA₁₇₁ mixes are shown in solid dark green (Panel A) and dark blue (Panel B) curves. s^* values for WT-FkpA-uOmpA₁₇₁ and G28K-FkpA-uOmpA₁₇₁ mixes are 3.18 ± 0.11 and 1.60 ± 0.10 Svedbergs, respectively. For WT-FkpA, calculated and experimental $g(s^*)$ curves for mix do not overlay, suggesting that WT-FkpA interacts with uOmpA₁₇₁ client. For G28K-

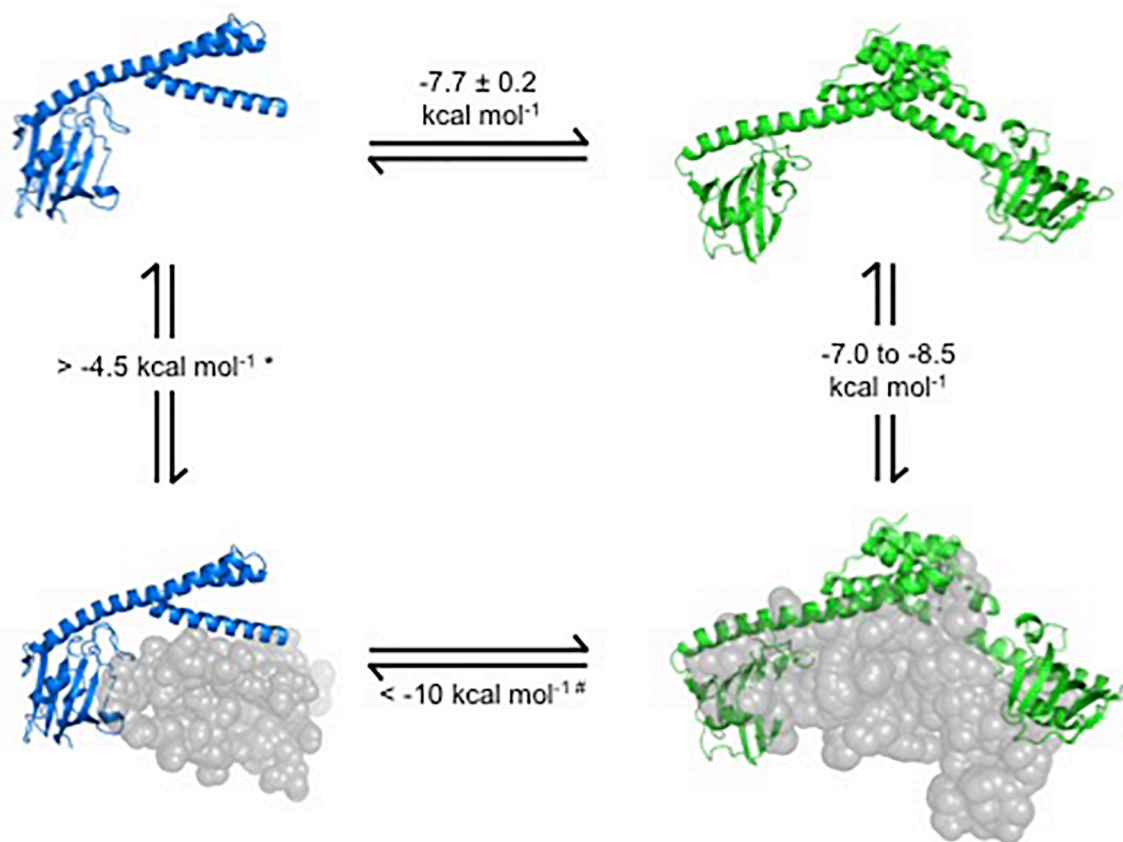
FkpA, the calculated and experimental $g(s^*)$ curves do overlay, suggesting that G28K-FkpA does not interact with the uOmpA₁₇₁ client.

Figure 2.6. Simulations suggest FkpA dimer and monomer bind to uOMP with μM and mM K_D values, respectively.



Panels A and D illustrate the structural models utilized for calculating the sedimentation coefficients of the monomer-FkpA-uOmpA₁₇₁ and dimer-FkpA-uOmpA₁₇₁ complexes, respectively. Panels B and E depict simulated sedimentation coefficient distributions for simulated data with the labeled range of equilibrium dissociation constants for the monomer-FkpA and dimer-FkpA association reactions with uOmpA₁₇₁ respectively. Panels C and F show the weight average sedimentation coefficients for the simulated data in Panels B and E as a function of equilibrium dissociation constant the monomer-FkpA and dimer-FkpA association reactions with uOmpA₁₇₁ respectively. Black horizontal lines indicate the range of values consistent with the experimentally determined weight average s^* for each dataset.

Figure 2.7. Thermodynamic cycle to summarize the new model for FkpA dimerization and uOMP binding reactions.



We measure the free energy of dimerization of FkpA in the absence of uOMP client to be $-7.7 \pm 0.2 \text{ kcal mol}^{-1}$ (top horizontal reaction). The vertical arrows indicate the association of the FkpA monomer and dimer with uOmpA₁₇₁ and these energies are estimated from SV simulations (Figure 2.6). The asterisk (*) on the monomer-FkpA binding to uOMP indicates that this experimental result was determined using the G28K variant of FkpA. Although this species may dimerize, we do not observe a G28K-FkpA dimer bound to uOMP in our SV experiments – this may be due to the low population of the G28K-FkpA/uOMP complex formed under these experimental conditions. Therefore the bottom horizontal reaction is not readily accessible in our experiments (#). Instead, I calculated this value due to the constraint that the thermodynamic

cycle must sum to zero; the estimated free energy of monomer-FkpA/uOMP recruiting an additional FkpA monomer to be $< -10 \text{ kcal mol}^{-1}$. This suggests that a monomer-FkpA/uOMP complex would associate with another FkpA monomer with nanomolar K_D value. All values reported here are for experiments conducted in 1 M urea at 20 °C. Additionally, all numerical values are indicated as negative for reactions proceedings from left to right or top to bottom.

2.6. Tables

Table 2.1. Summary of fitting for SE data on FkpA dimerization (20 mM Tris).

| <u>Temperature</u> (°C) | <u>Obligate Dimer Model</u> | | <u>Monomer <-> Dimer Model</u> | |
|----------------------------|-----------------------------|----------------------------|---|----------------------------|
| | <u>Molecular Weight</u> | <u>σ</u> | <u>K_{dim} (μM)</u> | <u>σ</u> |
| 4 | 47830 \pm 1370 | 5.26E-3 \pm 5.5E-4 | 2.46 \pm 1.46 | 5.62E-3 \pm 6.0E-4 |
| 26 | 47220 \pm 980 | 5.92E-3 \pm 9.2E-4 | 3.98 \pm 1.51 | 6.11E-3 \pm 9.8E-4 |
| 37 | 46590 \pm 690 | 5.40E-3 \pm 9.1E-4 | 4.96 \pm 1.49 | 5.80E-3 \pm 9.9E-4 |
| 40 | 45820 \pm 410 | 5.14E-3 \pm 5.2E-4 | 7.32 \pm 1.23 | 5.50E-3 \pm 4.7E-4 |

Summary of fitting output from WinNonLin v.1.06 for global fitting of FkpA sedimentation equilibrium data collected in 20 mM Tris (shown in Figure 2.1) (Johnson et al. 1981). σ indicates the standard deviation or square root of the variance for each fit. The predicted molecular weight of the FkpA dimer is 52450 kDa; because the molecular weight obtained from fitting the experimental data to the obligate dimer model is inconsistent with this predicted molecular weight, we exclude this model.

Table 2.2. Summary of fitting for SE data on FkpA dimerization (20 mM Tris, 1 M urea).

| <u>Obligate Dimer Model</u> | | | <u>Monomer <-> Dimer Model</u> | |
|-----------------------------|-------------------------|----------------------------|---|----------------------------|
| <u>Temperature</u> | | | | |
| <u>(°C)</u> | <u>Molecular Weight</u> | <u>σ</u> | <u>K_{dim} (μM)</u> | <u>σ</u> |
| 20 | 48900 \pm 580 | 5.26E-3 \pm 6.9E-4 | 1.92 \pm 0.64 | 5.15E-3 \pm 6.7E-4 |
| 37 | 41810 \pm 1220 | 7.63E-3 \pm 3.9E-4 | 24.9 \pm 6.29 | 6.33E-3 \pm 4.7E-4 |

Summary of fitting output from WinNonLin v.1.06 for global fitting of FkpA sedimentation equilibrium data collected in 20 mM Tris and 1 M urea (values shown in Figure 2.7) (Johnson et al. 1981). σ indicates the standard deviation or square root of the variance for each fit.

Table 2.3. Primers for FkpA-G28K cloning.

Primer Sequence

Forward primer GCTTATGCACTGAAAGCCTCGCTGGGTCGTTACATGG

Reverse primer CCATGTAACGACCCAGCGAGGCTTTCAGTGCATAAGC

Primers utilized for site-directed mutagenesis cloning of FkpA-G28K. Underlined codon highlights the site of the desired mutation.

**Chapter 3 – Novel Binding Mechanism for the Chaperone SurA and
unfolded OMPs**

3.1. Introduction

Unfolded or disordered proteins play a variety of critical functions in biology (Dyson and Wright 2005; Iakoucheva et al. 2002). For these unstructured proteins to perform their functions, they must first undergo accurate trafficking to ensure they arrive in their appropriate cellular environment. Chaperones and quality control systems are present in all cellular compartments to promote the efficient trafficking of unfolded client proteins, in addition to facilitating the folding of soluble proteins. Without chaperone proteins that interact with unfolded protein ensembles, some client proteins are prone to populate misfolded states and subsequently form aggregates that are potentially toxic to the cell (Plummer and Fleming 2016). Understanding how chaperones interact with unfolded client proteins will provide insight into their critical function in maintaining cellular proteostasis.

One example of chaperone-mediated biogenesis of unfolded proteins is the assembly pathway of unfolded outer membrane proteins (uOMPs) in Gram-negative bacteria. The *Escherichia coli* periplasmic chaperone system is an example of a chaperone network that specifically handles unfolded proteins to promote their folding and accurate biogenesis, which is a prerequisite for outer membrane integrity and consequent cellular survival. This network is composed of several periplasmic chaperones that interact with uOMPs to prevent misfolding and aggregation, while also promoting uOMP flux through productive folding pathways (Plummer and Fleming 2016). SurA is one of the chaperones involved this network and is known to play a critical role in uOMP trafficking, as it has been suggested to interact with the majority of OMP flux in the periplasm (Costello et al. 2016; Rizzitello, Harper, and Silhavy 2001; Sklar, Wu, Kahne, et al. 2007).

Biochemical characterization of SurA suggests this chaperone is specific for uOMPs.

SurA was first identified as a protein required for *E. coli* survival under stationary phase growth (Tormo, Almirón, and Kolter 1990). It was later shown that the SurA polypeptide is exported to the periplasm where it is a chaperone for uOMP trafficking, although it additionally contains two peptidyl-prolyl isomerase (PPIase) domains of the parvulin family (Rouviere and Gross 1996). Binding studies to synthetic peptides indicated that SurA preferentially binds to aromatic-rich sequences (Behrens-Kneip 2010; Bitto and McKay 2003, 2004; Hennecke et al. 2005). Interestingly, proline residues are not required for peptides to bind to SurA (Hennecke et al. 2005). Although these studies provide insight into the peptide sequences preferred for SurA binding, they do not give information about the interactions of SurA with its native, full-length uOMP clients.

Binding studies of SurA to its bona fide clients (i.e., uOMPs) are scarce due to the experimental difficulties of measuring binding of unfolded client proteins to a folded chaperone. The high propensity of uOMPs to aggregate in aqueous solvents complicates binding studies (Ebie Tan et al. 2010). Here we have overcome these problems and present the first measurements of interaction energies of SurA to a relevant uOMP client (e.g., uOmpA₁₇₁) under conditions that ensure the uOMP client is monomeric and the SurA chaperone is structurally intact.

Crystallographic studies of SurA hint at mechanisms for uOMP chaperone function.

The crystal structure of SurA was presented in 2002 (Bitto and McKay 2002). The N-terminal, PPIase-1, and C-terminal regions associate together to form a “core” domain; the PPIase-2 domain is connected to the “core” by two flexible linkers (25 Å in length; PDB: 1M5Y). Inspection of this structure revealed that the N/PPIase-1/C region of SurA contains an “extended crevice” that may accommodate short regions of client peptide. Indeed, later crystal

structures of SurA fragments revealed that peptides bind to this “core” domain (Xu et al. 2007). The PPIase-1 domain alone was crystallized in the presence of two aromatic rich peptides (i.e., WEYIPNV in PDB: 2PV1 and NFTLKFWDFRK in PDB: 2PV2); interestingly, in one of these structures this domain was observed to be dimeric. These structural studies provide an excellent source of knowledge on how SurA interacts with peptide clients in the context of a crystal lattice. We complement these results with solution studies to probe several previously unanswered questions, such as: what is the solution oligomerization, and likely functionally active, state of SurA? And how does SurA interact with full-length uOMP clients that are hundreds of amino acids longer than the crystallized peptides? We address these inquiries and incorporate our experimental constraints into a model that suggests how SurA binds to uOMPs and may facilitate their assembly via the OMP biogenesis pathway.

3.2. Methods

Determination of proline content and *cis/trans* isomer classification.

As SurA is known to contain two PPIase domains, we first inquired how important PPIase activity is for OMP biogenesis. To determine the extent to which OMPs require a prolyl-isomerase enzyme for assembly, we examined the proline content of the most abundant OMPs, along with the most abundant periplasmic proteins. The most abundant proteins in these classes have been previously reported and the selection for our analysis is indicated in Table 3.1 (Han, Kim, and Kim 2014; Vertommen et al. 2008). We also included the OMPs previously identified as SurA clients *in vivo* (Hennecke et al. 2005; Vertommen et al. 2009). For each selected protein, we utilized a Python script to parse the listed PDB file and enumerate the amino acid composition of each protein. The number of prolines in each protein included in our analysis is indicated in Tables 3.1 and 3.2. We have additionally plotted these values in Figure 3.1. In this figure, the dashed line indicates the average proline content of all proteins in the UniProt database (4.7%; accessed in March, 2017). We then utilized the dihedral measurement tool in Pymol to measure the backbone omega (ω) dihedral angle for all proline residues identified in our analysis. Four atoms define the ω dihedral angle: the carbonyl O from residue^{Pro-1}, the backbone C from residue^{Pro-1}, the N from the proline, and the C α from the proline. Proline residues with an ω angle of $\pm 180^\circ \pm 15^\circ$ are classified as *cis* (Table 3.1).

SurA protein was expressed and purified for analysis.

We introduced the gene of *E. coli* SurA into the pET28b vector between the Nde I and BamHI restriction sites with a C-terminal 6-Histidine tag. This construct lacks a signal sequence for export of protein to the periplasm. SurA was expressed and cells were lysed as in Chapter 2. The Histidine-tagged protein was isolated from cell lysate using a Ni Sepharose column as in

Chapter 2. Stock concentrations were determined with the theoretical extinction coefficient of $29450 \text{ M}^{-1} \text{ cm}^{-1}$ (Gill and von Hippel 1989).

SE analysis was utilized to investigate SurA oligomerization.

To determine the relevant oligomeric species of SurA, we completed analytical ultracentrifugation sedimentation equilibrium (SE) experiments (Figure 3.2). SurA was diluted into 20 mM Tris buffer (pH=8.0) and samples with $A_{280} = 0.90, 0.60,$ and 0.30 at a path length of 1.2 cm (corresponding to concentrations of 25, 17, and 8 μM respectively) were loaded into six-sector centerpieces and allowed to equilibrate at speeds of 20,000; 24,500; and 30,000 rpm in a Beckman Optima XL-A analytical ultracentrifuge with absorbance optics. Data were collected at 37 °C with radial scans ($\lambda=280 \text{ nm}$) acquired with 0.001 cm radial steps with 10 replicates. Equilibration was assessed with WinMatchv0.99 and data were subsequently trimmed using WinReEdit v.0999.0028 to regions where Beer's law applies (Johnson et al. 1981). Global fitting was completed utilizing WinNonLin v.1.06 (Johnson et al. 1981). For data analysis, we calculated reduced molecular weight values ($\sigma^{\text{Temperature}}$), partial specific values and buffer densities using Sednterp v.20130813 β (Laue et al. 1992). The values used were as follows: $\bar{v} = 0.7325 \text{ mL g}^{-1}$, $\rho = 0.9988 \text{ g mL}^{-1}$, $\eta = 1.0069 \text{ mPa}$; reduced molecular weight values were $\sigma^{20,\text{C}} = 2.26$ and $\sigma^{37,\text{C}} = 2.16$ for monomeric SurA at a rotor angular velocity (ω) of $2094.4 \text{ rad s}^{-1}$ (i.e., 20,000 rpm).

Because it is known that the periplasmic concentration of SurA may be modulated by cellular exposure to stress, we next inquired if SurA may oligomerize at higher concentrations (Dartigalongue, Missiakas, and Raina 2001). To assess the oligomeric state of SurA over a greater range of protein concentrations, we repeated the above experiment with a modified SE set-up. SurA was diluted into 20 mM Tris buffer (pH=8.0) to a final A_{280} of 1.0 at a path length of 0.3 mm (corresponding to concentration of 120 μM) and was loaded into a two-sector centerpiece

and allowed to equilibrate at speeds of 20,000; 24,500; and 30,000 rpm in a Beckman Optima XL-A analytical ultracentrifuge with absorbance optics. SE data were collected and analyzed as described above. These data are summarized in Figure 3.2B.

SANS analysis provides global structural information of macromolecules in solution.

The crystal structure of SurA suggests that the PPIase-2 domain is extended away from the core domain – we inquired if this conformation was populated in solution. To this end, we measured the radius of gyration (R_G) of SurA in solution utilizing small-angle neutron scattering (SANS). R_G is defined as the root-mean-squared distance of all atoms from the macromolecular center of mass (Jacques and Trewhella 2010); for proteins, this value will depend on the shape or distribution of atoms about the center of mass.

In SANS experiments, neutrons are scattered by macromolecules in solution to yield a scattering pattern that provides structural information about the molecules. The ability of any particular atom to scatter neutrons is represented by its scattering length (b in 10^{-12} cm) and the scattering lengths of several common atoms are given in Table 3.3 (Harroun, Wignall, and Katsaras 2006). Importantly, the b values for hydrogen and deuterium are opposite in sign, which allows for differential scattering of macromolecules with varying deuterium composition. This is a unique feature of SANS experiments, as these two isotopes scatter x-rays identically (Table 2.3). The ability of an entire macromolecule to scatter neutrons, termed the scattering length density (i.e., $\rho(r)$ in 10^{10} cm⁻²), is defined as the sum of coherent scattering lengths over all atoms within a given volume, V (cm³), normalized by δV :

$$\rho(r)\delta V = \sum b_i \quad (\text{Equation 3.1})$$

where:

$$b_{\text{neutron}} = \sum b_i + (n_H - n_{\text{Hex}})f_{\text{deut}}(b_D - b_H) + n_{\text{Hex}}f_{\text{excb}}f_{\text{D2O}}(b_D - b_H) \quad (\text{Equation 3.2})$$

b_i indicates a sum over all non-hydrogen and non-deuterium atoms. n_H and n_{Hex} are the number of total hydrogens and exchangeable hydrogens in the macromolecule, respectively. f_{deut} describes the deuterium content of the macromolecule; f_{exch} is the fraction of exchangeable protons; and f_{D_2O} is the fraction of D_2O in the solvent. The amplitude of the scattered wave, or structure factor (S), is given as:

$$S(Q) = \sum b_i \exp(iQ \cdot r) \quad (\text{Equation 3.3})$$

where this summation is over all atoms in a macromolecule and orientations, Q is the scattering vector, and r describes the location of the detector from a given atom. Measured intensity (I in cm^{-1}) is related to structure factor squared:

$$I(Q) \propto |S(Q)|^2 \quad (\text{Equation 3.4})$$

Another important parameter in SANS experiments is contrast (ρ in 10^{10} cm^{-2}). Contrast (ρ_C) is defined as the difference between the scattering length density of the macromolecule ($\bar{\rho}_m$) and the solvent (ρ_s):

$$\rho_C = \bar{\rho}_m - \rho_s \quad (\text{Equation 3.5})$$

An interesting consequence of the hydrogen/deuterium scattering lengths differing in sign is that the scattering length densities of H_2O ($-0.17 \times 10^{-12} \text{ cm}$) and D_2O ($1.92 \times 10^{-12} \text{ cm}$) are quite distinct. The scattering length density of D_2O is larger than most biological molecules, while that of H_2O is smaller than most biological molecules; therefore an appropriate mix of H_2O and D_2O can match the scattering length density of any biological molecule. This type of experiment is termed contrast matching and yields a scattering pattern with minimal contribution of the contrast matched (for a given component: $\rho_C = 0$, $S(Q) = 0$, $I(Q) = 0$). Although these types of experiments are not useful for analysis of single component systems (e.g., apo-SurA), we utilize them later to investigate two component systems (i.e., SurA in complex with uOMP).

All scattering experiments were collected in collaboration with Dr. Susan Kreuger at the National Institute of Standards and Technologies Center for Neutron Research (Gaithersburg, MD) as previously described (Zaccai et al. 2015). All scattering data presented here were collected on the NG3 30-m SANS Instrument (NIST). The $\lambda = 6 \text{ \AA}$ ($\Delta\lambda / \lambda = 0.15$) neutron beam was utilized to collect scattering profiles from all samples described here on a 2D position-sensitive detector (64 cm x 64 cm) with 128 x 128 pixels at resolution of 0.5 cm pixel⁻¹. For data processing, raw counts were normalized to the common monitor count and normalized to the incident beam flux at every pixel for absolute scaling. Radial averaging was utilized to produce scattering profiles. Sample-to-detector distances of 5.0 m and 1.5 m were used to cover range of $0.01 \text{ \AA}^{-1} < q < 0.4 \text{ \AA}^{-1}$.

For SANS experiments on apo-SurA, we prepared the SurA construct described above with a slightly modified protocol. After expression and purification, we further purified SurA by gel-filtration in 20 mM Tris and 200 mM NaCl (pH=8.0, GF buffer). SurA (40 μM) was injected onto a Superdex-200 10/300 GL (GE Healthcare Life Sciences) gel-filtration column in GF buffer with a flow rate of 0.6 mL/min. Fractions containing SurA were pooled and buffer exchanged into GF buffer containing 98% D₂O via centrifugation in an Amicon filter (Millipore) with a 10 kDa MWCO. For structural characterization of apo-SurA, we collected SANS datasets of protonated SurA in the presence of buffer containing 98% D₂O. Under these conditions, we expect high contrast between SurA and buffer and therefore appreciable neutron scattering. We collected scattering profiles of apo-SurA at two concentrations (1 and 3 mg/mL, corresponding to concentrations of 20 and 60 μM respectively). Data sets are shown in Figure 3.3, and fitting is summarized in Table 3.4.

For analysis of SANS datasets, we utilize the Guinier approximation to obtain two fit parameters: the macromolecule R_G (\AA) and the intensity at a scattering distance of 0 (i.e., $I(0)$ in cm^{-1}). This approximation estimates the intensity in low q (\AA^{-1}) regions as follows:

$$I(q) \sim I(0) \cdot \exp[-(1/3) \cdot R_G^2 \cdot q^2] \quad (\text{Equation 3.6})$$

$$\ln[I(q)] \sim \ln[I(0)] - (1/3) \cdot R_G^2 \cdot q^2 \quad (\text{Equation 3.7})$$

Therefore, linear regression of $\ln[I(q)]$ vs. q^2 yields information in the slope (i.e., R_G^2) and the intercept (i.e., $I(0)$). $I(0)$ is also calculated due to its known dependence on macromolecular concentration (C in mg mL^{-1}), contrast ($\Delta\rho$ in cm^{-2}), specific volume (\bar{v} in $\text{cm}^3 \text{g}^{-1}$), and molecular weight (M in kDa) (Sarachan, Curtis, and Krueger 2013):

$$I(0) = C \cdot \Delta\rho^2 \cdot \bar{v}^2 \cdot M \cdot N_A^{-1} \quad (\text{Equation 3.8})$$

N_A in the above formula is Avogadro's number. For each Guinier fit, we compare the fitted value of $I(0)$ from Equation 5.7 to the calculated value from Equation 5.8 for each experiment to ensure that samples contain homogeneous, monomeric species (Table 3.4).

Biochemical crosslinking was used to map the interaction interface between SurA and OMP clients.

We next studied how SurA interacts with its unstructured binding partners – unfolded OMP proteins. We utilized a biochemical approach to examine the interactions between uOMP clients and SurA. We incorporated an unnatural amino acid into the SurA polypeptide chain using amber suppression (Best 2009; Peeler and Mehl 2012). Briefly, we introduced the pDule2 plasmid (gift from the Sondermann Lab at Cornell University) into a bacterial expression strain – this plasmid encodes for the tRNA_{UAG} synthetase (under constitutive active expression) that incorporates *p*-azido-Phenylalanine (*p*AF) at the non-native TAG stop codon (Figure 3.4 and Figure 3.5). We also introduced a plasmid containing the SurA gene (pET28b) with a TAG stop

codon incorporated at a specific position (Table 3.5). Stop codons were cloned into the coding sequence of SurA either by site-directed mutagenesis or by the Berkeley QB3 MacroLab ‘Round-the-Horn’ cloning method. After induction of the SurA gene by addition of IPTG to the growth media, *pAF* is incorporated into the growing polypeptide chain by the engineered synthetase. This unnatural amino acid contains a reactive azide group that nonspecifically crosslinks to atoms within 3 to 4 Å upon exposure to UV light (Hagan and Staros 1984; Reddington et al. 2013). All SurA_{*pAF*} variants were expressed purified similarly to WT-SurA with slight modifications. One hour after inoculation of 500 mL bacterial cultures, *pAF* was added to a final concentration of 10 mM to the growth media. Full-length SurA_{*pAF*} variants were separated from truncation products by Ni Sepharose High Performance bench-top column as described above.

We used this library of SurA-*pAF* variants to understand which structural regions of the SurA chaperone are involved with binding to uOMP clients. 25 µM of each SurA *pAF* variant was mixed with 5 µM uOmpA₁₇₁ in 20 mM Tris (pH=8.0) and 1 M Urea in a 96-well plate. Mixtures were then irradiated with UV light (λ=254 nm) for 5 minutes using a Spectroline MiniMax UV Lamp (Fisher #11-992-662). Aliquots were taken for SDS-PAGE analysis both before and after exposure to UV light. These samples were subjected to electrophoresis using a 12% precast gel (Mini-PROTEAN TGX, Bio-Rad) at a constant voltage of 150 mV for 55 minutes at room-temperature (Figure 3.5B). Densitometry analysis on the loss of density of the uOmpA₁₇₁ band was utilized to quantitate crosslinking efficiency as follows:

$$\text{Efficiency} = [(\delta_{\text{OMP}}^{\text{pre}} - \delta_{\text{OMP}}^{\text{post}}) / \delta_{\text{OMP}}^{\text{pre}}] * 100 \quad (\text{Equation 3.9})$$

where δ indicates the band density of uOmpA₁₇₁. Crosslinking experiments were repeated with another 8 stranded β -barrel OMP, uOmpX and a larger 12-stranded β -barrel, uOmpLA (Figure

3.6). We have mapped these efficiencies onto the structure of SurA in Figure 3.7 to illustrate crosslinking hot-spots.

SANS was used to interrogate a SurA-uOMP complex.

Once we identified positions on SurA that have high crosslinking efficiencies to uOMP clients, we investigated the structural properties of this complex. We scaled up the crosslinking reaction for uOmpA₁₇₁ and SurA_{pAF}¹⁰⁵ and purified this complex by gel-filtration, using the protocol described above for apo-SurA. We collected SANS on this complex in 98% D₂O gel-filtration buffer with experimental set-up similar to that described above for apo-SurA. Guinier fitting this scattering profile yields to R_G of the entire complex (Figure 3.9A and 3.9D, Table 3.4).

To gain more structural insight into the conformation of the individual protein components in the complex, we utilized isotope labeling to modulate the contrast of the uOmpA₁₇₁ client. In Figure 3.8A, we plot the calculated scattering length density of protonated SurA (green), deuterated-OmpA₁₇₁ (gray dashed), and GF buffer (black dashed). Panel B shows the mass weighted contribution to total scattering of each component. Near the contrast match point of the protonated SurA (i.e., 43% D₂O), the intensity of total scattering originates primarily from the uOmpA₁₇₁ in the complex. This is only true for a complex composed of a protonated chaperone and deuterated uOMP client. Therefore deuterium was incorporated into the uOmpA₁₇₁ protein as previously described (d-uOmpA₁₇₁) (Zaccai et al. 2015). Briefly, we expressed d-uOmpA₁₇₁ to inclusion bodies in minimal M9 growth media containing D₂O and deuterated-glucose. To determine the extent of deuteration, which is a required parameter for contrast calculations, we utilized proton NMR (with the assistance of Dr. Ananya Majumdar and Henry J. Lessen). We collected NMR spectrum for preparations of both protonated and deuterated uOmpA₁₇₁ and estimated the loss in intensity of methyl- and methylene- chemical

groups upon deuteration to be 80% of total peak area. Therefore, we assigned the extent of deuteration of d-uOmpA₁₇₁ for SANS calculations as 80%.

SANS datasets on the SurA_{pAF}¹⁰⁵ variant crosslinked to d-uOmpA₁₇₁ were collected as described above in 0% and 30% D₂O GF buffer (Figure 3.9A-3.9C). We attempted to collect scattering profiles in 80% and 98% D₂O of this complex but the I(0) values from Guinier fitting indicated that these samples contained aggregates. It is known that exposure to high compositions of D₂O may promote self-association and aggregation of particularly hydrophobic proteins (Lee and Berns 1968).

Experimental R_G values were integrated into a SurA-OMP complex model.

We incorporated the R_G information from the SurA-uOMP SANS experiments as constraints for the construction of a model for this complex. We initially used torsional angle MD (TAMD) to construct an ensemble of uOmpA₁₇₁ conformations consistent with experimental R_G values (Zhang et al. 2017). We began with previously published conformations of OmpA₁₇₁ and constrained these conformations to states with an R_G value of 43 Å (trajectories provided by S. Kreuger) (Zaccai et al. 2015). For computational treatment of SurA, we assume that the chaperone conformation does not change appreciably upon complex formation (i.e., R_G = 33 Å). To form the complex, we manually aligned the extended conformation of uOmpA₁₇₁ with the crystal structure of SurA and performed constrained MD simulations. As above, we utilized CHARMM-GUI to construct this MD system of SurA with uOmpA₁₇₁ in a 156 x 156 x 156 Å box with 113,652 explicit waters and 200 mM NaCl. Constrained simulations were run for ~ 100 ns after the implementation of constraints at 25 °C. We utilized the colvar package to implement harmonic potential constraints on the R_G values of SurA and uOmpA₁₇₁ as follows: for SurA, the well potential was defined as 1.0, with lower and upper boundaries defined as 28 and 38 Å respectively. Lower and upper walls were defined as 32 and 34 Å respectively with

both wall constants set as 5.0. For uOmpA₁₇₁, the well potential was defined as 1.0, with lower and upper boundaries defined as 38 and 48 Å respectively. Lower and upper walls were defined as 42 and 44 Å respectively with both wall constants set as 5.0. No constraints were placed on the entire complex R_G value (Figure 3.10A). A representative complex conformer is shown in Figure 3.10B. To compare the structural properties of this conformation with our experimental scattering profiles, we calculated the theoretical scattering data for this complex under the experimental conditions, as described above using SasCalc (Sarachan, Curtis, and Krueger 2013; Watson and Curtis 2013). Comparisons of these theoretical scattering curves with our experimentally determined ones are shown in Figure 3.10C-E.

SurA-OMP binding was quantitated by sedimentation velocity experiments.

The above studies provide a structural model of a SurA-uOMP complex, but give us little quantitative understanding of the affinity for which these two proteins interact. To supplement our structural investigations, we examined the thermodynamics of binding between SurA and uOmpA₁₇₁. Previous studies have utilized intrinsic tryptophan (W) fluorescence as an observable to monitor binding of uOMP clients to chaperones (Moon et al. 2013). However, both SurA and OmpA₁₇₁ contain multiple Trp residues (4 and 5, respectively), which would complicate interpretation of fluorescence-detected binding. Instead, we used an absorbance-based observable by monitoring association of SurA and uOmpA₁₇₁ by sedimentation velocity (SV) analytical ultracentrifugation experiments. To reduce the relative contribution of SurA to the observed signal, we replaced all W residues in SurA with F (i.e., SurA-W233F/W343F/W375F/W413F, or SurA^{-4W}). We used site-directed mutagenesis and the primers outlined in Table 3.6 to clone this construct into the pET28b vector.

We determined buffer conditions that would be conducive for experimentally analyzing the association between SurA^{-4W} and uOmpA₁₇₁. Because urea is required to maintain uOMPs in

their monomeric conformations, we determined the range of urea concentrations under which SurA^{-4W} will retain its native conformation. To this end, we measured the degree of secondary structure of SurA^{-4W} at varying concentrations of urea by circular dichroism (CD) (Figure 3.11A). All CD measurements were collected in an Aviv CD spectrometer, Model 410 (Aviv Biomedical) in Hellma cuvettes with a path length of 1 cm. SurA^{-4W} was diluted to a final concentration of 1 μ M into 20 mM Tris (pH=8.0) with varying concentrations of urea. At each urea concentration after equilibration (i.e., \sim 1 week of incubation at room-temperature), we measured the CD signal at 220 nm of each sample using the kinetics experiment type. We monitored the signal for 90 seconds using a 1 sec interval and 4-second time constant. We averaged the signal over this time course and reported values reflect this time-averaged signal. At every urea concentration, we also collected the CD signal from a buffer only sample and subtracted this from the protein sample signal for buffer corrected CD signals reported in Figure 3.11A. We also confirmed that uOmpA₁₇₁ is monomeric under the buffer conditions for binding assays (i.e., 20 mM Tris and 1.5 M urea) by sedimentation velocity (SV) analytical ultracentrifugation (Figure 3.11B); this finding agrees with previously reported results (Danoff and Fleming 2011; Ebie Tan et al. 2010).

We used SV to determine the weight average sedimentation coefficient as an observable to monitor association of SurA^{-4W} and uOmpA₁₇₁ (Figure 3.11C). SurA^{-4W} was diluted into 20 mM Tris and 1.5 M urea to final concentrations ranging from 1 to 100 μ M in the presence of 5 μ M uOmpA₁₇₁. 400 μ L of sample was then loaded into a two-sector SV cell. Experiments were performed in an An-Ti60 rotor at 50,000 rpm with radial scans at 280 nm were acquired with 0.003 cm radial steps in continuous mode with zero time interval between scans. SV experiments were conducted at 20 °C with a Beckman Optima XL-A analytical ultracentrifuge using absorbance optics. All data were analyzed in DCDT+ v.2.4.2 (Philo 2006).

We also simulated SV data for this association reaction between SurA^{-4W} and uOmpA₁₇₁ using SEDANAL v6.01.6926 (Figure 3.12) (Stafford and Sherwood 2004). For these simulations, we consider two mixtures of SurA^{-4W} and uOmpA₁₇₁: 1 μ M SurA^{-4W}/5 μ M uOmpA₁₇₁ and 10 μ M SurA^{-4W}/5 μ M uOmpA₁₇₁. For each mixture, our simulations yield a predicted weight average sedimentation coefficient as a function of input equilibrium dissociation constant. For these simulations, we used the following input parameters: for SurA^{-4W}, MW = 46118 g mol⁻¹, sedimentation coefficient = 2.70 Svedbergs (calculated from the crystal structure) (García De La Torre, Huertas, and Carrasco 2000; Ortega, Amorós, and García De La Torre 2011), ρ increment (defined as $1 - \bar{v}\rho$) = 0.251, ϵ_{mass} = 0.162 L cm⁻¹ g⁻¹. For uOmpA₁₇₁, MW = 18875 g mol⁻¹, sedimentation coefficient = 1.40 Svedbergs (Danoff and Fleming 2011), ρ increment = 0.266, ϵ_{mass} = 2.483 L cm⁻¹ g⁻¹. For the SurA^{-4W}-uOmpA₁₇₁ complex, MW = 64993 g mol⁻¹, sedimentation coefficient = 3.10 Svedbergs (calculated from structural model shown in Figure 3.10B), ρ increment = 0.256, ϵ_{mass} = 0.836 L cm⁻¹ g⁻¹.

3.3. Results

SurA is monomeric at physiological concentrations.

To begin our investigation into the function of SurA, we initially determined the oligomerization state of this uOMP chaperone using SE experiments. Other periplasmic chaperones are known to function as higher order oligomers (Plummer and Fleming 2016). For SurA, this question had been previously addressed with crystallography. It was determined that both the PPIase-1 domain of SurA and a SurA fragment lacking the PPIase-2 domain in complex with peptide crystallized in dimeric conformations (PDB: 2PV3) (Xu et al. 2007). This finding raised the possibility that the full-length SurA protein may exist in both monomeric and dimeric states. We found that in a concentration range of 10 to 30 μM , the SE profiles of SurA are well described by a single-ideal species model that correctly recapitulates the molecular weight of a SurA monomer (Figure 3.2A). Because this experimental concentration range corresponds with the anticipated concentration of SurA in the periplasm (20 μM) (Arike et al. 2012; Masuda et al. 2009), we suggest that SurA is a monomer under biological conditions.

SurA has additionally been implicated in the σ^E bacterial stress response and is one of the chaperone genes that is upregulated by this transcriptional response to handle stress conditions in *E. coli* (Dartigalongue, Missiakas, and Raina 2001). To determine whether SurA may form higher order oligomers at higher concentrations, we repeated our SE experiments at 120 μM SurA. At this concentration, the single-ideal species model poorly fits the SE data (red dashed curves and red residuals in Figure 3.2B). Instead, these data are better fit with a monomer-dimer model and this fitting yields an equilibrium dissociation constant of 1160 ± 60 μM at 37 °C. Figure 3.2B depicts the absorbance profiles of both the monomeric and dimeric species for this representative dataset in blue and green, respectively. This representation shows

that the population of SurA dimer under these conditions is small relative to the monomer population.

We have incorporated the dimerization equilibrium data obtained from the experiment presented in Figure 3.2B into a species plot shown in Figure 3.2C. The monomer and dimer species populations are indicated as blue and green curves, respectively, with the experimentally observable concentration range shown in bold. The dashed vertical line indicates the anticipated periplasmic concentration of SurA under normal bacterial growth conditions. At 20 μM , the population of SurA monomer and dimer is expected to be 97% and 3% respectively. If SurA were upregulated 10-fold to a total concentration of 200 μM , this population should shift to 78% monomer and 22% dimer. At 2 mM total SurA concentration, we anticipate SurA to exist as 40% monomer and 60% dimer.

SurA monomer has solution properties similar to crystallized conformation.

We investigated the solution structure of the SurA monomer by SANS at two concentrations that are well below the concentrations at which dimer population is significant. From Guinier fitting the SANS profiles for apo-SurA presented in Figure 3.3A, we obtain an R_G for the SurA monomer in solution of $33.3 \pm 0.6 \text{ \AA}$ (Figures 3.3B-C, Table 3.4). This value is similar to the calculated value from the crystal structure using HydroPro (i.e., 32.6 \AA) (García De La Torre, Huertas, and Carrasco 2000; Ortega, Amorós, and García De La Torre 2011). These results suggest that the solution SurA monomer behaves on average like the crystallized conformation.

SurA interacts with uOMP clients with a delocalized interface.

Our findings suggest that crystal structure of SurA is similar to the ensemble present in solution – this finding is particularly puzzling as we know that SurA functions as a chaperone by

binding to unfolded OMP clients. There are no obvious binding sites for an unstructured partner on this expanded structure of SurA. To determine which regions of SurA are involved in uOMP interactions, we incorporated a photoactivatable unnatural amino acid (*p*AF) at 36 surface-exposed positions on SurA (Figure 3.4). We then mixed each of these SurA_{*p*AF} variants with a representative uOMP client, uOmpA₁₇₁, and measured the efficiency of crosslinking for each variant to a uOMP client. OmpA is a known client of SurA *in vivo* and these interactions are exclusively between the transmembrane region of OmpA (i.e., OmpA₁₇₁) and SurA (Hennecke et al. 2005; Vertommen et al. 2009), therefore we utilize uOmpA₁₇₁ in our experiments. Crosslinking efficiencies are highest for tested sites in the N-terminal and PPIase-1 regions of SurA (Figures 3.5 and 3.6A). Residues 59, 105, 245, and 260 in particular exhibit high crosslinking efficiencies. Lower efficiencies are observed for tested sites in the PPIase-2 and C-terminal regions.

Because SurA has been suggested to interact with clients of varying sequences and lengths (Hennecke et al. 2005; Vertommen et al. 2009), we repeated the above experiment with two other uOMP clients. OmpX and OmpLA are 8- and 12-stranded β -barrel OMPs, respectively, that behave as unfolded monomers under our experimental conditions (Ebie Tan et al. 2010). Binding efficiencies for OmpX are similar in magnitude to those of uOmpA₁₇₁ (Figure 3.6B), although those for uOmpLA are lower. This may indicate that OmpLA binds to SurA weaker than uOmpA₁₇₁ and uOmpX.

uOMP exists in an expanded conformation when in complex with SurA.

These crosslinking experiments provide novel insight into the binding interface on SurA, however they give little structural information on the conformation of the uOMP client in these complexes. To complement our crosslinking experiments, we collected SANS scattering profiles on a fully protonated SurA-uOMP complex in order to quantify the R_G of the entire complex.

We purified a crosslinked complex composed of SurA_{pAF}¹⁰⁵ and uOmpA₁₇₁ and collected the scattering profile of this complex in 98% D₂O to maximize the contrast and subsequent intensity for complex scattering (Figure 3.9A, gold). Guinier fitting of this data yields an R_G value of 38 Å for the entire complex.

As discussed in the Methods section above, varying the deuterium composition of the uOMP client and buffer allows for selective visualization of individual components in the complex. In Figure 3.8, we highlight the importance of this; for a complex composed of protonated SurA and deuterated uOmpA₁₇₁, the contribution of each protein to the total scattering will depend on the buffer D₂O content. Under buffer conditions that contrast match the protonated chaperone, the scattering primarily originates from the deuterated OMP in the complex. We take advantage of this property of neutron scattering by collecting scattering profiles of a complex composed of protonated-SurA_{pAF}¹⁰⁵ crosslinked to deuterated-uOmpA₁₇₁. We collected datasets under two buffer conditions: 0% and 30% D₂O buffer. At each of these conditions, the individual complex components contribute differentially to the total scattering intensity. At 0% buffer, the chaperone and client OMP contribute equally to the total intensity (Figure 3.8B.) Under the latter experimental conditions, the total scattering intensity of a complex composed for SurA_{pAF}¹⁰⁵ - deuterated-uOmpA₁₇₁ originates from the two components with 15% coming from the protonated-SurA and 85% due to the deuterated-uOmpA₁₇₁ (Figure 3.8B). Guinier fitting of data collected under these conditions yields an R_G value of 40 Å. Because the scattering is dominated by the uOmpA₁₇₁ component, we utilize this R_G value as an estimate for the R_G of uOmpA₁₇₁ in complex with SurA.

Constrained MD simulations yield SurA-uOMP complex structures consistent with experimental results.

To construct a model for the SurA-uOmpA₁₇₁ complex, we combined constrained TAMD and MD simulations. TAMD provides an efficient method to explore vast conformational space by using large time steps to sample backbone torsion angles, and we use this technique to produce conformational ensembles of uOmpA₁₇₁ (Zhang et al. 2017). To better understand the molecular details of how this uOmpA₁₇₁ interacts with SurA, we use traditional all-atom MD simulations. We simulated SurA in complex with uOmpA₁₇₁ and implemented constraints on the R_G values of SurA and uOmpA₁₇₁. These simulations produced conformations that exhibit R_G values consistent with those we have measured (Figure 3.10A). An example conformation is shown in Figure 3.10B. For the R_G values of SurA and the uOmpA₁₇₁ to be 33 and 43 Å, respectively, the uOmpA₁₇₁ must be expanded and extend away from SurA.

We can further assess the validity of this SurA-uOmpA₁₇₁ model by comparing its expected SANS curve to our experimental data. We utilized the NIST SasCalc server to predict the scattering curve of this example complex conformation under each condition that we have collected experimental SANS datasets (Figure 3.10C-E) (Sarachan, Curtis, and Krueger 2013). These predicted curves shown in Figure 3.10B are in black with the experimental data shown in purple, green, and gold in Panels C, D, and E respectively. These calculated curves agree well with the experimental results indicated for each panel.

We note that the conformation shown in Figure 3.10B represents one structural model that is consistent with our results. An inherent limitation to SANS is that we obtain low-resolution constraints for structural modeling (i.e., component and complex R_G values). While future work involves exploring other modeling techniques to sample conformational space to

yield complex structures compatible with our data, the representative model is the best model that reproduces our SANS dataset discovered to date.

SurA binds to uOMP client with a K_D in the micromolar range.

Previous studies have aimed to estimate the binding affinity of SurA to short peptides or OMP clients using non-equilibrium phage display assays (Bitto and McKay 2003, 2004). The use of non-native clients and non-equilibrium conditions precludes the interpretation of these measurements as true binding affinities. Here we quantify the binding of SurA to a native, monomeric uOMP client. One important consideration for using a native OMP client is that these experiments require the presence of urea to prevent the self-association of the uOMP; however, high concentrations of denaturant will cause unfolding of the chaperone protein. We have carefully chosen experimental conditions under which the chaperone is folded and the OMP client is unfolded and monomeric (Figure 3.11A-B). For these experiments, we use a variant of SurA (i.e., SurA^{-4W}) to minimize the convolution of our observable with signal contributions from the free chaperone. This variant is likely still able to interact with uOMP clients in a native manner as our crosslinking studies indicate that all four native Trp residues in SurA crosslink to uOMP clients with low efficiencies (Figure 3.6).

The weight average sedimentation coefficient for mixtures of SurA^{-4W} and uOmpA₁₇₁ as a function of [SurA^{-4W}] are shown for a representative binding experiment in Figure 3.11C. Globally fitting three experiments individually to a binding model yields a K_D of $17 \mu\text{M} \pm 4 \mu\text{M}$. To complement these experimental data, we simulated SV data for association reactions of SurA^{-4W} and uOmpA₁₇₁ with varying K_D values (Figure 3.12). We performed simulations for two different reaction mixture concentrations (i.e., $1 \mu\text{M}$ SurA^{-4W} and $5 \mu\text{M}$ uOmpA₁₇₁ in Panels A/B and $10 \mu\text{M}$ SurA^{-4W} and $5 \mu\text{M}$ uOmpA₁₇₁ in Panels C/D). These simulations require the

specification of the sedimentation coefficient of the SurA^{-4W}- uOmpA₁₇₁ complex. Due to our prior structural investigation and modeling, we are able to calculate that parameter for the complex presented in Figure 3.10B (i.e., 3.1 S). As shown in Figure 3.12, these simulations agree with our SV experimental data (Figure 3.11) and suggest that K_D values in the low to mid micromolar range are consistent with our experimental results.

3.4. Discussion

SurA is a dedicated chaperone for uOMP biogenesis.

The periplasmic chaperone network of *E. coli* is composed of several chaperones that traffic uOMPs through this cellular compartment. Of these chaperones, several have been suggested to be bifunctional: DegP functions as both a protease and chaperone; and FkpA exhibits both prolyl-isomerase and chaperone activity (Bothmann and Pluckthun 2000; Ge, Lyu, et al. 2014; Ge, Wang, et al. 2014a; Misra, Castilokeller, and Deng 2000). In terms of PPIase activity, FkpA has a catalytic efficiency that is approximately 100-fold greater than that of SurA (Behrens et al. 2001). Coupled with the observation that OMPs rarely contain *cis*-prolines that require isomerization prior to uOMP folding, we suspect that SurA is unlikely to be the periplasmic workhorse for PPIase activity (Figure 3.1, Tables 3.1-3.2). Instead, SurA may function solely as a chaperone for uOMP trafficking in the periplasm.

This suggestion begs the question: what is the function of the two parvulin domains of SurA if they are not required for prolyl-isomerization of client proteins? One recent suggestion is that PPIase-2 is necessary to modulate the transition between the “open” and “closed” functionally-relevant conformations of SurA (Soltes et al. 2016). However, the importance of PPIase-2 is refuted by the finding that PPIase-2 is not required for *in vivo* complementation of Δ *surA* phenotype; therefore, we suggest that this structural transition is likely not required for SurA function *in vivo* (Behrens et al. 2001). Although PPIase-2 is dispensable for SurA function, PPIase-1 is likely required for structural integrity of the N/PPIase-1/C terminal region. This structural unit has been reported to be responsible for the chaperone function of SurA (Behrens et al. 2001). Our studies support this as we find that this domain exhibits high crosslinking efficiencies for uOMPs (Figure 3.6).

SurA exhibits unique oligomerization properties and uOMP binding mechanism.

Other periplasmic chaperones are known to function as higher order oligomers: FkpA as a dimer, Skp as a trimer, and DegP as a trimer/hexamer (Plummer and Fleming 2016). Unlike these chaperones, we have discovered that SurA is monomeric under our experimental conditions and under physiological concentrations (Figure 3.2). Although our SE experiments were completed in the absence of uOMP client, our crosslinking data additionally support the interpretation that SurA interacts with uOmpA₁₇₁ in a 1 SurA: 1 uOMP stoichiometric manner (Figure 3.5B). Our results suggest that SurA is monomeric and does not utilize a mechanism for uOMP binding that involves oligomerization, at least for interactions with uOmpA₁₇₁.

Another key difference between SurA-uOMP interactions and other chaperones is found in the varying strengths of these interactions. We find the SurA binds to uOmpA₁₇₁ with a dissociation constant in the micromolar range (Figures 3.11 and 3.12). This K_D is similar in magnitude to previously reported measurements for binding of SurA to aromatic-rich peptides or OmpF₃₃₉ (Bitto and McKay 2003, 2004). This value is 1000-fold lower than the previously reported constants for binding of uOMP clients to DegP, Skp, or FkpA (Ge, Lyu, et al. 2014; S. Wu et al. 2011). Taken together, we suggest that SurA interacts with uOMP clients significantly weaker than other periplasmic chaperones. This seems paradoxical as SurA has been identified as the chaperone that handles most of the uOMP flux through the periplasm (Costello et al. 2016; Sklar, Wu, Kahne, et al. 2007). However, computational studies have shown that the periplasmic concentrations of chaperones and uOMPs are poised to allow for significant population of SurA-uOMP complexes. This stems from the balance of kinetic and thermodynamic partitioning between various uOMP species in the periplasm and is discussed at length in Chapter 5 (Costello et al. 2016).

The relatively weak binding of uOMPs to SurA compared to other chaperone-uOMP interactions may be a result of the difference in structural mechanism by which SurA interacts with uOMPs. Other chaperones are known to encapsulate uOMPs in internal cavities to physically shield them from the aqueous solvent or self-association reactions (Plummer and Fleming 2016) (Figure 3.13). In contrast, using SANS and biochemical crosslinking, we have discovered that SurA binds to expanded uOMP clients with a delocalized interface primarily located in the N-terminal and PPIase-1 regions. This type of delocalized interface between chaperones and unstructured binding partners has been recently reported for other chaperone systems (Horowitz et al. 2016; Huang et al. 2016). Taken together, our findings suggest that the uOMP client is expanded around SurA, essentially encapsulating SurA, whereas other chaperones enclose uOMP clients.

Structural model of SurA-uOMP complex suggests how SurA may facilitate uOMP folding in coordination with the BAM complex.

Of the periplasmic chaperones, only SurA has been crosslinked with the OM-localized BAM complex *in vivo*. For this reason, SurA is thought to play an active role in the uOMP folding pathway (Sklar, Wu, Kahne, et al. 2007; Wang et al. 2016). Complementary *in vitro* studies have also demonstrated that SurA promotes OMP folding, whereas other chaperones simply limit the formation of off-folding-pathway species (Thoma et al. 2015). Our structural model of the SurA-uOMP complex may explain these findings. Because the uOMP is expanded when in complex with SurA, significant regions of this client are extended away from the SurA chaperone. This means that the uOMP client may interact with both SurA and the BAM complex simultaneously (Figure 3.14). In contrast, this type of ternary complex is unlikely to form between DegP-uOMP or Skp-uOMP complexes as the uOMP is encapsulated with the chaperone-oligomeric cage (Figure 3.13).

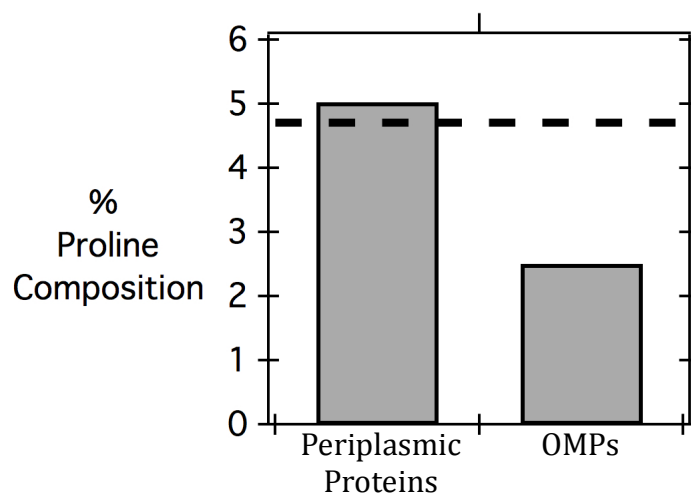
One important point for consideration is that the uOMP modeled into our SurA-uOMP complex may differ only slightly from uOMP conformations that would be sampled in the absence of SurA. Indeed, it has been shown that uOMPs sample on-folding-pathway conformations and can fold into bilayers in the absence of chaperones (Burgess et al. 2008; Gessmann et al. 2014). Moreover, the presence of SurA accelerates this process *in vitro* (Hagan and Kahne 2011; Hagan, Kim, and Kahne 2010). Together these observations suggest that SurA interacts with uOMPs in a way that slightly modulates the conformational ensemble of uOMPs to promote uOMP *in vitro* folding. Interestingly, it was recently shown that SurA is only required to accelerate *in vivo* folding of uOMPs by a factor of 10 to reproduce previously published phenotypes (Costello et al. 2016). Such a modest acceleration may result from the slight conformational bias imparted by SurA both *in vitro* and *in vivo* on the uOMP conformational ensemble.

Moving Forward: Expanding our understanding of how SurA accommodates uOMPs.

We have presented data that SurA handles uOMP clients via weak binding and a delocalized interface to promote their assembly *in vivo*. We suggest the theme of delocalized interactions between chaperones and unfolded client proteins is likely a common mechanism that chaperones utilize to modulate the folding trajectories of unstructured clients, as it has been proposed for several chaperone complexes (Horowitz et al. 2016; Huang et al. 2016). Moving forward, we aim to expand upon this understanding of SurA-uOMP interactions by investigating how SurA binds to other uOMP clients, as it is known to interact with several uOMP clients *in vivo* (Vertommen et al. 2009). It will be interesting to see how chaperone promiscuity relates to binding affinity and structural accommodation of uOMP clients.

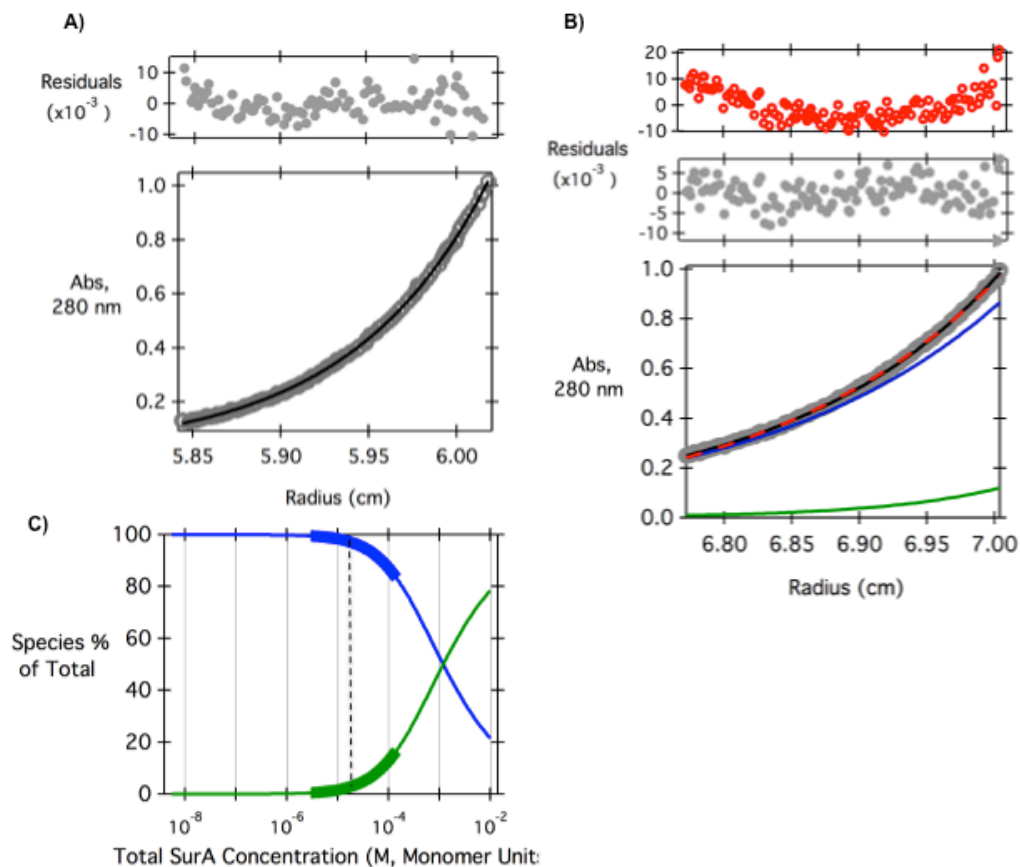
3.5. Figures

Figure 3.1. Analysis of Proline content for abundant periplasmic proteins and OMPs.



OMP sequences typically contain fewer prolines than periplasmic proteins and soluble proteins. Sequences of the most abundant OMP and periplasmic protein sequences were analyzed for proline content (Table 3.1) and are plotted above. The dashed horizontal line indicates the average proline content of all proteins in the UniProt database.

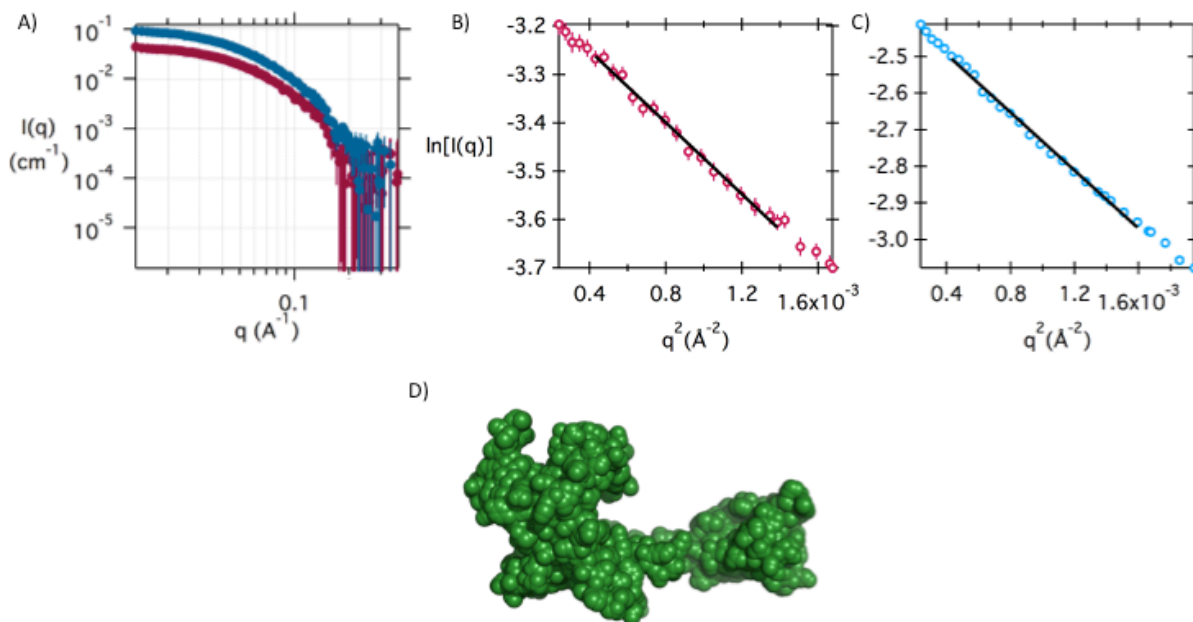
Figure 3.2. SE analysis of SurA at varying concentrations.



SurA is predominantly monomeric in solution at physiological concentrations and dimerizes with a dissociation constant in the millimolar range. Panel A shows a representative SE dataset collected for SurA at a total concentration of 30 μM . These data are well described by a single-ideal species model, which yields the molecular weight of SurA to be 43 ± 2 kDa, which agrees well with the calculated molecular weight of monomeric SurA (45 kDa). These values represent the average weight obtained from fitting three independent experiments and the standard deviation of fitting. The average number of degrees of freedom for individual fits is 850. Panel B indicates the SE results obtaining from repeating this experiment with a SurA concentration of 120 μM . Fitting this dataset with a single ideal species model (red dashed curve) yields non-

random residuals (in red). These data are better described by a model (black) that accounts for an equilibrium between monomeric (blue) and dimeric species (green). The K_D obtained from fitting these data is $1160 \pm 60 \mu\text{M}$. The average number of degrees of freedom for individual fits is 600 for these datasets. Panel C indicates the population of both the monomeric and dimeric SurA species as a function of SurA total monomeric concentration. The vertical dashed line shows the physiological concentration of SurA, while the thicker regions depict the concentration range accessible in our SE experiments. All data presented here at collected at 37 °C.

Figure 3.3. SANS data and structural model for apo-SurA.



Analysis of SANS data collected on apo-SurA indicates that SurA has an R_G value in solution consistent with that of the crystallized SurA conformation. We collected scattering profiles of apo-SurA at two concentrations (1 mg mL^{-1} , maroon; 3 mg mL^{-1} , blue; Panel A). Guinier fitting for both the low and high concentration datasets are shown in Panels B and C, respectively; this analysis yields an R_G value for SurA of $33.3 \pm 0.6 \text{ \AA}$. This value agrees well with the calculated R_G value for the crystal structure of SurA (33 \AA for PDB 1M5Y; Panel D) (García De La Torre, Huertas, and Carrasco 2000; Ortega, Amorós, and García De La Torre 2011).

Figure 3.4. Summary of the SurA sequence and sites of all mutations.

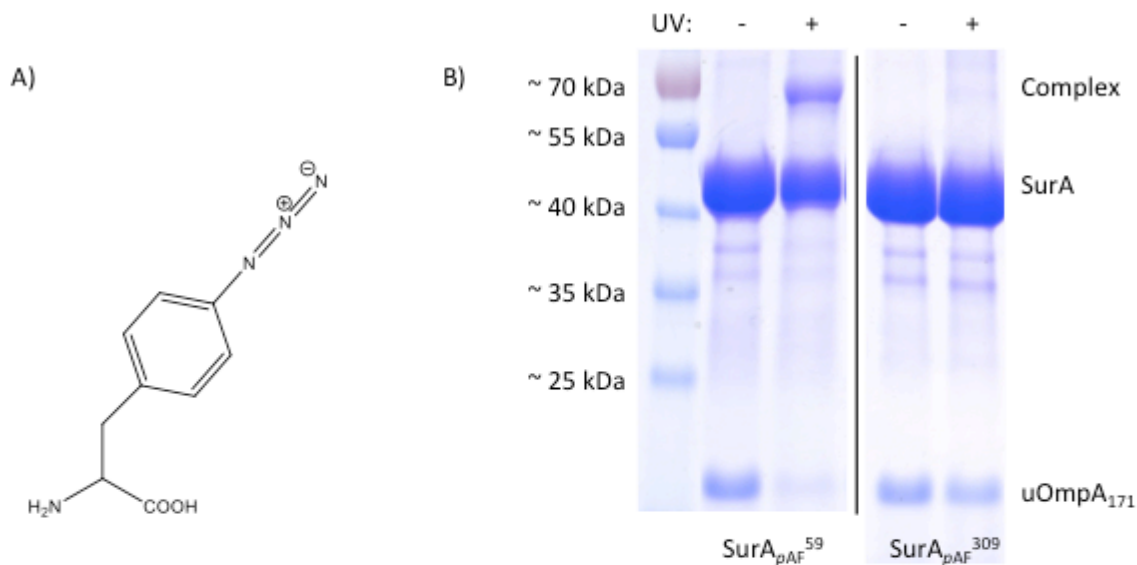
```

20                               69
MAPQVVDKVAAVVNNGVVLESDVDGLMQSVKLNAAQARQQLPDDATLRHQ
70                               119
IMERLIMDQIILQMGQKMGVKISDEQLDQAIANIAKQNNMTLDQMRSRLA
120                               169
YDGLNYNTYRNQIRKEMIISEVRNNEVRRRITILPQEVESLAQQVGNQND
170                               219
ASTELNLSHILIPLPENPTSDQVNEAESQARAIVDQARNGADFGKLAIAH
220                               269
SADQQALNGGQMGWGRIQELPGIFAQALSTAKKGDIVGPIRSGVGFHILK
270                               319
VNDLRGESKNISVTEVHARHILLKPSPIMTDEQARVKLEQIAADIKSGKT
320                               369
TFAAAAKEFSQDPGSANQGGDLGWATPDIFDPAFRDALTRLNKGQMSAPV
370                               419
HSSFGWHLIELLDTRNVDKTDAAQKDRAYRMLMNRKFSEEAASWMQEORA
420
SAYVKILSN

```

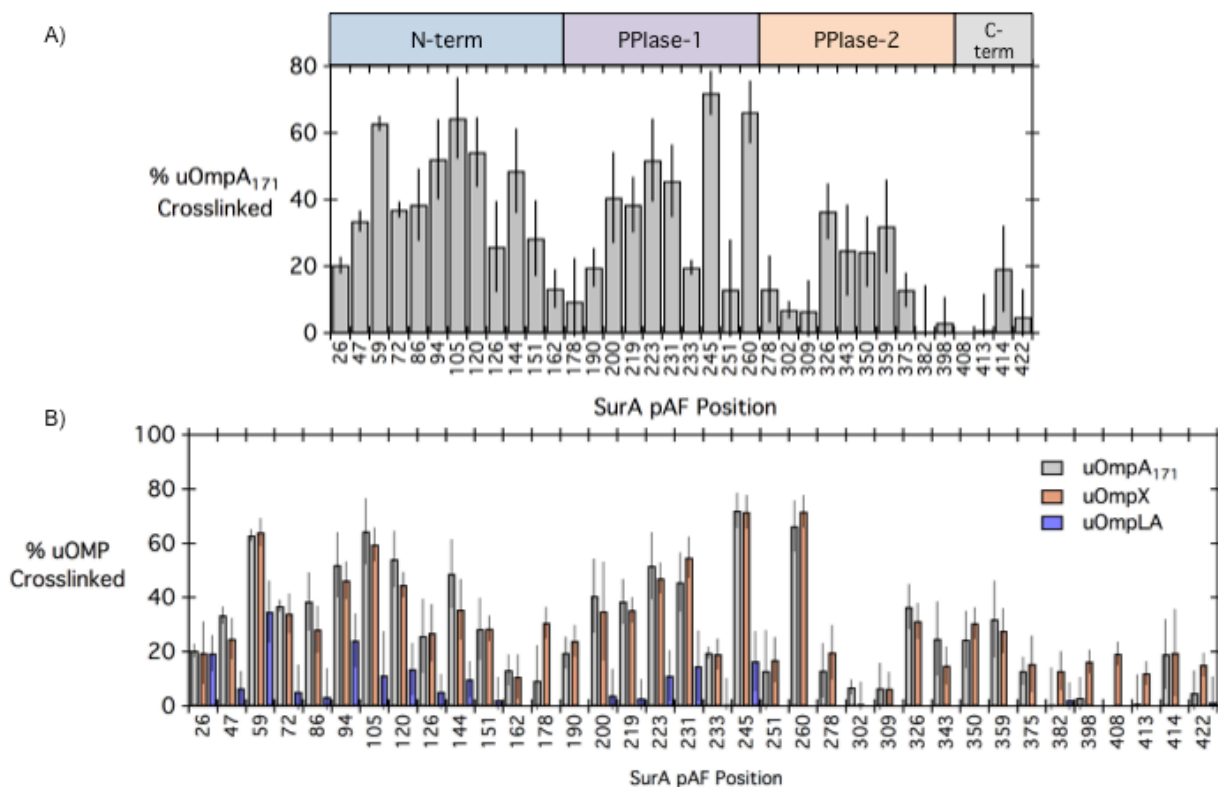
Amino acid numbering begins at 20, as the signal sequence encoding for export of SurA to the periplasm has been excluded from our constructs. The first and second parvulin PPIase domains are indicated in yellow and green, respectively. All positions mutated for incorporation of *p*AF are underlined. SurA contains 4 tryptophans (i.e., W233, W343, W375, and W413) shown in bold which are mutated to phenylalanine in the SurA^{-4W} construct.

Figure 3.5. *p*AF structure and representative SDS-PAGE gel of crosslinking reaction.



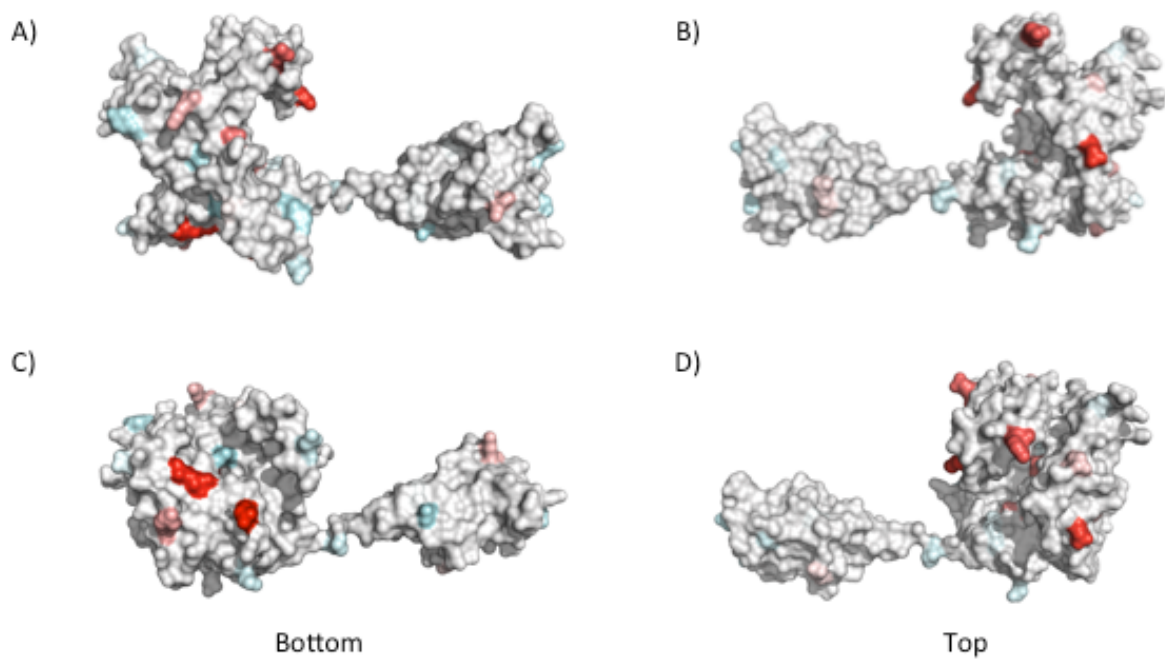
Decrease in density of uOmpA₁₇₁ SDS-PAGE band indicates crosslinking between SurA-*p*AF variants and uOMP. SurA_{*p*AF} variants are used for interrogation of binding with uOmpA₁₇₁ by crosslinking and subsequent SDS-PAGE analysis. The unnatural amino acid, *para*-azido-Phenylalanine (Panel A) was incorporated into SurA at 36 positions shown in Figure 3.4. This amino acid was chosen due to its ability to non-specifically crosslink to chemical moieties within 3 to 5 Å. Each SurA_{*p*AF} variant (25 μM) was mixed with uOmpA₁₇₁ (5 μM) and exposed to UV light (5 min). Samples were taken pre- and post- exposure to UV light and subjected to analysis by SDS-PAGE. As shown in Panel B, this experimental setup yields a higher apparent molecular weight species (“Complex”) for SurA_{*p*AF} variants (i.e., SurA_{*p*AF}⁵⁹). In addition to the formation of this band at ~ 70 kDa, we observe the loss in density of the uOmpA₁₇₁ band at ~ 20 kDa. For other variants, the formation of this complex band is minimal (i.e., SurA_{*p*AF}³⁰⁹).

Figure 3.6. Summary of crosslinking efficiencies for SurA-*pAF* variants and uOMPs.



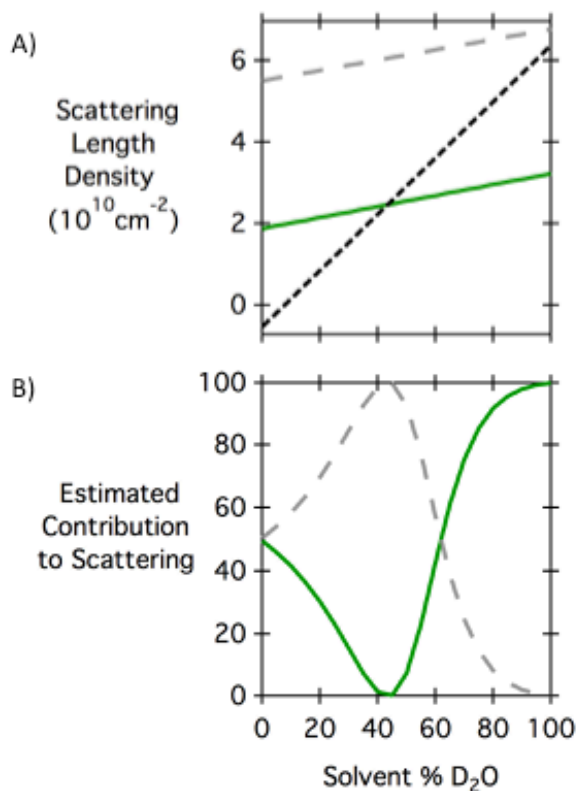
SurA_{*pAF*} variants with high crosslinking efficiency to uOMP clients are primarily located in the N-terminal and PPIase-1 regions. Panel A depicts the percentage of uOmpA₁₇₁ crosslinked to each tested SurA_{*pAF*} variant with the SurA regions labeled as follows: N-terminus (blue), PPIase-1 (purple), PPIase-2 (orange), and C-terminus (gray). Panel B includes the results from repeating the crosslinking experiments with two additional uOMP clients: uOmpX (tan) and uOmpLA (purple). We observe similar crosslinking efficiencies for uOmpA₁₇₁ and uOmpX, both of which are unfolded 8-stranded β -barrel OMPs. Qualitatively, crosslinking uOmpLA (12 stranded β -barrel) to our SurA_{*pAF*} variant library yields similar trends in that higher crosslinking efficiencies are observed for sites in the N-terminal and PPIase-1 regions; however, efficiencies for SurA crosslinking to uOmpLA are lower than uOmpA₁₇₁ for all tested sites.

Figure 3.7. Map of SurA_{pAF}-uOmpA₁₇₁ crosslinking results.



Structural map of SurA_{pAF}-uOmpA₁₇₁ crosslinking results suggests that SurA makes delocalized contacts centered on the N-terminus and PPIase-1 regions. Gradient shading was utilized to indicate high and low crosslinking results are colored in red and blue, respectively (PDB 1M5Y).

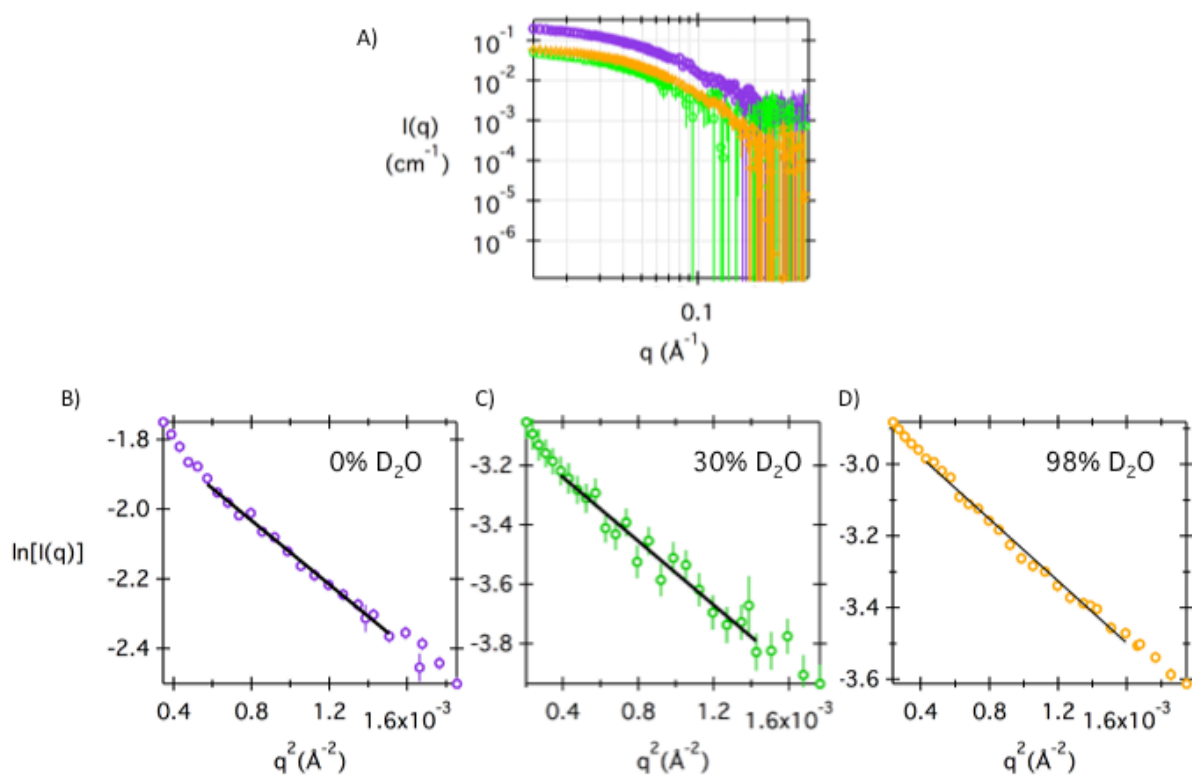
Figure 3.8. Scatter length density and contribution to total scattering calculations for protonated SurA and deuterated uOmpA₁₇₁.



Near the D₂O buffer composition at which protonated SurA is contrast matched, scattering from a complex of protonated SurA and deuterated uOmpA₁₇₁ will primarily originate from the uOMP. Panel A plots the scattering length density of protonated SurA (green), deuterated uOmpA₁₇₁ (gray dashed line), and GF buffer (black dashed line). The buffer D₂O content at which scattering length density of a protein component equals that of the buffer is termed the contrast match point; at this point, the protein component neutron scattering relative to the buffer is negligible and the component makes little to no contribution to the total sample scattering profile. For protonated SurA and deuterated uOmpA₁₇₁, the contrast match points are 43% and > 100 % D₂O content. Panel B illustrates the mass-weighted contribution to the total complex scattering of the individual components – protonated SurA (green) and deuterated

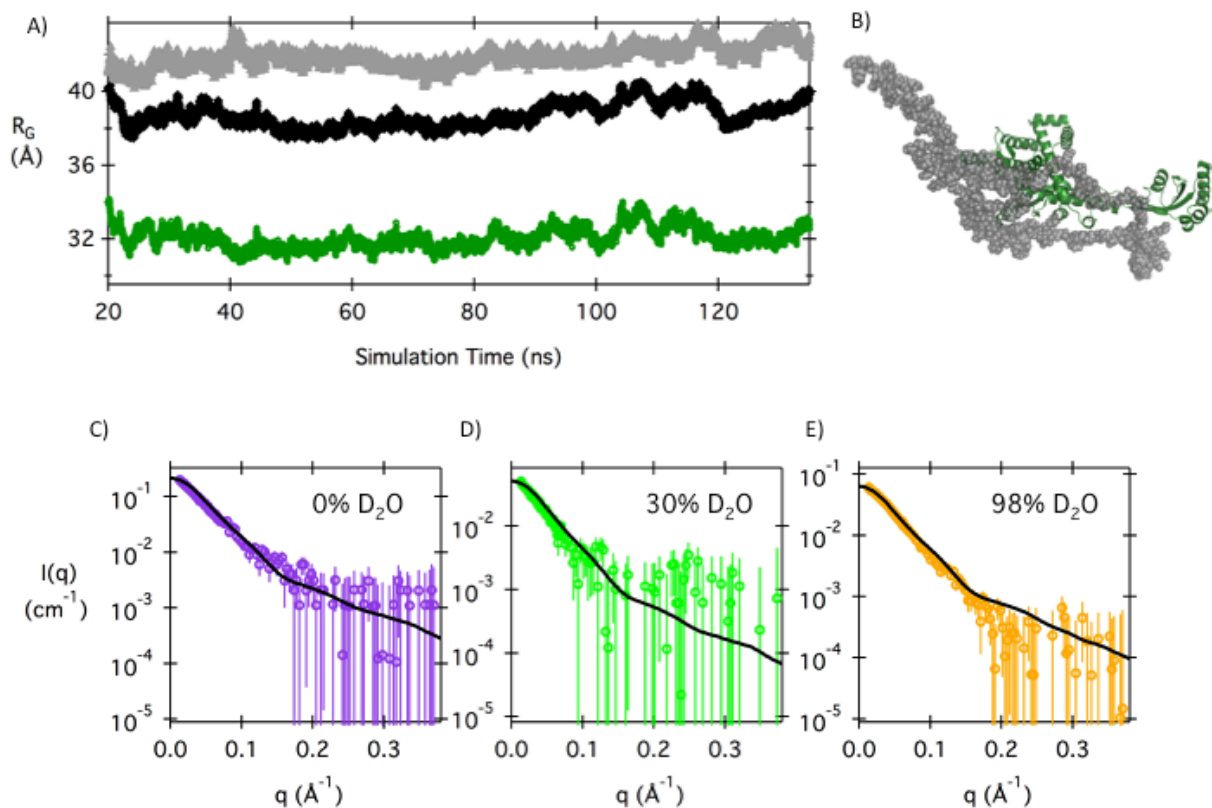
uOmpA₁₇₁ (gray, dashed). Near the contrast match point of SurA ($\sim 40\%$ D₂O), most of the scattering intensity originates from the uOMP in the complex.

Figure 3.9. Summary of SANS datasets and fitting for SurA-uOmpA₁₇₁ complex.



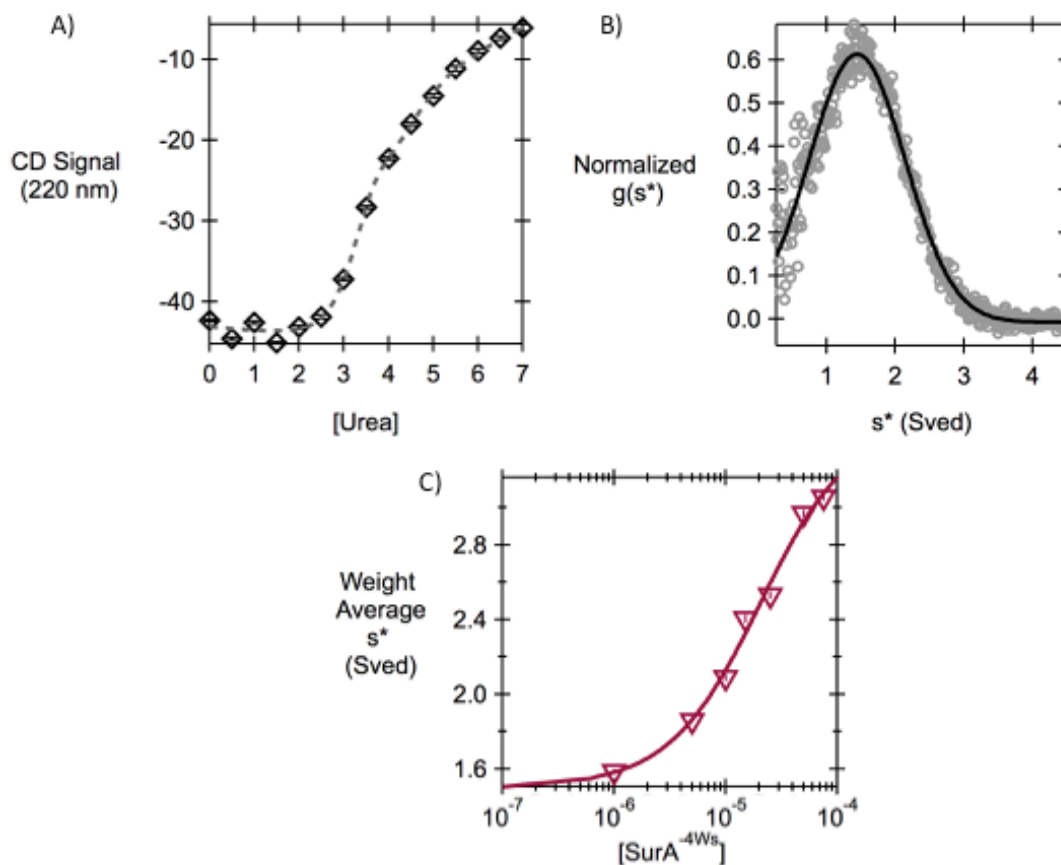
SANS datasets collected on complex of SurA crosslinked to uOmpA₁₇₁ provide R_G constraints for structural modeling. Scattering profiles of prot-SurA_{pAF}¹⁰⁵ crosslinked to deut-uOmpA₁₇₁ in 0% and 30% D₂O GF buffer are shown in purple and green, respectively; data collected for the complex containing prot-SurA_{pAF}¹⁰⁵ crosslinked to prot-uOmpA₁₇₁ in 98% D₂O buffer are shown in orange (Panel A). Guinier fitting for these datasets are shown in Panels B through D and summarized in Table 3.4.

Figure 3.10. MD analysis and SANS calculations for SurA-uOmpA₁₇₁ complex model.



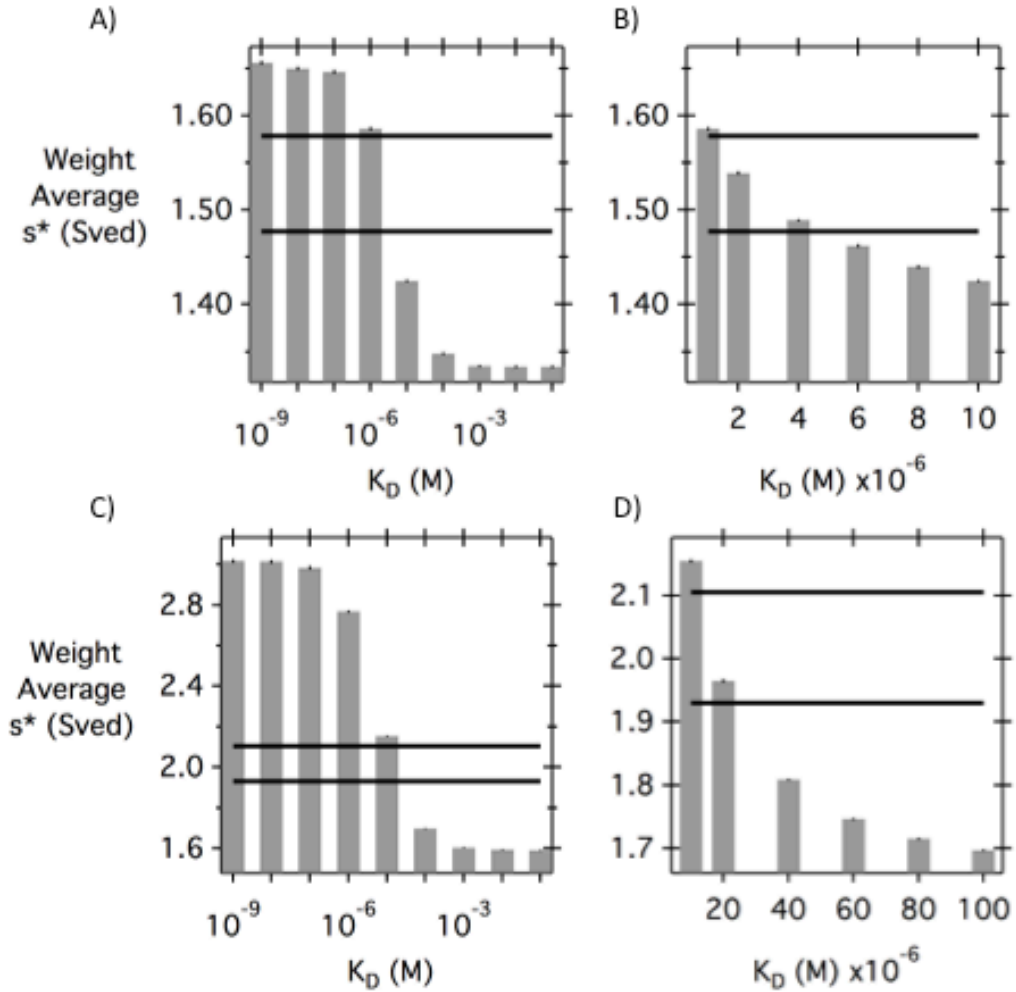
Structural model constructed from SANS R_G constraints produces conformation that yields simulated scattering curves that agree with experimentally determined data. We monitored the R_G of SurA (green), uOmpA₁₇₁ (gray), and the entire complex (black) for our constrained MD simulation. A representative complex conformation is shown in Panel B. For this particular conformation, we calculated the expected scattering curves (black) for the experimental complexes and buffer compositions shown in Figure 3.9.

Figure 3.11. SV data for SurA^{-4W} and uOmpA₁₇₁ mixtures and controls.



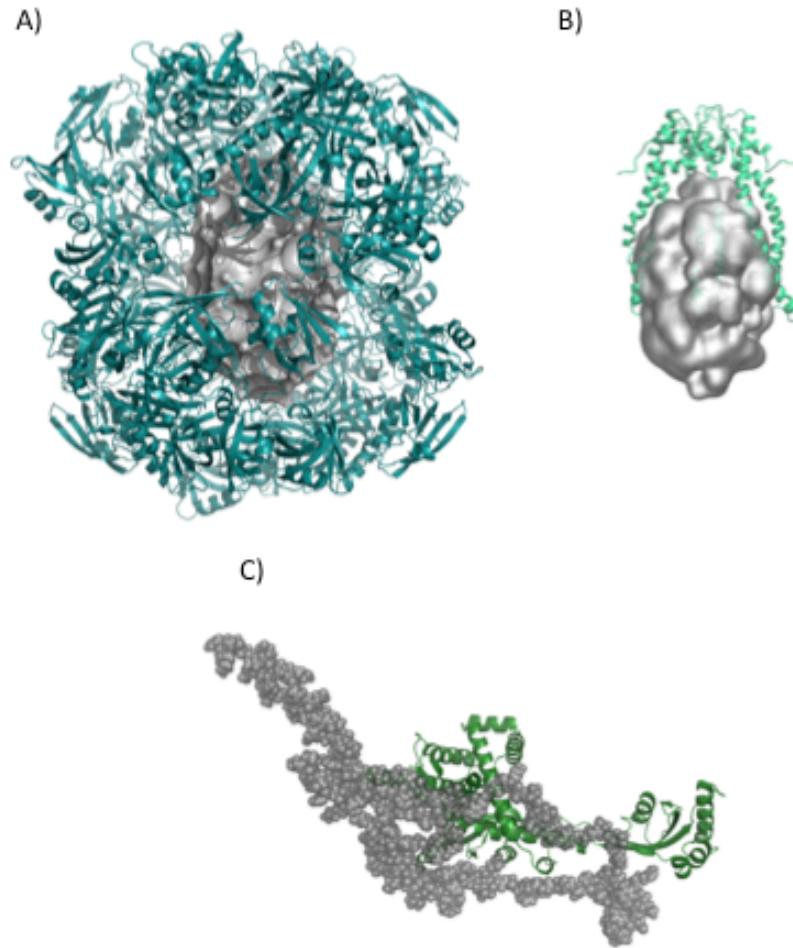
SurA^{-4W} binds to uOmpA₁₇₁ with a micromolar K_D under experimental conditions in which SurA^{-4W} is folded and uOmpA₁₇₁ is an unfolded monomer. SurA^{-4W} retains native secondary structures at urea concentrations lower than 2 M urea (Panel A). At 5 μ M uOmpA₁₇₁ concentration and 1.5 M urea, uOmpA₁₇₁ is monomeric as evidenced by the sedimentation coefficient distribution function being well described by a single species model (Panel B). Panel C shows the weight average sedimentation coefficient for mixtures of 5 μ M uOmpA₁₇₁ with varying concentrations of SurA^{-4W} measured in 1.5 M urea and 20 mM Tris (pH=8.0).

Figure 3.12. Simulation of SV data for SurA^{-4w} and uOmpA₁₇₁ as a function of K_D .



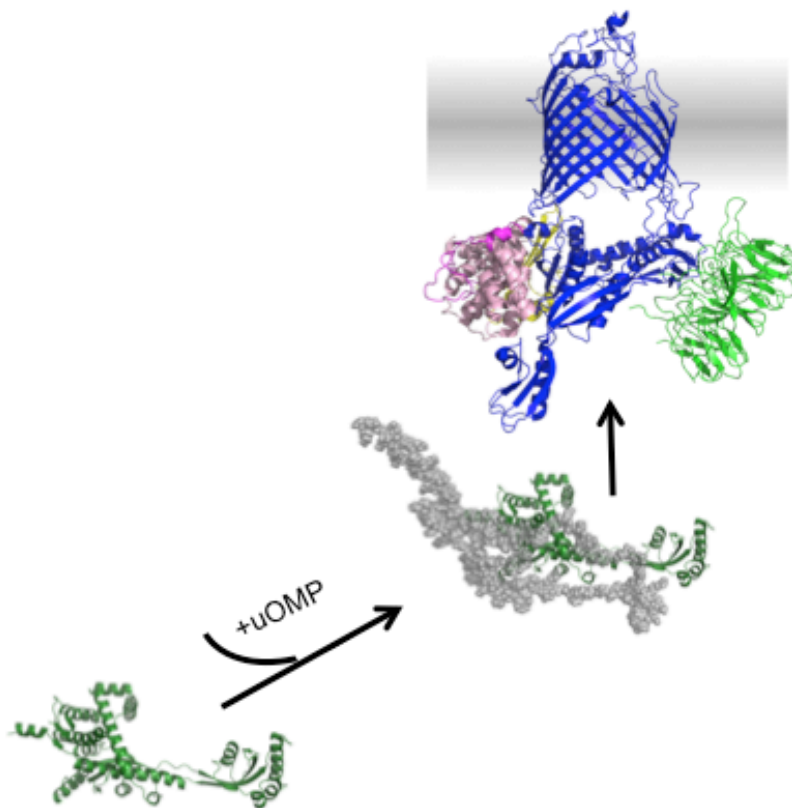
Simulations of SV data suggest that a micromolar K_D value is consistent with our experimental SV results for mixtures of SurA^{-4w} and uOmpA₁₇₁. Above, we plot the average weight average sedimentation coefficient obtained from simulations of two mixtures of SurA^{-4w} and uOmpA₁₇₁ with varying equilibrium dissociation constants (K_D). Simulations for a mixture of 1 μ M SurA^{-4w} and 5 μ M uOmpA₁₇₁ are shown in Panels A and B; simulations for a mixture of 10 μ M SurA^{-4w} and 5 μ M uOmpA₁₇₁ are shown in Panels C and D. Horizontal lines indicate the experimentally determined range of weight average sedimentation coefficients measured for these mixtures (Figure 3.11).

Figure 3.13. Summary of structures of chaperone bound uOMP complexes.



Unlike other periplasmic chaperones that encapsulate uOMP clients, SurA binds to uOMPs in an expanded, external conformation. Panels A and B depict structural models for complexes of uOMP clients (i.e., uOmpC and uOmpW) with the oligomeric chaperones, DegP and Skp respectively (Malet et al. 2012; Zaccai et al. 2015). Panel C depicts the expanded uOmpA₁₇₁ in our model of the SurA-uOmpA₁₇₁ complex presented in Figure 3.10B.

Figure 3.14. Mechanistic insight into SurA-uOMP interactions with the BAM complex.



The SurA-uOmpA₁₇₁ complex may interact with the BAM proteins in a manner that promotes uOMP assembly into the membrane. SurA associates with the uOMP client, which maintains an expanded structure in the SurA-uOMP complex. In this structural model, regions of the uOMP are extended away from the SurA chaperone and therefore capable of interacting with the periplasmic domains of the BAM complex.

3.6. Tables

Table 3.1. Summary of number of prolines in abundant OMPs and periplasmic proteins.

| | | <u>PDB</u> | <u>Total</u> <u>Residues</u> | <u>Total</u> <u>Prolines</u> | <u>cis</u> <u>Prolines</u> |
|---------------------------------------|---------------------|-------------|---------------------------------|---------------------------------|-------------------------------|
| Most Abundant OMPs | LamB | 1MAL | 421 | 8 | 1 |
| | OmpA ₁₇₁ | 1QJP | 169 | 8 | 0 |
| | OmpC | 2J1N | 346 | 3 | 0 |
| | OmpF | 3K19 | 340 | 4 | 0 |
| | OmpT | I78 | 297 | 9 | 0 |
| | OmpW | 2F1V | 191 | 6 | 0 |
| | <u>OmpX</u> | <u>1QJ9</u> | <u>148</u> | <u>4</u> | <u>1</u> |
| | FhuA | 2GRX | 555 | 24 | 0 |
| SurA Clients | LptD | 4Q35 | 760 | 32 | 1 |
| | <u>OmpA</u> | <u>1QJP</u> | <u>169</u> | <u>8</u> | <u>0</u> |
| | AgP | 1NT4 | 391 | 24 | 0 |
| | GlnH | 1WDN | 226 | 7 | 1 |
| Most Abundant Periplasmic Proteins | HdeA | 1DJ8 | 89 | 4 | 0 |
| | HdeB | 2XUV | 79 | 5 | 0 |
| | MalE | 1ANF | 370 | 21 | 0 |
| | OppA | 3TCH | 517 | 32 | 1 |
| | RbsB | 1URP | 271 | 9 | 0 |

Most abundant OMPs have fewer total prolines and cis-prolines than the most abundant periplasmic proteins. The total number of prolines and cis-prolines are provided for the most abundant OMPs and periplasmic proteins, along with previously identified *in vivo* clients of SurA (Han, Kim, and Kim 2014; Vertommen et al. 2008, 2009).

Table 3.2. Percentage of proline content in abundant OMPs and periplasmic proteins.

| | <u>% Pro</u> | <u>% Cis</u> |
|------------------------------------|--------------------|--------------|
| | <u>Composition</u> | |
| Most Abundant OMPs | 2.51 | 0.105 |
| SurA-preferred clients | 3.90 | 0.080 |
| Most Abundant Periplasmic Proteins | 5.04 | 1.96 |

Few *cis*-Prolines occur in OMPs. The percentage of prolines total and *cis*-prolines for the proteins listed in Table 3.1 are shown above. For OMP sequences, we considered the transmembrane regions only (Bitto and McKay 2004; Hennecke et al. 2005). SurA-preferred clients only contain 1 *cis*-proline (i.e., LptD).

Table 3.3. Scattering lengths of common atoms.

| <u>Atom</u> | <u>Nucleus</u> | <u>b (10^{-12} cm)</u> | <u>$f_{\text{x-ray}}$ (10^{-12} cm)</u> |
|-------------|-----------------|--|---|
| Hydrogen | ^1H | -0.374 | 0.28 |
| Deuterium | ^2H | 0.667 | 0.28 |
| Carbon | ^{12}C | 0.665 | 1.69 |
| Nitrogen | ^{14}N | 0.930 | 1.97 |
| Oxygen | ^{16}O | 0.580 | 2.25 |

The scattering lengths of common atoms and isotopes are given for both neutron (b) and x-ray ($f_{\text{x-ray}}$) scattering. Importantly, the neutron scattering length for hydrogen and deuterium are opposite in sign and this yields differential scattering for isotopically labeled macromolecules.

Table 3.4. Summary of SANS experiments and Guinier fitting parameters.

| <u>Protein</u> | <u>Concentration</u> (mg mL ⁻¹) | <u>Buffer</u> <u>Composition</u> | <u>Guinier Fitting</u> | | |
|--|--|-------------------------------------|--|-----------------------------|-----------------------------|
| | | | <u>I(0)</u> (cm ⁻¹) | <u>R_G</u> (Å) | <u>I(0)</u> <u>Ratio</u> |
| SurA | 1.0 | 98% D ₂ O | 4.49x10 ⁻² ± 5.3x10 ⁻⁴ | 33.3 ± 0.6 | 1.04 |
| | 3.0 | 98% D ₂ O | 9.67x10 ⁻² ± 6.0x10 ⁻⁴ | 34.5 ± 0.3 | 1.14 |
| SurA _{pAF} ¹⁰⁵ x p-uOmpA ₁₇₁ | 1.2 | 98% D ₂ O | 6.29x10 ⁻² ± 5.5x10 ⁻⁴ | 38.4 ± 0.5 | 0.97 |
| SurA _{pAF} ¹⁰⁵ | 3.0 | 0% D ₂ O | 2.10x10 ⁻¹ ± 1.8x10 ⁻³ | 41.6 ± 0.5 | 1.04 |
| x d-uOmpA ₁₇₁ | 3.0 | 30% D ₂ O | 4.92x10 ⁻² ± 1.5x10 ⁻³ | 40.7 ± 1.3 | 0.94 |

The ratio of the experimentally determined I(0) to the predicted value is calculated as described in the Methods section. I(0) ratios close to 1 indicate that samples contain monomeric species. For I(0) and R_G values, errors indicate the standard deviations from fitting.

Table 3.5. Primers used for cloning SurA-*p*AF variants.

| <u>Residue #</u> | <u>Primer</u> |
|------------------|---|
| D 26 | GCCCCCAGGTAGTCT <u>AG</u> AAAGTCGCAGCCGTCGTC |
| Q 47 | GCGACGTTGATGGATTAAATGT <u>AG</u> TCGGTAAAACGAACGCTGC |
| Q 59 | GCTCAGGCAAGGCAGT <u>AG</u> CTTCCTGATGACGCGAC |
| E 72 | GCGCCACCAAATCATGT <u>AG</u> CGTTTGATCATGGATCAAATC |
| K 86 | ATCCTGCAGATGGGGCAGT <u>AG</u> ATGGGAGTGAAAATCTC |
| E 94 | GTGAAAATCTCCGATT <u>AG</u> CAGCTGGATCAGGCGATTG |
| K 105 | GCGATTGCTAACATCGCGT <u>AG</u> CAGAACAACATGACGCTGGATC |
| Y 120 | ATGCGGAGTCGTCTGGCTT <u>AG</u> GATGGACTGAACTACAAC |
| N 126 | GCTTACGATGGACTGAACTACT <u>AG</u> ACCTATCGTAACCAGATCCGC |
| N 144 | ATCTCTGAAGTGCGTAACT <u>AG</u> GAGGTGCGTCGTC |
| T 151 | GTGCGTCGTCGCATCT <u>AG</u> ATCCTGCCGCA <u>AG</u> AAGTCGAATC |
| Q 162 | GTCGAATCCCTGGCGT <u>AG</u> CAGGTGGGTAAACCAAAACGAC |
| D 190 | CCGGAAAACCCGACCTCTT <u>AG</u> CAGGTGAACGAAGCG |
| R 200 | GCGGAAAGCCAGGCGT <u>AG</u> GCCATTGTTCGATCAGG |
| H 219 | AAGCTGGCGATTGCTT <u>AG</u> TCTGCCGACCAGCAG |
| Q 223 | ATTGCTCATTTCTGCCGACT <u>AG</u> CA <u>AG</u> CGCTGAACGGCG |
| M 231 | CTGAACGGCGGCCAGT <u>AG</u> GGCTGGGGCCGTATTCAGG |
| W 233 | CTGAACGGCGGCCAGATGGGCT <u>AG</u> GGCCGTATTCAGGAG |
| Q 245 | CCCGGGATCTTCGCCT <u>AG</u> GCATTAAGCACCGCG |
| K 251 | CAGGCATTAAGCACCGCGT <u>AG</u> AAAGG <u>AG</u> AACATTGTTG |
| R 260 | GACATTGTTGGCCCGATTT <u>AG</u> TCCGGCGTTGGCTTCC |
| K 278 | GCGCGGCGAAAGCT <u>AG</u> AAATATCTCGGTGACCG |
| Q 302 | CCGATCATGACTGACGAAT <u>AG</u> GCCCGTGTGAAACTGG |
| Q 309 | GCCCGTGTGAAACTGGAAT <u>AG</u> ATTGCTGCTGATATC |
| K 326 | ACTTTTGCTGCCGCAGCGT <u>AG</u> GAGTTCTCTCAGGATCC |
| D 350 | GCTACACCAGATATTTCT <u>AG</u> CCGGCCTTCCGTGACGC |
| R 359 | TTCCGTGACGCCCTGACTT <u>AG</u> CTGAACAAAGGTCAAATG |
| D 382 | TGGCATTTAATCGAACTGCTGT <u>AG</u> ACCCGTAATGTCTG |
| Y 398 | CAGAAAGATCGTGCAT <u>AG</u> CGCATGCTGATGAACCGTAAGTTCTCG |

| | | |
|---|-----|---|
| E | 408 | AACCGTAAGTTCTCGT <u>AGGAGG</u> CAGCAAGCTGGATG |
| M | 414 | GAAGAAGCAGCAAGCTGGT <u>AGC</u> AGGAACAACGTGCCAG |
| Y | 422 | CAACGTGCCAGCGCCT <u>AGGT</u> TAAAATCCTGAGC |

Mutations to the SurA gene are underlined.

Table 3.6. Primers used for cloning SurA^{-4W}.

| | <u>Primer</u> |
|-------|---|
| W233F | Forward: CCAGATGGGT <u>TTT</u> TGGCCGTATTCAGGAGTTGC Reverse: GCAACTCCTGAATACGGCC <u>AAA</u> ACCCATCTGG |
| W343F | Forward: CGATCTCGGC <u>TTT</u> GCTACACCAGATATTTTCGATCCGG Reverse: CGAAAATATCTGGTGTAGC <u>AAAG</u> CCGAGATCGCCG |
| W375F | Forward: GGTTCACTCTTCATTCGGC <u>TTT</u> CATTTAATCGAACTGCTGG Reverse: CGATTAAATG <u>AAAG</u> CCGAATGAAGAGTGAACCGGTGC |
| W413F | Forward: GGAAGAAGCAGCAAGC <u>TTT</u> ATGCAGGAACAACGTGCCAGC Reverse: CGTTGTTCTGTCAT <u>AAAG</u> CCTTGCTGCTTCTTCCGAGAACTTACG |

Mutations to the SurA gene are underlines.

Chapter 4 – BamA Alone Accelerates OMP Folding *in vitro* through a Catalytic Mechanism

Excerpts published as: Plummer, A. M., Fleming, K. G., (2015) *Biochemistry*, 54(39): 6009-6011

and

Plummer, A. M., Fleming, K.G., (2016) *Trends in Biochemical Sciences*, 41(10): 872-882.

4.1. Introduction

The functionally active, native conformations of Outer Membrane Proteins (OMPs) are folded into the Outer Membranes (OM) of Gram-negative bacteria. The assembly of OMPs is known to depend on the OMP BamA – this OM-localized β -barrel protein is evolutionary conserved from bacteria to eukaryotes and is known to play an essential role in uOMP assembly (Voulhoux, Bos, Geurtsen, Mols and Tommassen 2003). In *E. coli*, BamA associates with four lipoproteins: BamBCDE to form the β -Barrel Assembly Machinery (BAM) complex (Malinverni et al. 2006; Onufryk et al. 2005; Sklar, Wu, Gronenberg, et al. 2007; Wu et al. 2005). While each of these accessory lipoproteins has been implicated in maintaining OM integrity, only BamA and BamD are required for cell viability (Malinverni et al. 2006; Werner and Misra 2005). The essentiality of the BAM complex stems from its role in assembling uOMPs into the bacterial OM.

Recently solved crystal structures reveal that the BamA β -barrel has a unique seam.

In 2013, the first crystallographic structure of a full-length bacterial BamA was solved (Noinaj et al. 2013). This structural model contains the two domains of BamA: one transmembrane 16-stranded β -barrel domain and a series of five soluble POlypeptide-TRansport-Associated (POTRA) motifs. Each of these structural subunits has features that may contribute to the ability of BamA to assemble uOMPs into the OM of Gram-negative bacteria. In particular, this first structure of the β -barrel domain of BamA revealed a surprising result: instead of exhibiting a geometry that maximizes the number of hydrogen bonds between the N- and C-terminal β -strands, the crystal structure of the *Neisseria gonorrhoeae* BamA revealed that the N- and C-terminal β -strands of the β -barrel interact with only two hydrogen bonds to close the β -barrel, and the C-terminal β -strand is twisted and bends into the β -barrel. This “open” β -

barrel conformation has since been observed in crystallographic studies of *E. coli* BamA (Figure 4.1A and 4.1C) (Gu et al. 2016).

The non-canonical β -barrel seam of the *N. gonorrhoeae* BamA prompted the investigation of the role of movement of the N- and C-terminal β -strands in the function of this BamA homologue. Indeed, molecular dynamics (MD) simulations of the *N. gonorrhoeae* BamA in dimyristoyl-glycero-3-phosphatidylethanolamine gel-phase lipids suggest that β -strands 1 and 16 laterally open in the absence of uOMP client (Noinaj et al. 2013). Crosslinking experiments that covalently link β -1 to β -16 of *E. coli* BamA were found to be detrimental to cell viability, suggesting that lateral opening of these β -strands may play a pivotal role in the function of BamA (Noinaj et al. 2014).

Mechanisms involving lateral opening have been previously reported for other OMPs – this type of motion was first suggested to play a role in the function of the OMP PagP over 10 years ago (Ahn et al. 2004). Since then, several OMPs have been suggested to laterally open (e.g., TamA, PagP, FadL, OmpW, LptD) (Ahn et al. 2004; Dong et al. 2014; Gruss et al. 2013; Hearn et al. 2009; Hong et al. 2006). These β -barrels range in size from 8 to 16 β -strands and have a variety of substrates, including phospholipids and lipopolysaccharide (LPS). The unique crystallographic evidence for the open conformation of BamA β -barrel differs from the previous structural and biochemical data for other OMPs that have functional mechanisms involving lateral opening. Interestingly, the potential similarities for insertion of LPS and OMPs by lateral opening of LptD and BamA, respectively, suggests the two major components of the OM may be assembled by similar mechanisms.

How do the soluble POTRA motifs contribute to BamA function?

The POTRA motifs of BamA have a conserved $\beta 1$ - $\alpha 1$ - $\alpha 2$ - $\beta 2$ - $\beta 3$ architecture and may interact with client uOMPs through exposed β -sheets (Knowles et al. 2008). Genetic experiments suggest that the three POTRA motifs closest to the β -barrel (POTRA 3-5) are required for BAM function *in vivo* (Kim et al. 2007). Recent studies have indicated that the presence of all five BamA POTRA motifs accelerates uOMP folding *in vitro* to a greater extent than the presence of only one POTRA motif (Gessmann et al. 2014). Together, these findings imply that at least some of the POTRA motifs play a role in facilitating uOMP folding or these motifs are important for folding of BamA itself. Crystallographic, NMR, and small-angle x-ray scattering analyses of truncations of the POTRA motifs (e.g., POTRA 1-2) in the absence of the BamA β -barrel suggest that the five POTRA motifs may be divided into two rigid bodies (POTRA 1-2 and 3-5) connected by a flexible linker (Gatzeva-Topalova, Walton, and Sousa 2008; Gatzeva-Topalova et al. 2010). Rotational and lateral flexibility of these POTRA motifs may allow BamA to explore conformational space and populate conformations that promote uOMP folding, thereby playing a role in the assembly of uOMPs by the BAM complex.

The POTRA motifs of BamA also interact with the BamBCDE lipoproteins (Figure 4.1B). Crystal structures of individual POTRA motifs fused to BAM lipoproteins revealed that BamB and BamD interact with POTRA motifs 3 and 5, respectively (Bergal et al. 2015; Jansen, Baker, and Sousa 2015). The recently solved crystal and cryo-electron microscopy structures of BamACDE and the entire BAM complex suggest that the most extensive contacts between BamA and the BAM lipoproteins occurs between BamA POTRA 5 and BamD (Bakelar, Buchanon, and Noinaj 2016; Gu et al. 2016; Han et al. 2016; Iadanza et al. 2016). This interaction between BamA and BamD may be functionally important, because outcompeting this interaction with a BamD-derived peptide inhibits BAM complex formation (Hagan,

Wzorek, and Kahne 2015). Although it is not known how the entire BAM complex works together to facilitate OMP folding, it has been suggested that BamA functions *in vivo* via a functional mechanism involving recycling of BamA by BamD and BamE (Hagan and Kahne 2011; Rigel, Ricci, and Silhavy 2013). In this type of mechanism the BamA protein would be modified in some manner that is reversed by the presence of the lipoproteins BamD and BamE.

***In vitro* folding studies complement structural investigations of BamA function.**

Crystal structures of the BAM complex and its individual components provide valuable snapshots of the catalytic cycle of BAM-mediated uOMP folding. These crystallographic conformations likely represent stable reaction intermediates; if so, these structural data inherently only provide insight into local energetic minima along the functional pathway of BAM. To better understand the entire mechanistic picture of BAM-mediated OMP assembly, we have performed *in vitro* studies to reveal novel insight into the role of BamA in the BAM complex.

4.2. Methods

Expression and purification of denatured OMPs was performed according to previously published protocols (Burgess et al. 2008; Gessmann et al. 2014; Plummer, Gessmann, and Fleming 2015). Briefly, OMPs are expressed to inclusion bodies, which are recovered and denatured OMPs are resolubilized in 8 M urea (Figure 4.2A). OMPs are then diluted into 1 M urea in the presence of Large Unilamellar Vesicles (LUVs). For experiments reported in Figure 4.4, final component concentrations were: [OmpA] = 4 μ M, [Urea] = 1 M, [EDTA] = 2 mM, [Borate] = 20 mM, and [Lipid] = 3.2 mM. Under these conditions, OMPs spontaneously insert into LUVs. All folding reactions presented here are completed with stirring at 37 °C (10 Sample Thermoelectric Temperature Incubator, Model T-10, Aviv Biomedical). At appropriate time points, aliquots of the reaction were removed and quenched with SDS gel loading buffer as described previously (Gessmann et al. 2014). Quenched samples were subjected to electrophoresis immediately on 10% precast gels (Mini-PROTEAN TGX, Bio-Rad) at a constant voltage of 150 mV for 55 minutes at room temperature. Densitometry analyses were performed as previously described (Gessmann et al. 2014; Plummer, Gessmann, and Fleming 2015). We analyze OMP folding kinetics by SDS-PAGE, as OMPs exhibit characteristic shifts in apparent molecular weight between the folded and unfolded species, as shown in Figure 4.3 (Gessmann et al. 2014; Inouye and Yee 1973; Nakamura and Mizushima 1976).

All LUVs utilized in studies shown here are composed of mixtures of the synthetic lipids: 1,2-didecanoyl-*sn*-glycero-3-phosphoethanolamine (DiC₁₀-PE) and 1,2-didecanoyl-*sn*-glycero-3-phosphocholine (DiC₁₀-PC) (Avanti Polar Lipids) in given ratios. All LUVs were extruded to have 100 nm diameter and a final stock concentration of 10 mM in 20 mM borate (pH=10).

The protocol above monitors the spontaneous insertion of OMPs into LUVs – to investigate the effect of BamA on OMP folding kinetics, this protocol can be modified to incorporate BamA (Gessmann et al. 2014; Plummer, Gessmann, and Fleming 2015). For these experiments, 2 μ M BamA was prefolded into LUVs prior to the introduction of the unfolded OMP folding client, as shown in Figure 4.2B). For experiments reported in Figures 4.4, final component concentrations were: [BamA] = 2 μ M, [OmpA] = 2 μ M, [Urea] = 1 M, [EDTA] = 2 mM, [Borate] = 20 mM, and [Lipid] = 3.2 mM. It has been previously reported that varying protein:lipid ratios affect the kinetics of OMP folding (Gessmann et al. 2014; Kleinschmidt and Tamm 2002). To avoid the convolution of these effects, we introduce a negative control where OmpX is prefolded into LUVs prior to the introduction of the client OMP (i.e., OmpA). OmpX is not known to accelerate the folding of OmpA. Final component concentrations for this control are: [OmpX] = 2 μ M, [OmpA] = 2 μ M, [Urea] = 1 M, [EDTA] = 2 mM, [Borate] = 20 mM, and [Lipid] = 3.2 mM. Analysis of these folding reactions by SDS-PAGE was carried out as previously described; BamA migrates at a higher molecular weight than most OMP clients and therefore does not interfere with the detection of client OMP folding (Figure 4.3B). Additionally, OmpX migrates at a lower molecular weight than the OmpA client OMP and also does not interfere with monitoring client OMP folding (Figure 4.5).

To investigate the catalytic mechanism of BamA, we further modified the above protocol for BamA-mediated OMP folding. For BamA-mediated folding experiments presented in Figures 4.5 through 4.8, 1 μ M BamA was prefolded into LUVs with stirring at 37 °C for 3 h. The average concentration of BamA prefolded was $0.85 \pm 0.06 \mu$ M (average \pm standard deviation, n=5). For the negative control included in Figures 4.5 through 4.7, 1 μ M OmpX was prefolded into LUVs to maintain a constant protein: lipid (mole: mole) ratio when comparing

OmpA folding in the presence and absence of BamA. The average concentration of OmpX prefolded was $0.85 \pm 0.05 \mu\text{M}$ (average \pm standard deviation, $n=5$). $8 \mu\text{M}$ of OmpA was then added to the LUVs containing BamA or OmpX and folded with stirring at 37°C . For experiments reported in Figures 4.5 through 4.8, final component concentrations were: [BamA] or [OmpX] = $1 \mu\text{M}$, [OmpA] = $8 \mu\text{M}$, [Urea] = 1 M , [EDTA] = 2 mM , and [Lipid] = 1.6 mM . Aliquots of the OmpA folding reactions were taken: 10 m, 20 m, 40 m, 1 h, and 2 h after folding initiation. These samples were immediately quenched with SDS gel loading buffer, as described previously (Gessmann et al. 2014). Quenched samples were subjected to electrophoresis immediately on 12% precast gels (Mini-PROTEAN TGX, Bio-Rad) at a constant voltage of 150 mV for 55 minutes at room temperature. Densitometry analyses were performed as previously described (Gessmann et al. 2014; Plummer, Gessmann, and Fleming 2015).

4.3. Results

Because the functional *E. coli* BAM complex contains five proteins, our *in vitro* experiments deconvolute the effects of these components by studying the individual BAM proteins in isolation. To better understand how the essential BamA protein facilitates uOMP assembly, we investigated the role of BamA in the process of *in vitro* uOMP folding (Burgess et al. 2008; Gessmann et al. 2014; Plummer, Gessmann, and Fleming 2015).

BamA acts as an enzyme to accelerate uOMP folding *in vitro*.

The composition of the OM of *E. coli* plays a crucial role in BAM-mediated uOMP folding. *In vivo* uOMP folding occurs into the inner leaflet of the outer membrane, which contains both phosphoethanolamine (PE) and phosphoglycerol (PG) head groups (Kamio and Nikaido 1976; Osborn, Gander, Parisi, Carson 1972). This is coincidentally similar to the composition of the bacterial IM. Paradoxically, these biological head groups retard uOMP folding *in vitro*, creating a pronounced kinetic barrier for unassisted uOMP folding (Gessmann et al. 2014). This kinetic barrier effectively prohibits uOMP folding into the IM because such an event would certainly lead to dissipation of the proton gradient essential to sustain cell viability. Yet for uOMP folding into the OM, the BAM complex must overcome this same kinetic barrier – another remarkable feat that must be completed in the absence of an external energy source.

Because it has been previously shown that BamA accelerates uOMP folding into LUVs composed of synthetic lipids with PE head groups (Gessmann et al. 2014), we aimed to further understand these effects. Figure 4.4 shows kinetic traces for the folding of a representative uOMP (i.e., OmpA) into LUVs composed of 20% DiC₁₀-PE and 80% DiC₁₀-PC in the absence of any prefolded OMP (blue diamonds) and in the presence of prefolded OmpX (gray triangles) and BamA (black triangles). The presence of prefolded OmpX does not affect the folding trajectory of OmpA compared to OmpA folding in the absence of a prefolded OMP; however

the presence of BamA accelerates the folding of OmpA. This acceleration of OmpA is evidenced by that lack of lag phase in the folding kinetics of OmpA (i.e., increase in folding rate) – this kinetic effect translates into a greater fraction of OmpA folded at all time points in the presence of BamA than in the presence of OmpX. For example: at 300 s, no OmpA is folded in the presence of OmpX or absence of prefolded OMP; at this same time point in the presence of BamA, 30% of OmpA has attained its native structure. This analysis suggests that BamA accelerates the initial rate for process of uOMP folding into LUVs *in vitro*. Because uOMPs spontaneously insert into synthetic lipid bilayers *in vitro* and BamA accelerates this process, BamA exhibits properties of an enzyme in that it reduces the activation barrier to uOMP folding into biological membranes.

BamA accelerates uOMP folding through a catalytic mechanism.

The observation that BamA alone accelerates OMP folding *in vitro* raises the questions: can BamA alone repeatedly catalyze the folding of OMPs? Or is BamA irreversibly consumed by a stoichiometric interaction with OMPs and subsequently requires regeneration by the additional BAM subunits? To test this, we developed an experimental assay to determine if BamA is consumed during the acceleration of OMP folding. Our approach allows for differentiation between a stoichiometric and a catalytic mechanism of BamA function. Briefly, BamA is folded to completion into LUVs composed of synthetic lipids. The folded BamA is then presented with a high concentration of an OMP client of interest (i.e., 8 μM OMP client: 1 μM BamA). A stoichiometric mechanism would be characterized by consumption of BamA upon interaction with this client OMP – therefore, the maximal amount of client OMP that could be folded by BamA is limited to the amount of BamA folded. In contrast, if the ability of BamA to accelerate the folding of a client OMP involves a catalytic mechanism, BamA would not be consumed by

interacting with the OMP client and could productively interact with a greater amount of client OMP than the amount of folded BamA.

The client OMP utilized in this study is OmpA because it has previously been shown to undergo BamA-accelerated folding *in vitro* (D. Gessmann et al. 2014). Additionally, OmpA folds slowly through the always accessible intrinsic folding (i.e., BamA-independent) pathway under certain conditions. The unique folding profile of OmpA – limited intrinsic folding and known acceleration of folding by BamA – makes this client OMP ideal for this experimental setup. Figure 4.5 shows a representative SDS-PAGE gel for this modified experimental protocol. The quantity of BamA-catalyzed folded OmpA is defined as the difference at a given time point between the concentration of OmpA folded in the presence of BamA and the concentration of OmpA folded through the intrinsic pathway (Figure 4.6). Because the volumes of all experiments are identical, the concentrations of all species can serve as a proxy for their amounts. Figure 4.7 indicates that the concentration of OmpA folded by BamA into LUVs composed of 20% DiC₁₀-PE and 80% DiC₁₀-PC reaches 1.5 μ M after 1 hour. Densitometric analyses reveal that total amount of folded BamA under these conditions is approximately 0.9 μ M. Therefore the concentration of OmpA that interacts productively with BamA is greater than the concentration of folded BamA. This result suggests that BamA alone is able to repeatedly interact with client OMPs *in vitro* to accelerate their folding via a catalytic mechanism.

Hagan *et al.* previously reported that the reconstituted multi-protein BAM complex (BamABCDE) facilitates OMP folding with a turnover of approximately 1.6 OMPs per BAM (Hagan and Kahne 2011). Our findings suggest that BamA alone is responsible for the catalytic nature of the assembly cycle, as the measured turnover for BamA-catalyzed folding in our

experiments equals 1.7 OMPs per BamA. We therefore conclude that BamA itself is responsible for folding activity.

4.4. Discussion

BamA function involves two substrates: uOMPs and lipids.

Figure 4.4 indicates that BamA accelerates the folding of OMP clients, suggesting that BamA is an enzyme that reduces the activation barrier to uOMP folding. Prior studies have attempted to use the Michaelis-Menten kinetic model to determine the K_m for this enzymatic process, but conditions under which BamA was saturated were unattainable (Gessmann et al. 2014). We were able to estimate the K_m for this catalytic process to be high ($>20 \mu\text{M}$) suggesting the possibility that thermodynamically weak interactions occur between BamA and the uOMP client (Fleming 2015; Gessmann et al. 2014). These results raise the question: how can BamA accelerate uOMP folding if it only weakly interacts with the uOMP? This conundrum can be addressed by realizing that these weak protein-protein interactions are only one facet of the role of BamA. BamA-accelerated uOMP folding involves BamA interacting with two distinct substrates: the uOMP client and the surrounding lipid membrane.

It is entirely plausible that BamA promotes the formation of a membrane defect. Because such structures are known to accelerate uOMP folding, this has been suggested as one possible catalytic mechanism for uOMP-BAM mediated folding (Danoff and Fleming 2015b; Fleming 2015). Such a membrane defect is poorly defined structurally but may be represented by a hydrophobic mismatch between the surrounding lipid bilayer and the BamA β -barrel (Figure 4.9) (Fleming 2015; Noinaj et al. 2013). This type of hydrophobic mismatch has indeed been previously reported by computational studies that investigate BamA-lipid interactions. Together, biochemical, structural, and computational findings suggest that BamA and the surrounding lipid bilayer work together to facilitate uOMP folding.

Recent structural studies of BamA and the entire BAM complex have allowed for further speculation on BamA-lipid interactions (Bakelar, Buchanon, and Noinaj 2016; Iadanza et al.

2016; Noinaj et al. 2013). These studies have suggested that incomplete closure of the BamA β -barrel may play a role in a mechanism by which BamA laterally opens to facilitate OMP folding. Because lipids in the OM surround OMPs, this lateral gating hypothesis for the functional mechanism of BamA seems contradictory to the basic principles of thermodynamics, as the exposure of backbone hydrogen bonds is energetically costly. The BamA β -barrel interior is large enough to accommodate hundreds of water molecules, which would be exposed to hydrophobic lipids as the BamA β -barrel laterally opens. This process should result in a large energetic penalty that must be overcome by another compensating source of energy. Reconciling these thermodynamic considerations with the available structural information must be accomplished to elucidate the catalytic mechanism of BamA.

***In vitro* studies offer insight into function of BAM lipoproteins.**

It has previously been reported that BamDE are strictly required for regeneration of BamA upon interacting with an OMP client (Hagan and Kahne 2011; Rigel, Ricci, and Silhavy 2013). However, comparisons between the activity of BamA alone and the BAM complex have yielded similarities in the catalytic activity: both BamA and the entire BAM complex have been shown to facilitate multiple rounds of catalysis with turnover numbers in both cases equal to approximately 1.5 uOMPs/BamA or uOMPs/BAM, respectively (Hagan and Kahne 2011; Plummer and Fleming 2015). These findings suggest that BamA itself undergoes a cyclic catalytic mechanism that is accelerated *in vivo* by the additional lipoproteins BamBCDE.

Our data suggest that BamA alone possesses intrinsic regeneration ability. We speculate that BamDE must function to accelerate this basal regeneration of BamA *in vivo*, as the timescales of OMP folding measured in our *in vitro* assay are likely too slow to support bacterial growth (Ureta et al. 2007). This will enable OMP folding on a biologically relevant time scale.

Current studies are focusing on understanding how the different components of the BAM complex collaborate to facilitate uOMP folding *in vitro* and biogenesis *in vivo*.

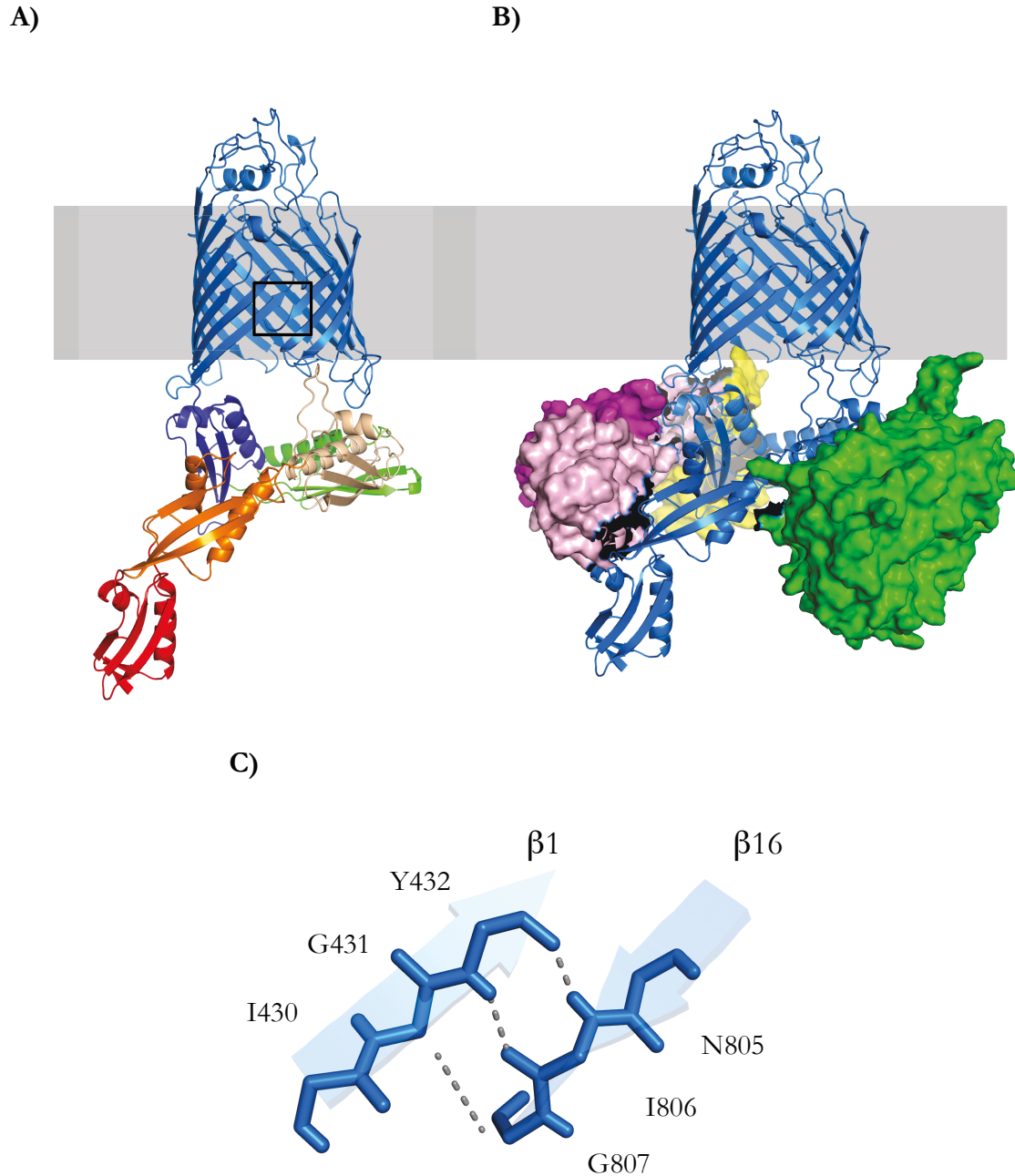
Moving Forward: Mechanistic insight into BamA-catalyzed OMP folding.

Our data suggest that BamA may repetitively and independently interact with uOMP clients. Proposed mechanisms for BamA-assisted OMP folding should be consistent with these findings. Potential BamA-assisted OMP folding mechanisms in the literature include: lateral opening of β -strands 1 and 16 to accommodate the uOMP client (Noinaj et al. 2013), local BamA-facilitated lipid deformations (Danoff and Fleming 2015b; Fleming 2015; Gessmann et al. 2014; Noinaj et al. 2013), and partial OMP folding inside of the BamA barrel (Albrecht et al. 2014). All of these potential mechanistic pathways may be compatible with a catalytic cycle pending no irreversible modification of BamA.

Here we have presented findings that BamA acts catalytically *in vitro* to independently and repetitively accelerate the folding of OMPs. These findings agree with the catalytic mechanism of BamA *in vivo* (Rigel, Ricci, and Silhavy 2013) and further validate *in vitro* OMP folding studies. Interestingly these complementary studies utilize different OMP clients, suggesting the ability of BamA to turnover is independent of OMP client identity. Conserved architecture and structural motifs between *E. coli* BamA and homologues in both prokaryotes (Maier et al. 2015) and eukaryotes (Kozjak et al. 2003) hint that uOMP folding mechanisms by these BamA homologues may also be catalytic. The molecular basis of this catalytic mechanism of BamA warrants further experimental investigation. Understanding the BamA role in acceleration of OMP folding aids in a more complete understanding of OMP biogenesis and provides insight into the function of the BAM complex.

4.5. Figures

Figure 4.1. Crystallographic studies suggest BamA β -barrel contains two domains and has unique seam.

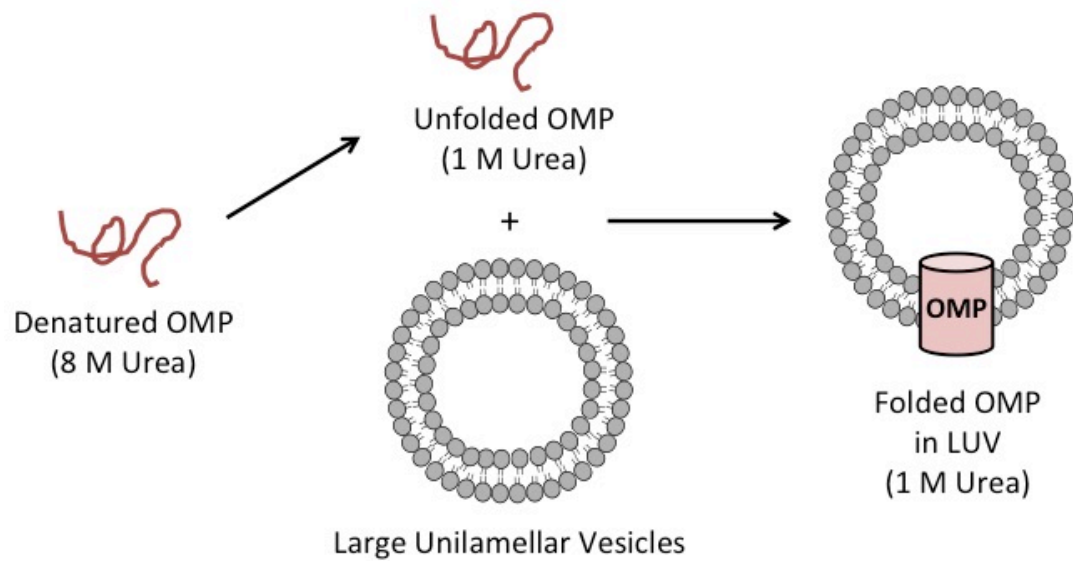


A) Two structural regions of *E. coli* BamA are indicated, with the β -barrel domain shown in blue and the soluble periplasmic POTRA motifs shown in red, orange, tan, green, and dark blue

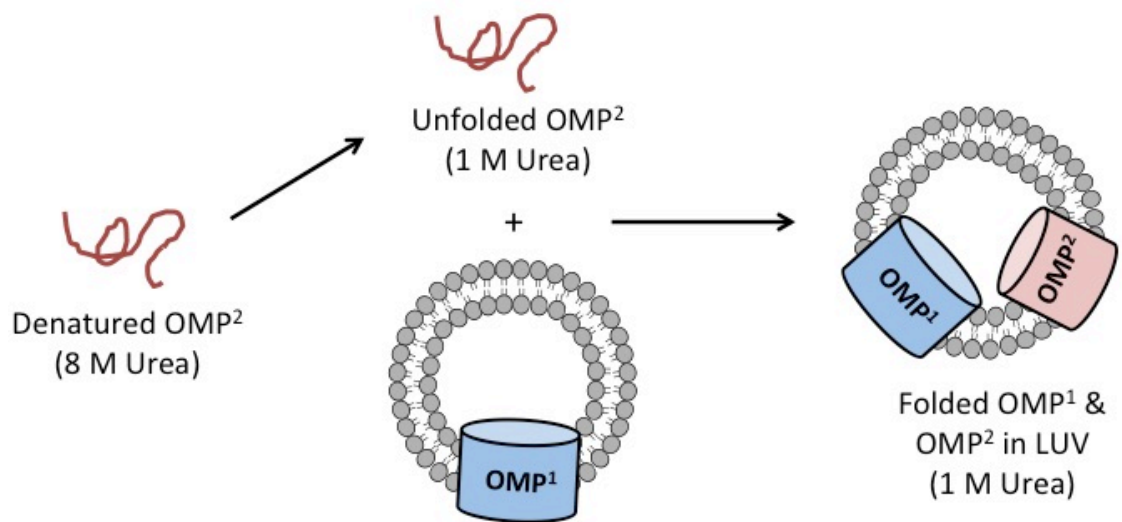
(POTRA 1 through 5, respectively). The membrane is indicated as a gray rectangle. The portion of the BamA β -barrel highlighted in Panel C is indicated with a box. B) BAM lipoproteins are shown as surfaces as indicated: BamB in green, BamC in purple, BamD in pink, and BamE in yellow. In this representation, the entire BamA protein is shown in blue. C) β -strands 1 and 16 of the *E. coli* BamA β -barrel are indicated. This β -barrel has a non-canonical seam because these two strands only interact via 3 hydrogen bonds, which are shown as gray dashed lines. PDB 5D0O and Pymol were utilized to make this figure.

Figure 4.2. Established protocols for intrinsic and BamA-mediated OMP folding *in vitro*.

A)



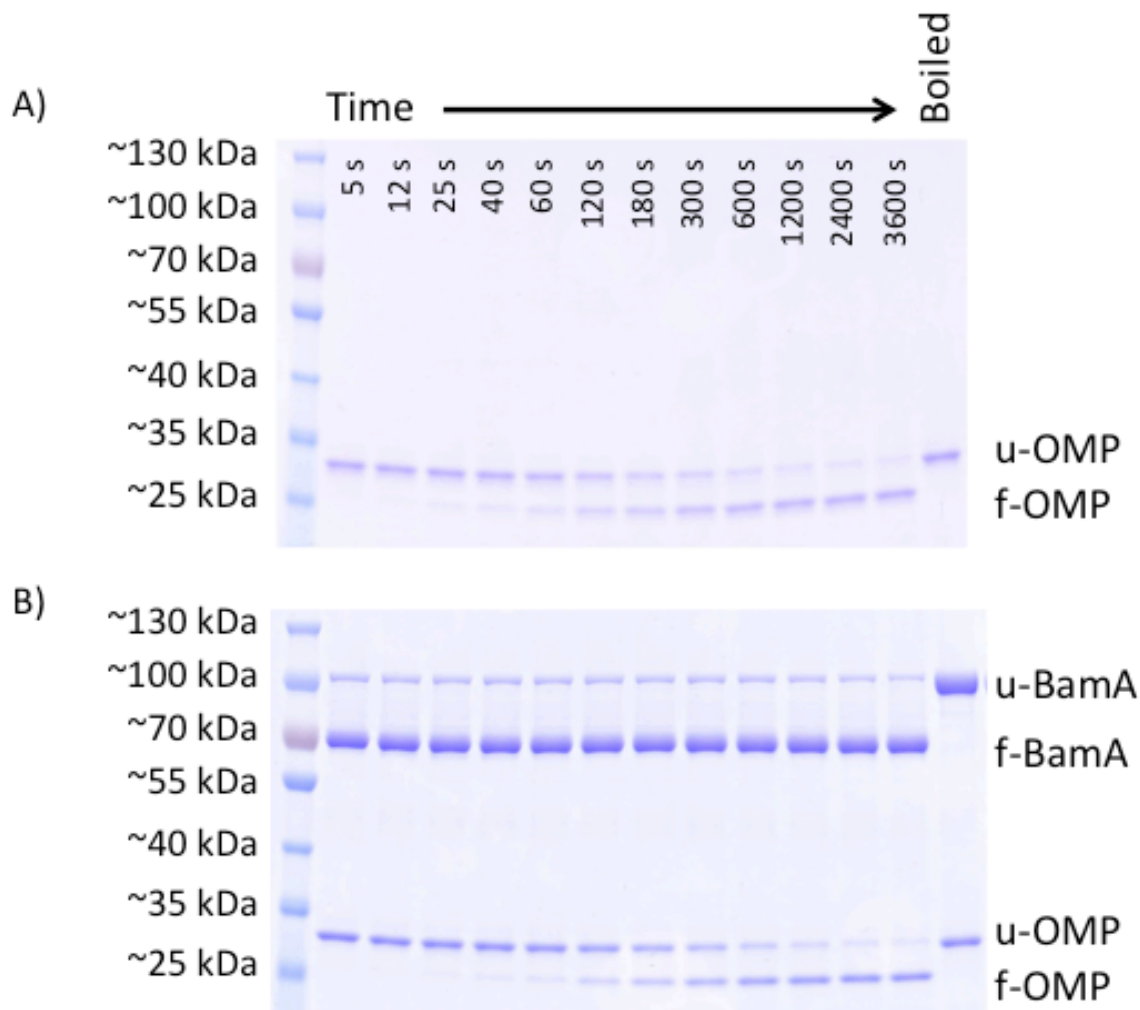
B)



In vitro experimental set-up for intrinsic OMP folding into LUVs (A). OMPs are expressed to inclusion bodies and resolubilized into 8 M urea. The OMP is then diluted into 1 M urea in the

presence of LUVs. OMPs spontaneously insert into LUVs under these conditions. B) *In vitro* experimental set-up for BamA-mediated OMP folding into LUVs. BamA is folded into LUVs as shown in Panel A and is indicated at OMP¹ in Panel B. A second OMP (i.e., OMP²) is then diluted from 8 M urea into 1 M urea in the presence of LUVs containing BamA. OMP² is termed the client OMP and this set-up is referred to as BamA-mediated OMP folding when OMP¹ is BamA.

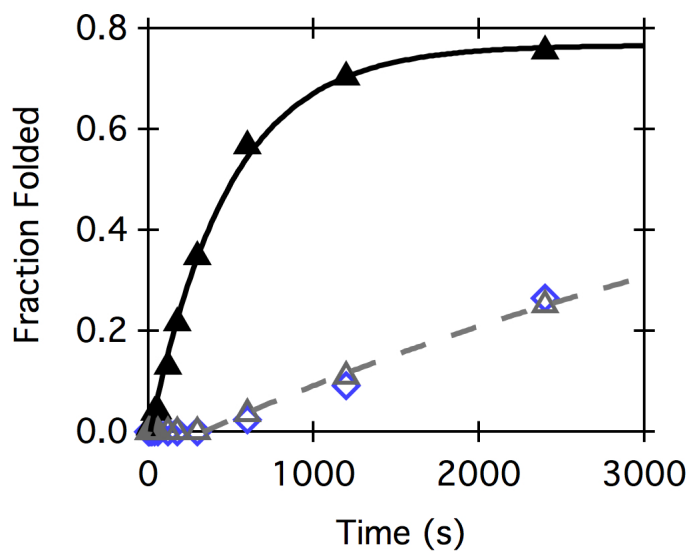
Figure 4.3. Unfolded and folded OMP species are distinguished by their distinct migration via SDS-PAGE.



A representative SDS-PAGE gel is shown for intrinsic folding (i.e., Figure 4.2A) of a representative uOMP into LUVs composed of 100% DiC₁₀-PC (i.e., OmpLA) (Panel A). Over time, the appearance of the band corresponding to folded OMP is observed – this species migrates with an apparent molecular weight of ~25 kDa. The disappearance of the band corresponding to the unfolded OMP species is also observed. This species migrates with an apparent molecular weight of ~32 kDa. A sample collected at the beginning of this experiment that was boiled is shown in the last lane. The density of this band is utilized to determine the

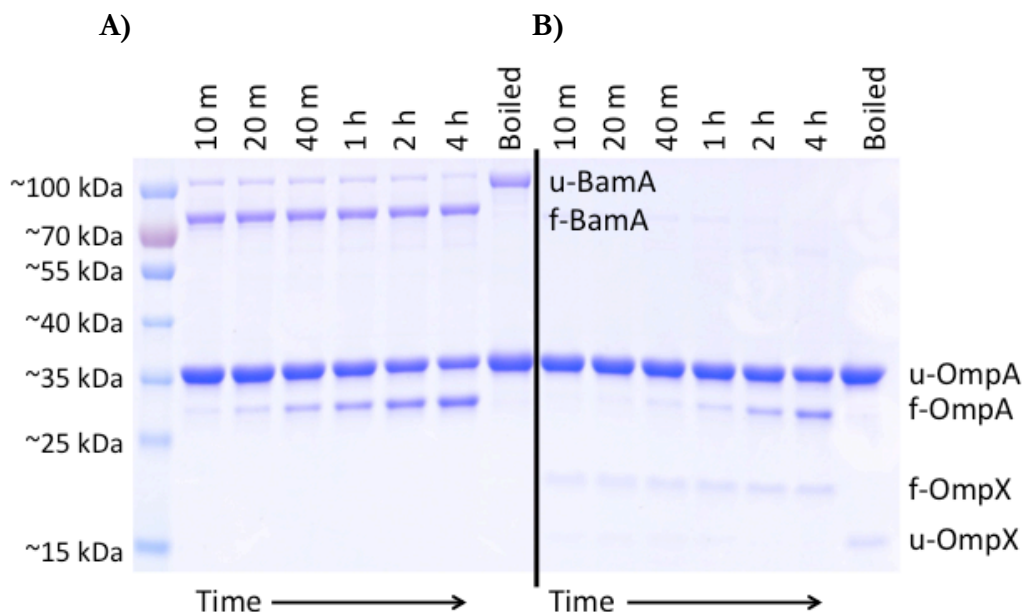
fraction folded of OmpLA at each time point. B) A representative SDS-PAGE gel is shown for BamA-mediated folding (i.e., Figure 4.2B) for a client uOMP into 100% DiC₁₀-PC LUVs (i.e., OmpLA). BamA is folded to completion prior to the addition of the client OMP and its extent of folding is constant throughout all experiments. The folded and unfolded BamA species migrate with apparent molecular weights of approximately 70 and 100 kDa, respectively.

Figure 4.4. BamA functions as an enzyme to accelerate OMP folding into LUVs.



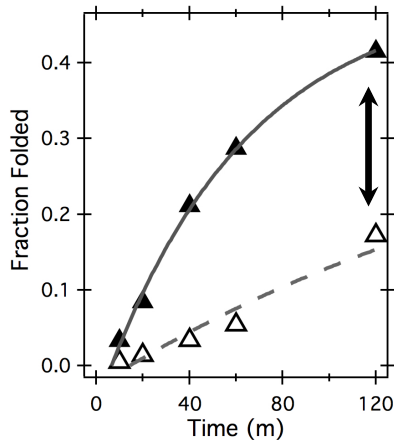
OmpA folds faster in the presence of BamA than in the presence of OmpX or absence of prefolded OMP. OmpA folding in the presence of prefolded BamA (black, filled triangles), OmpX (gray, open triangles), and no prefolded OMP (blue, open diamonds) into LUVs composed of 20% DiC₁₀-PE and 80% DiC₁₀-PC is shown above. This figure is reproduced from (Gessmann et al. 2014).

Figure 4.5. Under modified setup, OmpA folds in the presence of prefolded BamA than OmpX.



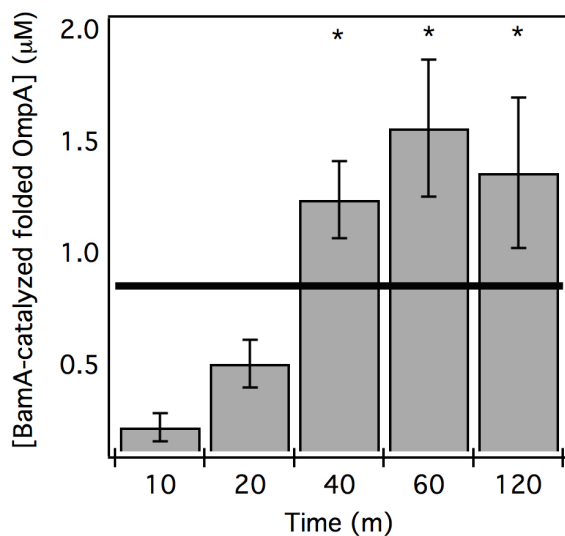
BamA folds more OmpA in 20% DiC₁₀-PE and 80% DiC₁₀-PC (A) than is folded through the intrinsic folding pathway (B) in modified experimental setup. A typical SDS-PAGE gel is shown. Experiment B is a negative control with OmpX prefolded to maintain a constant protein:lipid ratio when comparing folding in the presence and absence of BamA. OmpX does not accelerate the folding of other OMPs. Time points are 10 m, 20 m, 40 m, 1 h, 2 h, and 4 h. This figure is reproduced from (Plummer and Fleming 2015).

Figure 4.6. Kinetic trace of OmpA folding in the presence of BamA and OmpX.



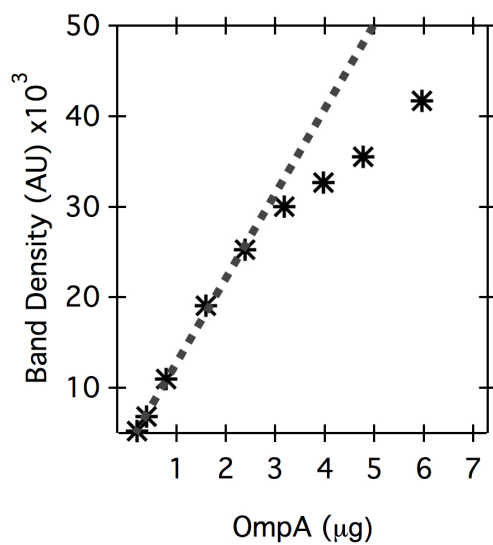
The folding profile of OmpA makes this client OMP ideal for this experimental setup. A representative kinetic trace of OmpA folding in the presence and absence of BamA is shown in dashed and solid lines respectively. The fraction of OmpA folded is plotted over time with filled or empty triangles indicating folding in the presence of BamA or OmpX, respectively. Double exponential fits are shown to guide the eye. The black vertical arrow indicates the amount of OmpA that is folded by BamA, which is defined as the difference between the concentration of OmpA folded in the presence and absence of BamA at a given time point. This figure is reproduced from (Plummer and Fleming 2015).

Figure 4.7. Concentration of OmpA folded by BamA exceeds the concentration of folded BamA.



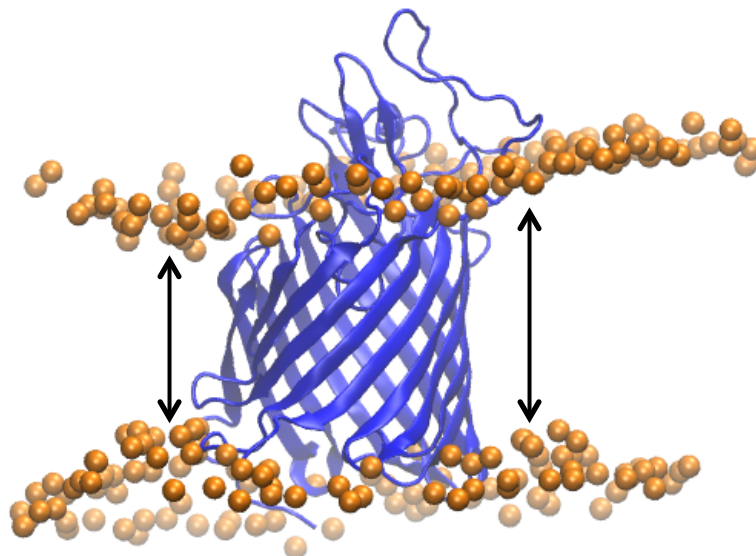
The amount of OmpA folded by BamA at each time point shown in Figures 4.5 and 4.6 is indicated. The horizontal line indicates the amount of BamA folded ($0.85 \pm 0.06 \mu\text{M}$). These reported concentrations are averages with standard deviations from multiple independent experiments ($n=5$) and are provided in Table 4.1. Asterisks indicate a significance of $p < 0.005$ as a result of a Student's t test. Statistical analyses were completed using Microsoft Excel. This figure is reproduced from (Plummer and Fleming 2015).

Figure 4.8. Linear range for concentration determination of OmpA by SDS-PAGE.



The experimental setup shown in Figures 4.5 through 4.7 remains in the linear range for concentration determination of OmpA by SDS-PAGE. Densitometry analyses reveal the linear range for concentration determination of OmpA ends at $\sim 3 \mu\text{g}$. SDS-PAGE samples for experiments presented here corresponds to OmpA mass amounts of $\sim 0.5 \mu\text{g}$. Previous work demonstrates OmpA is monomeric the concentrations ranges used here (Danoff and Fleming 2011). This figure is reproduced from (Plummer and Fleming 2015).

Figure 4.9. The BamA β -barrel may create defects in neighboring bilayer.



Lipid defects, such as hydrophobic mismatch, have been previously reported in molecular dynamics simulations of the BamA β -barrel (Noinaj et al. 2013). The BamA β -barrel is shown as a blue cartoon and the phospholipid phosphorus atoms are shown as orange spheres. This simulation was completed in a 1,2-dimyristoyl-sn-glycero-3-phosphoethanolamine (i.e., DiC₁₄-PE) lipid bilayer and the difference in hydrophobic thickness on the left and right sides of the β -barrel in this representation is ~ 16 Å. The BamA POTRA motifs have been excluded for clarity. VMD was utilized to create this figure. Dr. J.C. Gumbart graciously provided the MD trajectory. This figure is reproduced from (Plummer and Fleming 2016).

4.6. Tables

Table 4.1. Summary of BamA-catalyzed folded OmpA concentrations

| <u>Time (m)</u> | <u>[BamA-catalyzed folded OmpA] (μM)</u> |
|-----------------|--|
| 10 | 0.22 ± 0.06 |
| 20 | 0.51 ± 0.11 |
| 40 | 1.24 ± 0.17 |
| 60 | 1.56 ± 0.31 |
| 120 | 1.36 ± 0.34 |

Concentrations of OmpA folded by BamA exceed the concentration of folded BamA ($0.85 \pm 0.06 \mu\text{M}$). These reported concentrations are averages with standard deviations from multiple independent experiments ($n=5$). This table is reproduced from (Plummer and Fleming 2015).

**Chapter 5 – Dynamic Periplasmic Chaperone Reservoir Facilitates
Biogenesis of Outer Membrane Proteins**

Published as: Costello, S. M., Plummer, A. M., Fleming, P. J., Fleming, K. G., (2016) PNAS,
113(33): E4794-4800.

5.1. Introduction

The cellular envelope of Gram-negative bacteria is comprised of two membranes separated by an aqueous compartment termed the periplasm. The outer membrane of the cellular envelope contain integral β -barrel membrane proteins referred to as outer membrane proteins (OMPs) (Tamm, Hong, and Liang 2004; Walther, Rapaport, and Tommassen 2009). The outer membrane and OMPs provide the first barrier between bacteria and the environment and are essential to many important cellular processes including metabolic transport, bacterial virulence and antibiotic resistance (Bajaj et al. 2012; Nikaido 1989; Wimley 2003). Understanding the pathway by which OMPs traverse the periplasm and attain their native functional state is essential to an ability to manipulate this element of the bacterial cell.

The OMP biogenesis process is distinct from the folding of cytosolic proteins because it involves a unique collection of obstacles. First, OMPs do not adopt their folded conformations while in an aqueous environment (Ebie Tan et al. 2010). Rather, unfolded OMPs (uOMPs) must be transported across the periplasm to reach their native membrane. Because of their marginal solubility in water, this process must be tightly controlled to avoid aggregation. Second, structures of folded OMPs (fOMPs) show that these proteins contain water solvated residues in loops on the outer surfaces of bacteria. The desolvation and transport of these polar and ionizable side chains across the outer membrane represent significant kinetic barriers to OMP folding (Burgess et al. 2008a). Third, Gram-negative bacteria maintain a high density of fOMP in the expanding outer membrane (Jarosławski et al. 2009) that requires a considerable flux of uOMP transport across the periplasm followed by folding to replace OMP lost to dilution during growth (Rassam et al. 2015). Finally, all periplasmic chaperones, proteases, and folding machinery must operate without the free energy provided by ATP hydrolysis, unlike cytosolic proteins with similar roles (Wülfing and Plückthun 1994).

Due to the important cellular functions and the unique biogenesis pathway of OMPs, considerable effort has been applied to understanding the process of OMP folding and assembly. Many *in vitro* and *in vivo* studies have investigated various components involved in this pathway (Bitto and McKay 2004; Dartigalongue, Missiakas, and Raina 2001; Ge, Lyu, et al. 2014; Gessmann et al. 2014; Lazar and Kolter 1996; Moon et al. 2013; Plummer and Fleming 2015; Rouviere and Gross 1996; Sklar, Wu, Kahne, et al. 2007; Thoma et al. 2015; Vuong et al. 2008; Wu et al. 2005). However, *in vitro* experiments typically characterize individual components in isolation while *in vivo* studies are often incapable of deciphering how specific components are responsible for observed phenomena. Computational techniques can overcome these limitations by combining orthogonal sets of information and allowing for unique system-wide studies of multi-protein networks. This holistic approach is especially important when multiple competing reactions occur, as in the transit of uOMP through the periplasm of Gram-negative bacteria. In this cellular compartment, at least four distinct complexes between uOMPs and chaperones can form (i.e., uOMP binding to Skp, SurA, FkpA or DegP), and the emergent properties of periplasmic proteostasis cannot be evaluated without a consideration of this linkage. To date, no computational study has investigated OMP biogenesis in this comprehensive manner, yet this biological system is ideal for this type of analysis because many of the relevant protein species have been well studied in isolation (Walther, Rapaport, and Tommassen 2009).

Towards this end, we created a comprehensive mathematical framework, Outer Membrane Protein Biogenesis Model (OMPBioM), which incorporates known kinetic and thermodynamic parameters for many of the reactions related to uOMP transport across the periplasm. We used both deterministic and stochastic methods to calculate the time-dependent trajectories of uOMPs in the periplasm, to simulate and reproduce several single and double null strain phenotypes as well as the σ^E stress response, to gain insight into periplasmic dynamics

between uOMPs and chaperones, and to predict limits for the effective rate of β -Barrel Assembly Machinery (BAM)-assisted OMP folding. We discovered that OMP biogenesis involves timescales that are much longer than that of chaperone-uOMP complexes. Hundreds of chaperone-uOMP binding and unbinding events take place prior to uOMP folding, suggesting that chaperone-uOMP binding reactions are near equilibrium in the periplasm. Moreover, we find that periplasmic chaperones have distinct roles that complement each other, resulting in preferential flux to folding through a SurA-BAM catalyzed folding pathway. Finally, intricate mechanisms for OMP transport and folding that involve higher order complexes that span the width of the periplasm or that contain parallel chaperone folding pathways with comparable flux are not required to reproduce current experimental observations.

5.2. Methods

OMPBioM is composed of a series of ordinary differential equations that describe the flux of OMPs into and across the periplasm during the process of OMP biogenesis (Figure 5.1, Table 5.1-5.2). This model aims to capture biological phenomena by incorporating known kinetic and thermodynamic parameters. Deterministic simulations were used to solve the system of equations numerically using Matlab R2014b on a Macbook Pro running OS X Yosemite with a 2.5 GHz Intel Core i5 processor and 8 GB of RAM. The stochastic treatment utilized a system built in COPASI, where all simulations were performed using the Gibson Bruck method (Gibson and Bruck 2000).

OMPBioM Treatment: uOMP Synthesis

uOMP enters the periplasm by post-translational secretion across the inner membrane through the Sec translocon (Ruiz, Kahne, and Silhavy 2006). The rate of secretion of uOMP into the periplasm has a lower limit defined by the product of the minimum allowed steady state concentration of fOMP (copy number of 8,000 (Masuda et al. 2009), concentration within the model of 1.48×10^{-4} M) and the rate of dilution due to cellular replication (k_{44}). This estimated lower bound is 2.85×10^{-8} M/s. Additionally, a maximum synthesis rate can be estimated by the copy number of the Sec translocon complex (500 (Matsuyama et al. 1992)), as well as the rate of translocation (~ 20 amino acids per second (Tomkiewicz et al. 2006)) and the average length of a uOMP (400 amino acids), assuming complete occupancy of cellular translocons with uOMP substrate. This estimated upper bound is 4.61×10^{-7} M/s. The WT synthesis rate (k_1 , Figure 5.2, Table 5.1) is between these two limits.

OMPBioM Treatment: Chaperone Synthesis and Oligomerization

Upon translocation into the periplasm uOMP can interact with the chaperones Skp and FkpA, the chaperone/protease DegP, or the chaperone/folding catalyst SurA. Skp is a trimer that binds to and prevents the aggregation of uOMP (Schäfer, Beck, and Müller 1999; Walton and Sousa 2004). FkpA is a dimeric prolyl isomerase that is essential to the cellular response to heat shock (Arié, Sassoon, and Betton 2001; Ge, Lyu, et al. 2014; Ramm and Plückthun 2001). Due to temperature sensitivity and heat shock not being addressed in this work, the activity of FkpA is not assessed in detail except as described below. DegP is a serine endoprotease with several oligomeric states that has been reported to have both protease and chaperone activities (Ge, Wang, et al. 2014a; Iwanczyk, Leong, and Ortega 2011; Krojer, Sawa, et al. 2008). SurA is a monomeric prolyl isomerase that has been shown to bind to uOMP as well as interact with the β -Barrel Assembly Machinery (BAM) (Bitto and McKay 2004; Lazar et al. 1996; Sklar, Wu, Kahne, et al. 2007; Vuong et al. 2008). The mechanistic consideration in this model treats all nascent chaperones as monomeric in agreement with monomeric chaperone synthesis. Chaperone synthesis rates (k_{2-5}) are set to maintain known chaperone concentrations by replacing chaperones lost due to dilution (Table 5.3). Following synthesis, chaperones can undergo sequential reversible bimolecular oligomerization steps (k_{6-17}) until reaching the native apo-oligomerization state. Oligomerization rates have not been measured *in vitro*. However, fast oligomerization reactions with geometric constraints are typically on the order of $2 \times 10^6 \text{ M}^{-1} \text{ s}^{-1}$ (Northrup and Erickson 1992). For simplicity, all oligomerization steps are reduced to bimolecular reactions with rate constants equal to that of a typical fast protein-protein association reaction. Oligomerization is assumed to be favorable. Equilibrium dissociation constants for very favorable protein-protein association reactions as low as 10 fM have been observed, and we assume each bimolecular oligomerization step to be this favorable (Schreiber,

Buckle, and Fersht 1994). This treatment is consistent with intermediate and lower order oligomeric states not being observed *in vivo*.

OMPBioM Treatment: Chaperone Binding of uOMP

Binding of chaperones to uOMP occurs only from the relevant oligomerization state (i.e., SurA binds to uOMP as a monomer (Xu et al. 2007), Skp as a trimer (Qu et al. 2007), and FkpA as a dimer (Ramm and Plückthun 2000)). A simplified DegP mechanism was utilized in which DegP oligomerizes from a monomer, to a dimer, to a trimer, and then to a hexameric state. Although intermediate oligomerization states have not been observed, this treatment is used so that all oligomerization reactions between monomer and the binding active state are second order reactions. DegP binds to uOMP in hexamer units, ultimately forming dodecamers in a highly cooperative two-step mechanism.

Our mechanistic treatment of chaperone-uOMP binding is representative of the current understanding of expression levels and association reactions in the literature (Ishihama et al. 2008; Masuda et al. 2009; Moon et al. 2013; Sklar, Wu, Kahne, et al. 2007; Wu et al. 2011). Each of these proteins has been shown to bind uOMP *in vitro*. Reversible chaperone-uOMP binding rate constants (k_{18-27}) were determined using the binding half-times and equilibrium binding constants observed *in vitro* (Dlugosz, Bojarska, and Antosiewicz 2002; Wu et al. 2011). As binding rates and equilibrium constants have not been determined for all OMPs present in *E. coli*, the binding parameters available were used to describe a hypothetical, generic and representative OMP.

OMPBioM Treatment: OMP Folding

BAM is an outer membrane-localized protein complex that is essential for the folding and assembly of OMPs *in vivo* (Albrecht et al. 2014; Malinverni et al. 2006; Noinaj et al. 2013;

Onufryk et al. 2005; Werner and Misra 2005). Folding of uOMP can occur from unbound uOMP or from a chaperone-uOMP complex ($k_{34,36-40}$) (Gessmann et al. 2014; McMorran et al. 2013; Rouviere and Gross 1996). Only the unbound uOMP and SurA-catalyzed pathway depend on BAM ($k_{34,36}$) (Gessmann et al. 2014; Sklar, Wu, Kahne, et al. 2007; Vuong et al. 2008). Many details of either BAM pathway have yet to be elucidated, and we therefore allow folding through the SurA-BAM pathway at a faster rate than that of the BAM pathway without invoking a specific folding mechanism. This assumption results in physiologically consistent phenotype simulations (Figures 5.3 and 5.4). uOMP folding through the BAM pathway is assumed to be first order. This assumption is valid, as the concentration of the BAM complex does not limit folding *in vivo* (Malinverni et al. 2006). The rate of fOMP unfolding (k_{35}) is determined using the rate constant for folding (k_{34}) and the experimentally observed fOMP folding stability (Moon et al. 2013). We included all possible folding pathways, including BAM-independent folding catalyzed by Skp, DegP, SurA or FkpA, in our model (k_{37-40}) (Table 5.1). Of these chaperones only Skp has been shown to assist uOMP folding *in vitro* with an observed apparent first order rate constant of $1 \times 10^{-4} \text{ s}^{-1}$. However, this rate was measured in non-biological lipid composition in high curvature vesicles that are likely to result in a much greater rate than what occurs *in vivo*. Additionally, chaperone catalyzed BAM-independent folding would face a targeting problem, with the possibility of uOMPs folding into either the inner or outer membrane (Grabowicz, Koren, and Silhavy 2016). We therefore set the chaperone catalyzed BAM-independent folding rates in the model (k_{37-40}) to a low enough value to ensure that no uOMP folding into the inner membrane would occur. Folding rates have not been determined for folding through DegP, FkpA or SurA so the rates are assumed to be maximally equal to that of Skp-uOMP folding.

OMPBioM Treatment: uOMP Aggregation, Degradation and Dilution

uOMP aggregation and degradation reactions are also included within the model. Aggregation consists of a third order nucleation step followed by second order linear polymerization with rates representative of literature values (k_{42-43}) (Danoff and Fleming 2011). uOMP bound to DegP may be degraded, as DegP is a known processive protease (k_{28-33}) (Krojer, Sawa, et al. 2008). To capture the processive behavior of DegP we incorporate a simplified two-step degradation mechanism that does not require the explicit description of each possible partially degraded uOMP state. The mechanism of degradation consists of an initial peptide hydrolysis reaction that results in a folding incompetent substrate that is committed to degradation. The subsequent proteolysis rate constant represents the average amount of time DegP takes to degrade its substrate before dissociating. The primary mechanism for the replacement of fOMP is dilution (Lugtenberg and Alphen 1983; Rassam et al. 2015). This rate of dilution was calculated by assuming a half-time equal to a typical replication time for *E. Coli* (Pierucci 1972).

Kinetic Simulations

The rate of change of any species (x) is defined as the sum of the rates of all reactions that result in that species formation minus the sum of the rates of all reactions that consume that species:

(Equation 5.1)

$$\frac{d[x]}{dt} = \sum_{i=1}^{N_F} rate_{i,Formation} - \sum_{j=1}^{N_C} rate_{j,Consumption}$$

where N_F equals the number of reactions resulting in species formation and N_C equals the number of reactions that result in the species being consumed.

The product of the concentration of all reactants for a given reaction and a rate constant (k) equals the rate of that reaction:

(Equation 5.2)

$$rate_i = k_i \prod_{n=1}^{N_R} [Reactant_n]$$

where N_R equals the number of reactants in reaction i . Applying this procedure on the mechanistic treatment shown in Figure 5.1 results in the set of ordinary differential equations shown in Table 5.2.

As a simplification, all species are considered to be in the periplasm, as the outer membrane is not defined as a separate compartment. Therefore, fOMP concentration corresponds to the theoretical concentration if all fOMP were in the periplasm and not in the outer membrane. This treatment is appropriate, as within the model fOMP does not interact with any periplasmic species and concentrations can be converted to outer membrane copy number using the periplasmic volume. Stochastic simulations require the compartment volume to be defined so concentrations can be converted to compartment copy numbers. Cellular copy numbers for all species are calculated by assuming a periplasmic volume of 9×10^{-17} L (Stock, Rauch, and Roseman 1977).

WT and phenotype simulations were performed using the deterministic method outlined above. Initial conditions contained only free monomeric chaperones and synthesis rates that maintained the total concentrations defined by parameters in the literature. In the case of phenotype experiments, we set the initial concentration and synthesis rate of the appropriate chaperone (e.g., Skp in Δskp or SurA and Skp in $\Delta surA \Delta skp$) to zero. Phenotypes with a significant accumulation of uOMP required further parameterization of synthesis rate and

doubling time (Figure 5.2). Simulations were performed at timescales such that the system reached steady state (Figure 5.5).

The σ^E response was implemented where necessary by increasing the chaperone synthesis rates to reflect known chaperone concentrations under stress conditions (Table 5.4) (Dartigalongue, Missiakas, and Raina 2001). Additionally, the σ^E response involves the down regulation of uOMP synthesis (Mecsas et al. 1993; Onufryk et al. 2005).

Calculation of uOMP Periplasmic Lifetimes

To determine the average lifetime of a uOMP in the periplasm, a generic uOMP (uOMP_a) was synthesized at levels characteristic for a given phenotype. At t=0, expression of uOMP_a was set to zero and expression of a distinguishable uOMP with identical behavior (uOMP_b) was set to the initial expression level of uOMP_a. Subsequently, the fraction of total periplasmic uOMP that consists of uOMP_a was tracked over time. The decay of uOMP_a species was well described by a fit to an exponential decay, which resulted in a time constant representing the average uOMP lifetime. During the lifetime of a uOMP, it samples all forms, including free uOMP and chaperone-bound uOMP.

While computationally efficient, deterministic simulations do not explicitly account for each molecule in a system. Therefore, in addition to the deterministic simulations detailed above, we performed stochastic simulations to determine the average number of binding events experienced by a uOMP in the periplasm. The stochastic treatment utilized a system built in COPASI, with all simulations utilizing the Gibson Bruck algorithm (Gibson and Bruck 2000). A generic uOMP (uOMP_a) was synthesized at levels normal for that phenotype. At t=0 a *single* uOMP_a was replaced by an identical but distinguishable uOMP (uOMP_b). Each binding reaction

resulted in the creation of a species used only for the enumeration of binding events for a given uOMP (Figure 5.6, Table 5.5).

Stochastic simulations can occasionally reveal behavior that cannot be observed in the deterministic model. To ensure that the conclusions resulting from the deterministic simulations were not invalid due to unobservable stochastic behavior, the genetic and lifetime experiments were completed using both the deterministic and stochastic models. These were shown to agree (Figure 5.6). The agreement between the stochastic and deterministic simulations indicates that stochastic behavior does not significantly affect the conclusions reached by the deterministic model. Because of the outstanding efficiency of the deterministic model, this approach was utilized unless stochastic trajectories were specifically required.

Model Assumptions

During the creation of this model we made several simplifying assumptions: (1) because parameters have not been determined for all OMPs present in *E. coli*, we assume a generic and representative OMP behavior; (2) we consider only the major players in OMP biogenesis (e.g., BAM, SurA, DegP, Skp); (3) we consider *E. coli* under a limited set of growth conditions; and (4) we assume a constant rate of growth and rate of expression. Future work could expand the model to address all of these biological complexities: (1) this model has the potential to incorporate OMP heterogeneity when it comes to expression rate, folding, misfolding, binding, and aggregation and address the effect of mutations in both uOMP and quality control proteins on OMP biogenesis; (2) the complexity of the model could be increased to accommodate other cellular systems (e.g., DegS/RseA and disulfide bond formation); (3) modifications could be made to include other β -barrel assembly processes in other organisms as well as a greater degree of biological conditions including heat and pH stress; and (4) future work could include variation in parameters throughout the cell cycle.

5.3. Results

OmpBioM reproduces experimentally observed folded OMP levels and lifetimes.

Figure 5.1 shows the set of linked reactions involved in OMP biogenesis that we incorporated for this mechanistic investigation. OmpBioM deterministically simulates the biogenesis of a representative uOMP using parameters derived from direct observations of *E. coli* or from *in vitro* experiments of *E. coli* proteins. Tables 5.1 and 5.2 list the relevant rate constants and kinetic equations. We used cellular concentrations of known species (Masuda et al. 2009) to reproduce key experimental observables: genetic phenotypes, OMP copy number per cell and uOMP periplasmic lifetime.

Under wild-type (WT) conditions, the area density of fOMP in the outer membrane has been reported to be high, with a copy number per cell between 8,000 and 80,000 (Ishihama et al. 2008; Masuda et al. 2009). Others have shown that the periplasmic lifetime of a representative uOMP (i.e., LamB) is approximately two minutes (Ureta et al. 2007). We used these fOMP levels and periplasmic uOMP lifetime to assess the validity of our treatment of this system. Figure 5.3 shows the WT phenotype in which we obtain a fOMP copy number equal to 28,000, which agrees well with the known experimental values. Similarly, quantitation of periplasmic uOMP lifetime yields an average of one minute in WT cells (Figure 5.6 and Table 5.5), also in excellent agreement with the magnitude observed *in vivo*.

Single chaperone null mutant phenotypes reveal the importance of SurA activity and σ^E response.

We used the reaction scheme outlined in Figure 5.1 to simulate genetic mutants lacking specific chaperones. Four distinct single chaperone null strain simulations ($\Delta degP$, Δskp , $\Delta fkpA$ or $\Delta surA$) were independently performed and compared to the WT simulations and to known

biological phenotypes (Dartigalongue, Missiakas, and Raina 2001; Ge, Lyu, et al. 2014; Rouviere and Gross 1996). Figure 5.3 shows the individual $\Delta degP$, Δskp and $\Delta fkpA$ simulations display fOMP, free and aggregated uOMP concentration profiles that are similar to WT under normal growth conditions. These results are consistent with modest phenotypic effects observed in genetic studies of the null strains for each corresponding chaperone (Ge, Lyu, et al. 2014).

In contrast, SurA is the only single periplasmic chaperone that is known to cause a significant change in fOMP density when depleted (Ge, Lyu, et al. 2014; Rouviere and Gross 1996). Our simulations capture this genetic finding (Figure 5.3). The importance of SurA in OMP biogenesis arises from its dual functions, both of which are incorporated in OMPBioM: (i) SurA can bind to uOMP, thereby preventing aggregation; and (ii) SurA can facilitate the folding of uOMP (Bitto and McKay 2004; Lazar and Kolter 1996; Rouviere and Gross 1996; Sklar, Wu, Kahne, et al. 2007; Thoma et al. 2015; Vuong et al. 2008). Because SurA plays a prominent role in OMP folding, the loss of SurA *in vivo* results in the induction of the σ^E stress response (Ge, Lyu, et al. 2014; Rouviere and Gross 1996), a regulatory mechanism caused by accumulation of unfolded protein in the periplasm. For $\Delta surA$, activation of this envelope stress response results in an increase in chaperone expression and a reduction in uOMP expression; these experimental observations are incorporated into our $\Delta surA$ simulation (Table 5.4) (Onufryk et al. 2005; Rhodius et al. 2006).

To further investigate the role of the σ^E response in managing cellular fitness, we performed *surA* null simulations both in the absence ($\Delta surA^*$) and presence ($\Delta surA$) of a computational treatment of σ^E (Figure 5.7). The hypothetical $\Delta surA^*$ mutant has not been observed *in vivo*. Therefore, a computational comparison between the WT and $\Delta surA^*$ phenotypes is an opportunity to observe the molecular damage that may stimulate an *E. coli* envelope stress response. Figures 5.7 and 5.8 show that the virtual $\Delta surA^*$ results in a reduction

in fOMP and a 290 fold increase in the sum of free and aggregated uOMP compared to WT, consistent with suggestions that the accumulation of periplasmic uOMPs stimulates induction of σ^E (Mecsas et al. 1993).

To mimic the consequences of the stress response in the biologically relevant $\Delta surA$ phenotype, we parameterized OMP synthesis rates and chaperone levels to return fOMP amounts equivalent to those observed *in vivo*. Figure 5.7 shows this reduction in fOMP in $\Delta surA$ compared to WT, which agrees with experiments (13, 15). In addition, Figure 5.8 shows the incorporation of a stress response relieves the nearly 300-fold increase the sum of free and aggregated uOMP populations predicted by $\Delta surA^*$. Moreover, although these populations are lower with the stress response, they are not completely eradicated and are still ~ 10 -fold higher than WT levels. This, too, is consistent with the biologically observed $\Delta surA$ phenotype in which uOMP accumulates in the periplasm yet the conditions are still conducive to growth (Ge, Lyu, et al. 2014; Rouviere and Gross 1996). In addition, the average periplasmic lifetime of an OMP *in vivo* is 10-fold longer in $\Delta surA$ than in WT (Ureta et al. 2007), consistent with our observation that the average periplasmic lifetime in simulated $\Delta surA$ is 15-fold greater than that predicted for WT (Table 5.5). In sum, the agreement between the trends observed *in vivo* and in simulations for the implementation of $\Delta surA$ incorporating a σ^E response further validates the mechanism and parameters used for SurA function and our simulated σ^E response.

Simulations of double null chaperone strains suggest distinct roles for Skp and DegP.

Double null strains obtained by either gene deletion or depletion of periplasmic chaperones have documented phenotypes that can be more severe than single null mutants (Rizzitello, Harper, and Silhavy 2001; Sklar, Wu, Kahne, et al. 2007). *In vivo*, the absence of either DegP or Skp concurrent with the absence of SurA (e.g., $\Delta surA\Delta degP$ or $\Delta surA\Delta skp$) results in a

phenotype more severe than the phenotypes for either $\Delta surA$, $\Delta degP$, Δskp , or $\Delta skp\Delta degP$. This implies that the activities of Skp and DegP are more important in a $\Delta surA$ genetic background than in a WT cell and has been interpreted as evidence of parallel folding pathways in OMP biogenesis (Rizzitello, Harper, and Silhavy 2001; Sklar, Wu, Kahne, et al. 2007). To investigate the roles of these chaperones we simulated and compared the phenotypes of the double null mutants $\Delta skp\Delta degP$, $\Delta surA\Delta degP$, and $\Delta surA\Delta skp$ with a simulated σ^E stress response and appropriate doubling times (Figure 5.3, Table 5.4). Overall we find phenotypes consistent with *in vivo* observations. Similar to each of the single null mutants, Figure 5.3 shows that $\Delta skp\Delta degP$ is viable with minimal phenotypic consequences (Dartigalongue, Missiakas, and Raina 2001; Ge, Lyu, et al. 2014) whereas $\Delta surA\Delta skp$ and $\Delta surA\Delta degP$ mutants (both incorporating σ^E) show either an increase in free and aggregated uOMP or a decrease in the concentration of fOMP relative to the single $\Delta surA$ mutant (Figure 5.3 and 5.8), consistent with experimental results (Rouviere and Gross 1996; Sklar, Wu, Kahne, et al. 2007).

In addition, we observe a large fraction of protein degraded in the $\Delta surA\Delta skp$ simulation (~85%, Figure 5.3 hatched and Figure 5.9). This is attributed to not only the presence of the protease DegP (Ge et al. 2013; Krojer, Sawa, et al. 2008; Strauch, Johnson, and Beckwith 1989) but also the large population of free uOMP available for proteolysis. In contrast, free uOMP cannot be degraded in the $\Delta surA\Delta degP$ simulation because DegP is absent, and OMP can only fold independently of SurA, aggregate, or dilute away. As a consequence, $\Delta surA\Delta degP$ displays an *increase* in the fOMP population compared to either $\Delta surA$ or $\Delta surA\Delta skp$, consistent with *in vivo* findings (Sklar, Wu, Kahne, et al. 2007).

DegP functions primarily as a protease and is under kinetic control.

Although DegP has been suggested to function as both a chaperone and a protease (Castillo-Keller and Misra 2003; Ge et al. 2013; Krojer, Sawa, et al. 2008), our results from double null simulations suggest that the chaperone activity of DegP is not a significant contributor to OMP biogenesis. This conclusion is further supported by results from stochastic simulations that allow enumeration of chaperone-uOMP binding events. DegP is involved in <0.02% of the binding events under WT conditions and <0.4% of uOMP binding events under $\Delta surA$ conditions (Table 5.5). These low percentages suggest that the chaperone activity of DegP may be negligible under all tested conditions.

In what may seem like a contradiction, a significant fraction of uOMP is degraded under stressful conditions, with 71% and 85% of secreted uOMP degraded in the $\Delta surA$ and $\Delta surA \Delta skp$ simulations respectively (Figure 5.9). This phenomenon is a testament to the kinetic partitioning present in this system, with the relatively slow binding of DegP to uOMP substrate and the even slower dissociation of DegP being equally important (Table 5.1). The low population of uOMP, presence of other chaperones, and slow binding together prevent DegP from binding to and degrading uOMP under WT conditions, as evidenced by the low fraction bound and infrequent binding events observed (Table 5.5, Figure 5.10). However, under stress conditions the high population of free periplasmic uOMP (a 10 fold increase in $\Delta surA$, Figure 5.8) and prolonged periplasmic OMP lifetime (Table 5.5) allows a small but significant number of DegP binding events to occur. A high fraction of these binding events result in the degradation of the uOMP substrate because the timescales for DegP dissociation and degradation are similar. Therefore the binding, dissociation and degradation rates for DegP measured *in vitro* are capable of preventing the unnecessary degradation of uOMP under WT

conditions while also allowing for the degradation of substrate and alleviation of uOMP accumulation under stress conditions.

Skp-uOMP complexes are highly populated and display dynamic behavior.

Skp is thought to act as a “holdase” by binding to and preventing the aggregation of uOMP *in vitro* (McMorran et al. 2013; Walton and Sousa 2004; Wu et al. 2011). The binding of Skp to uOMP is thermodynamically favorable and kinetically fast (Table 5.1). The favorable binding results in a large population of Skp-uOMP complex at steady state (Figure 5.10). However, the association rate of Skp to uOMP is near diffusion limited, and the dissociation rate is on the millisecond time scale (Table 5.1). This dissociation time scale is several orders of magnitude shorter than the average periplasmic OMP lifetime under WT conditions, resulting in a large number of association and dissociation events for each OMP client (Table 5.5). Therefore, to the extent that the term “holdase” implies a long-lived Skp-uOMP complex, its usage is misleading. In contrast, the Skp-uOMP interactions are fleeting but populated to a significant extent. A consideration should be made for this dynamic nature of Skp binding when discussing the “holdase” activity. This specific binding kinetic behavior may play a unique role in controlling uOMP conformational populations. The unfolded client may explore a large configurational space, with certain conformations likely favoring either the folding or self-association reactions. We speculate that the fast binding to and dissociation from Skp may help to promote folding-competent or aggregation-incompetent conformations.

The folding rate enhancement provided by SurA is necessary but modest.

SurA is the only soluble chaperone implicated in the *in vivo* folding of uOMP; therefore we investigated this reported “foldase” activity (Lazar et al. 1998). OMPBioM treats the folding of a uOMP through SurA-BAM as faster than the BAM-only pathway. This is expressed using

the term “rate enhancement”, and this parameter is defined as the OMP folding rate through SurA-BAM divided by the OMP folding rate through BAM alone. To investigate the necessary magnitude of the rate enhancement provided by SurA we concurrently varied this parameter with the BAM folding rate (k_{fold}). Figure 5.4 shows this space (cyan) bounded by the known range of OMP periplasmic lifetimes (green) and further constrained by the summed concentration of free and aggregated uOMP (red) and the previously reported phenotype range for ΔsurA (grey). The value of the rate enhancement must be between 3 and 100 to satisfy these constraints, with a WT value of 10. Interestingly, for this physiological range of folding rates and rate enhancements, the majority (between 80 and >99%) of uOMP folds through the SurA-BAM pathway, providing further evidence that SurA plays a key role in OMP biogenesis (Figure 5.11).

It is worth noting that a 10-fold rate enhancement is modest relative to common folding catalyst rate enhancements (Rothman 1989). This observation may provide insight into the “foldase” mechanism of SurA. We speculate that the previously observed binding of SurA to uOMP and interaction of SurA and the BAM complex (Bitto and McKay 2004; Sklar, Wu, Kahne, et al. 2007; Vuong et al. 2008; Wu et al. 2011) simply increase local concentrations, which could be sufficient to provide the modest rate enhancement needed to reproduce phenotypes. For this reason, we propose that the experimentally observed folding catalytic ability of SurA is not necessarily indicative of an intricate folding catalytic mechanism. The details of SurA-BAM mediated OMP folding merit further biophysical investigation.

The estimated effective rate of uOMP folding by BAM is faster than *in vitro* observations.

The mechanistic details for how the BAM complex catalyzes uOMP folding are not well understood (Bakelar, Buchanon, and Noinaj 2016; Danoff and Fleming 2015b; Fleming 2015;

Noinaj et al. 2013, 2014; Plummer and Fleming 2015; Voulhoux, Bos, Geurtsen, Mols and Tommassen 2003). Even lacking this information, we can use OMPBioM to estimate the effective rate necessary for BAM-assisted OMP folding. This parameter must be large enough to prevent an accumulation of periplasmic uOMP but maintain a sufficient amount of fOMP under physiological uOMP synthesis and cellular replication rates. Under WT conditions, the BAM concentration is not rate limiting, as evidenced by no phenotypic effect if BamA levels are reduced 10-fold (Malinverni et al. 2006), therefore we do not explicitly consider BAM concentration effects. Figure 5.12 shows multiple simulation outputs as a function of both the uOMP synthesis rate and BAM-mediated OMP folding rate (i.e., k_{in} and k_{fold} , respectively). Contour lines indicate physiological upper and lower bounds for OMP periplasmic lifetime (green), fOMP copy number per cell (blue), and an upper bound of free and aggregated uOMP (red). Given these limitations, the effective OMP folding rate through the BAM pathway under WT conditions should range from $0.3\text{-}6 \times 10^{-2} \text{ s}^{-1}$.

This value is consistent with the copy numbers for BamA and total OMP and the replication time for *E. coli*. For a cell containing 200 BamA molecules (Masuda et al. 2009) and ~ 28000 fOMPS, the calculated turnover number for BamA would be 140 per cell generation. Assuming a generation time of one hour this results in an expected rate of $3.9 \times 10^{-2} \text{ s}^{-1}$. This calculated first order rate constant is in excellent agreement with the predicted range shown in Figure 5.12.

It is noteworthy that this effective rate constant is currently not attainable *in vitro*. The predicted lower limit (i.e., $0.3 \times 10^{-2} \text{ s}^{-1}$) is an order of magnitude faster than the rate observed for BAM protein A (BamA)-mediated OMP folding in non-native lipid conditions (Plummer and Fleming 2015) and the rate observed for SurA-BAM assisted *in vitro* folding in near native lipid conditions (Hagan and Kahne 2011). This indicates either that current *in vitro* analysis may be

incapable of capturing all of the details of SurA-BAM mediated folding or that additional factors are necessary for proper folding *in vivo*.

5.4. Discussion

Chaperones are dynamic uOMP periplasmic reservoirs.

Because uOMPs are essentially insoluble in monomeric forms in the aqueous milieu of the periplasm (Ebie Tan et al. 2010), periplasmic chaperones are essential for preventing accumulation of unfolded and aggregated species (Dartigalongue, Missiakas, and Raina 2001; Onufryk et al. 2005; Rhodius et al. 2006). Our simulations suggest that WT cells maintain a large reservoir of free chaperones while simultaneously creating a situation where essentially all periplasmic uOMP is bound (Figure 5.3 and 5.10). This is accomplished because the apparent total concentration of each chaperone is tuned to be above its respective equilibrium dissociation constant. This thermodynamic finding is complemented by the fact that kinetic rate constants for folding, binding and unbinding result in chaperone-bound uOMP lifetimes that are orders of magnitude shorter than OMP periplasmic lifetimes. Stated another way: periplasmic chaperones bind their client uOMPs stoichiometrically, are not saturated, and the rates of binding to and dissociating from chaperones are fast (e.g., msec) relative to folding (Wu et al. 2011) (Figure 5.10). This robust chaperone buffering capacity under WT conditions equips the cell with an ability to cope with mild stress quickly without the need to wait for a transcriptional regulatory response. More severe stress conditions will cause the population of free uOMP to increase, thus saturating the available chaperone network. Such a condition requires a consequent increase in the concentration of periplasmic chaperones and protease to maintain cell viability – this is exactly what the σ^E envelope regulatory response is known to accomplish (Rhodius et al. 2006). Interestingly, the modulation of only three parameters (chaperone concentration, uOMP synthesis rate, and rate of dilution) within OMPBioM is capable of capturing the expected phenotype of a genetic knockout that induces σ^E .

A strictly ordered set of reactions is not required to accurately represent OMP biogenesis.

There are known examples of escort mechanisms that shuttle molecules across the periplasm via consecutive protein-protein interactions in which the transported molecule is never free in solution (May et al. 2015). Some of these mechanisms involve stable interactions between soluble proteins with binding partners that are embedded in the inner and outer membranes, essentially forming a physical bridge spanning the periplasm. Accordingly, models for OMP biogenesis have been presented in the literature that include a similar highly ordered mechanism that involves periplasmic chaperones handing uOMP from the Sec translocon to the BAM machinery (Lyu and Zhao 2014). Evidence for these models includes the *in vivo* observation of chaperones binding to partially translocated uOMP as well as chaperones interacting with the BAM folding machinery (Harms et al. 2001; Ureta et al. 2007). Our model considers neither a sequential set of reactions nor the formation of a multi-protein complex that spans the periplasm. Yet OMPBioM still reproduces biological observations. Therefore, these intricate escort mechanisms are not required to explain the process of OMP biogenesis.

Rather, our findings suggest that these biological observations are simply a consequence of the conditions in the periplasm and distinct time scales for key reactions. The abundance of unbound chaperone (Figure 5.10) coupled with the fast rates of chaperone binding (e.g., msec) and the slow rate of translocation (e.g., sec), could explain the experimental observation of chaperones binding to uOMP translocation intermediates. Additionally, OMP lifetimes are at least an order of magnitude longer than the timescales necessary for dissociation of a chaperone-uOMP complex. Therefore, the data to date for OMP maturation can be modeled by simple consideration of thermodynamic and kinetic parameters. This results in a stochastic non-directed process that ends with OMP folding and accurately describes known observables.

One disadvantage of a deterministic treatment is that this methodology cannot track single uOMP trajectories. We therefore complemented these with stochastic simulations to enumerate the binding events per uOMP. Stochastic simulations result in an average of 348 binding (and unbinding) events per uOMP before folding occurs (Figure 5.13A, Table 5.5). Figure 5.13B shows a representative binding trajectory of a single uOMP highlighting the stochastic nature of its interactions. Taken together with the prolonged OMP lifetimes (i.e., 59 sec, Table 5.5), this abundance of chaperone binding events is not consistent with a continuous physical pathway across the periplasm. Although we recognize that neither computational nor experimental kinetic experiments can disprove a more complex model, the lack of evidence supporting a linear physical pathway for OMP biogenesis along with the ability to explain all available data with a simpler mechanism suggests the treatment presented in this model is the most parsimonious at this time.

Skp and DegP may not form a productive parallel folding pathway.

Depletion of either Skp or DegP alone results in a similar phenotype compared to WT, but $\Delta_{surA}\Delta_{skp}$ or $\Delta_{surA}\Delta_{degP}$ result in a phenotype where either fOMP is depleted from the outer membrane or uOMP is accumulated in the periplasm compared to the single null mutant Δ_{surA} (Figure 5.3) (Rizzitello, Harper, and Silhavy 2001; Sklar, Wu, Kahne, et al. 2007). This observation has been used as evidence that Skp and DegP form a folding pathway that is parallel to the SurA-BAM pathway and is essential when SurA is removed from the periplasm (Rizzitello, Harper, and Silhavy 2001; Sklar, Wu, Kahne, et al. 2007). Indeed, folding can formally occur in our model from a complex with any chaperone or from free uOMP (Figure 5.1). However, we observe negligible folding flux through Skp and DegP because the rate constants employed in this mathematical model are relatively low, and neither Skp nor DegP have been shown to interact with the BAM folding machinery.

Nevertheless, to further investigate the role of Skp in catalyzing OMP folding we increased the folding catalytic activity of Skp to be equal to that of SurA. Figure 5.14 shows that the phenotypes resulting from this implementation are not consistent with biological observations. In this hypothetical scenario, none of the Δ_{surA} mutants show perturbations in OMP profiles except the double null $\Delta_{surA}\Delta_{skp}$. Therefore, not only is physiologically relevant folding from Skp or DegP not required, including it in OMPBioM yields phenotypes that are in conflict with experimental results (Dartigalongue, Missiakas, and Raina 2001; Ge, Lyu, et al. 2014; Rouviere and Gross 1996).

Instead of folding catalytic activity, we suggest the main role of Skp and DegP is quality control under stress conditions. The loss of the folding ability of SurA results in the accumulation of free and aggregated uOMP in the periplasm in which free uOMP is still able to fold through the BAM pathway but at a slower rate. This results in the increased levels of uOMP in the periplasm that requires the quality control mechanisms – provided by Skp and DegP – to manage this accumulation. Our results suggest that the loss of these quality control mechanisms is the origin of the importance of these two periplasmic proteins under stress conditions.

Kinetic partitioning prevents uOMP aggregation and degradation under WT conditions.

The kinetic and thermodynamic parameters for the intermediate processes in OMP biogenesis are of special interest due to the lack of an external energy source (i.e., ATP) in the periplasm (Wülfing and Plückthun 1994). Previous work has suggested that the thermodynamic stability of fOMP drives partitioning of uOMP from the relatively stable chaperone complexes to the even more stable native state (Moon et al. 2013). The fact that BamA is essential to cellular viability provides evidence that the kinetics of OMP folding is of the utmost importance as well (Voulhoux, Bos, Geurtsen, Mols and Tommassen 2003). When known thermodynamic and kinetic parameters are implemented into this model, additional relationships between these

two different classes of parameters and this biogenesis pathway are revealed. The relatively slow kinetics of OMP folding result in long periplasmic lifetimes for OMPs, leading to uOMP-chaperone binding reactions poised near equilibrium. Therefore, the populations of free uOMP and chaperone-bound OMP are essentially defined by their binding energies. Under these steady state conditions, the combination of low free uOMP concentrations and aggregation/degradation rate constants that are even slower than folding rate constants prevents aggregated and degraded species from populating to a significant extent. In essence, such states are kinetically inaccessible despite being thermodynamically favorable. We conclude that a finely tuned balance between thermodynamic and kinetic effects maximizes OMP folding and minimizes aggregation and unnecessary degradation.

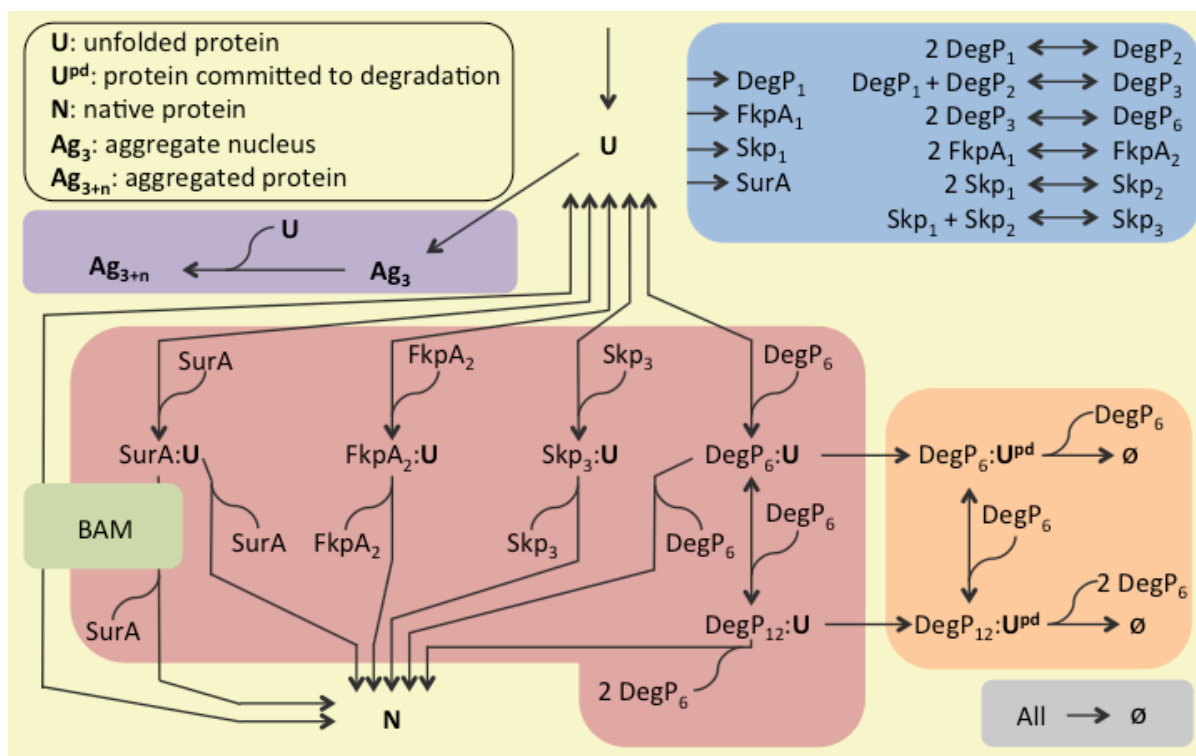
Periplasmic conditions provide simple solutions to challenges faced by OMP biogenesis.

OMP biogenesis is subject to obstacles that are not present in cytoplasmic protein folding systems. OMPBioM simulations indicate that the cell is able to overcome all of these barriers simply by regulating the presence of periplasmic chaperones, proteases and folding catalysts. The folding catalytic ability of BAM and SurA in combination with the chaperone ability of Skp and FkpA and the protease activity of DegP are sufficient to (i) prevent an accumulation of free uOMP and therefore aggregated uOMP, (ii) overcome the kinetic barriers to folding, (iii) maintain fOMP concentrations at sufficient levels, and (iv) accomplish all this in the absence of mechanisms that use ATP. The remedy to the many challenges OMPs face during biogenesis is remarkably simple. The inclusion of chaperones and folding catalysts at biologically observed concentrations with binding, aggregation and degradation rates observed *in vitro* and *in vivo* results in cellular conditions that promote efficient folding of OMP and prevent an accumulation of free and aggregated uOMP in the periplasm. Overall, OMPBioM provides a holistic window into understanding how OMP populations are determined by periplasmic

processes. This system can be easily modified in the future to incorporate new thermodynamic and kinetic information to further investigate any future mechanistic hypotheses for OMP biogenesis.

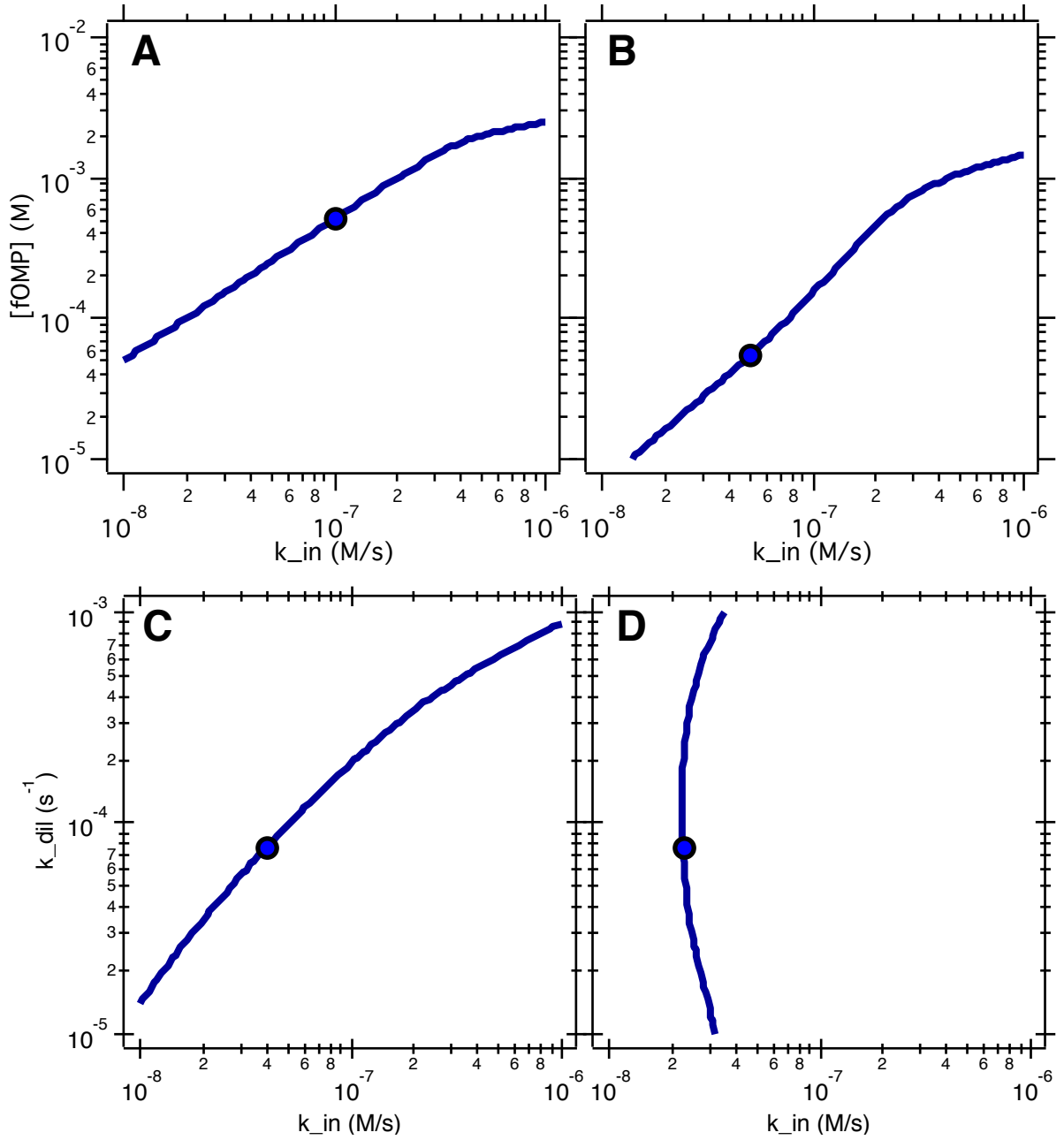
5.5. Figures

Figure 5.1. Diagram of mechanistic treatment used in OMPBioM.



The downward vertical arrow at the top of the figure indicates uOMP synthesis and translocation. Nascent uOMP (U) can either interact with itself through the aggregation pathway (purple), bind to chaperone (red) prior to folding into its native state (N), or be degraded (orange). Chaperones enter the system as monomers before undergoing oligomerization into a binding competent oligomerization state indicated by subscript (blue). All species are subject to a rate of dilution (gray). Chaperones are regenerated upon uOMP folding or unbinding. Folding pathways that are accelerated by BAM implicitly are shown (green). This figure is reproduced from (Costello et al. 2016).

Figure 5.2. Phenotype construction in OMPBioM.

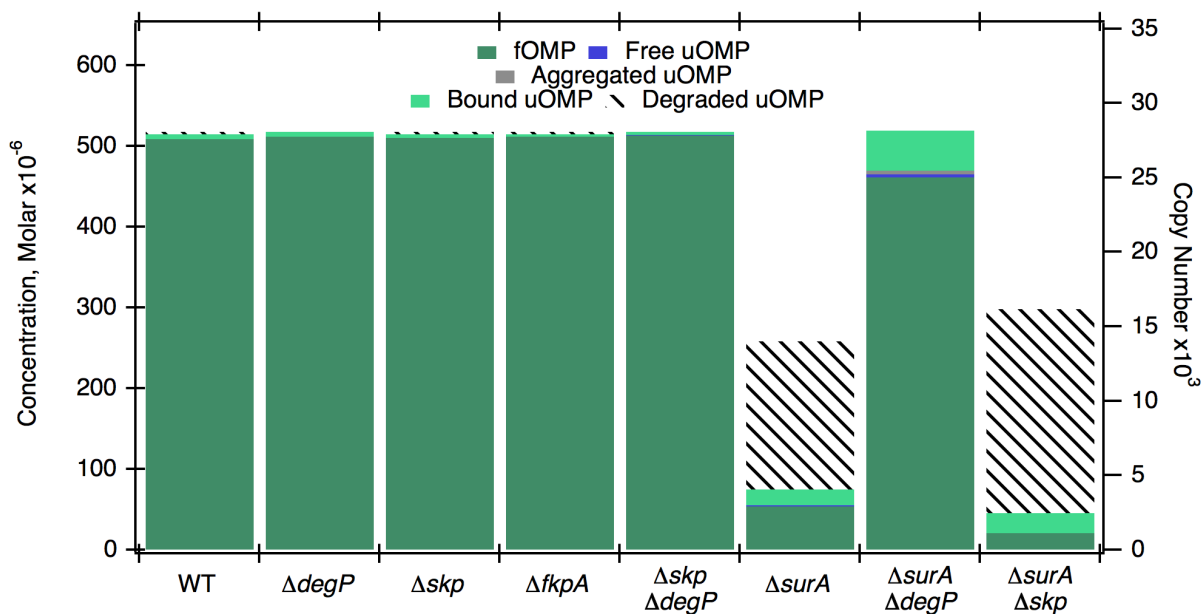


Contour lines showing synthesis and dilution parameterization for WT (A), $\Delta surA$ (B), $\Delta surA \Delta degP$ (C) and $\Delta surA \Delta skp$ (D). (A) The fOMP concentration at steady state as a function of uOMP synthesis rate under WT conditions. A uOMP synthesis rate of 1×10^{-7} M s $^{-1}$ returns a fOMP concentration indicated by the filled circle of 509.34×10^{-6} M (or 5.1×10^{-4}) (copy number

27605 assuming a envelope volume of 9×10^{-17} L) consistent with the expected WT copy number.

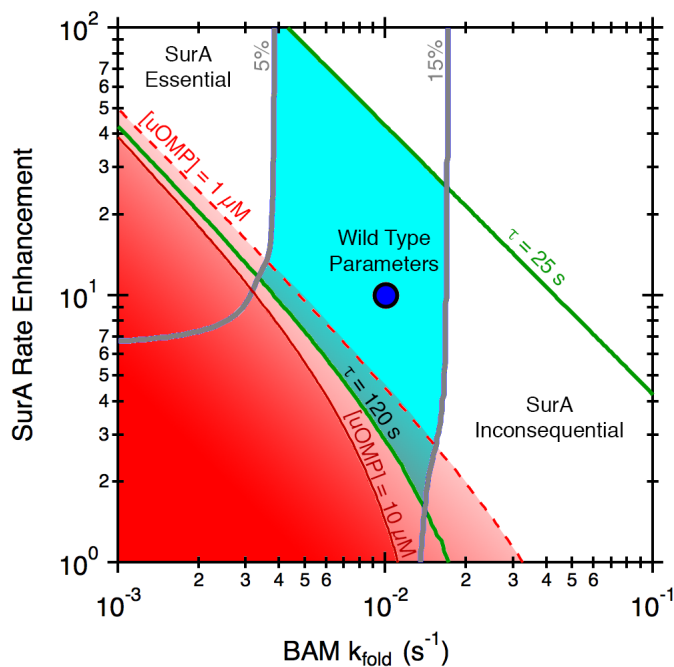
(B) The fOMP concentration at steady state as a function of uOMP synthesis rate under $\Delta surA$ conditions. To achieve a 90% reduction in the steady state fOMP concentration compared to WT (as indicated by the biological phenotype), the uOMP synthesis rate must be reduced by 50% (5×10^{-8} M s⁻¹). (C) The contour line representing a fOMP concentration equal to 90% that of WT as a function of both uOMP synthesis and the rate of dilution under $\Delta surA \Delta degP$ conditions. Assuming the rate of dilution decreases (replication time increases) by a factor of 2.5, the synthesis rate would need to be 4×10^{-8} M s⁻¹. (D) The contour line representing a fOMP concentration equal to 4% that of WT as a function of both uOMP synthesis and the rate of dilution under $\Delta surA \Delta skp$ conditions. Assuming the rate of dilution decreases (replication time increases) by a factor of 2.5, the synthesis rate would need to be 2.3×10^{-8} M s⁻¹. This parameterization yields OMP profiles consistent with those reported in the literature (32). This figure is reproduced from (Costello et al. 2016).

Figure 5.3. Simulated phenotypes in OMPBioM.



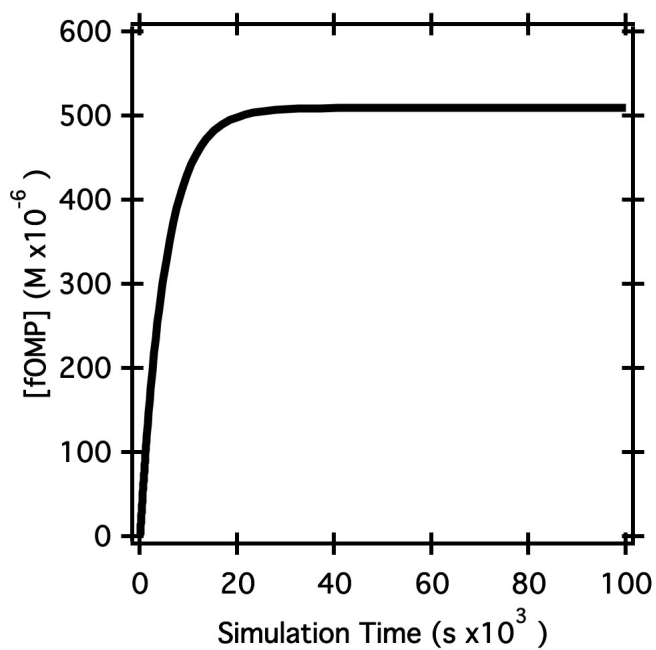
The steady state concentrations of each OMP species in the simulations for the WT and indicated chaperone single and double null mutants are shown. Species include fOMP (dark green), free monomeric uOMP (blue), aggregated uOMP (grey), bound uOMP (light green), and degraded uOMP (hatched lines). Bound uOMP is the sum of uOMP bound to all chaperones, including SurA, Skp, FkpA, and DegP. The x-axis indicates simulated phenotypes. Simulations indicate minimal populations of free and aggregated uOMP are present under WT and mild phenotype conditions. Simulated σ^E responses are included for $\Delta surA$, $\Delta surA \Delta degP$, and $\Delta surA \Delta skp$. Data are provided in tabular form in Table 5.6. This figure is reproduced from (Costello et al. 2016).

Figure 5.4. Summary of simulations to investigate folding rate enhancement provided by SurA.



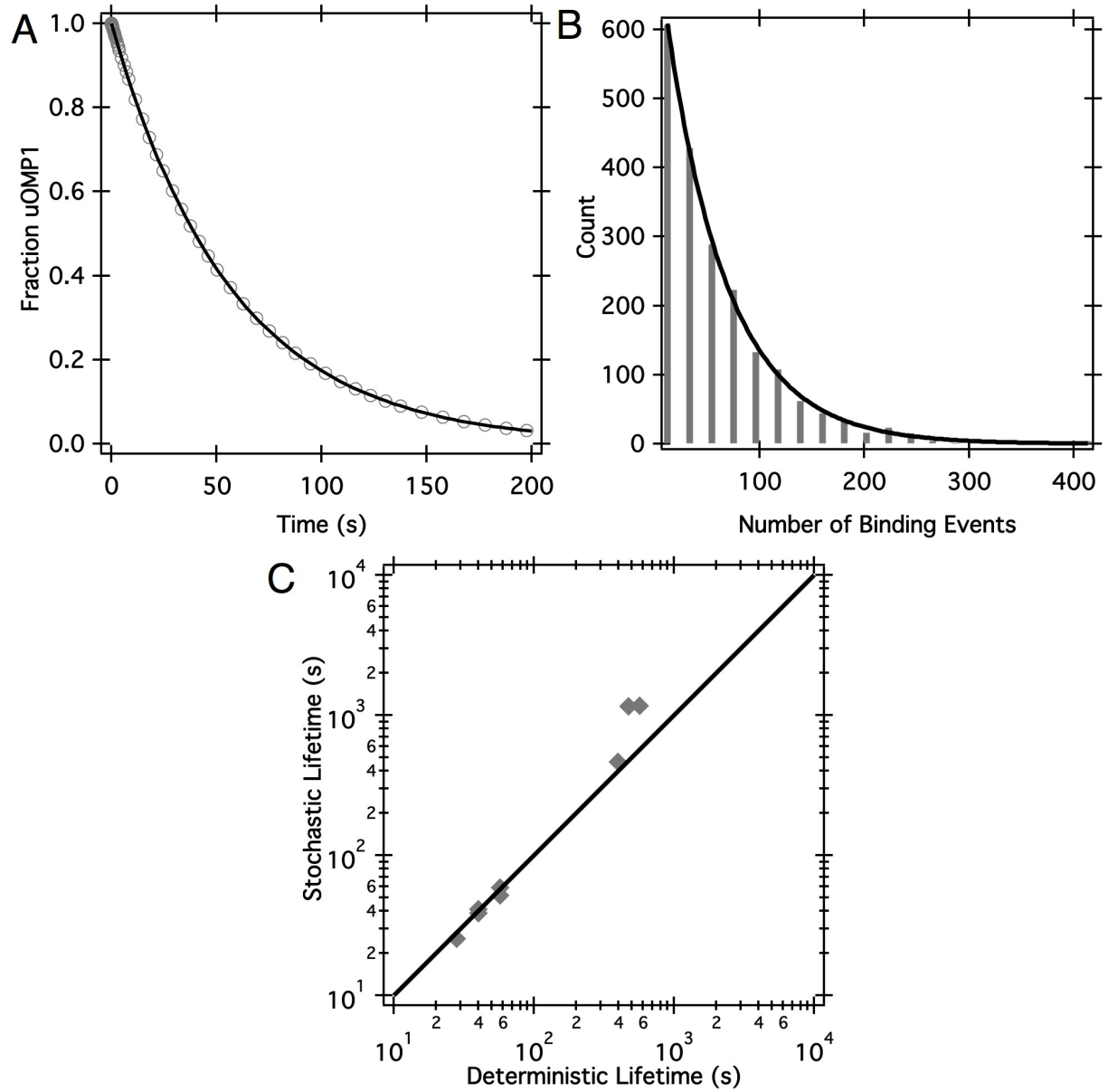
The rate enhancement provided by SurA is defined as the folding rate constant for SurA-BAM divided by the folding rate constant for BAM-only. Shown are contour lines for OMP periplasmic lifetime (green), and summed concentration of free and aggregated uOMP (red). The concentration of fOMP in the $\Delta surA$ simulation and WT simulation are related, where the $\Delta surA$ simulation is expected to return a concentration of fOMP $\sim 10\%$ that of the WT simulation (13). The limits defining where the fOMP concentration in the $\Delta surA$ simulation is 5% or 15% of the WT simulation are shown as grey contour lines. If this value is less than 5% SurA is more essential than expected, and if the value is greater than 15% SurA is more inconsequential than expected. The cyan shaded area indicates the parameter space that results in lifetimes, free and aggregated uOMP concentrations, and fOMP concentrations that agree with experimental observations. This reveals a mild rate enhancement (3-100) is required to recapitulate experimental observations. This figure is reproduced from (Costello et al. 2016).

Figure 5.5. Representative steady state simulation.



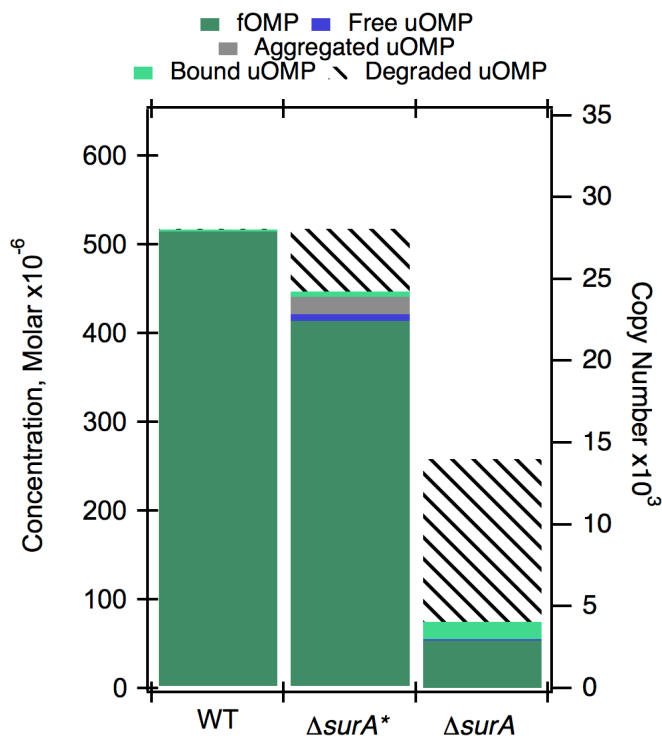
The fOMP concentration over time for a typical WT simulation is shown. Starting from a concentration of zero, [fOMP] reaches steady state in less than 100,000 seconds. Simulations are run for 500,000 seconds to ensure steady state is approached. This figure is reproduced from (Costello et al. 2016).

Figure 5.6. Lifetime measurements by stochastic and deterministic modeling methods.



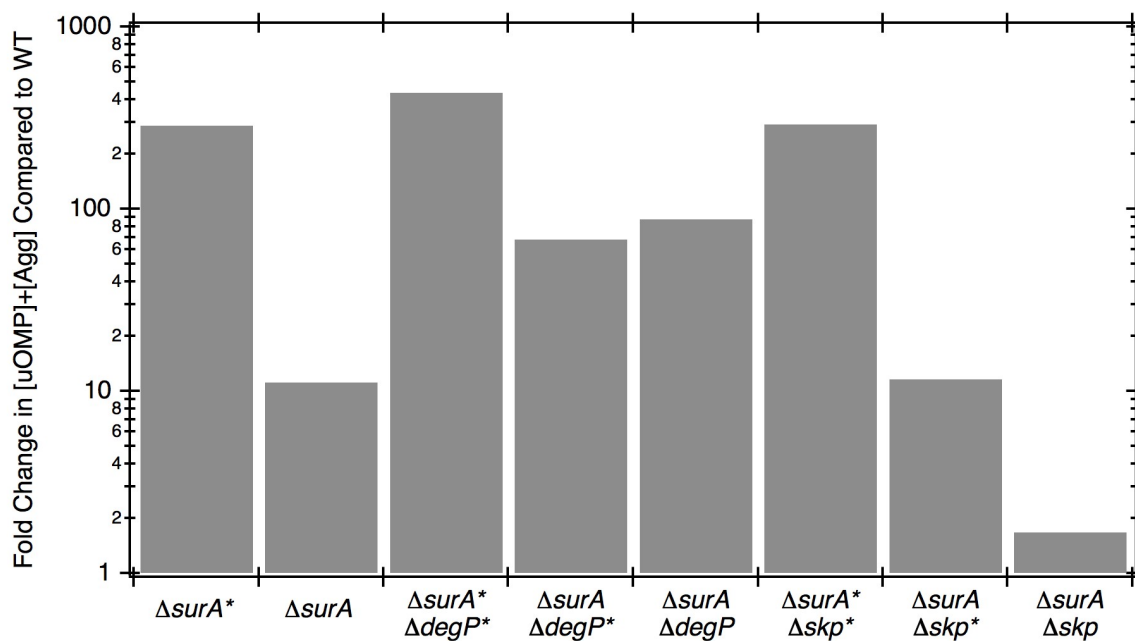
(A) WT periplasmic uOMP lifetime for the deterministic model; (B) Plotted is the distribution of lifetimes for the stochastic model. (C) Correlation between the stochastic and deterministic lifetimes for each null strain phenotype. A line of agreement (Slope=1 y-int=0) is shown for reference. This figure is reproduced from (Costello et al. 2016).

Figure 5.7. OMP populations for simulations with varying σ^E treatments.



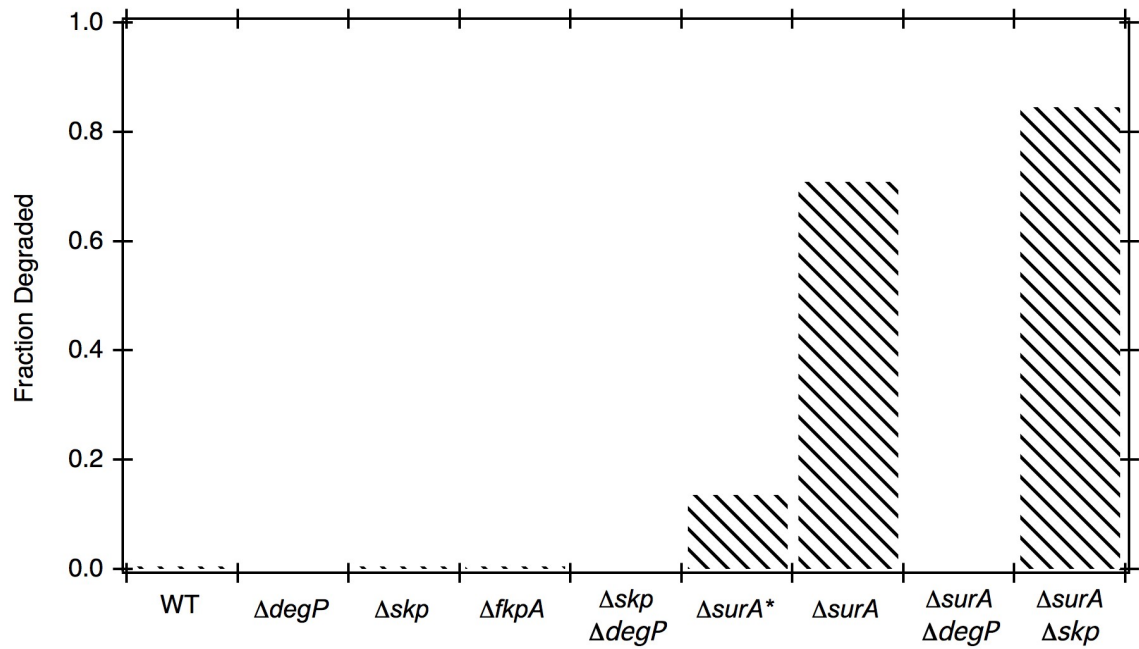
Induction of a model σ^E response alleviates uOMP accumulation at the cost of fOMP depletion. Species include fOMP (dark green), free monomeric uOMP (blue), aggregated uOMP (grey), bound uOMP (light green), and degraded uOMP (hatched lines). Asterisk indicates the deletion was executed without any additional change in uOMP expression or chaperone expression. This figure is reproduced from (Costello et al. 2016).

Figure 5.8. Change in [uOMP] + [Agg] for various phenotypes treatments.



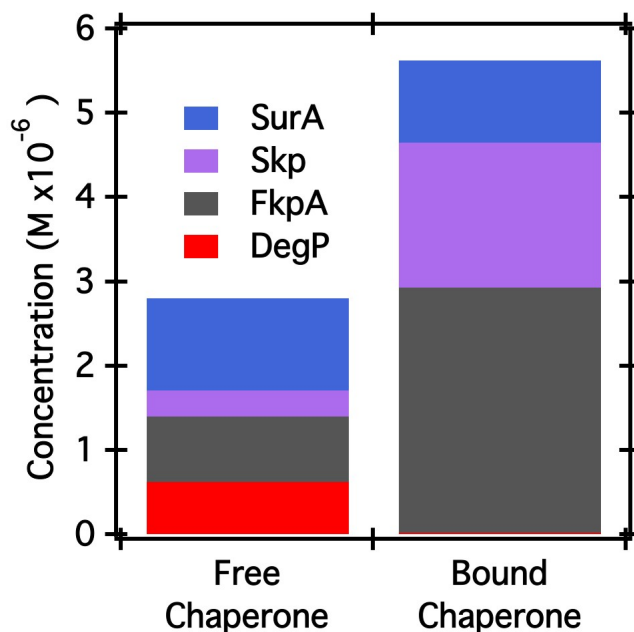
The loss of SurA increases aggregated and free uOMP species in the periplasm. Strains lacking SurA show increases in the sum of their free and aggregated OMP species in the periplasm. The fold increases in the sum of the free and aggregated OMP are referenced to the WT sum and are indicated by the left axis scaling. Asterisks indicate the knockout was executed without any additional change in uOMP expression or chaperone expression. This figure is reproduced from (Costello et al. 2016).

Figure 5.9. Fraction of degraded OMP for phenotype simulations.



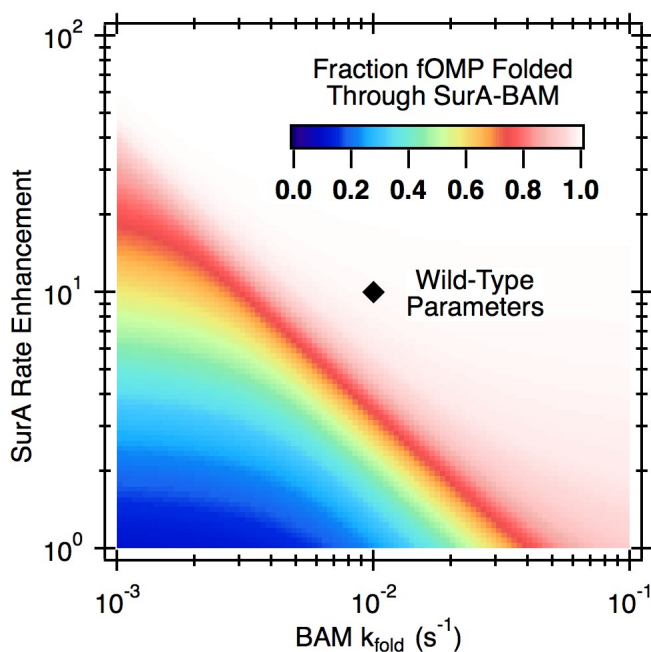
The fraction of secreted uOMP that is degraded by DegP under each relevant genetic condition is shown. The loss of SurA and increase in DegP concentration result in an increase in the fraction of secreted uOMP that is degraded. Asterisks indicate the virtual null phenotype that was executed without any additional change in uOMP expression or chaperone expression. This figure is reproduced from (Costello et al. 2016).

Figure 5.10. Concentrations of free and bound chaperone species in WT simulations.



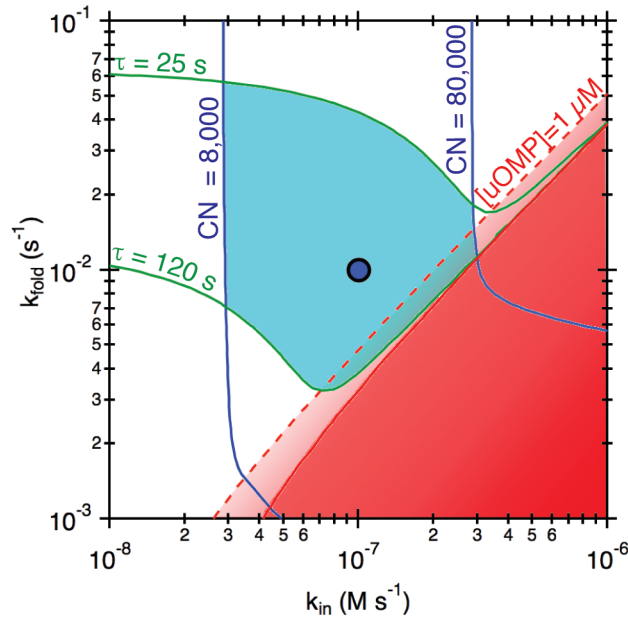
There is a large chaperone reservoir of unbound chaperones. Although >98% of uOMP is bound to chaperone, a significant amount of chaperone is unbound under WT conditions. The simulated concentrations of periplasmic species under WT conditions are plotted. Chaperone species represent the binding competent oligomerization states (i.e., DegP hexamer, Skp trimer, FkpA dimer, SurA monomer). The concentrations of total chaperone are above each of their respective dissociation constants and no chaperone is saturated with uOMP, indicating a reservoir capable of stoichiometric binding of additional uOMP. This figure is reproduced from (Costello et al. 2016).

Figure 5.11. Summary of simulations to determine SurA rate-enhancement for OMP folding.



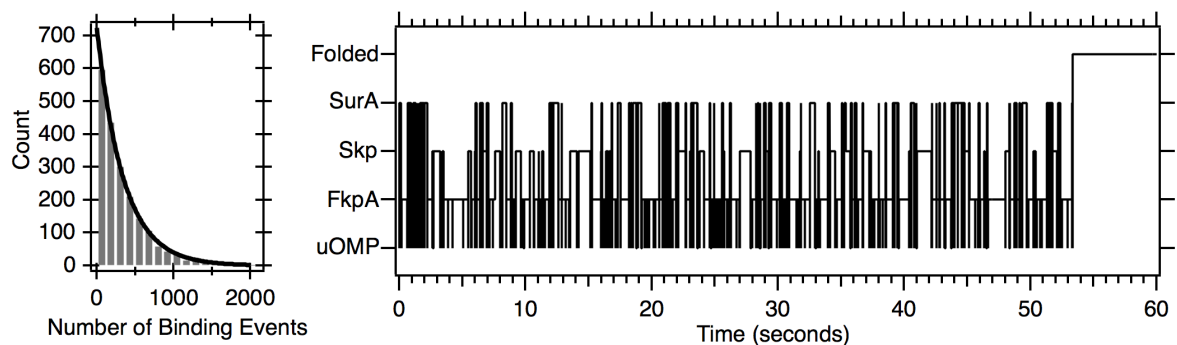
OMPs travel through the SurA-BAM folding pathway, irrespective of the folding rate enhancement provided by SurA. The fraction of OMP folded through SurA for different combinations of BAM folding rates and SurA rate enhancement is plotted. The rate enhancement provided by SurA is defined as the folding rate constant for SurA-BAM divided by the folding rate constant for BAM. This graph shows that greater than 99% of OMP folds through SurA for the WT parameter combination. This figure is reproduced from (Costello et al. 2016).

Figure 5.12. Assessment of *in vivo* BAM folding rates.



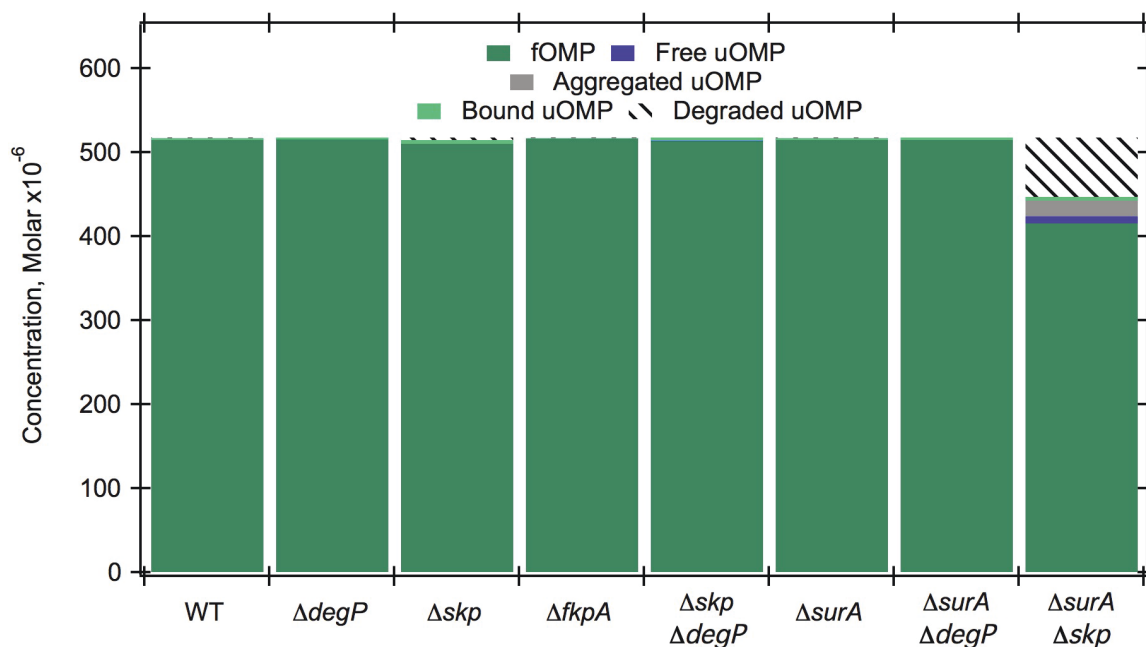
Shown are the contour lines for OMP periplasmic lifetimes (green) and copy number per cell (CN) (blue) as a function of co-variation of the periplasmic input rate (k_{in}) and the effective BAM folding rate (k_{fold}). The parameter space allowed by the known values for OMP lifetimes and CN is indicated in cyan. The dashed red line indicates the boundary where the concentration of free and aggregated uOMP in the periplasm equals 1 μM ; this is a viable parameter space. The solid red line is the $\text{uOMP} + \text{Aggregate} = 10 \mu\text{M}$ boundary; this concentration would be expected to induce the envelope stress response. The increasing red shading in the bottom right corner indicates increasing accumulation of uOMP in the periplasm; these levels would be expected to lead to cell death. This figure is reproduced from (Costello et al. 2016).

Figure 5.13. Summary of stochastic simulations of uOMP flux.



OMP biogenesis is highly dynamic with many binding events occurring in between uOMP synthesis and folding. Panel A shows the number of binding events for each synthesized uOMP under WT conditions. Fitting this data to an exponential decay results in an average number of binding events of 348. Panel B shows a representative trajectory (600,000 steps) of binding events for a single (representative) uOMP over its periplasmic lifetime; between every binding event, the OMP is released to form free uOMP before it is bound by another chaperone. This particular OMP has a periplasmic lifetime of 54 seconds. Table 5.5 shows the number of binding events and lifetime for simulated phenotypes. This figure is reproduced from (Costello et al. 2016).

Figure 5.14. Summary of phenotypes with hypothetical folding mechanism.



Increasing the Skp catalyzed folding rate to be equal to the SurA-BAM catalyzed folding rate results in OMP populations that are inconsistent with experimentally observed phenotypes. Phenotypes generated from simulation with WT parameters except that the Skp folding rate (k_{38}) was set equal to that of SurA-BAM (k_{36}). This shows that the fOMP copy numbers are not consistent with the phenotypes of most mutants. In particular, if Skp could catalyze folding to the same extent as SurA, the Δ_{surA} phenotype would show no change in fOMP concentration, which is inconsistent with experiments. This figure is reproduced from (Costello et al. 2016).

5.6. Tables

Table 5.1. Summary of reactions and WT rate constants within the model.

| <u>Reaction</u> | <u>Rate Constant</u> | <u>Value</u> | <u>Units</u> | <u>Citations</u> |
|------------------------------|--------------------------|-----------------------|--------------|---|
| $\emptyset \rightarrow uOMP$ | k_1 | 1.00×10^{-7} | $M s^{-1}$ | (Koebnik, Locher, and Van Gelder 2000; Lugtenberg and Alphen 1983; Matsuyama et al. 1992; Rassam et al. 2015; Stock, Rauch, and Roseman 1977; Tomkiewicz et al. 2006) |

Synthesis rate determined by estimated total fOMP concentration under WT conditions (Figure 5.2). A lower bound can be calculated from the rate of dilution due to replication (k_{44} , $1.93 \times 10^{-4} s^{-1}$) and an estimate of the lowest allowed concentration of fOMP under WT conditions (copy number of 8,000 (Masuda et al. 2009), concentration within the model of $1.48 \times 10^{-4} M$). This results in a lower bound of $2.85 \times 10^{-8} M s^{-1}$. An estimate of the upper bound can be calculated by assuming a translocon copy number of 500 (Matsuyama et al. 1992), and average uOMP length of 400 amino acids and a rate of translocation of 20 amino acids per second (Tomkiewicz et al. 2006). Assuming maximum translocon occupancy, this would result in an upper bound on the rate of uOMP periplasmic entry of $4.61 \times 10^{-7} M s^{-1}$. Our parameter falls between these two

| <u>Reaction</u> | <u>Rate Constant</u> | <u>Value</u> | <u>Units</u> | <u>Citations</u> |
|---|--------------------------|------------------------|-----------------|--|
| bounds. | | | | |
| $\emptyset \rightarrow SurA$ | k_2 | 4.00×10^{-10} | $M s^{-1}$ | (Masuda et al. 2009; Stock, Rauch, and Roseman 1977) |
| $\emptyset \rightarrow Skp_1$ | k_3 | 1.18×10^{-9} | $M s^{-1}$ | (Masuda et al. 2009; Stock, Rauch, and Roseman 1977) |
| $\emptyset \rightarrow FkpA_1$ | k_4 | 1.42×10^{-9} | $M s^{-1}$ | (Masuda et al. 2009; Stock, Rauch, and Roseman 1977) |
| $\emptyset \rightarrow DegP_1$ | k_5 | 7.47×10^{-10} | $M s^{-1}$ | (Masuda et al. 2009; Stock, Rauch, and Roseman 1977) |
| Chaperone synthesis rates (k_{2-5}) set to the rate necessary to maintain a desired steady state concentration with the determined rate of dilution (k_{44}). The desired steady state concentration was determined using the copy numbers observed in (Masuda et al. 2009) (Table 5.3) and a periplasmic volume of 9×10^{-17} L (Stock, Rauch, and Roseman 1977). | | | | |
| $2 Skp_1 \rightarrow Skp_2$ | k_6 | 2.00×10^6 | $M^{-1} s^{-1}$ | (Northrup |

| <u>Reaction</u> | <u>Rate Constant</u> | <u>Value</u> | <u>Units</u> | <u>Citations</u> |
|--------------------------------------|--------------------------|-----------------------|-----------------|--|
| | | | | and Erickson 1992) |
| $Skp_2 \rightarrow 2 Skp_1$ | k_7 | 2.00×10^{-8} | s^{-1} | (Schreiber, Buckle, and Fersht 1994) |
| $Skp_1 + Skp_2 \rightarrow Skp_3$ | k_8 | 2.00×10^6 | $M^{-1} s^{-1}$ | (Northrup and Erickson 1992) |
| $Skp_3 \rightarrow Skp_1 + Skp_2$ | k_9 | 2.00×10^{-8} | s^{-1} | (Schreiber, Buckle, and Fersht 1994) |
| $2 FkpA_1 \rightarrow FkpA_2$ | k_{10} | 2.00×10^6 | $M^{-1} s^{-1}$ | (Northrup and Erickson 1992) |
| $FkpA_2 \rightarrow 2 FkpA_1$ | k_{11} | 2.00×10^{-8} | s^{-1} | (Schreiber, Buckle, and Fersht 1994) |
| $2 DegP_1 \rightarrow DegP_2$ | k_{12} | 2.00×10^6 | $M^{-1} s^{-1}$ | (Northrup and Erickson 1992) |
| $DegP_2 \rightarrow 2 DegP_1$ | k_{13} | 2.00×10^{-8} | s^{-1} | (Schreiber, Buckle, and Fersht 1994) |
| $DegP_1 + DegP_2 \rightarrow DegP_3$ | k_{14} | 2.00×10^6 | $M^{-1} s^{-1}$ | (Northrup and Erickson |

| <u>Reaction</u> | <u>Rate Constant</u> | <u>Value</u> | <u>Units</u> | <u>Citations</u> |
|--|--------------------------|-----------------------|-----------------|---|
| | | | | 1992) |
| $DegP_3 \rightarrow DegP_1 + DegP_2$ | k_{15} | 2.00×10^{-8} | s^{-1} | (Schreiber, Buckle, and Fersht 1994) |
| $2 DegP_3 \rightarrow DegP_6$ | k_{16} | 2.00×10^6 | $M^{-1} s^{-1}$ | (Northrup and Erickson 1992) |
| $DegP_6 \rightarrow 2 DegP_3$ | k_{17} | 2.00×10^{-8} | s^{-1} | (Schreiber, Buckle, and Fersht 1994) |
| <p>All chaperone oligomerization reactions are assumed to be bimolecular, fast (Northrup and Erickson 1992) and favorable (Schreiber, Buckle, and Fersht 1994). Fast oligomerization reactions with geometric constraints are typically on the order of $2 \times 10^6 M^{-1} s^{-1}$ (Northrup and Erickson 1992), and equilibrium dissociation constants for very favorable protein-protein association reactions as low as 10 fM (Schreiber, Buckle, and Fersht 1994). The product of these two values returns a dissociation rate constant of $2 \times 10^{-8} s^{-1}$.</p> | | | | |
| $uOMP + SurA \rightarrow uOMP:SurA$ | k_{18} | 1.05×10^8 | $M^{-1} s^{-1}$ | (Dlugosz, Bojarska, Antosiewicz 2002; Wu et al. 2011; Xu et al. 2007) |
| $uOMP:SurA \rightarrow uOMP + SurA$ | k_{19} | 1.11×10^1 | s^{-1} | (Dlugosz, Bojarska, Antosiewicz 2002; Wu et |

| <u>Reaction</u> | <u>Rate Constant</u> | <u>Value</u> | <u>Units</u> | <u>Citations</u> |
|---|--------------------------|--------------------|-----------------|--|
| | | | | al. 2011; Xu et al. 2007) |
| $uOMP + Skp_3 \rightarrow uOMP:Skp_3$ | k_{20} | 1.75×10^8 | $M^{-1} s^{-1}$ | (Dlugosz, Bojarska, Antosiewicz 2002; Qu et al. 2007; Wu et al. 2011) |
| $uOMP:Skp_3 \rightarrow uOMP + Skp_3$ | k_{21} | 2.80×10^0 | s^{-1} | (Dlugosz, Bojarska, Antosiewicz 2002; Qu et al. 2007; Wu et al. 2011) |
| $uOMP + FkpA_2 \rightarrow uOMP:FkpA_2$ | k_{22} | 2.39×10^8 | $M^{-1} s^{-1}$ | (Dlugosz, Bojarska, Antosiewicz 2002; Ge, Lyu, et al. 2014; Ramm and Plückthun 2001; Wu et al. 2011) |
| $uOMP:FkpA_2 \rightarrow uOMP + FkpA_2$ | k_{23} | 5.98×10^0 | s^{-1} | (Dlugosz, Bojarska, Antosiewicz |

| <u>Reaction</u> | <u>Rate Constant</u> | <u>Value</u> | <u>Units</u> | <u>Citations</u> |
|--|--------------------------|--------------------|-----------------|--|
| | | | | 2002; Ge, Lyu, et al. 2014; Ramm and Plückthun 2001; Wu et al. 2011) |
| $uOMP + DegP_6 \rightarrow uOMP: DegP_6$ | k_{24} | 1.14×10^5 | $M^{-1} s^{-1}$ | (Dlugosz, Bojarska, Antosiewicz 2002; Kim, Grant, and Sauer 2011; Krojer, Sawa, et al. 2008; Wu et al. 2011) |
| $uOMP: DegP_6 \rightarrow uOMP + DegP_6$ | k_{25} | 1.02×10^1 | s^{-1} | (Dlugosz, Bojarska, Antosiewicz 2002; Kim, Grant, and Sauer 2011; Krojer, Sawa, et al. 2008; Wu et al. 2011) |

| <u>Reaction</u> | <u>Rate Constant</u> | <u>Value</u> | <u>Units</u> | <u>Citations</u> |
|---|--------------------------|--------------------|-----------------|--|
| $uOMP:DegP_6 + DegP_6 \rightarrow uOMP:DegP_{12}$ | k_{26} | 1.00×10^8 | $M^{-1} s^{-1}$ | (Dlugosz, Bojarska, Antosiewicz 2002; Kim, Grant, and Sauer 2011; Krojer, Sawa, et al. 2008; Wu et al. 2011) |
| $uOMP:DegP_{12} \rightarrow uOMP:DegP_6 + DegP_6$ | k_{27} | 8.94×10^3 | s^{-1} | (Dlugosz, Bojarska, Antosiewicz 2002; Kim, Grant, and Sauer 2011; Krojer, Sawa, et al. 2008; Wu et al. 2011) |
| <p>Chaperone-uOMP binding half times and equilibrium constants were reported in (Wu et al. 2011) and converted to rate constants using (Dlugosz, Bojarska, Antosiewicz 2002). Binding of chaperones to uOMP occurs only from the relevant oligomerization state (i.e., SurA binds to uOMP as a monomer (Xu et al. 2007), Skp as a trimer (Qu et al. 2007), and FkpA as a dimer (Ramm and Plückthun 2000)). DegP binds to uOMP in hexamer units, ultimately forming dodecamers in a highly cooperative two-step mechanism, consistent with the structures observed in (Krojer, Sawa, et al. 2008).</p> | | | | |

| <u>Reaction</u> | <u>Rate Constant</u> | <u>Value</u> | <u>Units</u> | <u>Citations</u> |
|---|--------------------------|-----------------------|-----------------|--|
| $uOMP: DegP_6 \rightarrow uOMP^{pd}: DegP_6$ | k_{28} | 1.00×10^0 | s^{-1} | (Hedstrom 2002; Kim, Grant, and Sauer 2011; Krojer, Sawa, et al. 2008) |
| $uOMP: DegP_{12} \rightarrow uOMP^{pd}: DegP_{12}$ | k_{29} | 1.00×10^0 | s^{-1} | (Hedstrom 2002; Kim, Grant, and Sauer 2011; Krojer, Sawa, et al. 2008) |
| $uOMP^{pd}: DegP_6 + DegP_6 \rightarrow uOMP^{pd}: DegP_{12}$ | k_{30} | 1.00×10^8 | $M^{-1} s^{-1}$ | (Hedstrom 2002; Kim, Grant, and Sauer 2011; Krojer, Sawa, et al. 2008) |
| $uOMP^{pd}: DegP_{12} \rightarrow uOMP^{pd}: DegP_6 + DegP_6$ | k_{31} | 8.94×10^3 | s^{-1} | (Hedstrom 2002; Kim, Grant, and Sauer 2011; Krojer, Sawa, et al. 2008) |
| $uOMP^{pd}: DegP_6 \rightarrow DegP_6$ | k_{32} | 3.00×10^{-2} | s^{-1} | (Hedstrom 2002; Kim, Grant, and |

| <u>Reaction</u> | <u>Rate Constant</u> | <u>Value</u> | <u>Units</u> | <u>Citations</u> |
|--|--------------------------|------------------------|--------------|---|
| | | | | Sauer 2011; Krojer, Sawa, et al. 2008) |
| $uOMP^{pd}: DegP_{12} \rightarrow 2 DegP_6$ | k_{33} | 3.00×10^{-2} | s^{-1} | (Hedstrom 2002; Kim, Grant, and Sauer 2011; Krojer, Sawa, et al. 2008) |
| <p>Proteolysis by DegP is modeled as a processive reaction. uOMP bound to either the hexameric form or the dodecameric form of DegP can undergo a hydrolysis step with a rate defined by the k_{cat}. This rate constant ($k_{28,29}$) is representative of values observed in serine proteases (Hedstrom 2002). Following initial hydrolysis, the partially degraded uOMP is then committed to degradation and DegP is regenerated at a rate that is representative of the typical k_{cat} and the average number of peptide bonds in a typical uOMP (~ 400) ($k_{32,33}$).</p> | | | | |
| $uOMP \rightarrow fOMP$ (BAM-only) | k_{34} | 1.00×10^{-2} | s^{-1} | (Gessmann et al. 2014; Ureta et al. 2007) |
| $fOMP \rightarrow uOMP$ | k_{35} | 1.00×10^{-17} | s^{-1} | (Moon et al. 2013) |
| $uOMP: SurA \rightarrow fOMP + SurA$ (SurA-BAM) | k_{36} | 1.00×10^{-1} | s^{-1} | (Bennion et al. 2010; Gessmann et al. 2014; Sklar, Wu, |

| <u>Reaction</u> | <u>Rate Constant</u> | <u>Value</u> | <u>Units</u> | <u>Citations</u> |
|---|--------------------------|-----------------------|-----------------|--|
| | | | | Kahne, et al. 2007; Ureta et al. 2007; Vuong et al. 2008) |
| $uOMP: SurA \rightarrow fOMP + SurA$ | k_{37} | 1.00×10^{-9} | s^{-1} | |
| $uOMP: Skp_3 \rightarrow fOMP + Skp_3$ | k_{38} | 1.00×10^{-9} | s^{-1} | (Patel et al. 2009) |
| $uOMP: FkpA_2 \rightarrow fOMP + FkpA_2$ | k_{39} | 1.00×10^{-9} | s^{-1} | |
| $uOMP: DegP_6 \rightarrow fOMP + DegP_6$ | k_{40} | 1.00×10^{-9} | s^{-1} | |
| $uOMP: DegP_{12} \rightarrow fOMP + 2 DegP_6$ | k_{41} | 1.00×10^{-9} | s^{-1} | |
| <p>OMP folding rates through BAM ($k_{34,36}$) are representative of what has been observed <i>in vivo</i> (Ureta et al. 2007).</p> <p>fOMP unfolding rate is determined using the folding rate and folding stabilities observed <i>in vitro</i> (Moon et al. 2013).</p> <p>Chaperone-uOMP folding is assumed to be slow enough that flux is negligible, as BAM-independent folding would face a targeting problem allowing uOMP to fold into both the inner and outer membranes. Less than 0.001 copies of a uOMP can fold through this pathway per generation.</p> | | | | |
| $3 uOMP \rightarrow uOMP_{Nucleus}$ | k_{42} | 3.50×10^2 | $M^{-2} s^{-1}$ | (Collins et al. 2004; Danoff and Fleming 2011; García-Fruitós et al. 2011; |

| <u>Reaction</u> | <u>Rate Constant</u> | <u>Value</u> | <u>Units</u> | <u>Citations</u> |
|---|--------------------------|-----------------------|---------------------------------|--|
| | | | | Hortschansky et al. 2005; Lin et al. 2008; Usui et al. 2009) |
| $uOMP + uOMP_{Nucleus} \rightarrow uOMP_{Aggregate} + uOMP_{Nucleus}$ | k_{43} | 5.00x10 ⁵ | M ⁻¹ s ⁻¹ | (Collins et al. 2004; Danoff and Fleming 2011; García- Fruitós et al. 2011; Hortschansky et al. 2005; Lin et al. 2008; Usui et al. 2009) |
| Aggregation consists of a third order nucleation step followed by second order linear polymerization with rates representative of literature values | | | | |
| $All \rightarrow \emptyset$ | k_{44} | 1.93x10 ⁻⁴ | s ⁻¹ | (Lugtenberg and Alphen 1983; Pierucci 1972; Rassam et al. 2015) |
| This rate of dilution (k_{44}) was calculated by assuming a half-time equal to a typical replication time for <i>E. coli</i> (Pierucci 1972) | | | | |

The speed of any given reaction is defined by the reaction stoichiometry, rate constant, and reactant concentrations. Citations and notes for each of the obtained values are listed. This table is reproduced from (Costello et al. 2016).

Table 5.2. Ordinary Differential Equations for each species within the model.

| <u>Eqn #</u> | <u>Equation</u> | | |
|------------------|----------------------------|---|---|
| 1 | $\frac{d[uOMP]}{dt}$ | = | $ \begin{aligned} &k_1 - k_{34}[uOMP] + k_{35}[fOMP] - k_{18}[uOMP][SurA] \\ &\quad - k_{20}[uOMP][Skp_3] - k_{22}[uOMP][FkpA_2] \\ &\quad - k_{24}[uOMP][DegP_6] + k_{19}[uOMP:SurA] \\ &\quad + k_{21}[uOMP:Skp_3] + k_{23}[uOMP:FkpA_2] \\ &\quad + k_{25}[uOMP:DegP_6] - 3k_{42}[uOMP]^3 \\ &\quad - k_{43}[uOMP][uOMP_{Nucleus}] - k_{44}[uOMP] \end{aligned} $ |
| 2 | $\frac{d[fOMP]}{dt}$ | = | $ \begin{aligned} &k_{34}[uOMP] + k_{36}[uOMP:SurA] + k_{37}[uOMP:SurA] \\ &\quad + k_{38}[uOMP:Skp_3] + k_{39}[uOMP:FkpA_2] \\ &\quad + k_{40}[uOMP:DegP_6] + k_{41}[uOMP:DegP_{12}] \\ &\quad - k_{35}[fOMP] - k_{44}[fOMP] \end{aligned} $ |
| 3 | $\frac{d[SurA]}{dt}$ | = | $ \begin{aligned} &k_2 - k_{18}[uOMP][SurA] + k_{19}[uOMP:SurA] \\ &\quad + k_{36}[uOMP:SurA] + k_{37}[uOMP:SurA] \\ &\quad - k_{44}[SurA] \end{aligned} $ |
| 4 | $\frac{d[uOMP:SurA]}{dt}$ | = | $ \begin{aligned} &k_{18}[uOMP][SurA] - k_{19}[uOMP:SurA] - k_{36}[uOMP:SurA] \\ &\quad - k_{37}[uOMP:SurA] - k_{44}[uOMP:SurA] \end{aligned} $ |
| 5 | $\frac{d[Skp_1]}{dt}$ | = | $ \begin{aligned} &k_3 - 2k_6[Skp_1]^2 + 2k_7[Skp_2] - k_8[Skp_1][Skp_2] + k_9[Skp_3] \\ &\quad - k_{44}[Skp_1] \end{aligned} $ |
| 6 | $\frac{d[Skp_2]}{dt}$ | = | $ \begin{aligned} &k_6[Skp_1]^2 - k_7[Skp_2] - k_8[Skp_1][Skp_2] + k_9[Skp_3] \\ &\quad - k_{44}[Skp_2] \end{aligned} $ |
| 7 | $\frac{d[Skp_3]}{dt}$ | = | $ \begin{aligned} &k_8[Skp_1][Skp_2] - k_9[Skp_3] - k_{20}[uOMP][Skp_3] \\ &\quad + k_{21}[uOMP:Skp_3] + k_{38}[uOMP:Skp_3] \\ &\quad - k_{44}[Skp_3] \end{aligned} $ |
| 8 | $\frac{d[uOMP:Skp_3]}{dt}$ | = | $ \begin{aligned} &k_{20}[uOMP][Skp_3] - k_{21}[uOMP:Skp_3] - k_{38}[uOMP:Skp_3] \\ &\quad - k_{44}[uOMP:Skp_3] \end{aligned} $ |

| <u>Eqn</u> <u>#</u> | <u>Equation</u> | | |
|------------------------|-----------------------------|---|--|
| 9 | $\frac{d[FkpA_1]}{dt}$ | = | $k_4 - 2k_{10}[FkpA_1]^2 + 2k_{11}[FkpA_2] - k_{44}[FkpA_1]$ |
| 10 | $\frac{d[FkpA_2]}{dt}$ | = | $k_{10}[FkpA_1]^2 - k_{11}[FkpA_2] - k_{22}[uOMP][FkpA_2]$ $+ k_{23}[uOMP:FkpA_2] + k_{39}[uOMP:FkpA_2]$ $- k_{44}[FkpA_2]$ |
| 11 | $\frac{d[uOMP:FkpA_2]}{dt}$ | = | $k_{22}[uOMP][FkpA_2] - k_{23}[uOMP:FkpA_2]$ $- k_{39}[uOMP:FkpA_2] - k_{44}[uOMP:FkpA_2]$ |
| 12 | $\frac{d[DegP_1]}{dt}$ | = | $k_5 - 2k_{12}[DegP_1]^2 + 2k_{13}[DegP_2] - k_{14}[DegP_1][DegP_2]$ $+ k_{15}[DegP_3] - k_{44}[DegP_1]$ |
| 13 | $\frac{d[DegP_2]}{dt}$ | = | $k_{12}[DegP_1]^2 - k_{13}[DegP_2] - k_{14}[DegP_1][DegP_2]$ $+ k_{15}[DegP_3] - k_{44}[DegP_2]$ |
| 14 | $\frac{d[DegP_3]}{dt}$ | = | $k_{14}[DegP_1][DegP_2] - k_{15}[DegP_3] - 2k_{16}[DegP_3]^2$ $+ 2k_{17}[DegP_6] - k_{44}[DegP_3]$ |
| 15 | $\frac{d[DegP_6]}{dt}$ | = | $k_{16}[DegP_3]^2 - k_{17}[DegP_6] - k_{24}[uOMP][DegP_6]$ $+ k_{25}[uOMP:DegP_6]$ $- k_{26}[uOMP:DegP_6][DegP_6]$ $+ k_{27}[uOMP:DegP_{12}]$ $- k_{30}[uOMP^*:DegP_6][DegP_6]$ $+ k_{31}[uOMP^*:DegP_{12}]$ $+ k_{32}[uOMP^*:DegP_6]$ $+ 2k_{33}[uOMP^*:DegP_{12}]$ $+ k_{40}[uOMP:DegP_6] + 2k_{41}[uOMP:DegP_{12}]$ $- k_{44}[DegP_6]$ |

| <u>Eqn</u> <u>#</u> | <u>Equation</u> | | |
|------------------------|--------------------------------------|---|--|
| 16 | $\frac{d[uOMP: DegP_6]}{dt}$ | = | $k_{24}[uOMP][DegP_6] - k_{25}[uOMP: DegP_6]$ $- k_{26}[uOMP: DegP_6][DegP_6]$ $+ k_{27}[uOMP: DegP_{12}] - k_{28}[uOMP: DegP_6]$ $- k_{40}[uOMP: DegP_6] - k_{44}[uOMP: DegP_6]$ |
| 17 | $\frac{d[uOMP: DegP_{12}]}{dt}$ | = | $k_{26}[uOMP: DegP_6][DegP_6] - k_{27}[uOMP: DegP_{12}]$ $- k_{29}[uOMP: DegP_{12}] - k_{41}[uOMP: DegP_{12}]$ $- k_{44}[uOMP: DegP_{12}]$ |
| 18 | $\frac{d[uOMP_{Aggregate}]}{dt}$ | = | $k_{43}[uOMP][uOMP_{Nucleus}] - k_{44}[uOMP_{Aggregate}]$ |
| 19 | $\frac{d[uOMP_{Nucleus}]}{dt}$ | = | $k_{42}[uOMP]^3 - k_{44}[uOMP_{Nucleus}]$ |
| 20 | $\frac{d[uOMP^{pd}: DegP_6]}{dt}$ | = | $k_{28}[uOMP: DegP_6] - k_{30}[uOMP^*: DegP_6][DegP_6]$ $+ k_{31}[uOMP^*: DegP_{12}]$ $- k_{32}[uOMP^*: DegP_6] - k_{44}[uOMP^*: DegP_6]$ |
| 21 | $\frac{d[uOMP^{pd}: DegP_{12}]}{dt}$ | = | $k_{29}[uOMP: DegP_{12}] + k_{30}[uOMP^*: DegP_6][DegP_6]$ $- k_{31}[uOMP^*: DegP_{12}]$ $- k_{33}[uOMP^*: DegP_{12}]$ $- k_{44}[uOMP^*: DegP_{12}]$ |
| 22 | $\frac{d[uOMP^{Degraded}]}{dt}$ | = | $k_{32}[uOMP^*: DegP_6] + k_{33}[uOMP^*: DegP_{12}]$ $- k_{44}[uOMP_{Degraded}]$ |

This table is reproduced from (Costello et al. 2016).

Table 5.3. Chaperone concentrations determined by proteomics studies.

(Masuda et al. 2009)

| <u>Protein</u> | <u>Copy Number</u> | <u>Concentration (M)</u> |
|----------------|--------------------|--------------------------|
| SurA | 112 | 2.07×10^{-6} |
| Skp | 328 | 6.05×10^{-6} |
| FkpA | 398 | 7.34×10^{-6} |
| DegP | 208 | 3.84×10^{-6} |

Observed monomeric chaperone copy numbers from proteomic data. Concentrations are determined by assuming a periplasmic volume of 9×10^{-17} L. This table is reproduced from (Costello et al. 2016).

Table 5.4. Rate constant values implemented in the σ^E response.

| <u>Simulated Null Phenotype</u> | <u>Reaction</u> | <u>Rate Constant</u> | <u>Value</u> | <u>Units</u> | <u>Citations and Notes</u> |
|-------------------------------------|------------------------------|--------------------------|-----------------------|--------------|---|
| Δ_{surA} | $\emptyset \rightarrow uOMP$ | k_1 | 5.00×10^{-8} | $M s^{-1}$ | (Koebnik, Locher, and Van Gelder 2000; Lugtenberg and Alphen 1983; Matsuyama et al. 1992; Rassam et al. 2015) |
| $\Delta_{surA}\Delta_{degP}$ | $\emptyset \rightarrow uOMP$ | k_1 | 4.00×10^{-8} | $M s^{-1}$ | (Koebnik, Locher, and Van Gelder 2000; Lugtenberg and Alphen 1983; Matsuyama et al. 1992; Rassam et al. 2015) |
| $\Delta_{surA}\Delta_{skp}$ | $\emptyset \rightarrow uOMP$ | k_1 | 2.30×10^{-8} | $M s^{-1}$ | (Koebnik, Locher, and Van Gelder 2000; Lugtenberg |

| | | | | | |
|---|--------------------------------|----------|-----------------------|------------|--|
| | | | | | and Alphen 1983; Matsuyama et al. 1992; Rassam et al. 2015) |
| $\Delta_{surA},$ $\Delta_{surA}\Delta_{degP}$ | $\emptyset \rightarrow Skp_1$ | k_3 | 4.71×10^{-9} | $M s^{-1}$ | (Dartigalongue, Missiakas, and Raina 2001; Masuda et al. 2009) |
| $\Delta_{surA}, \Delta_{surA}\Delta_{degP},$ $\Delta_{surA}\Delta_{skp}$ | $\emptyset \rightarrow FkpA_1$ | k_4 | 4.27×10^{-9} | $M s^{-1}$ | (Dartigalongue, Missiakas, and Raina 2001; Masuda et al. 2009) |
| $\Delta_{surA},$ $\Delta_{surA}\Delta_{skp}$ | $\emptyset \rightarrow DegP_1$ | k_5 | 5.23×10^{-9} | $M s^{-1}$ | (Dartigalongue, Missiakas, and Raina 2001; Masuda et al. 2009) |
| $\Delta_{surA}\Delta_{degP}, \Delta_{surA}\Delta_{skp}$ | $All \rightarrow \emptyset$ | k_{43} | 7.7×10^{-5} | s^{-1} | (Lugtenberg and Alphen 1983; Rassam et al. 2015) |

Values for uOMP synthesis determined using known change in fOMP concentration (see Figure 5.2). Chaperone expression levels were determined by multiplying the WT synthesis levels by the

fold increase in expression observed in (Dartigalongue, Missiakas, and Raina 2001). This table is reproduced from (Costello et al. 2016).

Table 5.5. Enumeration of binding events and lifetimes from stochastic simulations.

| <u>Simulated Null</u> <u>Phenotype</u> | <u>Average Number of Binding Events</u> | | | | | <u>Lifetime</u> <u>(s)</u> |
|---|---|------------|-------------|-------------|--------------|-------------------------------|
| | <u>SurA</u> | <u>Skp</u> | <u>FkpA</u> | <u>DegP</u> | <u>Total</u> | |
| Wild Type | 110±1.4 | 51.3±1.0 | 183±4.9 | 0.06 | 348±6.7 | 58.8±1.2 |
| $\Delta degP$ | 101±4.8 | 42.3±2.0 | 158.9±7.4 | N/A | 308±9.6 | 51.7±2.2 |
| Δskp | 107±2.6 | N/A | 170±5.0 | 0.07 | 279±6.7 | 38.8±0.8 |
| $\Delta fkpA$ | 106±5.5 | 45.2±2.0 | N/A | 0.07 | 150±7.5 | 25.4±1.4 |
| Δskp $\Delta degP$ | 111±3.3 | N/A | 180±3.4 | N/A | 294±9.4 | 41.1±1.6 |
| $\Delta surA$ | N/A | 541±26 | 1528±93 | 8.5±1 | 2742±389 | 464±18 |
| $\Delta surA$ $\Delta degP$ | N/A | 1215±99 | 3518±326 | N/A | 4663±440 | 1172±134 |
| $\Delta surA$ Δskp | N/A | N/A | 6625±221 | 9.5±1 | 8678±471 | 1159±38.8 |

Hundreds of binding events between chaperones and a uOMP occur during the uOMP periplasmic lifetime. Shown are the average number of binding events and lifetimes measured for the WT and mutant strains. All binding event data, other than that for DegP (because the numbers are small), are well described by a single exponential distribution as expected. Values are the mean of the distribution determined by fitting to a single exponential followed by the associated error from the fit. The distribution for DegP binding events was not well described

by an exponential decay. Instead the average number of binding events is reported (the sum of observed binding events over the number of simulations). N/A indicates chaperone species is not present in a given simulation. Data were collected by analyzing 1000 uOMP trajectories (2000 for WT). This table is reproduced from (Costello et al. 2016).

Table 5.6. Tabular form of Figure 5.3.

| <u>Simulated Null</u> <u>Phenotype</u> | <u>[fOMP]</u> | <u>Free</u> <u>uOMP</u> | <u>Aggregated</u> <u>uOMP</u> | <u>Degraded</u> <u>uOMP</u> | <u>Bound</u> <u>uOMP</u> |
|---|----------------------------|----------------------------|----------------------------------|--------------------------------|-----------------------------|
| Wild Type | 509.34 $\times 10^{-6}$ | 9.47×10^{-8} | 3.83×10^{-13} | 3.07×10^{-6} | 5.63×10^{-6} |
| $\Delta degP$ | 512.41 $\times 10^{-6}$ | 9.58×10^{-8} | 4.00×10^{-13} | 0 | 5.61×10^{-6} |
| Δskp | 511.04 $\times 10^{-6}$ | 9.53×10^{-8} | 3.92×10^{-13} | 3.09×10^{-6} | 3.91×10^{-6} |
| $\Delta fkpA$ | 512.21 $\times 10^{-6}$ | 9.57×10^{-8} | 3.99×10^{-13} | 3.10×10^{-6} | 2.73×10^{-6} |
| Δskp $\Delta degP$ | 514.13 $\times 10^{-6}$ | 9.64×10^{-8} | 4.11×10^{-13} | 0 | 3.90×10^{-6} |
| $\Delta surA$ | 54.40 $\times 10^{-6}$ | 1.05×10^{-6} | 5.71×10^{-9} | 1.84×10^{-4} | 2.00×10^{-5} |
| $\Delta surA$ $\Delta degP$ | 462.22 $\times 10^{-6}$ | 3.56×10^{-6} | 4.74×10^{-6} | 0 | 4.90×10^{-5} |
| $\Delta surA$ Δskp | 20.69 $\times 10^{-6}$ | 1.59×10^{-7} | 1.91×10^{-11} | 2.53×10^{-4} | 2.52×10^{-5} |

All concentrations are in Molar units. This table is reproduced from (Costello et al. 2016).

Concluding Remarks

Prior to the studies presented here, many questions remained unanswered about the molecular details of the assembly pathways of OMPs in *E. coli*. It has been established that the chaperones SurA, FkpA, Skp, and DegP facilitate OMP trafficking by associating with unfolded OMPs in the periplasm (Bothmann and Pluckthun 2000; Ge, Lyu, et al. 2014; Lazar and Kolter 1996; Schäfer, Beck, and Müller 1999; Sklar, Wu, Kahne, et al. 2007; Strauch, Johnson, and Beckwith 1989). However, it is unclear how SurA and FkpA bind to uOMP clients to prevent their self-association without forming oligomeric cages like Skp and DegP. It is also unknown which oligomeric species are relevant for uOMP binding for the chaperones SurA, FkpA, and DegP. A complicating feature for consideration of the *in vivo* function of these three chaperones is that they each exhibit a chaperone-independent enzymatic function; yet the relationship between the enzymatic and chaperone activities of these bifunctional chaperone proteins is undetermined.

In addition to these open questions about chaperone-uOMP interactions, it is also unclear how BamA works in collaboration with the BAM lipoproteins to facilitate the folding of OMPs into the bacterial OM. Recent structural work has provided atomistic details of the BAM protein interactions in the absence of OMP clients (Bakelar, Buchanon, and Noinaj 2016; Han et al. 2016; Iadanza et al. 2016; Noinaj et al. 2013). Complementary *in vitro* studies are just beginning to probe the catalytic mechanism of BamA (Gessmann et al. 2014). Still many questions remain, such as: how does BamA interact with uOMP clients? What are the functions of the BamBCDE lipoproteins in this process? What is the role of the BamA β -barrel seam and the lipid bilayer in this process?

Lastly, decades of biochemical characterization of this system have provided a wealth of literature that makes the OMP biogenesis pathway a prime target for computational modeling. Holistic modeling for this pathway had not been completed to parse out the complex interplay

between the proposed kinetic and thermodynamic partitioning mechanisms for OMP flux through the periplasm. It was previously undetermined if such a computational model could recapitulate the immense amount of genetic and biochemical data reported on the components of this pathway.

Our findings provide invaluable insight into the roles of FkpA, SurA, and the OMP-folding enzyme BamA, along with a holistic model for the entire OMP biogenesis pathway in *E. coli*. For our investigation of periplasmic chaperones, we have focused our experimental work on two prolyl-isomerases that are known to participate in OMP assembly: FkpA and SurA (Chapters 2 and 3). These two chaperones have not been as well-characterized structurally or biochemically as the chaperone Skp (Sandlin, Zaccai, and Fleming 2015; Schäfer, Beck, and Müller 1999; Sklar, Wu, Kahne, et al. 2007; Thoma et al. 2015; Walton et al. 2009; Walton and Sousa 2004; Zaccai et al. 2015) and the details of how these proteins interact with uOMPs are previously unreported.

FkpA populates monomeric and dimeric species, which exhibit distinct functions.

We have presented evidence that the oligomerization of FkpA is a critical reaction for consideration of the function of this chaperone, as FkpA populates both monomeric and dimeric states. Further, we discover that these two oligomers have distinct affinities for uOMP clients, with the dimer binding uOMPs 1000-fold tighter than the monomer. These findings raise the question – why is the dimerization equilibrium for FkpA poised to populate both oligomeric species if only one of them is capable of interacting with uOMPs? We propose that the FkpA monomer and dimer function as a PPIase and uOMP-chaperone, respectively, and both of these activities are critical for *in vivo* maintenance of the periplasmic and OM proteomes.

These results highlight the varying importance of the two functions of a bifunctional chaperone under various growth conditions. It is known that FkpA is one of the genes

upregulated upon cell stress (i.e., σ^E) (Dartigalongue, Missiakas, and Raina 2001) and we suggest that this shift in FkpA concentration will increase the amount of FkpA dimer/chaperone in the periplasm. This allows the periplasmic chaperone system to better handle increased concentrations of misfolding OMPs under these stress conditions. Overall, our findings highlight the modulation of relative populations of various oligomers of FkpA under normal and stress bacterial growth conditions and may explain the importance of FkpA under σ^E stress conditions.

The isolation of FkpA oligomers and assignment of distinct functions to these species raises exciting prospects for better understanding the activities of bifunctional enzymes/chaperones. Moving forward, an interesting new avenue for chaperone studies involves identifying the *in vivo* clientele pools for each of these functional states of FkpA; that is, which periplasmic proteins or OMPs require prolyl-isomerization by the FkpA monomer prior to folding? Also, *in vivo* OMP binding partners for the FkpA dimeric chaperone have not been ascertained. In addition to determining the clients of various chaperone functional states, it will be interesting to evaluate this type of relationship for other bifunctional chaperones, such as DegP.

Proposed model of SurA-uOMP complex raises exciting prospects.

We find that oligomerization is likely not relevant for the binding of SurA to uOMP clients. This raised the question of how SurA structurally accommodates unfolded OMP binding partners. Modeling of a SurA-uOMP complex has not previously been reported likely due to the short-lived nature of this complex and aggregation-prone uOMP. By combining biochemical crosslinking with neutron scattering experiments, we show that the uOMP populates an

expanded conformation in this complex, and we suggest this is significant for the ability of SurA to promote folding of uOMPs both *in vitro* and *in vivo* in coordination with the BAM complex.

SurA is different from the periplasmic chaperones Skp and DegP, because it lacks an internal cavity to accommodate uOMPs. Our structural model for the SurA-uOMP complex adds insight into the field of OMP biogenesis by presenting an apparent paradox: SurA is known to play a pivotal role in OMP biogenesis, which requires protection of uOMP from aggregation. Yet our model suggests that SurA binds to uOMPs in a manner that leaves regions of the client OMP exposed and likely able to associate with other free uOMPs or SurA-uOMP complexes, in addition to productive interactions with the BAM complex for folding. OMPBioM simulations suggest that the concentration of free uOMP in the periplasm is likely negligible (Costello et al. 2016), therefore we exclude the possibility that uOMP bound to SurA may form aggregates with free uOMP in a biologically relevant context. However, further structural investigations and modeling will be required to understand if uOMP bound to SurA may associate with other SurA-uOMP complexes.

Additionally, our work raises several further questions about how SurA associates with uOMP clients. As shown in Figure 1.2, many unique OMPs are present in the OM and SurA is known to interact with several OMP clients (Vertommen et al. 2009). Our discovery that SurA binds to uOMPs with a delocalized interface suggests a promiscuous binding mechanism for these interactions; however, it is unclear how SurA may accommodate uOMPs with soluble periplasmic domains (i.e., full-length OmpA, Figure 1.2). It was shown that Skp interacts with these types of clients with the folded OMP domain in several orientations (Zaccai et al. 2015). It will be exciting to see if SurA exhibits a similar plasticity in bound uOMP conformation and soluble domain orientation. Our protocols for combining unnatural amino acid incorporation, biochemical crosslinking, and SANS allow for future studies of complexes formed between SurA

and a variety of uOMP clients. These methods are also likely applicable for studies with other chaperones of interest, including FkpA.

***In vitro* analysis of BamA function complement structural studies.**

BamA is required for *E. coli* viability and is known to facilitate OMP folding *in vivo* and *in vitro*, although details of its functional mechanism were previously unreported (Gessmann et al. 2014; Voulhoux, Bos, Geurtsen, Mols and Tommassen 2003). Many structural studies have been recently reported on the BAM complex; these studies allow for visualization of static protein conformations but are limited in their insight into the mechanism of protein function. Our *in vitro* investigation of BamA-accelerated OMP folding allows for a controlled assessment of how BamA affects OMP folding. This established protocol allows for experimental manipulation of the client OMP identity and concentration, denaturant concentration, and lipid composition. By utilizing this assay, we can deconvolute the effects of these parameters on BamA function *in vitro* and ask specific questions about how this enzyme works.

In Chapter 4, we have modified previous protocols to present BamA with a relatively high concentration (i.e., 8 μ M OmpA, 1 μ M BamA) of client OMP to determine the turnover number of this enzyme. Comparisons between the activity of BamA alone and the BAM complex have yielded similarities in the catalytic activity: both BamA and the entire BAM complex have been shown to facilitate multiple rounds of catalysis with turnover numbers in both cases equal to approximately 1.5 (Hagan and Kahne 2011; Plummer and Fleming 2015). These findings suggest that BamA itself undergoes a cyclic catalytic mechanism that is accelerated *in vivo* by the additional lipoproteins BamBCDE.

Future modifications of this *in vitro* assay will allow for further probing of the BamA-accelerated OMP folding mechanism. Here we highlight two future directions for this work that incorporate the plethora of structural information recently reported on the BAM complex.

Moving forward, it will be interesting to systematically incorporate the BamBCDE lipoproteins into this *in vitro* assay to determine their contribution to BAM-mediated OMP folding. We hypothesize that these lipoproteins will further accelerate OMP folding, yet their differential importance reported through genetics experiments suggests they may do so to varying extents. Additionally, we suggest that this assay should be utilized to investigate the importance of residues identified as functionally critical through crystallographic analyses. Figure 4.1 highlights the non-canonical seam of the *E. coli* BamA protein: it has been suggested that this geometry of β -sheet and intra-strand hydrogen bonding is important for BAM complex function (Noinaj et al. 2014). Our experimental assay is the ideal set-up for testing this idea: mutations to lock the $\beta 1$ and $\beta 16$ strands of BamA in a closed conformation (i.e., Cysteine residues on these adjacent strands that are covalently linked by a disulfide bond) could be incorporated into this enzyme to construct a variant with limited seam dynamics. The enzymatic activity of variants of this nature could be tested to further probe the importance of the BamA seam in accelerating OMP folding *in vitro*.

OMPBioM is the first computational model of OMP biogenesis.

Most biochemical and biophysical investigations study protein-protein interactions under experimental conditions that are far removed from the relevant biological conditions. Our above experiments all fall into this classification. Although we aim to emulate biologically relevant parameters by utilizing native uOMPs as chaperone binding clients and native *E. coli* head groups for kinetics assays, we are inherently simplifying our experimental conditions to understand how the individual components of the OMP biogenesis work in isolation. To better understand how the entire trafficking system manages OMP flux through the periplasm, we have incorporated previously published thermodynamic and kinetic information into the first

computational model of OMP biogenesis (Chapter 5). Our model provides novel insight into the functions of the periplasmic chaperones, kinetic partitioning of uOMP species, and estimation of *in vivo* OMP folding rates. These types of parameters are challenging, if not impossible, to determine experimentally. We additionally have redefined current models for OMP biogenesis by suggesting that OMPs dynamically bind to the periplasmic chaperone reservoir and non-directionally partition toward the OM (Costello et al. 2016). These findings reinforce the previously proposed idea that the thermodynamics of uOMP-chaperone binding and folding may drive the biological process of OMP trafficking and assembly (Moon et al. 2013).

This computational study has been pivotal to the current understanding of this network and we greatly look forward to future applications of this model to probe various aspects of this system. It has recently come to our attention that the introduction of slow-folding OMP variants into the *E. coli* periplasm presents particular challenges to the OMP assembly machinery (Peterson, J.H.; Plummer, A. M.; Fleming, K. G.; Bernstein, H. D; *in preparation*) (Wzorek et al. 2017). Some slow-folding OMPs saturate the chaperone network and lead to lethal phenotypes, while other OMPs stall on the BAM complex. This type of experimental data allows us to ask – which parameters incorporated into OMPBioM must be changed to reproduce this distinct *in vivo* behavior (Tables 5.1 and 5.2)? Our current version of OMPBioM incorporates a representative OMP client, which we recognize is an oversimplification of the OMP biogenesis system that handles many unique OMPs (Figure 1.2). As experimental *in vivo* information becomes readily available on how the periplasmic chaperones and BAM complex interact with distinct OMPs, we will use this data to further develop our OMPBioM simulations. Additionally, as *in vitro* biochemical investigations as those presented in Chapters 2 and 3 are published, we hope to incorporate the most up-to-date *in vitro* data into our model as well.

Overall, the experimental and computational studies presented here provide essential details for understanding the trafficking and assembly of OMPs. This process is a prerequisite for the formation of an intact membrane system in Gram-negative bacteria and subsequent virulence and antibiotic permeation of cells. We highlight the importance of chaperone-uOMP and BAM-uOMP binding interactions as promising targets for anti-virulence drugs and important factors for consideration with regard to antibiotic resistance in *E. coli*.

References

- Ahn, Victoria E et al. 2004. "A Hydrocarbon Ruler Measures Palmitate in the Enzymatic Acylation of Endotoxin." *The EMBO journal* 23(15): 2931–41.
- Albrecht, Reinhard et al. 2014. "Structure of BamA, an Essential Factor in Outer Membrane Protein Biogenesis." *Acta Crystallographica Section D: Biological Crystallography* 70(6): 1779–89.
- Arié, Jean Philippe, Nathalie Sassoon, and Jean Michel Betton. 2001. "Chaperone Function of FkpA, a Heat Shock Prolyl Isomerase, in the Periplasm of Escherichia Coli." *Molecular Microbiology* 39(1): 199–210.
- Arike, L et al. 2012. "Comparison and Applications of Label-Free Absolute Proteome Quantification Methods on Escherichia Coli." *Journal of proteomics* 75(17): 5437–48.
- Arnold, Konstantin, Lorenza Bordoli, Jürgen Kopp, and Torsten Schwede. 2006. "The SWISS-MODEL Workspace: A Web-Based Environment for Protein Structure Homology Modelling." *Bioinformatics* 22(2): 195–201.
- Bajaj, Harsha et al. 2012. "Antibiotic Uptake through Membrane Channels: Role of Providencia Stuarii OmpPst1 Porin in Carbapenem Resistance." *Biochemistry* 51(51): 10244–49.
- Bakelar, J, S K Buchanon, and N Noinaj. 2016. "The Structure of the β -Barrel Assembly Machinery Complex." *Science* 351(6269): 180–86.
- Behrens-Kneip, Susanne. 2010. "The Role of SurA Factor in Outer Membrane Protein Transport and Virulence." *International Journal of Medical Microbiology* 300(7): 421–28.
- Behrens, S et al. 2001. "The SurA Periplasmic PPIase Lacking Its Parvulin Domains Functions in Vivo and Has Chaperone Activity." *EMBO Journal* 20: 285–94.
- Bennion, Drew, Emily S Charlson, Eric Coon, and Rajeev Misra. 2010. "Dissection of β -Barrel Outer Membrane Protein Assembly Pathways through Characterizing BamA POTRA 1 Mutants of Escherichia Coli." *Molecular microbiology* 77(5): 1153–71.
- Bergal, Hans Thor, Alex Hunt Hopkins, Sandra Ines Metzner, and Marcelo Carlos Sousa. 2015.

- “The Structure of a BamA-BamD Fusion Illuminates the Architecture of the β -Barrel Assembly Machine Core.” *Structure* 24: 1–9.
- Best, Michael D. 2009. “Click Chemistry and Bioorthogonal Reactions: Unprecedented Selectivity in the Labeling of Biological Molecules.” *Biochemistry* 48(28): 6571–84.
- Biasini, Marco et al. 2014. “SWISS-MODEL: Modelling Protein Tertiary and Quaternary Structure Using Evolutionary Information.” *Nucleic Acids Research* 42(W1): 252–58.
- Bishop, Russell E. 2005. “The Lipid A Palmitoyltransferase PagP: Molecular Mechanisms and Role in Bacterial Pathogenesis.” *Molecular Microbiology* 57(4): 900–912.
- Bitto, Eduard, and David B McKay. 2002. “Crystallographic Structure of SurA, a Molecular Chaperone That Facilitates Folding of Outer Membrane Porins.” *Structure (London, England: 1993)* 10(11): 1489–98.
- . 2003. “The Periplasmic Molecular Chaperone Protein SurA Binds a Peptide Motif That Is Characteristic of Integral Outer Membrane Proteins.” *The Journal of biological chemistry* 278(49): 49316–22.
- . 2004. “Binding of Phage-Display-Selected Peptides to the Periplasmic Chaperone Protein SurA Mimics Binding of Unfolded Outer Membrane Proteins.” *FEBS letters* 568(1–3): 94–98.
- Bordoli, Lorenza et al. 2009. “Protein Structure Homology Modeling Using SWISS-MODEL Workspace.” *Nature protocols* 4(1): 1–13.
- Bothmann, H, and A Pluckthun. 2000. “The Periplasmic Escherichia Coli Peptidylprolyl Cis,trans-Isomerase FkpA. I. Increased Functional Expression of Antibody Fragments with and without Cis-Prolines.” *J Biol Chem* 275: 17100–105.
- Braun, Volkmar et al. 2015. “Import and Export of Bacterial Protein Toxins.” *International Journal of Medical Microbiology* 305(2): 238–42.

- Brown, Eric D., and Gerard D. Wright. 2016. “Antibacterial Drug Discovery in the Resistance Era.” *Nature* 529(7586): 336–43.
- Bulieris, Paula V, Susanne Behrens, Otto Holst, and Jörg H Kleinschmidt. 2003. “Folding and Insertion of the Outer Membrane Protein OmpA Is Assisted by the Chaperone Skp and by Lipopolysaccharide.” *The Journal of biological chemistry* 278(11): 9092–99.
- Burgess, Nancy K, Thuy P Dao, Ann Marie Stanley, and Karen G Fleming. 2008a. “Beta-Barrel Proteins That Reside in the Escherichia Coli Outer Membrane in Vivo Demonstrate Varied Folding Behavior in Vitro.” *The Journal of biological chemistry* 283(39): 26748–58.
- Burmann, Björn M, Congwei Wang, and Sebastian Hiller. 2013. “Conformation and Dynamics of the Periplasmic Membrane-Protein-Chaperone Complexes OmpX-Skp and tOmpA-Skp.” *Nature structural & molecular biology* 20(11): 1265–72.
- Cao, Weihuan, and Mary Konsolaki. 2011. “FKBP Immunophilins and Alzheimer’s Disease: A Chaperoned Affair.” *Journal of Biosciences* 36(3): 493–98.
- Castillo-Keller, Maria, and Rajeev Misra. 2003. “Protease-Deficient DegP Suppresses Lethal Effects of a Mutant OmpC Protein by Its Capture.” *Journal of Bacteriology* 185(1): 148–54.
- CDC, U.S. Department of Health and Human Services. 2013. Antibiotic resistance threats in the United States, 2013 *Antibiotic Resistance Threats in the United States, 2013*.
- Chen, R, and U Henning. 1996. “A Periplasmic Protein (Skp) of Escherichia Coli Selectively Binds a Class of Outer Membrane Proteins.” *Molecular microbiology* 19(6): 1287–94.
- Collins, Sean R., Adam Douglass, Ronald D. Vale, and Jonathan S. Weissman. 2004. “Mechanism of Prion Propagation: Amyloid Growth Occurs by Monomer Addition.” *PLoS Biology* 2(10).
- Costello, Shawn M., Ashlee M. Plummer, Patrick J. Fleming, and Karen G. Fleming. 2016. “Dynamic Periplasmic Chaperone Reservoir Facilitates Biogenesis of Outer Membrane

- Proteins.” *Proceedings of the National Academy of Sciences* 113(33): E4794–4800.
- Cumby, Nichole et al. 2015. “The Phage Tail Tape Measure Protein, an Inner Membrane Protein and a Periplasmic Chaperone Play Connected Roles in the Genome Injection Process of E. coli Phage HK97.” *Molecular Microbiology* 96(3): 437–47.
- Dlugosz, M., Bojarska E., and J. M. Antosiewicz. 2002. “A Procedure for Analysis of Stopped-Flow Transients for Protein – Ligand Association.” 51: 179–93.
- Dalbey, Ross E, Peng Wang, and Andreas Kuhn. 2011. “Assembly of Bacterial Inner Membrane Proteins.” *Annual review of biochemistry* 80(May): 161–87.
- Danese, P N, and T J Silhavy. 1997. “The sigmaE and the Cpx Signal Transduction Systems Control the Synthesis of Periplasmic Protein-Folding Systems in Escherichia Coli.” *Genes & Development* 11: 1183–93.
- Danoff, Emily J., and Karen G. Fleming. 2015a. “Aqueous, Unfolded OmpA Forms Amyloid-Like Fibrils upon Self-Association.” *Plos One* 10(7): e0132301.
- . 2015b. “Membrane Defects Accelerate Outer Membrane β -Barrel Protein Folding.” *Biochemistry* 54(2): 97–99.
- Danoff, Emily J, and Karen G Fleming. 2011. “The Soluble, Periplasmic Domain of OmpA Folds as an Independent Unit and Displays Chaperone Activity by Reducing the Self-Association Propensity of the Unfolded OmpA Transmembrane β -Barrel.” *Biophysical chemistry* 159(1): 194–204.
- Dartigalongue, C, D Missiakas, and S Raina. 2001. “Characterization of the Escherichia Coli Sigma E Regulon.” *The Journal of biological chemistry* 276(24): 20866–75.
- Dattilo, Sandro et al. 2015. “Heat Shock Proteins and Hormesis in the Diagnosis and Treatment of Neurodegenerative Diseases.” *Immunity & Ageing* 12(1): 1–19.
- Dong, Haohao et al. 2014. “Structural Basis for Outer Membrane Lipopolysaccharide

- Insertion.” *Nature* 511(6): 52–56.
- Van Duyne, G. D. et al. 1993. “Atomic Structures of the Human Immunophilin FKBP-12 Complexes with FK506 and Rapamycin.” *J Mol Biol* 229: 105–24.
- Dwyer, Robert S. et al. 2014. “Folding LacZ in the Periplasm of Escherichia Coli.” *Journal of Bacteriology* 196(18): 3343–50.
- Dyson, H Jane, and Peter E Wright. 2005. “Intrinsically Unstructured Proteins and Their Functions.” *Nature reviews. Molecular cell biology* 6(3): 197–208.
- Ebie Tan, Alexandra et al. 2010. “Self-Association of Unfolded Outer Membrane Proteins.” *Macromolecular bioscience* 10(7): 763–67.
- Fairman, James W., Nicholas Noinaj, and Susan K. Buchanan. 2011. “The Structural Biology of B-Barrel Membrane Proteins: A Summary of Recent Reports.” *Current Opinion in Structural Biology* 21(4): 523–31.
- Falsafi, Sajad, and Zahra Karimi. 2011. “Sasa.tcl.”
http://www.ks.uiuc.edu/Research/vmd/ mailing_list/ vmd-l/ att-18670/ sasa.tcl.
- Fleming, Karen G. 2015. “A Combined Kinetic Push and Thermodynamic Pull as Driving Forces for Outer Membrane Protein Sorting and Folding in Bacteria.” *Philosophical Transactions of the Royal Society B* 370.
- García-Fruitós, Elena et al. 2011. “Biological Role of Bacterial Inclusion Bodies: A Model for Amyloid Aggregation.” *The FEBS journal* 278: 2419–27.
- García De La Torre, J, M L Huertas, and B Carrasco. 2000. “Calculation of Hydrodynamic Properties of Globular Proteins from Their Atomic-Level Structure.” *Biophysical journal* 78(2): 719–30.
- Gatzeva-Topalova, Petia Z., Troy A. Walton, and Marcelo C. Sousa. 2008. “Crystal Structure of YaeT: Conformational Flexibility and Substrate Recognition.” *Structure* 16(12): 1873–81.

- Gatzeva-Topalova, Petia Zvezdanova, Lisa Rosa Warner, Arthur Pardi, and Marcelo Carlos Sousa. 2010. "Structure and Flexibility of the Complete Periplasmic Domain of BamA: The Protein Insertion Machine of the Outer Membrane." *Structure* 18(11): 1492–1501.
- Ge, Xi, Zhi-Xin Lyu, et al. 2014. "Identification of FkpA as a Key Quality Control Factor for the Biogenesis of Outer Membrane Proteins under Heat Shock Conditions." *Journal of bacteriology* 196(3): 672–80.
- Ge, Xi, Rui Wang, et al. 2014a. "DegP Primarily Functions as a Protease for the Biogenesis of beta-Barrel Outer Membrane Proteins in the Gram-Negative Bacterium Escherichia Coli." *FEBS Journal* 281: 1226–40.
- Georgopoulos, C., and W. J. Welch. 1993. "Role of the Major Heat Shock Proteins as Molecular Chaperones." *Annual Review of Cell Biology* 9: 601–34.
- Gessmann, D. et al. 2014. "Outer Membrane β -Barrel Protein Folding Is Physically Controlled by Periplasmic Lipid Head Groups and BamA." *Proceedings of the National Academy of Sciences* 111(16): 5878–83.
- Gibson, Michael A, and Jehoshua Bruck. 2000. "Efficient Exact Stochastic Simulation of Chemical Systems with Many Species and Many Channels." *J. Phys. Chem. A* 104(9): 1876–89.
- Giese, Kim C., and Elizabeth Vierling. 2002. "Changes in Oligomerization Are Essential for the Chaperone Activity of a Small Heat Shock Protein in Vivo and in Vitro." *Journal of Biological Chemistry* 277(48): 46310–18.
- Gill, Stanley C., and Peter H. von Hippel. 1989. "Calculation of Protein Extinction Coefficients from Amino Acid Sequence Data." *Analytical Biochemistry* 182(2): 319–26.
- Gothel, S. F., and M. A. Marahiel. 1999. "Peptidyl-Prolyl Cis-Trans Isomerases, a Superfamily of ubiquitous folding catalysts." *Cell Mol Life Sci* 55(3): 423–36.

- Grabowicz, Marcin, Daria Koren, and Thomas J Silhavy. 2016. “The CpxQ sRNA Negatively Regulates Skp To Prevent Mistargeting of β -Barrel Outer Membrane Proteins into the Cytoplasmic Membrane.” 7(2): 1–8.
- Gruss, Fabian et al. 2013. “The Structural Basis of Autotransporter Translocation by TamA.” *Nature Structural & Molecular Biology* 20(11): 1318–20.
- Gu, Yinghong et al. 2016. “Structural Basis of Outer Membrane Protein Insertion by the BAM Complex.” *Nature* 531(7592): 64–69.
- Gunnarsen, Kristin S et al. 2010. “Periplasmic Expression of Soluble Single Chain T Cell Receptors Is Rescued by the Chaperone FkpA.” *BMC Biotechnology* 10(8).
- . 2013. “Chaperone-Assisted Thermostability Engineering of a Soluble T Cell Receptor Using Phage Display.” *Scientific reports* 3(1162): DOI: 10.1038/srep01162.
- Hagan, B., and J. V. Staros. 1984. *Azides and Nitrenes: Reactivity and Utility*. Orlando, FL: Academic Press.
- Hagan, Christine L., and Daniel Kahne. 2011. “The Reconstituted Escherichia Coli Bam Complex Catalyzes Multiple Rounds of B-Barrel Assembly.” *Biochemistry* 50(35): 7444–46.
- Hagan, Christine L, Seokhee Kim, and Daniel Kahne. 2010. “Reconstitution of Outer Membrane Protein Assembly from Purified Components.” *Science (New York, N.Y.)* 328(5980): 890–92.
- Hagan, Christine L, Joseph S Wzorek, and Daniel Kahne. 2015. “Inhibition of the β -Barrel Assembly Machine by a Peptide That Binds BamD.” *Proceedings of the National Academy of Sciences of the United States of America* 112(7): 2011–16.
- Han, Long et al. 2016. “Structure of the BAM Complex and Its Implications for Biogenesis of Outer-Membrane Proteins.” *Nature Structural & Molecular Biology* 23(3): 192–96.
- Han, Mee-Jung, Jin Young Kim, and Jung a Kim. 2014. “Comparison of the Large-Scale

- Periplasmic Proteomes of the Escherichia Coli K-12 and B Strains.” *Journal of bioscience and bioengineering* 117(4): 437–42.
- Harms, Nellie et al. 2001. “The Early Interaction of the Outer Membrane Protein PhoE with the Periplasmic Chaperone Skp Occurs at the Cytoplasmic Membrane.” *Journal of Biological Chemistry* 276(22): 18804–11.
- Harroun, T. A., G. D. Wignall, and J. Katsaras. 2006. *Neutron Scattering in Biology: Techniques and Applications*. eds. J. Fitter, T. Gutberlet, and J. Katsaras. Springer Berlin Heidelberg New York.
- Haslbeck, Martin, Titus Franzmann, Daniel Weinfurtner, and Johannes Buchner. 2005. “Some like It Hot: The Structure and Function of Small Heat-Shock Proteins.” *Nature structural & molecular biology* 12(10): 842–46.
- Hearn, Elizabeth M. et al. 2009. “Transmembrane Passage of Hydrophobic Compounds through a Protein Channel Wall.” *Nature* 458(7236): 367–70.
- Hedstrom, Lizbeth. 2002. “Serine Protease Mechanism and Specificity.” *Chemical Reviews* 102: 4501–23.
- Hennecke, Gerrit et al. 2005. “The Periplasmic Chaperone SurA Exploits Two Features Characteristic of Integral Outer Membrane Proteins for Selective Substrate Recognition.” *Journal of Biological Chemistry* 280: 23540–48.
- Hong, Heedeok, Dimki R. Patel, Lukas K. Tamm, and Bert van den Berg. 2006. “The Outer Membrane Protein OmpW Forms an Eight-Stranded β -Barrel with a Hydrophobic Channel.” *Journal of Biological Chemistry* 281(11): 7568–77.
- Horne, S. M., and K. D. Young. 1995. “Escherichia Coli and Other Species of the Enterobacteriaceae Encode a Protein Similar to the Family of Mip-like FK506-Binding Proteins.” *Archives of Microbiology* 163(5): 357–65.

- Horowitz, Scott et al. 2016. “Visualizing Chaperone-Assisted Protein Folding.” *Nature Structural & Molecular Biology* 23(7): 691–97.
- Hortschansky, Peter et al. 2005. “The Aggregation Kinetics of Alzheimer ’ S B-Amyloid Peptide Is Controlled by Stochastic Nucleation.” *Protein Science* 14: 1753–59.
- Hu, Kaifeng, Veniamin Galus, and Konstantin Pervushin. 2006. “Structural Plasticity of Peptidyl - Prolyl Isomerase sFkpA Is a Key to Its Chaperone Function As Revealed by Solution NMR.” *Biochemistry* 45: 11983–91.
- Huang, Chengdong, Paolo Rossi, Tomohide Saio, and Charalampos G. Kalodimos. 2016. “Structural Basis for the Antifolding Activity of a Molecular Chaperone.” *Nature* 537: 202–6.
- Hullmann, Julia et al. 2008. “Periplasmic Chaperone FkpA Is Essential for Imported Colicin M Toxicity.” *Molecular microbiology* 69(4): 926–37.
- Humphrey, William, Andrew Dalke, and Klaus Schulten. 1996. “VMD: Visual Molecular Dynamics.” *Journal of Molecular Graphics* 14(1): 33–38.
- Iadanza, Matthew G. et al. 2016. “Lateral Opening in the Intact β -Barrel Assembly Machinery Captured by Cryo-EM.” *Nature Communications* 7(12865): DOI: 10.1038/ncomms12865.
- Iakoucheva, Lilia M. et al. 2002. “Intrinsic Disorder in Cell-Signaling and Cancer-Associated Proteins.” *Journal of Molecular Biology* 323(3): 573–84.
- Inouye, M, and M L Yee. 1973. “Homogeneity of Envelope Proteins of Escherichia Coli Separated by Gel Electrophoresis in Sodium Dodecyl Sulfate.” *Journal of bacteriology* 113(1): 304–12.
- Ishihama, Yasushi et al. 2008. “Protein Abundance Profiling of the Escherichia Coli Cytosol.” *BMC Genomics* 9(102).
- Iwanczyk, Jack, Vivian Leong, and Joaquin Ortega. 2011. “Factors Defining the Functional

- Oligomeric State of Escherichia Coli DegP Protease.” *PloS one* 6(4): e18944.
- Jacques, David A, and Jill Trewhella. 2010. “Small-Angle Scattering for Structural Biology--Expanding the Frontier While Avoiding the Pitfalls.” *Protein Science* 19(4): 642–57.
- Jagadish, Nirmala et al. 2016. “Heat Shock Protein 70-2 (HSP70-2) Overexpression in Breast Cancer.” *Journal of experimental & clinical cancer research* 35(150): DOI 10.1186/s13046-016-0425-9.
- Jansen, Katarina Bartoš, Susan Lynn Baker, and Marcelo Carlos Sousa. 2015. “Crystal Structure of BamB Bound to a Periplasmic Domain Fragment of BamA, the Central Component of the β -Barrel Assembly Machine.” *Journal of Biological Chemistry* 290(4): 2126–36.
- Jarosławski, Szymon, Katia Duquesne, James N. Sturgis, and Simon Scheuring. 2009. “High-Resolution Architecture of the Outer Membrane of the Gram-Negative Bacteria *Roseobacter Denitrificans*.” *Molecular Microbiology* 74(5): 1211–22.
- Jo, S., T. Kim, V. G. Iyer, and W. Im. 2008. “CHARMM-GUI: A Web-Based Graphical User Interface for CHARMM.” *Journal of computational chemistry* 29(11): 1859–65.
- Johnson, M L, J J Correia, D A Yphantis, and H R Halvorson. 1981. “Analysis of Data from the Analytical Ultracentrifuge by Nonlinear Least-Squares Techniques.” *Biophysical journal* 36(3): 575–88.
- Jolly, Caroline, and Richard I Morimoto. 2000. “Role of the Heat Shock Response and Molecular Chaperones in Oncogenesis and Cell Death.” *Journal of the National Cancer Institute* 92(19): 1564–72.
- Justice, Sheryl S et al. 2005. “Periplasmic Peptidyl Prolyl Cis-Trans Isomerases Are Not Essential for Viability, but SurA Is Required for Pilus Biogenesis in Escherichia Coli.” *Journal of bacteriology* 187(22): 7680–86.
- Kamio, Y, and H Nikaido. 1976. “Outer Membrane of Salmonella Typhimurium: Accessibility

- of Phospholipid Head Groups to Phospholipase c and Cyanogen Bromide Activated Dextran in the External Medium.” *Biochemistry* 15(12): 2561–70.
- Kim, Seokhee et al. 2007. “Structure and Function of an Essential Component of the Outer Membrane Protein Assembly Machine.” *Science* 317: 961–64.
- Kim, Seokhee, Robert A Grant, and Robert T Sauer. 2011. “Covalent Linkage of Distinct Substrate Degrons Controls Assembly and Disassembly of DegP Proteolytic Cages.” *Cell* 145(1): 67–78.
- Kim, Seokhee, and Robert T Sauer. 2012. “Cage Assembly of DegP Protease Is Not Required for Substrate-Dependent Regulation of Proteolytic Activity or High-Temperature Cell Survival.” *Proceedings of the National Academy of Sciences* 109(19): 7263–68.
- Kleinschmidt, Jörg H. 2015. “Folding of β -Barrel Membrane Proteins in Lipid Bilayers — Unassisted and Assisted Folding and Insertion.” *Biochimica et Biophysica Acta (BBA) - Biomembranes* 1848(9): 1927–43.
- Kleinschmidt, Jörg Helmut, and Lukas K. Tamm. 2002. “Secondary and Tertiary Structure Formation of the β -Barrel Membrane Protein OmpA Is Synchronized and Depends on Membrane Thickness.” *Journal of Molecular Biology* 324(2): 319–30.
- Knowles, Timothy J. et al. 2008. “Fold and Function of Polypeptide Transport-Associated Domains Responsible for Delivering Unfolded Proteins to Membranes.” *Molecular Microbiology* 68(5): 1216–27.
- Koebnik, R, K P Locher, and P Van Gelder. 2000. “Structure and Function of Bacterial Outer Membrane Proteins: Barrels in a Nutshell.” *Molecular microbiology* 37(2): 239–53.
- Kozjak, Vera et al. 2003. “An Essential Role of Sam50 in the Protein Sorting and Assembly Machinery of the Mitochondrial Outer Membrane.” *The Journal of biological chemistry* 278(49): 48520–23.

- Krojer, Tobias, Karen Pangerl, et al. 2008. "Interplay of PDZ and Protease Domain of DegP Ensures Efficient Elimination of Misfolded Proteins." *Proceedings of the National Academy of Sciences of the United States of America* 105(22): 7702–7.
- Krojer, Tobias, Justyna Sawa, et al. 2008. "Structural Basis for the Regulated Protease and Chaperone Function of DegP." *Nature* 453(7197): 885–90.
- De Las Peñas, A, L Connolly, and C A Gross. 1997. "SigmaE Is an Essential Sigma Factor in Escherichia Coli." *Journal of bacteriology* 179(21): 6862–64.
- Laue, T. M., B. D. Shah, T. M. Ridgeway, and S. L. Pelletier. 1992. "Computer-Aided Interpretation of Analytical Sedimentation Data for Proteins." In *Analytical Ultracentrifugation in Biochemistry and Polymer Science*, 90–125.
- Lazar, Sara W., Marta Almirón, Antonio Tormo, and Roberto Kolter. 1998. "Role of the Escherichia Coli SurA Protein in Stationary-Phase Survival." *Journal of Bacteriology* 180(21): 5704–11.
- Lazar, S W, and R Kolter. 1996. "SurA Assists the Folding of Escherichia Coli Outer Membrane Proteins." *Journal of bacteriology* 178(6): 1770–73.
- Lee, J J, and D S Berns. 1968. "Protein Aggregation. The Effect of Deuterium Oxide on Large Protein Aggregates of C-Phycocyanin." *The Biochemical journal* 110(3): 465–70.
- Lee, Jumin et al. 2016. "CHARMM-GUI Input Generator for NAMD, GROMACS, AMBER, OpenMM, and CHARMM/OpenMM Simulations Using the CHARMM36 Additive Force Field." *Journal of Chemical Theory and Computation* 12(1): 405–13.
- Li, Shulian et al. 2014. "Upregulation of Heat Shock Factor 1 Transcription Activity Is Associated with Hepatocellular Carcinoma Progression." *Molecular Medicine Reports* 10(5): 2313–21.
- Lin, Ming-Shen et al. 2008. "Investigation of the Mechanism of Beta-Amyloid Fibril Formation

- by Kinetic and Thermodynamic Analyses.” *Langmuir* 24(7): 5802–8.
- Lipinska, Barbara, Maciej Zylicz, and Costa Georgopoulos. 1990. “HtrA (DegP) Protein, Essential for Escherichia Coli Survival at High Temperatures, Is an Endopeptidase.” *Journal of bacteriology* 172(4): 1791–97.
- Lugtenberg, Ben, and Loek Van Alphen. 1983. “Molecular Architecture and Functioning of the Outer Membrane of Escherichia Coli and Other Gram-Negative Bacteria.” *Biochimica et Biophysica Acta* 737: 51–115.
- Lugtenberg, E.J.J, and R Peters. 1976. “Distribution of Lipids in Cytoplasmic and Outer Membranes of Escherichia Coli K12.” *Biochimica et biophysica acta* 441: 38–47.
- Lyu, Zhi Xin, and Xin Sheng Zhao. 2014. “Periplasmic Quality Control in Biogenesis of Outer Membrane Proteins.” *Biochemical Society Transactions* 43(2): 133–38.
- Maier, Timm et al. 2015. “Conserved Omp85 Lid-Lock Structure and Substrate Recognition in FhaC.” *Nature Communications* 6(May): 7452.
- Malet, Hélène et al. 2012. “Newly Folded Substrates inside the Molecular Cage of the HtrA Chaperone DegQ.” *Nature structural & molecular biology* 19(2): 152–57.
- Malinverni, Juliana C et al. 2006. “YfiO Stabilizes the YaeT Complex and Is Essential for Outer Membrane Protein Assembly in Escherichia Coli.” *Molecular microbiology* 61(1): 151–64.
- Masuda, Takeshi, Natsumi Saito, Masaru Tomita, and Yasushi Ishihama. 2009. “Unbiased Quantitation of Escherichia Coli Membrane Proteome Using Phase Transfer Surfactants.” *Molecular & cellular proteomics : MCP* 8: 2770–77.
- Matsuyama, S., Y. Fujita, K. Sagara, and S. Mizushima. 1992. “Overproduction, Purification and Characterization of SecD and SecF, Integral Membrane Components of the Protein Translocation Machinery of Escherichia Coli.” *Biochimica et Biophysica Acta - Protein Structure and Molecular Enzymology* 1122(1): 77–84.

- May, J. M. et al. 2015. "Lipopolysaccharide Transport to the Cell Surface: Periplasmic Transport and Assembly into the Outer Membrane." *Philosophical Transactions of the Royal Society B: Biological Sciences* 370(1679).
- McMorran, Lindsay M et al. 2013. "Dissecting the Effects of Periplasmic Chaperones on the in Vitro Folding of the Outer Membrane Protein PagP." *Journal of molecular biology* 425(17): 3178–91.
- Mecasas, J et al. 1993. "The Activity of Sigma E, an Escherichia Coli Heat-Inducible Sigma-Factor, Is Modulated by Expression of Outer Membrane Proteins." *Genes & development* 7(12B): 2618–28.
- Mecasas, Joan et al. 1993. "The Activity of an Escherichia Coli Heat-Inducible R-Factor , Is Modulated by Expression of Outer Membrane Proteins." : 2618–28.
- Minoia, Andrea. 2010. "Rgyr.tcl." <http://chembytes.wdfiles.com/local--files/yasc-vmd/rgyr.tcl>.
- Misra, R., M. Castilokeller, and M. Deng. 2000. "Overexpression of Protease-Deficient DegP(S210A) Rescues the Lethal Phenotype of Escherichia Coli OmpF Assembly Mutants in a degP Background." *Journal of Bacteriology* 182(17): 4882–88.
- Missiakas, Dominique, Jean-michel Betton, and Satish Raina. 1996. "New Components of Protein Folding in Extracytoplasmic Compartments of Escherichia Coli SurA, FkpA, and Skp/OmpH." *Molecular cell* 21(4): 871–84.
- Moon, C Preston et al. 2013. "Membrane Protein Thermodynamic Stability May Serve as the Energy Sink for Sorting in the Periplasm." *Proceedings of the National Academy of Sciences of the United States of America* 110(11): 4285–90.
- Murakami, Satoshi, Ryosuke Nakashima, Eiki Yamashita, and Akihito Yamaguchi. 2002. "Crystal Structure of Bacterial Multidrug Efflux Transporter AcrB." *Nature* 419(6907): 587–93.
- Nakamura, K, and S Mizushima. 1976. "Effects of Heating in Dodecyl Sulfate Solution on the

- Conformation and Electrophoretic Mobility of Isolated Major Outer Membrane Proteins from *Escherichia Coli* K-12.” *Journal of biochemistry* 80(6): 1411–22.
- Nikaido, H. 1989. “Outer Membrane Barrier as a Mechanism of Resistance.” *Antimicrobial agents and chemotherapy* 33(11): 1831–36.
- Noinaj, Nicholas et al. 2013. “Structural Insight into the Biogenesis of β -Barrel Membrane Proteins.” *Nature* 501(7467): 385–90.
- . 2014. “Lateral Opening and Exit Pore Formation Are Required for BamA Function.” *Structure* 22(7): 1055–62.
- Northrup, S H, and H P Erickson. 1992. “Kinetics of Protein-Protein Association Explained by Brownian Dynamics Computer Simulation.” *Proceedings of the National Academy of Sciences of the United States of America* 89(8): 3338–42.
- O’Reilly, A. O. et al. 2014. “Chaperone-Mediated Native Folding of a β -Scorpion Toxin in the Periplasm of *Escherichia Coli*.” *Biochimica et Biophysica Acta* 1840: 10–15.
- Onufryk, Christina, Marie-Laure Crouch, Ferric C Fang, and Carol A Gross. 2005. “Characterization of Six Lipoproteins in the sigmaE Regulon.” *Journal of bacteriology* 187(13): 4552–61.
- Ortega, A., D. Amorós, and J. García De La Torre. 2011. “Prediction of Hydrodynamic and Other Solution Properties of Rigid Proteins from Atomic- and Residue-Level Models.” *Biophysical Journal* 101(August): 892–98.
- Ortiz-Suarez, Maite L. et al. 2016. “Full-Length OmpA: Structure, Function, and Membrane Interactions Predicted by Molecular Dynamics Simulations.” *Biophysical Journal* 111(8): 1692–1702.
- Osborn, M. J., Gander, J. E., Parisi, R., Carson, J. 1972. “Mcromolecules: Mechanism of Assembly of the Outer Membrane of Salmonella Typhimurium: Site of Syntehsis of

- Lipopolysaccharide.” *Journal of Biological Chemistry* 247: 3962–72.
- Padiolleau-Lefèvre, Séverine et al. 2006. “Expression of a Functional scFv Fragment of an Anti-Idiotypic Antibody with a β -Lactam Hydrolytic Activity.” *Immunology Letters* 103: 39–44.
- Patel, Geetika J, Susanne Behrens-Kneip, Otto Holst, and Jörg H Kleinschmidt. 2009. “The Periplasmic Chaperone Skp Facilitates Targeting, Insertion, and Folding of OmpA into Lipid Membranes with a Negative Membrane Surface Potential.” *Biochemistry* 48(43): 10235–45.
- Peeler, J. C., and R. A Mehl. 2012. “Site-Specific Incorporation of Unnatural Amino Acids as Probes for Protein Conformational Changes.” *Methods in Molecular Biology* 794: 125–34.
- Philo, John S. 2006. “Improved Methods for Fitting Sedimentation Coefficient Distributions Derived by Time-Derivative Techniques.” *Analytical biochemistry* 354(2): 238–46.
- Pierucci, O. 1972. “Chromosome Replication and Cell Division in Escherichia Coli at Various Temperatures of Growth.” 109(2): 848–54.
- Plummer, Ashlee M., and Karen G. Fleming. 2015. “BamA Alone Accelerates Outer Membrane Protein Folding In Vitro through a Catalytic Mechanism.” *Biochemistry* 54: 6009–11.
- . 2016. “From Chaperones to the Membrane with a BAM!” *Trends in Biochemical Sciences* 41(10): 872–82.
- Plummer, Ashlee M, Dennis Gessmann, and Karen G Fleming. 2015. “The Role of a Destabilized Membrane for OMP Insertion.” *Methods in Molecular Biology* 1329: 57–65.
- Powers, Evan T, David L Powers, and Lila M Gierasch. 2012. “FoldEco: A Model for Proteostasis in E. Coli.” *Cell reports* 1(3): 265–76.
- “PyMOL.” *The PyMOL Molecular Graphics System, Version 1.3 Schrödinger, LLC.*
- Qu, Jian et al. 2007. “The Trimeric Periplasmic Chaperone Skp of Escherichia Coli Forms 1:1 Complexes with Outer Membrane Proteins via Hydrophobic and Electrostatic

- Interactions.” *Journal of Molecular Biology* 374(1): 91–105.
- Ramm, K, and A Plückthun. 2000. “The Periplasmic Escherichia Coli Peptidylprolyl Cis,trans-Isomerase FkpA. II. Isomerase-Independent Chaperone Activity in Vitro.” *The Journal of biological chemistry* 275(22): 17106–13.
- . 2001. “High Enzymatic Activity and Chaperone Function Are Mechanistically Related Features of the Dimeric E. Coli Peptidyl-Prolyl-Isomerase FkpA.” *Journal of molecular biology* 310(2): 485–98..
- Rassam, Patrice et al. 2015. “Supramolecular Assemblies Underpin Turnover of Outer Membrane Proteins in Bacteria.” *Nature* 523: 333-36.
- Reddington, Samuel C. et al. 2013. “Different Photochemical Events of a Genetically Encoded Phenyl Azide Define and Modulate GFP Fluorescence.” *Angewandte Chemie - International Edition* 52(23): 5974–77.
- Rhodium, Virgil A. et al. 2006. “Conserved and Variable Functions of the Sigma E Stress Response in Related Genomes.” *PLoS Biology* 4(1): 0043–0059.
- Rigel, Nathan W, Dante P Ricci, and Thomas J Silhavy. 2013. “Conformation-Specific Labeling of BamA and Suppressor Analysis Suggest a Cyclic Mechanism for β -Barrel Assembly in Escherichia Coli.” *Proceedings of the National Academy of Sciences of the United States of America* 110(13): 5151–56.
- Rizzitello, A, Jill R Harper, and Thomas J Silhavy. 2001. “Genetic Evidence for Parallel Pathways of Chaperone Activity in the Periplasm of Escherichia Coli.” *Journal Of Bacteriology* 183(23): 6794–6800.
- Rothman, J E. 1989. “Polypeptide Chain Binding Proteins: Catalysts of Protein Folding and Related Processes in Cells.” *Cell* 59(4): 591–601.
- Rouviere, P. E., and C. A. Gross. 1996. “SurA, a Periplasmic Protein with Peptidyl-Prolyl

- Isomerase Activity, Participates in the Assembly of Outer Membrane Porins.” *Genes & Development* 10(24): 3170–82.
- Ruiz, Natividad, Daniel Kahne, and Thomas J Silhavy. 2006. “Advances in Understanding Bacterial Outer-Membrane Biogenesis.” *Nature reviews. Microbiology* 4(1): 57–66.
- Sandlin, Clifford W., Nathan R. Zaccai, and Karen G. Fleming. 2015. “Skp Trimer Formation Is Insensitive to Salts in the Physiological Range.” *Biochemistry* 54(48): 7059–62.
- Sarachan, Kathryn L., Joseph E. Curtis, and Susan Krueger. 2013. “Small-Angle Scattering Contrast Calculator for Protein and Nucleic Acid Complexes in Solution.” *Journal of Applied Crystallography* 46(6): 1889–93.
- Sassoon, N, J P Arié, and J M Betton. 1999. “PDZ Domains Determine the Native Oligomeric Structure of the DegP (HtrA) Protease.” *Molecular microbiology* 33(3): 583–89.
- Saul, F.A. et al. 2004. “Structural and Functional Studies of FkpA from Escherichia Coli, a Cis/trans Peptidyl-Prolyl Isomerase with Chaperone Activity.” *Journal of Molecular Biology* 335(2): 595–608.
- Schäfer, Ute, Konstanze Beck, and Matthias Müller. 1999. “Skp, a Molecular Chaperone of Gram-Negative Bacteria, Is Required for the Formation of Soluble Periplasmic Intermediates of Outer Membrane Proteins.” *Journal of Biological Chemistry* 274(35): 24567–74.
- Scholz, Christian et al. 2005. “Functional Solubilization of Aggregation-Prone HIV Envelope Proteins by Covalent Fusion with Chaperone Modules.” *Journal of Molecular Biology* 345: 1229–41.
- Schreiber, G, A M Buckle, and a R Fersht. 1994. “Stability and Function: Two Constraints in the Evolution of Barstar and Other Proteins.” *Structure (London, England : 1993)* 2(10): 945–51.
- Schwalm, Jaclyn, Tara F. Mahoney, Garner R. Soltes, and Thomas J. Silhavy. 2013. “Role for

- Skp in LptD Assembly in Escherichia Coli.” *Journal of Bacteriology* 195(16): 3734–42.
- Sklar, Joseph G, Tao Wu, Luisa S Gronenberg, et al. 2007. “Lipoprotein SmpA Is a Component of the YaeT Complex That Assembles Outer Membrane Proteins in Escherichia Coli.” *Proceedings of the National Academy of Sciences of the United States of America* 104(15): 6400–6405.
- Sklar, Joseph G, Tao Wu, Daniel Kahne, and Thomas J Silhavy. 2007. “Defining the Roles of the Periplasmic Chaperones SurA, Skp, and DegP in Escherichia Coli.” *Genes & development* 21(19): 2473–84.
- Soltes, Garner R., Jaclyn Schwalm, Dante P. Ricci, and Thomas J. Silhavy. 2016. “The Activity of *Escherichia Coli* Chaperone SurA Is Regulated by Conformational Changes Involving a Parvulin Domain.” *Journal of Bacteriology* (January): JB.00889-15.
- Stafford, Walter F., and Peter J. Sherwood. 2004. “Analysis of Heterologous Interacting Systems by Sedimentation Velocity: Curve Fitting Algorithms for Estimation of Sedimentation Coefficients, Equilibrium and Kinetic Constants.” *Biophysical Chemistry* 108(1–3): 231–43.
- Stock, Jeffry B., Barbara Rauch, and Saul Roseman. 1977. “Periplasmic Space in Salmonella Typhimurium.” *The Journal of biological chemistry* 252.
- Strauch, K L, K Johnson, and J Beckwith. 1989. “Characterization of DegP, a Gene Required for Proteolysis in the Cell-Envelope and Essential for Growth of Escherichia Coli at High Temperature.” *Journal of Bacteriology* 171(5): 2689–96.
- Tamm, Lukas K., Heedeok Hong, and Binyong Liang. 2004. “Folding and Assembly of β -Barrel Membrane Proteins.” *Biochimica et Biophysica Acta - Biomembranes* 1666(1–2): 250–63.
- Thoma, Johannes, Björn M Burmann, Sebastian Hiller, and Daniel J Müller. 2015. “Impact of Holdase Chaperones Skp and SurA on the Folding of β -Barrel Outer-Membrane Proteins.” *Nature Structural & Molecular Biology* 22(10): 795–802.
- Thompson, Natalie J et al. 2014. “Substrate Occupancy at the Onset of Oligomeric Transitions

- of DegP.” *Structure (London, England : 1993)* 22(2): 281–90.
- Tomkiewicz, Danuta et al. 2006. “SecA Supports a Constant Rate of Preprotein Translocation.” *Journal of Biological Chemistry* 281(23): 15709–13.
- Tormo, A, M Almirón, and R Kolter. 1990. “SurA, an Escherichia Coli Gene Essential for Survival in Stationary Phase.” *Journal of bacteriology* 172(8): 4339–47.
- Trandinh, C C, G M Pao, and M H Saier. 1992. “Structural and Evolutionary Relationships among the Immunophilins: Two Ubiquitous Families of Peptidyl-Prolyl Cis-Trans Isomerases.” *The FASEB Journal* 6(15): 3410–20.
- Ureta, Alejandro R., Robert G. Endres, Ned S. Wingreen, and Thomas J. Silhavy. 2007. “Kinetic Analysis of the Assembly of the Outer Membrane Protein LamB in Escherichia Coli Mutants Each Lacking a Secretion or Targeting Factor in a Different Cellular Compartment.” *Journal of Bacteriology* 189(2): 446–54.
- Usui, Kenji et al. 2009. “Site-Specific Modification of Alzheimer’s Peptides by Cholesterol Oxidation Products Enhances Aggregation Energetics and Neurotoxicity.” *Proceedings of the National Academy of Sciences of the United States of America* 106: 18563–68.
- Veiga, Esteban, Víctor De Lorenzo, and Luis Angel Fernández. 2004. “Structural Tolerance of Bacterial Autotransporters for Folded Passenger Protein Domains.” *Molecular Microbiology* 52(4): 1069–80.
- Vertommen, Didier et al. 2008. “The Disulphide Isomerase DsbC Cooperates with the Oxidase DsbA in a DsbD-Independent Manner.” *Molecular Microbiology* 67(November 2007): 336–49.
- . 2009. “Characterization of the Role of the Escherichia Coli Periplasmic Chaperone SurA Using Differential Proteomics.” *Proteomics* 9(9): 2432–43.
- Vogt, Joachim, and Georg E. Schulz. 1999. “The Structure of the Outer Membrane Protein OmpX from Escherichia Coil Reveals Possible Mechanisms of Virulence.” *Structure* 7(10):

1301–9.

- Vollmer, Waldemar, and Ute Bertsche. 2008. “Murein (Peptidoglycan) Structure, Architecture and Biosynthesis in Escherichia Coli.” *Biochimica et Biophysica Acta - Biomembranes* 1778(9): 1714–34.
- Voulhoux, R., Bos, M. P., Geurtsen, J., Mols, M., and J. Tommassen. 2003. “Role of a Highly Conserved Bacterial Protein in Outer Membrane Protein Assembly.” *Science* 299: 262–66.
- Vuong, Phu et al. 2008. “Analysis of YfgL and YaeT Interactions through Bioinformatics, Mutagenesis, and Biochemistry.” *Journal of Bacteriology* 190(5): 1507–17.
- Walther, Dirk M., Doron Rapaport, and Jan Tommassen. 2009. “Biogenesis of β -Barrel Membrane Proteins in Bacteria and Eukaryotes: Evolutionary Conservation and Divergence.” *Cellular and Molecular Life Sciences* 66(17): 2789–2804.
- Walton, Troy A et al. 2009. “The Cavity-Chaperone Skp Protects Its Substrate from Aggregation but Allows Independent Folding of Substrate Domains.” *Proceedings of the National Academy of Sciences of the United States of America* 106(6): 1772–77.
- Walton, Troy A, and Marcelo C Sousa. 2004. “Crystal Structure of Skp, a Prefoldin-like Chaperone That Protects Soluble and Membrane Proteins from Aggregation.” *Molecular cell* 15(3): 367–74.
- Wang, Shanshan et al. 2016. “Expression of Antioxidant Molecules and Heat Shock Protein 27 in Thyroid Tumors.” *Journal of cellular biochemistry* 117: 2473–81.
- Wang, Yan et al. 2016. “A Supercomplex Spanning the Inner and Outer Membranes Mediates the Biogenesis of β -Barrel Outer Membrane Proteins in Bacteria.” *Journal of Biological Chemistry* 291(32): 16720–29.
- Watson, Max C., and Joseph E. Curtis. 2013. “Rapid and Accurate Calculation of Small-Angle Scattering Profiles Using the Golden Ratio.” *Journal of Applied Crystallography* 46(4): 1171–77.

- Werner, John, and Rajeev Misra. 2005. "YaeT (Omp85) Affects the Assembly of Lipid-Dependent and Lipid-Independent Outer Membrane Proteins of Escherichia Coli." *Molecular microbiology* 57(5): 1450–59.
- White, D. A., W. J. Lennarz, and C. A. Schnaitman. 1972. "Distribution of Lipids in the Wall and Cytoplasmic Membrane Subfractions of the Cell Envelope of Escherichia Coli." *Journal of Bacteriology* 109(2): 686–90.
- Wimley, William C. 2003. "The Versatile β -Barrel Membrane Protein." *Current Opinion in Structural Biology* 13: 404–11.
- Wu, Emilia L. et al. 2014. "E. Coli Outer Membrane and Interactions with OmpLA." *Biophysical Journal* 106(11): 2493–2502.
- Wu, Si et al. 2011. "Interaction between Bacterial Outer Membrane Proteins and Periplasmic Quality Control Factors: A Kinetic Partitioning Mechanism." *The Biochemical journal* 438(3): 505–11.
- Wu, Tao et al. 2005. "Identification of a Multicomponent Complex Required for Outer Membrane Biogenesis in Escherichia Coli." *Cell* 121(2): 235–45.
- Wülfing, Christoph, and Andreas Plückthun. 1994. "Protein Folding in the Periplasm of Escherichia Coli." *Molecular Microbiology* 12(5): 685–92.
- Wzorek, Joseph S. et al. 2017. "Membrane Integration of an Essential β -Barrel Protein Prerequires Burial of an Extracellular Loop." *Proceedings of the National Academy of Sciences*.
- Xu, Xiaohua, Shuying Wang, Yao-Xiong Hu, and David B McKay. 2007. "The Periplasmic Bacterial Molecular Chaperone SurA Adapts Its Structure to Bind Peptides in Different Conformations to Assert a Sequence Preference for Aromatic Residues." *Journal of molecular biology* 373(2): 367–81.
- Zaccai, Nathan R. et al. 2015. Methods in enzymology *Deuterium Labeling Together with Contrast*

Variation Small-Angle Neutron Scattering Suggests How Skp Captures and Releases Unfolded Outer Membrane Proteins. 1st ed. Elsevier Inc.

Zhang, Weihong et al. 2017. “Combined Monte Carlo/Torsion-Angle Molecular Dynamics for Ensemble Modeling of Proteins , Nucleic Acids and Carbohydrates.” : Submitted.

Curriculum Vitae

Asblee M. Plummer

3120 Saint Paul St, Apt A201, Baltimore, MD 21218 • (910) 818-6500 • Aplumme9@jhu.edu

Born: August 12, 1990 in Fayetteville, North Carolina

Education

2012 – *Current* Ph.D. Molecular Biophysics Johns Hopkins University
Baltimore, MD

Expected Graduation: June, 2017

2008 – 2012 B.S. Chemistry North Carolina State
Raleigh, NC University

Publications

Plummer, A. M., Bubbs, Q. R., Fleming, K. G., Chaperone FkpA Populates Oligomers that Exhibit Distinct Functions, *J. Biological Chemistry*, *Submitted*.

Mo, G. C. H., Ross, B., Hertel, F., Manna, P., Yang, X., Greenwald, E., Booth, C., **Plummer, A. M.**, Tenner, B., Chen Z., Wang, Y., Kennedy, E. J., Cole, P. A., Fleming, K. G., Palmer, A., Jimenez, R., Xiao, J., Dedecker, P., Zhang, J., (2017) Genetically-Encoded Biosensors for Visualizing Live-cell Biochemical Activity at Superresolution, *Nature Methods*, *Accepted*.

Plummer, A. M., Fleming, K. G., (2016) From Chaperones to the Membrane with a BAM!, Review in *Trends in Biochemical Sciences*, 41(10), 872-882.

Costello, S. M., **Plummer, A. M.**, Fleming, P. J., Fleming, K. G., (2016) Dynamic periplasmic chaperone reservoir facilitates biogenesis of outer membrane proteins, *PNAS*, 113(33), E4794-E4800.

Plummer, A. M., Fleming, K. G., (2015) BamA Alone Accelerates Outer Membrane Protein Folding In Vitro through a Catalytic Mechanism, *Biochemistry*, 54(39), 6009-11.

Plummer, A. M.*, Gessmann, D.*, Fleming, K. G., (2015) The role of a destabilized membrane for OMP insertion, *Methods in Molecular Biology*, 1329, 57-65. (*Co-authors)

Gessmann, D., Chung, Y. H., Danoff, E. J., **Plummer, A. M.**, Sandlin, C. W., Zaccai, N. R., Fleming, K. G., (2014) Outer membrane β -barrel protein folding is physically controlled by periplasmic lipid head groups and BamA, *PNAS*, 111, 5878-5883.

Plummer, A. M., Thompson, M. K., Franzen, S. (2013) Role of Polarity of the Distal Pocket in the Control of Inhibitor Binding in Dehaloperoxidase-Hemoglobin, *Biochemistry*, 52, 2218–2227.

Grants and Fellowships

| | | |
|-----------------------|------------------------------|----------------------------------|
| 2014 – <i>Current</i> | Recipient | NSF Graduate Research Fellowship |
| 2012 | George E. Owen Fellowship | Johns Hopkins University |
| 2011 | Undergraduate Research Grant | NC State University |

Research Experience

2013 – *Current* ***Graduate Student (Dept of Biophysics, JHU, Lab of K. Fleming)***

My Ph.D. research aims to understand how outer membrane proteins (OMPs) interact with two protein folding factors: SurA and BamA.

- *How does the soluble chaperone SurA bind to unfolded OMPs?* I isolated a SurA-uOMP complex by biochemical crosslinking and constructed a structural model for this complex by integrating analytical ultracentrifugation, circular dichroism and fluorescence spectroscopy, and small-angle neutron scattering experimental data.
- *How does BamA accelerate folding of client OMPs?* I quantitated the catalytic turnover number of BamA by developing a SDS-PAGE kinetics assay.
- *How do transmembrane (TM) arginines affect the folding kinetics and assembly of OMPs?* I introduced arginines into TM regions of an OMP sequence and quantitated the kinetics of folding for these variants in the presence of BamA using SDS-PAGE. I maintained a collaboration with H. Bernstein (NIH), who studies the in vivo assembly of these variants.

2014 – 2016

Mentor to Undergraduate Researchers:

Shawn Costello, Quenton Bubb

Shawn's project was to develop a holistic MATLAB model for OMP biogenesis. Quenton's project was to experimentally investigate solution properties of the chaperone FkpA. I worked actively with both students to ensure the success of their research. Towards this end, my activities were as follows:

- Designed computational and experimental projects for respective students
- Numerous one-on-one meetings with undergraduates to keep projects on track
- Helped undergraduate students understand relevant literature
- Trained students in presentation skills and laboratory techniques
- Actively collaborated in the writing of Shawn Costello's *PNAS* paper

2011

Undergraduate Summer Research Fellow (Dept of Chemistry, U.T. Knoxville, Lab of S. Campagna)

- *What structural features impart inherent stability to the antioxidant glutathione?* I synthesized analogs of glutathione and probed their structures using mass spectrometry.

2010 – 2012

Undergraduate Researcher (Dept of Chemistry, NCSU Laboratory of S. Franzen)

- *What are the important features of the substrate-binding cavity of the enzyme Dehaloperoxidase?* I designed and studied mutants utilizing UV-Vis kinetics, Resonance Raman, molecular dynamics, and X-ray crystallography experiments.
- Conducted X-ray crystallography experiments at Argonne National Laboratory

2010

Undergraduate Researcher – Study Abroad (Zhejiang University, Hangzhou, China)

- Collaborated with local students to complete molecular dynamics simulations of protein variants

Conference Activity and Participation

Talks

| | | |
|------|-------------------------|---|
| 2016 | Invited Speaker | JHU IBR Retreat (Baltimore, MD) |
| 2016 | Invited Speaker | Gibbs Society of Biothermodynamics Conf. (Carbondale, IL) |
| 2016 | Student-invited Speaker | JHU PMB Student Evening Series |
| 2015 | Student-invited Speaker | JHU PMB Student Evening Series |
| 2011 | Invited Speaker | Local A.C.S. Meeting (Raleigh, NC) |

Poster Presentations and Attended Conferences

| | | |
|------|---------------------|---|
| 2017 | Poster Presentation | Biophysical Society Conf. (New Orleans, LA) |
| 2016 | Attendee/Recruiter | Annual Biomedical Research Conf. for Minority Students (Tampa, FL) |
| 2016 | Attendee | International Physics of Living Systems Conference (Boston, MA) |
| 2016 | Poster Presentation | Biophysical Society Conf. (Los Angeles, CA) |
| 2015 | Student Organizer | JHU IBR Retreat (Baltimore, MD) |

| | | |
|------|------------------|--|
| 2015 | Poster Presenter | Gordon Research Conf. (Waltham, MA) |
| 2015 | Poster Presenter | Biophysical Society Conf. (Baltimore, MD) |
| 2014 | Poster Presenter | Gibbs Society of Biothermodynamics Conf. (Carbondale, IL) |
| 2014 | Poster Presenter | JHU IBR Retreat (Baltimore, MD) |
| 2014 | Attendee | Molecular Biophysics of Membranes FASEB Meeting (Big Sky, MT) |
| 2014 | Attendee | DE Membrane Protein Symposium (Newark, DE) |
| 2013 | Poster Presenter | Biophysical Society Conf. (Philadelphia, PA) |
| 2011 | Poster Presenter | Biophysical Society Conf. (Baltimore, MD) |
| 2010 | Poster Presenter | State of North Carolina Undergraduate Research & Creativity Symposium (Raleigh, NC) |

Teaching Experience

| | | |
|------|---|--------------------------|
| 2016 | <i>Participant</i> in Preparing Future Faculty Certification Program | Johns Hopkins University |
|------|---|--------------------------|

| | | |
|---------------------------|--|--|
| 2016 | <i>Co-instructor</i> for Advanced Seminar in Membrane Protein Structure, Function & Pharmacology | Johns Hopkins University |
| 2013 | <i>Teaching Assistant</i> for Physical Chemistry of Biological Macromolecules | Johns Hopkins University |
| 2010 – 2012 | <p><i>Peer Supervisor/Academic Coach</i></p> <ul style="list-style-type: none"> Supervised peer Supplemental Instruction leaders and critiqued their sessions weekly Supported other leaders in the development of skills needed to facilitate productive review sessions Analyzed study skills of General Chemistry students in one-on-one meetings and formulated study plans with these students | University Tutorial Center, North Carolina State University |
| 2010 – 2012 | <p><i>Supplemental Instruction Leader</i></p> <ul style="list-style-type: none"> Facilitated 3 weekly review sessions to help students better understand material in General Chemistry 1, 2, and Organic Chemistry | University Tutorial Center, North Carolina State University |
| <i>Community Outreach</i> | | |
| 2014, 2016 | <i>Volunteer</i> for U.S. Science and Engineering Festival | Washington, DC |
| 2013 - <i>Current</i> | <i>Summer Mentor</i> for Biophysics Research for Baltimore Teens | Johns Hopkins University Dept. of Biophysics |